Heating of fetal bone by diagnostic ultrasound

Doody, Claire

Award date:
1998

Awarding institution:
University of Bath

Heating of Fetal Bone by Diagnostic Ultrasound

submitted by Claire Doody

for the degree of PhD

of the University of Bath

1998

ProQuest LLC
789 East Eisenhower Parkway
P.O. Box 1346
Ann Arbor, MI 48106-1346

Abstract

Most pregnant women in the Western world undergo an ultrasound examination and so it is important to ensure that exposure of the embryo or fetus does not produce unwanted effects. It is known that ultrasound can heat tissue, especially bone, and so this thesis explores the degree to which fetal bone might be heated during a pulsed Doppler examination. This is done both by carrying out measurements and by developing computer models.

Thermal measurements on human fetal thoracic vertebrae of gestational age ranging from 14 to 39 weeks are reported. The bone samples were insonated in vitro with an ultrasound beam which had power and intensity values typical of those from a clinical scanner operating in pulsed Doppler mode. Temperature rises ranging from 0.6°C to 1.8°C were observed after five minutes, with approximately 75% of the temperature rise occurring in the first minute.

Two approaches to computer modelling are described. These are the heated disc technique, which is commonly used to model the temperature rise generated by an ultrasound beam, and finite element modelling, a more general approach used to obtain solutions to differential equations. The degree to which our limited knowledge of the properties of fetal tissue affect our ability to make accurate predictions of in vivo heating is explored. It is shown that the present uncertainty in the value of the thermal conductivity and attenuation coefficient of fetal bone can lead to significant uncertainty in predictions of heating. The degree to which the simplifications inherent in the heated disc model affect the results will also be discussed. The results from the models are compared with the experimental measurements in order to estimate the attenuation coefficient of the bone.

Acknowledgements

There are many people I would like to thank for their help and support during the course of this work. Special thanks must go to my supervisors: Andy Baker, for believing that we would get there in the end; Francis Duck for sharing his great knowledge and enthusiasm and Victor Humphrey for stepping in just when it got difficult. I must also thank Professor Peter Soothill and Dr Helen Porter of St Micheal's Hospital, Bristol without whose assistance I would never have been able to carry out many of the heating measurements.

I am also extremely grateful to the many people in the ultrasonics laboratory at the University of Bath and in medical physics at the Royal United Hospital for their help and encouragement. It would have been much less fun without their friendship.

I must also thank Bournemouth University for funding this work and for arranging my timetable so that it was possible. Thanks are also due to my colleagues and students at Bournemouth for coping with my many absences.

Finally I would like to thank Malcolm for his love and understanding.

Table of Contents

Chapter 1
Introduction

"Diagnostic ultrasound has been widely used in clinical medicine for many years with no proven deleterious effects. However, as the use of ultrasound increases, with the introduction of new techniques and a broadening of the medical indications for ultrasound examinations, continual vigilance is essential to ensure its continued safe use."
(European Federation of Societies for Ultrasound in Medicine and Biology, 1996)

Ultrasound imaging is routinely used as a diagnostic tool for investigating many parts of the body and it is estimated that more than one out of every four imaging studies in the world is an ultrasound examination (Goldberg, 1997). It is important, therefore, to ensure that exposure to ultrasound does not cause unwanted biological effects. At present no reported potentially adverse effect of diagnostic exposure to ultrasound has been convincingly reproduced by a second, independent research team (ter Haar, 1996). There is evidence, however, that the power output from diagnostic machines may be rising (Henderson, Willson, Jago & Whittingham, 1995; Henderson, Whittingham & Dunn, 1997) and a broad range of ultrasound intensities is used in the different diagnostic modalities currently available. Over the past ten years new developments in ultrasound, such as colour flow imaging and transvaginal imaging, have led to new exposure conditions and it is important that these are investigated to ensure that they are not hazardous.

Mechanisms for producing biological changes are often classified as either thermal or non-thermal; this latter group includes mechanisms such as cavitation, acoustic streaming and radiation stress effects. This thesis, however, is concerned with thermal effects, particularly heating of fetal bone, which has been shown to experience a greater temperature rise than soft tissue under identical exposure conditions (Drewniak, Carnes & Dunn, 1989).

1.1. Exposure of the Fetus to Ultrasound.

Most pregnant women in the Western world now undergo an ultrasound examination (Williams, 1991). This could involve exposure from one, or more, of the following diagnostic modalities:

- B-mode: real time imaging which gives a grey-scale display of the structures insonated in which the brightness of each pixel depends upon the amplitude of the received echo;
- M-mode: display of one scan line against time, most frequently used in cardiac imaging;
- Pulsed Doppler: the display of a graph of the frequency (or velocity) spectrum against time for the signal returning from a designated length of one scan line, used to study blood flow;
- Doppler imaging: the colour-coding of part of a B-mode image so that regions in which tissue, usually blood, is moving are coloured according to either the tissue velocity or the power in the Doppler-shifted signal.

While most pregnant women in the U.K. are likely to undergo a B-mode examination at between 15 - 20 weeks, a Doppler examination of any kind is less common. B-mode examinations allow the structure of fetal organs to be examined, looking, for example, at the chambers of the heart. They also allow fetal measurements to be obtained and these can be used either to confirm the age or to monitor the growth of the fetus. Doppler studies allow non-invasive studies of the fetal and maternal circulation (Kurjak, Alfirevic & Miljan, 1988) and transabdominal pulsed Doppler is a well-established technique for evaluating the later stages of pregnancy. Transvaginal pulsed Doppler and Doppler imaging have been used to assess blood flow in first-trimester pregnancies (Dillon, Case, Ramos, Holland & Taylor, 1993; Montenegro, Matias, Areias & Barros, 1997).

The range of intensity values used by the different modalities is reflected in the European Federation of Societies for Ultrasound in Medicine and Biology (EFSUMB) Clinical Safety Statement for Diagnostic Ultrasound (EFSUMB, 1996). The advice given ranges from that for B-mode, which states that "there is no evidence to withhold B-mode scanning, including the routine scanning of every woman during pregnancy" to more

cautious statements regarding the use of Doppler mode ultrasound: "In general, the informed use of Doppler ultrasound is not contra-indicated. However, at maximum machine settings, significant thermal effects at bone surfaces cannot be excluded". The increased sensitivity of the embryo during the first trimester is also noted and "Until further scientific information is available, investigations using pulsed Doppler ultrasound at maximum output levels in which the embryo lies within the ultrasonic beam, are considered inadvisable".

It can be seen that concerns over the safety of ultrasound have been raised and that further work is necessary to allowed informed debate to take place about what are safe exposure conditions. It should be remembered however that "mis-diagnosis is far more dangerous than any effect that might result from ultrasound exposure" (WFUMB, 1997)

1.2. Scope of This Thesis.

This thesis is concerned with the heating of fetal bone during diagnostic exposure to ultrasound, particularly exposure to a pulsed Doppler field. This modality was chosen because the beam remains stationary, leading to a relatively small volume of tissue being insonated for an extended period of time and increasing the likelihood of significant heating. Fetal bone was chosen because, as has already been noted, bodies such as EFSUMB have identified the bone surface as a region where thermal effects may occur. The one piece of published work on measurements of heating in human fetal bone (Drewniak et al., 1989), however, only includes data from samples up to 108 days gestational age, less than half way through pregnancy.

The temperature rise that can be generated in fetal bone by an ultrasound beam with power and intensity values typical of those from a clinical scanner operating in pulsed Doppler mode has been measured. The samples were of fetal thoracic vertebrae with gestational age ranging from 14 - 39 weeks, i.e. from approximately a third of the way through pregnancy to nearly full term. Results are presented showing how the temperature rise varies with gestational age and the application of these results to in-vivo heating is discussed. These results and those obtained on fetal bone by other authors are then compared with the Thermal Index, an indicator of temperature rise that is now displayed on most modern scanners.

In the second half of this thesis techniques for modelling bone heating are reviewed and two types of model implemented. The first, the heated disc model, calculated the temperature rise along the axis of the ultrasound beam by carrying out a numerical integration of an approximate point-source solution to the bio-heat transfer equation. The second model used the finite element technique, which is a standard numerical approach used to obtain a solution to the differential equation governing heat flow. This latter technique can model more complex geometries and estimate the temperature rise anywhere in the field but at greater computational cost. It allows the appropriate thermal properties to be used in each tissue layer, a feature that is not present in the analytical techniques commonly used to predict heating due to diagnostic ultrasound. The degree to which our limited knowledge of the properties of fetal tissue affect our ability to make accurate predictions of in-vivo heating is explored and the modelled and measured results are compared in order to estimate the attenuation coefficient of the bone. Finally suggestions are made about further work that is necessary in this field.

Chapter 2

Biological Effects of Ultrasound Induced Hyperthermia

2.1. Introduction.

There are a variety of approaches that can be used to investigate the safety of ultrasound and these were divided into three groups by Williams (1983):

- mechanistic studies which look at the various mechanisms which may result in the modification of tissue;
- bioeffects studies which attempt to identify the acoustic parameters which cause a detectable change in biological systems;
- epidemiological studies which carry out a statistical comparison of a population of subjects who have been exposed with a control population.

The mechanistic approach would separate out an effect such as hyperthermia and study it separately from other effects, such as cavitation and streaming, while a bioeffects study might identify the acoustic power levels needed to cause cell damage without identifying which mechanism was causing the damage. However, when studying an effect thought to be caused by ultrasound, it may not always be possible to state the mechanism which caused the effect or, in an epidemiological study, to explain way there is a difference between the exposed group and the control group.

2.2. Mechanistic Studies

Studies have investigated the effect of raising tissue temperature both in cell cultures and in animals. Cells rely upon chemical reactions occurring at the proper rate and these reaction rates are controlled by enzymatic activity, which has a temperature dependence described by the Q_{10} rule (Miller & Ziskin, 1989). This states that for every 10°C elevation in temperature there is a doubling in enzymatic activity. However, at approximately 50°C the protein constituents of enzymes become degraded and enzymatic activity decreases and ultimately ceases. This results in cell death.

Cell production is also affected by temperature, with the cell cycle time lengthening if the cells are above or below the ideal incubation temperature and stopping completely once the temperature reaches a certain level. For mammalian cells the temperature for maximal cell growth is in the range 33-39°C (Barnett, ter Haar, Ziskin, Nyborg, Maeda & Bang, 1994).

Biological effects that have been observed when cell temperatures are in the range 40 45°C include microscopic changes such as shrinkage of the cytoplasm and nuclei, leakage of proteins through capillary membranes and oedema formation (Overgaard, 1983; Barnett et al., 1994). Barnett, Edwards and Martin (1991) demonstrated changes in the bone marrow cells of adult guinea pigs at threshold exposures of 43°C for 3 minutes and 42°C for 6 minutes.

The fact that there is a relationship between the duration of the temperature elevation and the temperature rise needed to cause cell damage has been noted by many authors (Lele, 1977; Sapereto & Dewey, 1984; Miller & Ziskin, 1989; Barnett et al., 1994). The threshold level appears to be at around 40°C, as no thermal damage has been observed below this. Above this threshold the severity of thermal injury is proportional to the logarithm of the exposure duration. For temperatures of less than 43°C it is possible to define a boundary line below which there have been no observed biological effects (Miller & Ziskin, 1989). This exposure time (in minutes) is given by:

$$t = 4^{(43 - T)} \qquad \text{(Equation 2.1)}$$

where T is the temperature (in °C). Combinations of temperature elevation and exposure duration falling below this line would be considered unlikely to produce any harm. However, there is not a clear consensus on whether absolute temperature or temperature elevation is the biologically relevant parameter (Barnett et al., 1994). Much of the data reviewed came from animals whose normal core temperature is higher than that of humans and so this leads to doubts about the applicability of Equation 2.1.

The World Federation for Ultrasound in Medicine and Biology (WFUMB) reviewed the effects of heat on prenatal development (WFUMB, 1992). They considered the evidence for embryonic or fetal

death and for teratogenic effects (those causing congenital malformations). Prenatal death was seen in many species after temperature elevations in the range 1.2 - 3.9°C had been maintained for a period of hours, with the embryo being most vulnerable pre-implantation. Temperature increases of the same magnitude during organogenesis have been shown to cause teratogenic effects such as neural tube defects and microcephaly. In general, embryos are more susceptible to damage than the more developmentally advanced fetuses. However it is also necessary to consider the relative sensitivity of different tissue types. The neurones of the developing fetal brain are considered to be the most susceptible to the effects of ultrasound induced heating (Barnett, Rott, ter Haar, Ziskin & Maeda, 1997) and any deficit of cells caused by cell death in the early stages of development may not be made up for later.

There are still uncertainties in the application of results from animal studies. Most of the studies into hyperthermia involve whole body heating and there is little information available on the effects that might result from localised heating. An ultrasound beam a few millimetres wide could encompass the whole of an embryo or a very small part of a fetus. There is a high probability that the consequences of heating a small volume of tissue will not be detected unless the target tissue is a critical sensory pathway or organ. The potential for ultrasound induced heating causing damage to small important structures, such as the developing pituitary gland, has not been fully studied (Barnett et al., 1997).

The effect of heating tissue from the nervous system was studied by Yamane et al (Yamane, Tateishi, Cho, Manabe, Yamanashi, Dezawa, et al., 1992). The spinal cord of rabbits was heated to a maximum of 47°C, either momentarily or for 30 minutes, using RF radiation and the temperature measured with a thermosensor placed in the epidural space. If the tissue was heated to below 45°C the spinal cord evoked potential (SCEP) was depressed with the change in amplitude being most severe at start of heating but then improving; the signal returned to normal after heating had ceased. At 45°C and above the amplitude of the SCEP did not return to normal and this lead the authors to conclude that "44°C in the epidural space is the highest tolerable temperature for normal spinal cord function". This paper also quotes a study by Uchiyama, Yashiro, Takahashi & Homma (1989) in which amplitude changes in the SCEP

were not noted at 44°C and below (although the amplitude was only measured after 30 minutes) while at 45°C and above amplitude changes were observed and the recovery was incomplete.

2.3. Bioeffects Research

Many authors have studied the biological effects of ultrasound and it is clear that ultrasound can induce changes in tissue morphology, tissue function and biochemical composition and activity. The intensity levels used in studies vary from those relevant to diagnostic ultrasound to the high intensities used in ultrasound surgery and so, since this thesis is concerned with the safety of diagnostic ultrasound, this review is limited to effects that have been observed with intensity levels at, or close to, those used in diagnosis. Much of the work prior to 1983 was reviewed by Williams (1983) and the bioeffects reported range from changes in DNA through increased fetal movement during insonation to changes in reflexes in animals born after insonation in utero. There are, however, serious doubts about the cause of some of the effects seen in many of the papers, with questions being raised about whether the effects could be due to some feature of the experimental method. One problem pointed out by Hedrick and Hykes (1991) is that in vitro studies usually involve molecules dissolved in an aqueous solution. This solution may contain a high level of dissolved gas and so enhance cavitation. Many studies have looked at cell samples in vitro.

Reports of changes induced by ultrasound include both increases and decreases in the rate of DNA and protein synthesis and in the intracellular concentrations of various ions. This would seem to be in keeping with the effects of temperature on enzyme activity and cell production that have already been discussed.

Other effects observed include differences in cell motility (ability to move) and the shape and behaviour of the cell surface (Liebeskind, Padawer, Wolley & Bases, 1981; Liebeskind, Padawer, Wolley & Bases, 1982). Fibroblasts grown in tissue culture were insonated using a commercial diagnostic machine and when the surface of cells was studied they showed a large number of folds or projections. These only disappeared, with the cells returning to their normal appearance, once the cells had grown to the stage were they were touching their neighbours. Morphological changes were also observed, including

changes in composition of the nucleus and the cytoplasm. Various groups have looked for genetic effects on the cell by counting the number of sister chromatids exchanges (SCEs). These occur when the two identical chromatids, of which each chromosome is composed, exchange DNA and the number of these present is thought to indicate the level of repair activity within the nucleus (Williams, 1983). While some reports show an increase in SCEs most are negative and specific attempts to replicate certain claimed ultrasound-induced effects have failed. These discrepancies may indicate the presence of a factor other than ultrasound which is affecting the results or it may be that inertial cavitation is occurring in the positive studies but not the negative ones (Miller, Miller & Brayman, 1996).

When the effects of ultrasound on the fetus have been investigated the studies also seem to contain conflicting results. Murai (1975) reported significant differences in the grasp reflex and vocalisation response of rats insonated in utero but there was also a significant difference between animals whose mothers had been restrained for the length of the experiment but not insonated and offspring of unrestrained animals. A later study by Brown (1981) in which higher powers were used but for a shorter time (3 minutes rather than 5 hours) didn't show any effect on reflex development. A report by David (1965) that detected an increase in fetal movement when the fetuses were subjected to ultrasound led to attempts to duplicate the study; three of which gave negative results and one positive.

More recent studies into ultrasound bioeffects have found a range of transient effects and have suggested mechanisms that may be causing them. Siddiqi, Plessenger, Meyer and Woods (1990) have demonstrated a decrease in the amplitude of the auditory brainstem response to a series of clicks during insonation in neonatal lambs, with values returning to normal once insonation stops. This effect was not seen in lambs insonated at two weeks of age. Although the mechanism causing the effect is unclear it is suggested that it may be due to interference with axonal conduction mediated through changes in surface myelin. Another suggestion is that the effect is due to the inner ear responding to the ultrasound, due to the pulse repetition frequency of the scanner, and that this response reduced the amplitude of the measured signals.

Tarantal et al. (1995) found reduced birth weights and third trimester neutrophil counts in monkey fetuses and neonates frequently (on over 30 occasions) exposed to ultrasound prenatally. The scanner used in this study was a commercial system used in "triple mode", i.e. combined B mode, colour and pulsed Doppler. Blood sampling showed that there was a reduction in one type of the hematopoetic progenitors (cells associated with the formation of blood) which had previously been shown to be uniquely sensitive to heat when compared to other progenitor populations. A reduction in insulin-like growth factor binding protein was also observed which is an observation previously noted in human fetuses with inter-uterine growth retardation (IUGR). No long term ramifications were observed, however, with all the animals resuming a normal course of postnatal development.

2.4. Epidemiological Studies

When Ziskin and Petitti (1988) reviewed the evidence for ultrasound bioeffects they stated that "Epidemiological studies and surveys and widespread clinical usage over 25 years have yielded no evidence of any adverse effects from diagnostic ultrasound". They also pointed out however that " the inability to find convincing proof from epidemiology or from physicians experience does not preclude the possibility of it happening". Since this was published some studies have pointed to the possibility of bioeffects. Newnham, Evans, Micheal, Stanley and Landau (1993) studied two groups of pregnant women. One group received a single ultrasound imaging scan at 18 weeks while others received ultrasound imaging and continuous wave Doppler flow studies at 18, 24, 28, 34 and 38 weeks gestation. The results suggested that there was a increase in the number of growth restricted fetuses from the group undergoing multiple examinations. This study was not designed to look for the adverse effects of ultrasound however and the authors suggested that there is need for another study designed specifically to look at the effect of ultrasound exposure on fetal growth. The results from this trial are inconsistent with the available data on birthweight from randomised trials on diagnostic imaging ultrasound. Ultrasound screened children are on average heavier at birth than unscreened children in all other randomised trails on ultrasound imaging (Salvensen, 1997).

Salvensen, Vatten, Eik-Nes, Hugdahl and Bakketeig (1993) found a link between ultrasound during pregnancy and the proportion of children

who are not right-handed. If the dominant hand is used as an indicator of cerebral dominance then the normal high prevalence of right handedness means that random changes to the hemispheres will increase left handedness. This finding was more significant in boys than girls an observation which fits the hypothesis that the male fetal brain is more vulnerable than the female fetal brain. Kieler, Axelsson, Haglund, Nilsson & Salvensen (1998) also found an increased prevalence of non-right handedness in boys who underwent ultrasound screening in early pregnancy compared to a non-screened group and while this did not demonstrate an association between non-right handedness and ultrasound screening in early pregnancy, when comparisons between exposed and non-exposed boys were performed such an association could not be ruled out .

Other outcomes which individual epidemiological studies have suggested may be linked to ultrasound exposure include dyslexia (Stark, Orleans, Haverkamp & Murphy, 1984) and delayed speech development (Campbell, Elford & Brant, 1993) but there are flaws in these studies which may account for the findings. In the study by Stark et al numerous statistical comparisons were made, as they were looking at a wide range of outcomes including measurements of hearing, visual acuity, cognitive function and behaviour. As Williams (1991) points out, the more possible effects that are studied the greater the chance of finding a significant difference between groups due purely to random variations in outcome. The study of speech development is rather small and was not assessed blind, which leads Salvensen (1997) to suggest that the results should be viewed cautiously. A study by Salvensen (1994) actually found that screened children were less likely to be referred to a speech therapist, although it should be noted that this study was not originally designed to look at speech development and the finding may have been due to chance.

2.5. Discussion

It can be seem that ultrasound has the potential to cause biological changes, with one mechanism for this being the increase in temperature of tissue. The extent to which bioeffects occur in clinical practice is not yet clear, however. and it should be noted that "no reported potentially adverse effect has been convincingly reproduced by a second, independent team" (ter Haar, 1996). However the fact that the output

from diagnostic machines has risen considerably over recent years (Henderson et al., 1995; Henderson et al., 1997) means that there is a need for continuing vigilance. It seems unlikely that ultrasound can be causing a significant increase in gross abnormalities, as these would have been detected by the epidemiological studies and so any damage that is caused by ultrasound exposure in utero must be subtle, delayed, or infrequent (Hedrick & Hykes, 1991). The study by Newnham showing an increase in low birthweight babies after exposure to Doppler ultrasound indicates the need for further work although this study seems to conflict with studies on the effect of ultrasound imaging.

After reviewing the report of a symposium on the 'Safety of Ultrasound in Medicine' held in 1996, WFUMB (1997) made a series of recommendations; these include the following:

"A diagnostic exposure that elevates embryonic and fetal in situ temperature above 41°C (4°C above normal temperature) for 5 minutes or more should be considered potentially hazardous For diagnostic ultrasound systems capable of producing a tissue temperature increase greater than 1.5°C above normal, users should be provided with worst-case estimates of the temperature increase in all pertinent operating modes."

The European Federation of Societies for Ultrasound in Medicine and Biology's (EFSUMB) 1996 safety statement states that "there is no reason to withhold B or M-mode scanning for any clinical application" and "the informed use of Doppler ultrasound is not contra-indicated". However, "at maximum output settings, significant thermal effects at bone surfaces can not be excluded". The statement advises to user to make use of exposure information and to act prudently to limit exposure of critical structures, including bone. Guidelines such as these, together with display standards giving the user an indication of the temperature rise that could be induced and so help to reduce the risk of bioeffects.

2.6. Chapter Summary

In reviewing the literature it has been found that temperatures in the range 40 - 45°C can effect tissue in a variety of ways including changes in the structure of cells and the rate of cell production It has been shown that a temperature elevation of 1.2 - 3.9°C, if maintained for a period of hours, can cause teratogenic effects if it occurs during organogenesis and

in many species lead to prenatal death. There is a relationship between the duration of the temperature elevation and the temperature at which damage occurs. Ultrasound exposure at diagnostic levels has been associated with a range of effects from changes to DNA to differences in the reflexes of animals insonated in utero. There is much conflicting evidence, however, and it appears that cavitation may have a role in many of the observed effects. Recent epidemiological data has suggested a possible link between ultrasound exposure and an increase in both the number of growth restricted fetuses and the prevalence of non right-handedness. Further work is needed in these areas. The safety statements published by the World and European federations give guidelines for the safe use of ultrasound and indicate the need to be vigilant. The fact that bone is seen as a critical structure and that significant thermal effects at bone surfaces can not be excluded makes the study of heating in fetal bone worthwhile.

Chapter 3
The Properties of Bone

3.1. Introduction

The degree to which a layer of bone is heated by an ultrasound field will depend upon the nature of both the ultrasound field and the bone. This interaction is complex as it has been shown that the thermal properties of bone depend on both the macroscopic structure, for example whether the bone is cancellous or compact, and the microscopic structure, for example the orientation of the collagen fibres (Biyikli, Modest & Tarr, 1986). The attenuation of the ultrasound field is also dependent on the bone structure (Travakoli & Evans, 1992). Fetal bone is even more complex than adult bone as it is changing throughout pregnancy.

3.2. Bone Development

Bones are classified as either cartilaginous or membranous depending upon whether they develop within cartilage or a connective tissue membrane. Ossification, the laying down of bone mineral, occurs within a connective tissue membrane in, for example, the frontal and parietal bones of the cranial vault, while the long bones and vertebrae develop first as cartilage and then ossify. Apart from the more rapid development of membranous bone there is no essential difference between these types (Duggan, 1993) and newly-formed bone is invariably cancellous in nature (Craigmyle, 1986). The first evidence of skeletal formation occurs about four weeks after conception and ossification begins at about the 8th or 9th week.

Both ossification processes begin within a region of mesenchyme. This is a composite of primitive connective cells lying in gel-like ground substance containing immature collagen fibres. In intramembranous ossification the mesenchyme condenses at the ossification centres and some of the cells differentiate into osteoblasts (bone forming cells). These produce osteoid or prebone, a substance rich in collagen, which is deposited outside the cells. Ossification occurs when osteoid is converted into bone by the deposition of the bone mineral, calcium phosphate between, on and within the collagen fibres. Individual shafts of bone, known as trabeculae are laid down and as the bone develops these increase in length and join each other to produce a lattice of primary

cancellous bone. Each bone has a relatively large unossified area among the bony trabeculae. It is only close to the time of birth that this type of bone begins to transform into compact bone.

In ossification in cartilage, there is an intermediate stage, in which mesenchyme condenses and the cells differentiate into cartilage-forming cells. These construct a model of the bone out of cartilage. Bone formation begins within these cartilaginous models towards the end of the second month of gestation and it is at about this time that bone can be reliably identified on an ultrasound scan (Andrews, 1993). Ossification occurs as the cartilage is penetrated by blood vessels and bone mineral is laid down around these. At the centre of the model the cartilage cells begin to degenerate and are eroded by vascular connective tissue and this area turns into the marrow cavity. A thin membrane surrounds the cartilage and osteoblasts just beneath this begin to deposit bone around the shaft, forming the periosteum. Close to the time of birth this begins to transform into compact bone.

3.2.1. Development of the spine

Late in the third week of development the embryo is three-layered and the midline of the middle layer is occupied by the notochord, which is the primitive axial supporting structure. On each side of the notocord is a continuous column of mesoderm most of which, as the embryo grows, becomes divided into short segments called somites. The cells in part of each somite then migrate medially, envelop the notocord and go on to contribute to the axial skeleton.

The tissue begins to turn into cartilage about six weeks after conception with centres of chondrification appearing in the vertebral body (the centrum) and the neural arch. Chrondrification spreads until a cartilaginous vertebral column is completed (Fitzgerald, 1978). Ossification begins towards the end of the second month and three primary centres of ossification are seen in each vertebra: one in the centrum (the vertebral body) and one in each half of the neural arch. In the centra ossification centres first appear in the lower thoracic / upper lumber region and ossification spreads rapidly in a regular manner in both cephalic and caudal directions reaching the second sacral vertebra at the bottom of the spine by week 22 (England, 1990). The ossification process is not complete until long after birth, however, and at birth each vertebra has three bony parts connected by cartilage (Pansky, 1982). In the

thoracic vertebrae, which will be used for the measurements in this study, centres of ossification appear first in the neural arches and then, within a week ossification of the vertebral bodies begins.

3.2.2. Development of the skull

Ossification of the cranial bones begins around the end of the second month with the bones of the vault undergoing intramembranous development. The growth of these bones in the fetal period has been described by Ohtsuki (1977); as they are membranous bones the growth occurs by formation of the trabeculae laid down radially from ossification centres and so the thickness of the bone varies depending on where it is measured. Table 3.1 gives the thickness from fourth month to term measured at an ossification centre.

Table 3.1: Thickness of fetal skull bones

	Thickness (mm)			
Age (months)	**Frontal**	**Parietal**	**Occipital**	**Temporal**
4-5	0.07	0.1	0.30	0.04
6	0.14	0.22	0.67	0.10
7	0.25	0.42	1.36	0.18
8	0.29	0.50	1.58	0.21
9 - 10	0.40	0.54	1.65	0.32

(from Ohtsuki, 1977)

The fact that not all of the bone is ossified and that it does not have a regular structure, makes it difficult to predict the way sound will propagate through it. It is, however, rich in collagen and is therefore likely to be highly absorbing. The thickness of some of the bones is of the order of a wavelength and so the effect of resonances needs to be considered.

The variation of mineralisation with gestational age of human fetal cranial bones was determined by Duggan (1993) who reanalysed data obtained by Trotter (1972). This showed that although the mean ash content increases with age, the percentage of ash content and hence the degree of mineralisation varies little between 20 weeks and term, being

66 ± 1% throughout this period. This observation may not be true for all bones, however, as the cartilaginous bones develop more slowly.

3.3. Thermal Properties of Bone

3.3.1. Thermal conductivity

In order to model bone heating it is necessary to know the thermal properties of the material. This is not a simple task for bone as these are likely to depend upon the structure of the bone and hence be different for different types of bone. Thermal conductivity of tissue is a function of composition and structure (Bowman, 1981). Table 3.2 summaries the values quoted for thermal conductivity of adult human bone. It can be seen that these range differ by more than an order of magnitude.

Table 3.2: Thermal conductivity of human bone.

Author	Type of Bone	Thermal conductivity ($W\ m^{-1}K^{-1}$)
Gordon et al (1976)	Cancellous	0.58
Graf and Stein (1979)	In vivo sternum	0.36
Bowman et al (1979)	Fresh cancellous	0.39
Biyikli (1986)	Fresh femur	0.3
Biyikli (1986)	Dry femur	0.2
Lundskog (1972)	Dry bone	3.35
Zelenov (1985)	Femur axial	12
Zelenov (1985)	Femur radial	9.5

Reasons suggested for this wide range of values include differences in experimental method, the wet or dry condition of the bone and the direction of heat flow (Moses, Witthaus, Hogan & Laster, 1995). Biyikli measured the thermal conductivity using a cut bar apparatus modified to prevent radial heat loss whereas Zelenov used a hot plate technique designed for samples with low thermal conductivity in which radial heat loss is prevented through the use of thermal guard rings. The difference in these two sets of results can not be attributed purely to equipment however, as the hot plate technique does not always give higher results. Moses obtained values for equine cortical bone of 9.5 $W\ m^{-1}K^{-1}$ using a modified cut bar technique and 0.8 $W\ m^{-1}K^{-1}$ using a hot plate apparatus.

Moses suggested that Biyikli obtained such a low result because the bone sample was very thin and the temperature was measured in the surrounding material. This resulted in the thermal contact between the bone and the surrounding material having a major influence on the result. Neither can the range of values be attributed solely to the state of hydration of bone. Moses and Biyikli both compared the values for wet and dry samples and got a variation of the order of 0.1 W $m^{-1}K^{-1}$.

The orientation of the bone will affect the measurement but this does not appear to make a large enough difference to explain the range of observations. Zelenov measured the thermal conductivity in both the radial and the axial direction and found a difference of over 30% in the two values.

It is useful to compare the values quoted for bone with those of other materials. To this end Table 3.3 gives values for a range of materials. It can be seen that the values of Zelenov are rather high, being closer to metals such as steel than to water which makes up 23% of trabecular bone (with another 30% of bone being composed of protein) (Duck, 1990). Thermal conductivity values for other biological hard tissues such as tooth are below 1 W m^{-1} K^{-1} (Duck, 1990) and so the results of Zelenov and Lundskog appear to be out of line with what one would expect of a biological material.

Table 3.3: Thermal conductivities of some non-biological materials.

Material	Thermal Conductivity (W m^{-1} K^{-1})
Brass	104
Concrete	0.934
Steel, stainless	13.8
Teflon	3.48
Water (15°C)	0.595

Values taken from: Therapeutic Heat and Cold (Lehmann, 1983).

There appear to be significant difficulties in determining the thermal conductivity of bone even in samples from the same part of the body. A variety of factors seem to lead to the uncertainty in the measurements including the difficulty in ensuring good thermal contact between the sample and the surrounding materials, the small size of the samples and

the need to obtain one-dimensional heat flow. Even if the values of Zelenov and Lundskog are discounted the values still differ by more than a factor of two. This uncertainty over the value for adult bone suggests that measurements of fetal bone, where the samples are smaller and likely to be more variable, could present considerable difficulties.

3.3.2. Specific heat

Values of the specific heat of bone are also needed if thermal modelling is to be carried out. Many values have been collected together by Duck (1990) and these, with a few additions, are shown in Table 3.4.

Table 3.4: Specific heat values for bone.

Author (date)	Type of Bone	Specific Heat (J kg^{-1} K^{-1})
Henschel (1943)	Human cortical	1300
Lehnmann and Johnson (1958)	Pig, cancellous	2110
Lundskog (1972)	Dry, human	1250
Chen (1976)	Cow, femur	1100
Clattenburg (1975)	Cow, cancellous	1150 - 1730
Gordon (1976)	Human cortical	1590
	Human, cancellous	1590
Morley (1986)	Cow, cortical	1330
	Pig, cortical	1360
Biyikli (1986)	Human, femur, fresh	1500 - 2370
	Human, femur, dry	1140 - 1640

In composite materials the specific heat may be estimated as the sum of heat capacities of each fractional component (Duck, 1990) and so one might expect different values to be obtained for cortical and cancellous bone. It is also to be expected that dry samples will have a lower value than fresh ones as water has a higher specific heat than any of the other components. Biyikli studied samples from different positions along the femur and the influence of the water content could be seen. At the ends of the femur, where the bone consisted primarily of cancellous material, the specific heat of the fresh samples was approximately 2200 J kg^{-1} K^{-1} while at middle where there was a thick layer of compact material and the fluid content was lower (approximately 20% by mass compared to 40%) the value was 1700 J kg^{-1} K^{-1}. The specific heat of the dry samples

appeared to be fairly consistent along the length of the bone, the range of values in the table above coming from scatter around the mean value.

3.4. Attenuation and Absorption of Ultrasound

When a wave passes through tissue the amount of energy in the beam decreases. This loss in energy, the attenuation, is due to refraction, reflection, scattering and absorption. In biological tissues it is generally not possible to describe interactions between individual particles and the wave and so the attenuation is generally described in terms of bulk scattering and absorbing properties (Bamber, 1986). If reflections at tissue interfaces are neglected, the intensity attenuation coefficient μ can be considered to be made up of two components, a scattering coefficient, μ_s and an absorption coefficient, μ_a, such that

$$\mu = \mu_s + \mu_a$$

and the power in the beam varies with distance z as

$$W = W_0 \exp(-\mu z)$$

where W_0 is the initial power (at $z = 0$).

The amplitude attenuation coefficient is generally expressed as α where $\mu = 2\alpha$.

When considering absorption and attenuation it is helpful to consider the basic processes that occur before going on to consider the behaviour of a complex material like bone.

3.4.1. Absorption in homogeneous liquid-like media

The frequency dependence of ultrasonic absorption in homogenous media, for example solutions of biopolymers such as proteins, has been said to suggest that the absorption is due to relaxation processes (Bamber, 1997). These arise when the wave repeatedly perturbs the media and so at any time the wave energy is shared among a number of different forms of energy: translational, molecular vibrational and structural and lattice vibrational and structural. As the pressure fluctuates there is a redistribution of the energy between these states but with a time lag that results in the degradation of the wave energy into heat (Bamber, 1986). The amplitude absorption coefficient due to a single relaxation process is given by:

$$\alpha_R = \frac{A_R f^2}{1+\left(f/f_R\right)^2} \qquad \text{(Equation 3.1)}$$

where A_R is a constant and f_R is the relaxation frequency corresponding to the time constant for the process. Absorption in solutions of biopolymers is usually modelled by summing a series of such processes with different relaxation frequencies and then adding the absorption of water due to shear viscosity η_s. This gives the following equation for the amplitude absorption coefficient α_a:

$$\alpha_a = f^2\left(\frac{16\pi^2\eta_s}{3\rho_o c^3} + \sum_i \frac{A_{Ri}}{1+\left(f/f_{Ri}\right)^2}\right) \qquad \text{(Equation 3.2)}$$

where ρ_o and c and the density of and speed of sound in the solution and i indicates a summation over a number of relaxation processes each with a relaxation frequency f_{Ri}

Holmes and Challis (1996) demonstrated that the acoustic absorption of the proteins lysozyme and bovine serum albumin within the 2 - 60 MHz range can be modelled using the sum of two single relaxation processes plus a residual component which may represent a relaxation process with $f_R > 100$ MHz.

The full range of relaxation processes that cause absorption in tissue is not known but one relaxation process the occurs at physiological pH involves proton transfer between the imidazole ring of histidyl residue, which is found in many proteins and the hydrogen phosphate ion:

$$-IH^+ + HPO_4^{--} \Leftrightarrow -I + H_2PO_4^-.$$

Here -IH^+ and -I represent respectively the protonated and neutral forms of the imidazole ring (Edmonds, 1982). Slutsky (1981) estimated the contribution to tissue absorption by this mechanism and produced results almost equal to observed values. This work makes the assumption that the total protein absorption is the sum of the constituent amino-acid absorptions, which is almost certainly not the case but it was a significant step forward in the understanding of tissue absorption (Evans, 1986). Slutsky (1996) also demonstrated that the chemical relaxation associated with perturbation of proton-exchange equilibria may make a fairly large

contribution to the ultrasonic absorption in tissue where inorganic phosphate was accumulated at the expense of other forms of phosphate, as might happen to cells that have exhausted glucose after anaerobic glycolysis. The absorption coefficients calculated using this assumption were comparable with those observed in excised heart muscle. Bamber (1997) states that at physiological pH the most important relaxation mechanisms are believed to arise from perturbation of the hydration layers of macromolecules, involving structural relaxation between the number of water molecules at any instant in a free or bound state.

3.4.2. Viscoelasticity

Although the high water content of tissue has led many authors to consider it as a liquid-like medium, strictly speaking tissue is viscoelastic (Kagawa, Takeuchi & Yamabuchi, 1986). In perfectly viscous materials the applied stress in proportional to the rate of change of the resulting strain, but independent of the strain itself; while in elastic materials Hooke's law applies and the stress is proportional to the strain. Viscoelastic materials exhibit a combination of these properties. At low frequencies they will exhibit primarily viscous behaviour but as the frequency increases this changes and the behaviour becomes elastic. In modelling the macroscopic aspects of viscoelasticity there are many possible ways of combining the elastic and viscous components. The attenuation coefficient is related to the ratio of the real and imaginary components of the longitudinal elastic modulus (M' and M") by the following equation:

$$a\lambda = M''/M'.$$

The form of M is dependent on the model chosen but this, and therefore the attenuation, will depend upon frequency.

3.4.3. Attenuation in solids

The elastic properties of a solid differ from those of an ideal fluid in two major respects (Bhatia, 1967):

- solids possess rigidity and can support shear waves;
- solids are usually anisotropic, so that the velocity of a wave depends upon its direction of propagation.

In a polycrystalline material the wave effectively enters a new medium at each grain boundary (Kuttruff, 1991). This is true even if the grains are

chemically identical because they are anisotropic and so the elastic constants depend upon the direction in which they are stressed. The sound wave will therefore be partially reflected from each grain boundary. The overall effect depends upon the size of the grains in relation to the wavelength. When $\lambda >> d$ (the mean grain diameter) the attenuation is proportional to f^4, Rayleigh's law, but as the frequency increases so that $0.3\lambda < d < \lambda$ the variation in the scattering coefficient approaches f^2. In cases where the wavelength is small compared to the grain size, a frequency independent portion of the absorption coefficient is observed which can be explained by the reflections at the grain boundaries and the refraction of sound entering the interior of the grain. At these frequencies there is also an elastic hysterisis, corresponding to sliding processes at the grain boundaries and this is directly proportional to the frequency.

Thermoelastic relaxation also contributes to the attenuation in polycrystalline solids. In this process heat flows between local temperature differences which have arisen due to differing stress-strain relationships in the randomly oriented grains (Bamber, 1986).

3.4.4. Attenuation of ultrasound in bone

The interaction of ultrasound with bone has been studied for a variety of reasons. These include investigations into the feasibility of imaging through bone and studies of bone structure as well as measurements of bone heating. Definitive identification of the absorption mechanisms is rendered difficult by the complexity of the bony microstructure (Lakes, Yoon & Katz, 1985) and the degree of absorption has been found to differ markedly between different types of bone. Wu and Cumberley (1997) stated that attenuation in cancellous bone is at least an order of magnitude greater than that in compact bone due to the scattering contribution.

The difficulty in obtaining attenuation values for bone has been evident since Heuter (1952) carried out measurements on human skull bones. In this study specimens were taken post mortum from seven autopsies and from different parts of the skull. When the author tried to prepare the samples, e.g. by grinding, it was found that their consistency, and thereby their attenuation changed. This meant that only the natural variation in thickness between different samples could be used to determine the attenuation and the reflection loss. Considerable variation was noted

between samples and part of this was ascribed to variations in their structure. It was found that the attenuation exhibited a highly non-linear frequency dependence in the range 0.3 - 3.5 MHz and it was suggested that there was a strong similarity to the results obtained by Mason in polycrystalline metals (Mason, 1950). This led the author to conclude that the energy loss occurred through scattering.

Fry and Barger (1978) also studied human skulls bones, including an infant skull, and they obtained the only attenuation data available on immature human bone. A broadband technique was used in which the change in insertion and reflection loss with frequency was calculated from the Fourier coefficients of the waveforms. The insertion loss (IL) and the reflection loss (R) were defined as follows:

$$IL = 20 \log |P_y| / |P'_y|$$

$$R = 20 \log |P_z| / |P_x|$$

where P_y and P'_y are the Fourier coefficients of the pressure waveforms at point y with and without the skull present respectively, P_x is the Fourier coefficient of the pressure waveform before it is incident of the bone and P_z after reflection from the bone surface. Measurements were carried out over a 0.4 - 2 MHz frequency range. The three layers of the adult skull, inner, diploe and outer, were found to have different properties and in some frequency ranges the scattering loss in the diploe was found to be causing the non-linear dependence. The inner and outer layers of the skull are of compact bone while the diploe is cancellous and has blood and fat filled pores. The size of these pores is of the same order of magnitude as the wavelength of sound at frequencies close to 1 MHz. At the lower end of the measured frequency band scattering was found to give a variation of attenuation that goes as the fourth power of the frequency, as would be expected from Rayleigh scattering, and it would seem likely that this is what produced the frequency dependence in Heuter's measurements. At frequencies greater than about 1.3 MHz the wavelength of the sound in the diploe was less than three times the characteristic diameter of the pores and the insertion loss changed to f^2.

The infant skull sample was 0.74 mm thick and did not have a diploe layer. The insertion loss reached a maximum value of 4 dB at a frequency of about 1 MHz. The absence of the diploe completely eliminated the

large increase in loss with increasing frequency. The reflection losses varied from 3 dB (50% of power reflected) to 20 dB (10% of power reflected); it should be noted that the definitions were such that a lower reflection loss corresponds to less power being transmitted into the skull. The peak reflection loss was at around 1.9 MHz which was thought to be a resonance frequency of the bone layer. In order to calculate the attenuation coefficients of the samples the constituent layers of some of the adult skull samples were separated, allowing the properties of the layers to be measured directly. When the contribution that reflection made to the insertion coefficient was allowed for, the values of absorption coefficients obtained at 1 MHz were 1.7 Np cm^{-1} for the outer table and 2.2 Np cm^{-1} for the inner table. The value of the attenuation coefficient for the infant skull was less than half the value of that for the outer table of the adult skull over the range in which both were measured (0.5 - 2 MHz); the attenuation value at 3 MHz being approximately 2 Np cm^{-1}. Two samples of the diploe, one of which was said to have a finer grain than the other, were measured and at 3 MHz the attenuation values were between 12 and 16 Np cm^{-1}.

Most studies suggest that, except where the bone sample contains diploe, the frequency dependence of the attenuation varies in a nearly linear fashion over diagnostic frequencies. Adler and Cook (1975) reported the frequency dependence of the absorption coefficient of dog tibia to be almost linear with frequency over the range 3 - 5 MHz. The values quoted are shown in Table 3.5.

The data in Table 3.5 includes measurements made at a variety of temperatures. Those of Fry and Barger were made at body temperature (37°C), while those of Adler and Cook and of Lakes, Yoon and Katz were carried out at room temperature (22 - 24 °C). The temperatures at which the rest of the measurements were made are not recorded. Kishimoto (1958) studied the change in the attenuation coefficient of horse bone with temperature over the range 0 - 60°C, for frequencies between 1.4 and 4.5 MHz. For the temperature range 20 - 40°C the attenuation coefficient at 2.86 MHz was found to be in the range 5.2 - 5.6 Np cm^{-1} and increased with temperature. Duck (1991) analysed the data in this paper and derived an approximate temperature coefficient of 0.017 Np cm^{-1} $°C^{-1}$. This would mean that making measurements at body temperature (37°C), rather than room temperature (22°C), would increase the

Table 3.5: Attenuation Values for Bone

Author (date)	Type of Bone	Frequency (MHz)	Attenuation (Np cm^{-1})
Heuter (1952)	Whole skull	3	6.9
Fry & Barger (1978)	Outer table of adult skull	3	4
	Outer table of adult skull	5	6
	Diploe, adult skull	3	12 - 16
	Infant skull	3	2
Adler & Cook, (1975)	Dog tibia	3	1.5
		5	2.2
Lakes, et al. (1985)	Compact human femur	3.5	2.5
		5	3.2
Lees & Klopholz (1992)	Cow compact femur, longitudinally	5	4
	Cow compact femur, radially	5	6
Wu & Cumberley (1997)	Bovine compact femur	5	1.7 - 2.3

attenuation coefficient by approximately 0.26 Np cm^{-1}. It will be shown in Section 9.4 that the effect that changing the attenuation coefficient has on the temperature rise depends upon a variety of factors, including the thickness of the bone and its thermal properties; this, therefore, makes it difficult to give a single figure for the influence of the initial temperature on the temperature rise. This is aggrevated by the fact that the attenuation coefficients measured by Kishimoto are towards the top end of the range of values quoted for bone and it is not clear whether the figure derived by Duck is directly applicable to samples with a lower attenuation coefficicent. It would appear, however, by inspection of Figures 9.3 and 9.4 that an increase in attenuation coefficient of 0.26 Np cm^{-1} would, at most, lead to a 25% increase in temperature rise and in most cases the increase would be much less than this. A temperature coefficient of this magnitude suggests that temperature differences are not responsible for the range of attenuation values quoted in Table 3.5.

Lakes et al. (1985) measured attenuation in femoral compact bone from cows and for a human cadaver. In both cases the samples were cut so that their axes were aligned with the microstructure of the sample and the variation of attenuation with direction was studied. For the human samples the attenuation in the longitudinal direction, i.e. along the bone, appeared to vary linearly with frequency between 1 and 6 MHz. The attenuation was approximately 2.5 Np cm^{-1} at 3.5 MHz and 3.2 Np cm^{-1} at 5 MHz. In the radial direction, across the bone, there was no steady increase in attenuation over the 1 - 6 MHz range with all the results being in the range 5 ± 1 Np cm^{-1}. It was noted that there was not a sharp maximum in the graph of attenuation against frequency as would be expected in a regular structure when the wavelength equalled twice the size of the unit cell. Two possible reasons were given for this absence: aperiodicity in the microstructure of bone or the fact that the cement structure between the trabeculae was nearly as stiff as the trabeculae at ultrasonic frequencies, hence making the bone appear more like a homogenous structure than one which was fibrous.

Lees and Klopholz (1992) also studied the influence of propagation direction on attenuation. Samples were cut wet from compact cow femurs in both the longitudinal and the radial direction. For both sets of samples the variation of attenuation was roughly linear over the range 5 - 50 MHz. Between 50 - 100 MHz the attenuation appeared to increase more slowly with frequency, although readings were only taken at 50 and 100 MHz. This difference in attenuation in the two directions, 4 Np cm^{-1} longitudinally compared to 6 Np cm^{-1} radially was attributed to the fact that if the wave path is along one of the bone fibres it has an unbroken path whereas if it is misaligned the wave strikes interfaces and is scattered.

Wu and Cumberley (1997) measured attenuation of shear and longitudinal waves in bovine compact bone over the frequency range 4 - 10 MHz. For both types of wave the attenuation was found to vary approximately linearly with frequency and the ratio of attenuation coefficient for shear waves to that for longitudinal waves was found to be 1.5.

Little information is available about cancellous bone. Other than the data for absorption in the diploe layer of the skull, quoted above, most of the information comes from authors whose interest has been in ultrasonic

measurements of bone density. This is a broadband technique and the frequencies used, typically 0.4 - 1 MHz, are lower than those used in imaging. This makes it difficult to compare actual numerical values but it is still possible to obtain useful information from their results. Travakoli and Evans (1992) studied the relationship between the structure of bovine cancellous bone and its attenuation. By the application of static loads they were able to decrease the porosity by up to 35% (i.e. from approximately 40% to 5%) and in doing so caused the attenuation to decrease by a factor of between 2.3 and 3.3 depending on the sample. They concluded that the attenuation depends mostly on the structure of the sample rather than on the component materials. Nicholson, Haddaway and Davie (1994) measured the speed of sound and the broadband ultrasonic attenuation in human trabecular bone from the lumbar vertebrae. They found significant differences in both parameters when the orientation of the bone was changed and concluded that these must be due to differences in the structural configuration of the bone associated with the different axes. It should be noted, however, that these specimens were from adults and, as such, had the pronounced alignment of the trabeculae along the cranio-caudal axis which arises due to the fact that this is the direction in which load is generally applied. Fetal bone has not experienced this loading and so may not have this structure. Attempts have been made to model the frequency dependence of ultrasonic attenuation in cancellous bone. McKelvie and Palmer (1991) used Biot theory which was developed to model ultrasonic propagation in porous rock. This considers factors such as the porosity of the material, the ultrasonic parameters and material densities. It was found that the theoretical results did not reproduce the experimental results clearly enough to be used as a complete explanation. The reasons given for this included the fact that some of the key parameters used in the model had to be estimated and the fact that scattering was not included.

3.5. Discussion

It can be seen that defining the thermal properties of bone is a far from straightforward task. Part of the reason for this is that bone is not a simple material, rather it is a class of materials which, while all sharing the property of being calcified, may differ markedly in their structure. It is necessary, therefore, to define the type of bone being studied. Sekins and Emery (1983) point out that "in employing thermal conductivity values, and other thermophysical properties as well, it is important to note the

conditions of applicability (temperature, pressure, direction of heat flow relative to orientation of the material's components and fibres, etc.) of the property values. In regard to biological properties, this is especially important". There are still large uncertainties even once the type of bone is defined, as can be seen from the range of values quoted for thermal conductivity. Even if the outliers are excluded there is still a factor of two between results quoted for cancellous bone. The difficulties associated with carrying out measurements on biological samples, caused by factors such as the small sample volume and the need to prevent the sample from drying out, seem to cause considerable problems. There does not appear to be any information available on fetal bone.

The attenuation coefficient of compact bone has been measured by a number of groups and appears to have a value in the range 1.5 - 4 Np cm^{-1} at 3 MHz and 1.7 - 6 Np cm^{-1} at 5 MHz. The exact value has been shown to depend upon the direction of propagation. The only data available for immature bone are the measurements carried out by Fry and Barger on infant skull and these suggest that the attenuation coefficient is approximately half that of the outer layer of adult skull. This paper also gives attenuation values for the cancellous bone in the diploe layer which are much higher than those of either adult compact or infant bone.

The proportion of the attenuation coefficient that is due to scattering is unclear. The attenuation of the diploe was shown to be highly dependent on frequency, as the pores are of the same order of magnitude as the wavelength of ultrasound at diagnostic frequencies. The f^4 frequency dependence found in part of the spectrum would suggest that Rayleigh scattering was occurring. Data available from ultrasonic bone density measurements shows that the structure of cancellous of bone, as opposed to the composition, is important in determining the attenuation and so this too would indicate that scattering is significant. The amount of scattering will depend upon the relative size of any structures within the bone and the wavelength of the ultrasound. For fetal bone this is likely to change with gestational age but unfortunately, as is the case for the thermal properties, no values are available for this type of tissue.

Having reviewed the properties of bone the next step is to investigate how ultrasound effects this type of tissue. The evidence presented in this chapter suggests that factors such as the type of bone and its age will need to be considered.

3.6 Chapter Summary

It has been shown that bone development starts early in pregnancy with cartilage models of bones such as the vertebrae beginning to form about 6 weeks after conception and bone mineral starting to be laid down at 8 - 9 weeks. Newly formed bone is cancellous in nature and it is only close to the time of birth that some of this transforms into compact bone; ossification is not, however, complete at the time of birth. The thermal properties of adult bone are poorly defined, especially the thermal conductivity, where quoted values differ by more than an order of magnitude. No data appear to be available for fetal bone. The attenuation coefficient of adult compact bone is reported to be in the range 1.5 - 4 Np cm^{-1} at 3 MHz and the available data suggest that infant bone has an attenuation coefficient about half that of adult bone. It has been suggested that the attenuation of cancellous bone is much higher than that of compact bone but the exact value seems to be highly dependent on structure.

Chapter 4
Effect of Ultrasound on Bone

4.1. Introduction

When an ultrasonic wave is incident on a layer of bone the energy from the wave will split into different components. Part of the energy will be reflected, either from the bone surface or through scattering inside the bone; some will be absorbed and so generate heat and some will be transmitted through the bone. In trying to assess the effect of ultrasound on bone it is necessary to consider both the temperature rise that will occur due to energy being absorbed and any structural effects that may be a result of this or of the propagation of a pressure wave through the medium.

4.2. Observations of Bone Heating by Ultrasound

The initial studies into the temperature rise generated in bone were carried out because excessive bone heating was seen as a barrier to the use of ultrasound as a therapeutic agent (Bender, Herrick & Krusen, 1953; Herrick, 1953). These experiments on dog femur showed that the temperature rise in the bone cortex was twice that next to the transducer or in the bone marrow. Lehmann, Delateur, Warren and Stonebridge (1967) measured the temperature rise in the soft tissue, cortical bone, cancellous bone and marrow of pig thighs. The temperature rise was highest in cancellous bone, being in live animals, on average, 1°C (28%) higher than that at the bone surface.

Many recent studies have been concerned with the heating effects of diagnostic ultrasound, with the main area of concern being exposure of the fetus. The fact that the temperature rise generated in fetal bone is much larger than that in soft tissue was demonstrated by Drewniak et al. (1989). They insonated fetal femurs and found, for a frequency of 1 MHz, that the initial rate of temperature increase in a 108 day gestational age specimen was 30 times that in soft tissue. The rate of heating depended upon the age of the fetus, being 15 times greater in a the 108 day specimen than one 59 days old. The influence of age was also demonstrated by Carstensen, Child, Norton and Nyborg (1990) who used young and old mice placed in a water bath to model fetal exposure at different stages of

development. These were positioned so that the focal zone of a 3.6 MHz focused transducer intersected with a thermocouple placed at the rear of the skull bone. For a temporal average focal intensity of 1.5 W cm^{-2} the temperature increase after 1.5 minutes was 5.6°C for old mice (> 6 months) and 3.5°C for young mice (< 17 weeks).

Bosward, Barnett, Wood, Edwards and Kossoff (1993) also found that the maximum temperature rise close to bone correlated with gestational age when they measured ultrasound-induced temperature elevations in guinea-pig brains. A 120 s exposure to a 3.2 MHz beam with a spatial peak, temporal average intensity (I_{spta}) of 2.9 W cm^{-2} and of 260 mW power produced a mean temperature increase adjacent to the parietal bone of 1.2°C at 30 days gestation and 5.2°C at 60 days. The role played by the bone was demonstrated by removing it and measuring the temperature rise at the same distance from the transducer as before. When this was done the temperature rise for the 60 day old fetus was 2.6°C. This paper also demonstrates the fact that I_{spta} is not a good predictor of temperature rise, a fact that ter Haar had already demonstrated for soft tissues (ter Haar, Duck, Starritt & Daniels, 1989). The temperature rise was measured with the transducer at two distances from the brain, giving different beam diameters. The power output was increased when measurements were taken close to the transducer so that, although the beam diameter was greater, the value of the I_{spta} for the two beams was within 25%. Typically the temperature rise was 3 - 4 times greater using the wider beam.

Margulies, Abraham, Way and Ziskin (1992) demonstrated that the position at which the highest temperature rise occurs depends upon the structure of the region being insonated and may not necessarily be at the front of the bone. Six day old rat pups were insonated with a beam of spatial average intensity 2.5 W cm^{-2} and frequency 2.25 MHz for five minutes and the temperature measured next to the scalp, where the beam entered, and in the mouth of the pup in contact with the hard palate. The observed temperature rise was 7°C at the scalp and 9°C next to the hard palate. This difference in temperature elevation was thought to be due to a combination of the soft tissue-air interface causing ultrasound to be reflected, hence increasing the effect of the ultrasound exposure, and greater absorption of ultrasound by the bone of the palate.

The above papers indicate the possibility of inducing significant heating in bone, including fetal and neonatal bone, using ultrasound at diagnostic levels. However, the ultrasound beams used are in some cases quite unlike those generated by diagnostic scanners; those used by Duggan, for example, were much wider than diagnostic beams and the spatial average temporal average intensity used by Margulies was greater than that which would normally be used for pulsed Doppler measurements. This makes it difficult to predict the temperature rise that might occur during routine scanning. Measurements using beams with characteristics closer to those from diagnostic scanners have been made on bone encased in tissue mimicking material (TMM). O'Neill, Winkler and Wu (1994) exposed adult human compact bone (femur) encased in TMM to a 3.2 MHz beam with power, at the transducer face, of 100 mW. The -6 dB beam diameter was 1.7 mm and the attenuation in the TMM meant that the power incident on the bone was 65mW; both these values are within the range quoted by Duck (1991) for pulsed Doppler equipment. The measured temperature rise after 1200 s was 6.6°C. This paper also notes that in preliminary tests the temperature rises observed in some cancellous bone samples were higher than those reported for compact bone. Wu et al. (1995) measured temperature rises generated by a commercial diagnostic ultrasound system in a phantom consisting of human temporal bone and TMM. Significant temperature rises (between 1.9 - 11 °C) were found at the upper and lower surfaces of the bone.

Another factor that has been studied is the effect of perfusion on heating. Blood flowing through the bone and surrounding tissues will remove heat from the area and so reduce the observed temperature rise. Studies that use dead tissue, such as those by Bosward, O'Neill and Wu, do not include this effect and so may overestimate the heating that would occur in-vivo. Lehmann (1967) attempted to quantify this effect by measuring the temperature increase before and after the animal studied was killed. The mean reduction, caused by perfusion, was 1.1°C (24%) at the bone surface, 1.5°C (25%) in cancellous bone and 0.8°C (47%) in bone marrow. Duggan (1995) studied the effect of perfusion on ultrasound induced temperature rise in late gestation fetal sheep in utero. The temperature rise observed in dead fetuses was 3.0°C for a power of 0.6 W and 12.5°C at 2 W. In live fetuses the values obtained were lower by 43% and 30% respectively. However, Horder, Barnett, Edwards and Kossoff (1997) observed much smaller differences when they measured the temperature

rise in guinea-pig fetal brain tissue when an ultrasound beam was focused on the parietal or sphenoid bone. The reduction in temperature rise in the live fetus, relative to the dead one, was 1% in the younger age category and 13% in the older, near term, fetus.

It can be seen from these results that it is not possible to use a single value to account for the effect of perfusion. Duggan suggests a range of factors that might be responsible for differences including beam area, bone composition and age and the positioning of the thermocouples.

These studies show that the temperature rise generated in bone will depend not only on the properties of the ultrasound beam but also on the properties of the target including gestational age and perfusion. This makes it difficult to use the results obtained from animal studies to predict heating in human fetal bone, as the composition of that bone, the change in size with gestational age and the degree of perfusion may all be different.

4.3. Structural and Histological Effects of Ultrasound on Bone

If ultrasound has an effect on bone this may either be due directly to the sound field or it may be due to the temperature rise resulting from absorption of the ultrasound beam. Little information is available about the effect of small temperature rises in bone although there is evidence that larger temperature rises can cause changes. Dekhtyar, Gamza, Tatarinov and Jansons (1995) measured ultrasound velocity changes with temperature over the range 20 - 80°C and found that the greatest decrease was at 35 - 65°C in collagen and 55 - 70 °C in whole bone. Exoelectron spectroscopy was also used to study the surface layer of the bone. This showed thermally induced variations in the electron structure of bone tissue at 55°C. Neither the reversibility or the biological consequences of these changes was discussed, although it was suggested that the fact that the spectral maximum and the greatest velocity gradient in bone both occurred at 55°C was connected with the partial denaturation of the collagen.

Many of the studies looking for structural changes in bone due to ultrasound date back to the early days of therapy and were carried out with power levels far higher that those used in diagnosis. Bender, Janes and Herrick (1954) exposed the femurs of dogs to power levels of 5 W and above for 2 minutes. No histological changes were found in the bone

cortex but there were changes to the marrow. For measured temperature rises below 7°C the main finding was haemorrhage while when the temperature rise was above this level osteogenesis and fibrosis were observed. DeForest, Herrick, Janes and Krusen (1953) exposed the hind legs of dogs and rabbits to similar power levels and found that a range of destructive effects, including fractures, could be seem on x-rays.

Studies have found that at lower power levels ultrasound can have a beneficial effect on fracture healing. Pilla, Mont, Nasser, Khan Figueiredo, Kaufman et al. (1990) observed an acceleration of fracture healing in rabbits when exposed for 20 minutes a day to 1.5 MHz ultrasound of intensity (I_{sata}) 30 mW cm^{-2}. The authors measured the temperature rise at the end of the heating period to be 0.1°C and so suggest that this is not a thermal response. Few details are given in this paper, however, about how and where the temperature was measured and it may be that the maximum temperature rise was missed. The effective radiating area of the transducer used in this study was 3.88 cm^2 and if this is used as an estimate of the beam area, a power output of 116 mW and a beam diameter of 2.2 cm are obtained. If these figures are inserted into formulae given by Carstensen et al. (1990) for the temperature rise generated when an ultrasound beam is incident on a layer of bone and it is assumed that 60% of the power is converted into heat, the value obtained is over 1.5°C, which makes the measured temperature rise of 0.1°C seem very small. Reher, Elbeshir, Harvey, Meghji and Harris (1997) found that 5 minutes exposure of mice frontal and parietal bones to ultrasound of intensity (I_{sata}) 0.1 W cm^{-2} and frequency 3 MHz stimulates bone formation, while if the intensity was raised to 1 or 2 W cm^{-2} synthesis of collagen and noncollagenous protein was inhibited. In this paper the temperature rise was measured in the culture medium surrounding the bone and ranged from 0.0°C at 0.1 W cm^{-2} to 1.8°C at 2 W cm^{-2}. These values led the authors to conclude that non-thermal effects were responsible for the effects. These conclusions need to be viewed with some scepticism, however, as the temperature rise in the bone is not known. Wang, Lewallen, Bolander, Chao, Ilstrup and Greenleaf (1994) also observed beneficial effects from low intensity ultrasound (30 mW cm^{-2}) in that it accelerated fracture repair in rabbits. No attempt was made to measure temperature during this study.

4.4. Effect of Direct Heating on Bone

Eriksson and Albrektsson (1983) studied the long term effects of heating rabbit tibia. A special thermal chamber was implanted into the bone and left in place for a period of 10 weeks before any heating studies were carried out During this time the surrounding bone tissue grew into the chamber and could be observed by removing the layers of skin covering the chamber. A heating element and thermocouple were inserted into the chamber so that controlled temperature rises could be generated. It was found that heating the bone to 50°C for 1 minute or 47°C for 3 minutes caused the composition of the bone to change over a period of 20 - 50 days. The borders of the trabeculae became less demarcated and bone resorption occurred. After 40 - 60 days there was, in many cases, 30 - 40% less bone compared to what had been observed prior to heating and 150 - 200% more fat cells. When the bone was heated to 47°C for one minute the effects were not as marked. Bone resorption was noticed in 2 out of 5 rabbits and in these cases about 10% of the originally observed bone disappeared. In the other three cases only minor bone resorption was noted and this was difficult to separate from the normal bone remodelling process.

4.5. Secondary Heating of Tissue Surrounding the Bone

Any temperature rise that occurs in bone means that it also acts as a secondary heat source acting on the surrounding tissue. Lehmann et al. (1967) found that when the temperature rise inside the bone was 4.7 K, the temperature rise at the bone surface was only one degree lower, causing the heating of important joint structures to be in the therapeutic range. In the temperature measurements on fetal guinea-pigs carried out by Bosward et al. (1993) significant temperature increases were measured in the tissue adjacent to bone. Temperature rises of 0.8 K were also measured in the middle of the cerebral hemispheres, compared to 5.2 K directly under the skull, and the rate of heating at this point led the authors to suggest that the temperature rise occurred due to heat conduction from the parietal bones. The significance of secondary heating was discussed by Barnett et al. (1997) who pointed out that many parts of the central nervous system are encased in bone and these tissues are particularly susceptible to elevated temperatures. The potential for ultrasound induced heating causing damage to small important structures, such as the developing pituitary gland, is not clear.

4.6. Discussion

It can be seen that ultrasound exposure from a diagnostic scanner is capable of inducing biologically significant temperature rises in bone and that intensities levels of around 0.1 W cm^{-2} can have a biological effect. Factors that have been shown to influence the temperature rise include the ultrasound exposure parameters, e.g. power and frequency, and the properties of the tissue being insonated, including:

- the type of bone, compact or cancellous;
- the gestational age of fetal bone;
- the presence of perfusion;
- structures surrounding the bone, e.g. tissue-air interfaces.

There is, however, a shortage of data on heating in human fetal bone using exposure conditions relevant to diagnostic ultrasound and the complexity of the situation makes it difficult to extrapolate the results from animal models. It was decided, therefore, to carry out measurements on human fetal bone and these are reported in the next chapter.

4.7. Chapter Summary

It can be seen that diagnostic ultrasound has the potential to generate temperature rises in bone that are greater than the 4°C that the WFUMB state may be hazardous under certain conditions. Heating of fetal bone appears to be age dependent, although the data available for human fetal bone only considers samples of age up to 108 days (15.5 weeks) and so it is not possible to predict what will happen in the latter part of pregnancy. The temperature rise that occurs in bone not only affects the bone itself but also causes the bone to act as a secondary source heating the surrounding tissue. Perfusion may act to reduce the temperature rise but values obtained for the effect of this vary greatly.

Chapter 5

Heating Measurements in Fetal Bone

5.1. Introduction

It is clear from the literature that there is very little experimental data on heating of human fetal bone by ultrasound. Furthermore there is little physical data available which might allow accurate modelling of this situation. It was decided, therefore, to measure the temperature rise generated in human fetal bone by a beam with characteristics typical of those which are emitted from a diagnostic scanner. To date there is no data available on ultrasonic heating of human fetal bone during the second half of pregnancy and so a range of samples of different ages were obtained in order to study the change in temperature rise with gestational age. These results, combined with work by others into factors such as perfusion and attenuation in maternal tissue, could then be used to make predictions about the temperature rise that might occur in-vivo. It was intended to model the system and so not only did the temperature have to be measured accurately but the position at which the temperature was measured needed to be well defined.

5.2. The Ultrasound Beam

The expense and high level of use of clinical scanners made it impractical to use one for the majority of the heating measurements and consequently a single element transducer was used. This was driven in such a way as to give a beam similar to that emitted from a scanner operating in pulsed Doppler mode. (A comparison of the output from the transducer and measured values from clinical pulsed Doppler equipment is shown in Figure 5.3 and is discussed later in this section.) A 3.5 MHz probe was chosen, as this is typical of the frequency used for clinical examinations. Figure 5.1 shows the equipment used to generate the beam. The characteristics of the function generator signal are shown in Table 5.1. For all of the reported measurements these values were set within the range given by the centre value ± uncertainty.

Figure 5.1: Generation of the Ultrasound Beam.

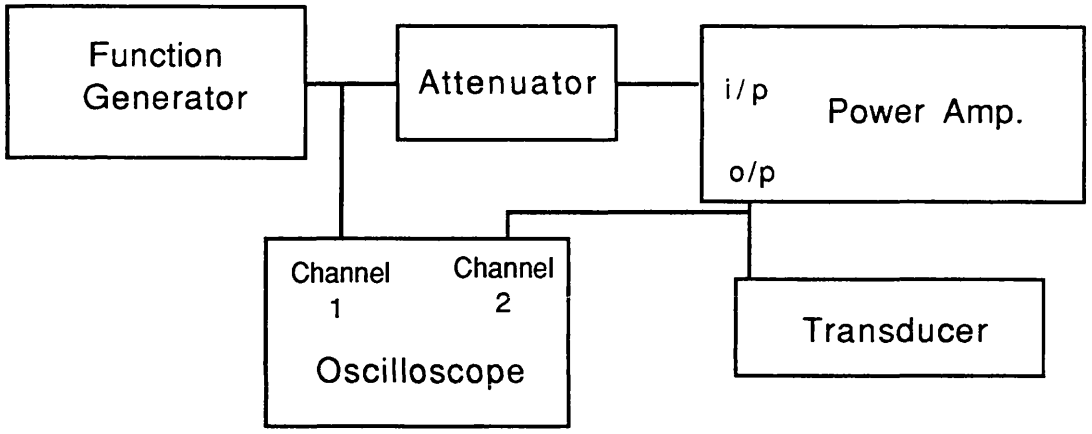

Table 5:1. Characteristics of Signal used to Excite Probe.

	Centre Value	Uncertainty
Frequency (MHz)	3.5	0.05
Pulse repetition rate (kHz)	6.8	0.1
Pulse length (μs)	4.6	0.1

Two power amplifiers were used in the study (ENI models A150 and 240L), one with a gain of 50 dB and the other 55 dB. The amplitude of the signal from the function generator was reduced when the higher gain amplifier was used. Channel 2 of the oscilloscope was used to monitor the signal going to the transducer. The oscilloscope used (Lecroy 9310) had the facility to record the mean value and standard deviation of the rms amplitude of the displayed signal over a period of time and so this facility was used to ensure that the output from the amplifier was stable over the period of data acquisition and that it did not vary between acquisitions. To do this the timebase on the scope was set to 20 μs per division so that two pulses were displayed at any time. This meant that a change in either the pulse repetition frequency or the pulse amplitude should change the displayed value for the mean rms amplitude. Tests showed that if the mean rms amplitude was within the

range 2.70 ± 0.05 V the output from the transducer should not vary by more than 2 mW.

Measurements of the ultrasonic beam were carried out using a NPL Beam Calibrator (BECA) system (Preston, 1988). This uses a multi-element hydrophone array constructed from two layers of polyvinylidene fluoride (PVDF) each of thickness 0.025 mm. The array consists of a line of 21 elements each of diameter 0.5 mm, with centres spaced 1 mm apart. Each element has an amplifier mounted in the hydrophone housing and corrections are applied to the signal from each channel to compensate for differences in the overall sensitivities of the hydrophone/amplifier channels. Data are acquired at 60 MHz with 8 bit resolution. The accuracy of the calibration of the system depends upon the frequency. The uncertainty in the pressure readings, at the 95% confidence level, are 8% at 2 MHz and 9% at 5 MHz; as the intensity is proportional to the pressure squared this means that the uncertainty in the intensity values, due to errors in the calibration, is in the range 16 - 18%. The overall uncertainty in the measurements is greater than this, however, as it includes factors such as the effects of hydrophone rotation and spatial averaging. Preston quotes typical uncertainty values for results from an automatic scanner operating at 3.5 MHz. These are shown in Table 5.2. All the sources of error listed in the table apply to a single element transducer as well as an automatic scanner.

Longitudinal plots of the time-averaged intensity[1], peak positive pressure and peak negative pressure are shown in Figure 5.2. The intensity profile of the beam at 70 mm and 80 mm from the probe face, the two positions at which heating measurements were made, is shown in Figure 5.3 In each case two orthogonal measurements have been made and both are plotted to given an indication of the degree of symmetry in the beam. As the beamwidth was so narrow extra sets of reading were obtained by translating the hydrophone 0.5 mm so that the elements were located to fill in the 'gaps' from the previous set of readings. These augmented plots are shown in Figure 5.4.

---

[1] Unless otherwise stated intensity will be used to refer to local time-averaged intenity values.

Table 5.2: Typical values of percentage uncertainty in the determination of acoustic parameters for an automatic scanner operating at 3.5 MHz using BECA

Source	p+	p-	Beamwidth	Pulse duration	Ispta
Calibration	8.5	8.5	-	-	17
Bandwidth	14		13	4	9
Digitisation	2	2	4	4	4
Gain	7	7	7		14
Spatial averaging	5	2	10	2	8
Pulse repetition rate					0.01
Hydrophone tilt	0.4	0.4	0.4		0.8
Total systematic	21	13	21	7	29
Random	4	2	1	1	2
Overall (95 % confidence level)	22	13	22	8	30

(from Preston, 1988)

The beam characteristics which, with the exception of the acoustic power, were determined by BECA are shown in Table 5.3. These are the mean values from measurements made in two orthogonal planes. This table also gives values of exposure quantities for pulsed Doppler equipment from a survey reported by Duck (1991). This collated 'worst case' values, i.e. the conditions of maximum exposure for each scanner/probe combination tested and the typical values given are an approximate median of these worst case values (Duck, 1998). It can be seen that for all the quantities listed the value from the single element probe falls within the range quoted for clinical equipment. The acoustic power and the beam diameter were chosen to be close to the typical values as these are two of the parameters used directly in many calculations of temperature rise (Bly, Vlahovich and Hussey, 1992; Carstensen et al., 1990; NCRP, 1992). More recent studies have included a more limited range of exposure parameters but it appears from these that exposure levels are increasing (Duck & Henderson, 1998). This is discussed in Section 6.2.

Figure 5.2: Longitudinal plots of the beam.

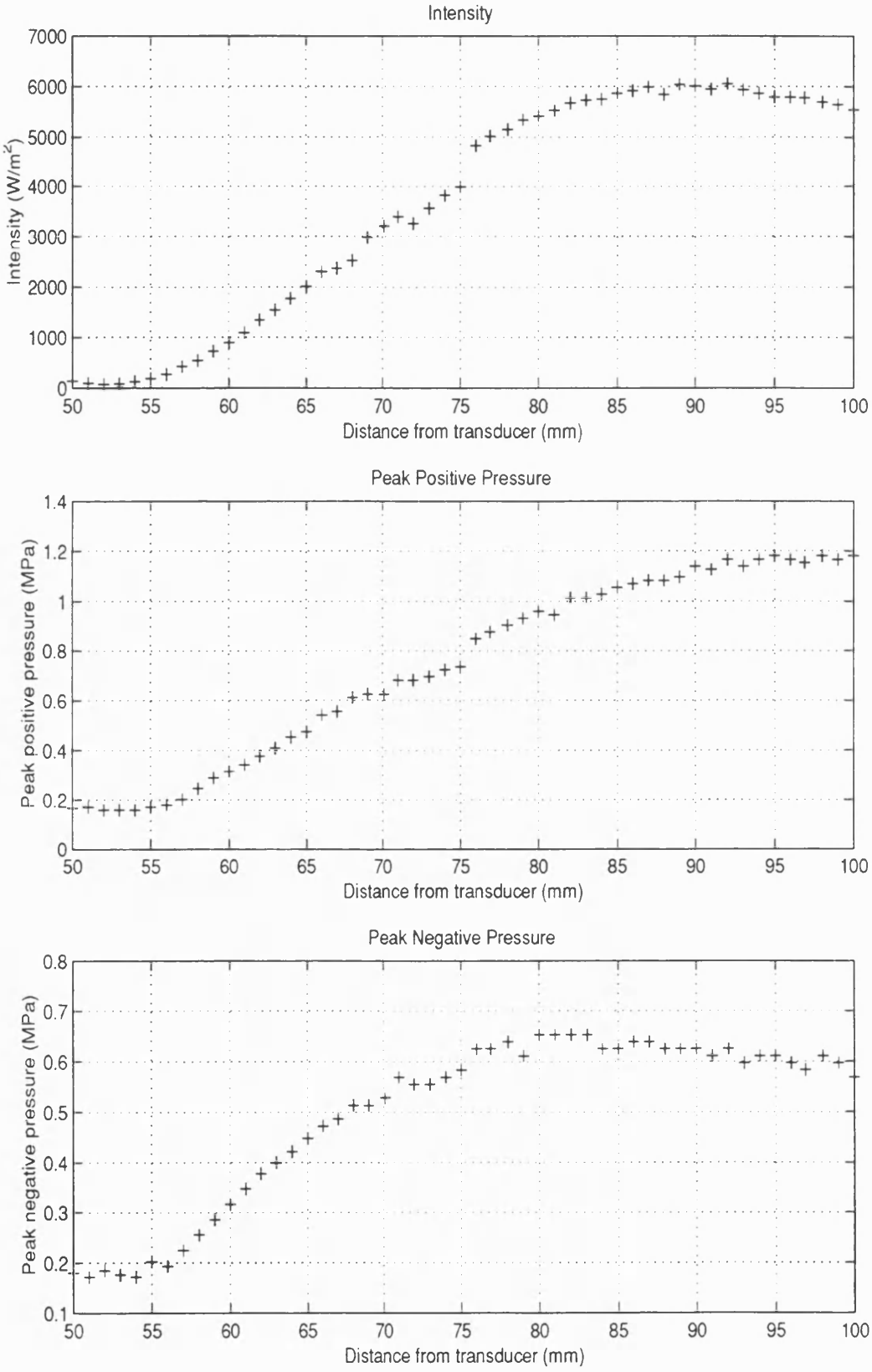

Figure 5.3: Intensity distribution.

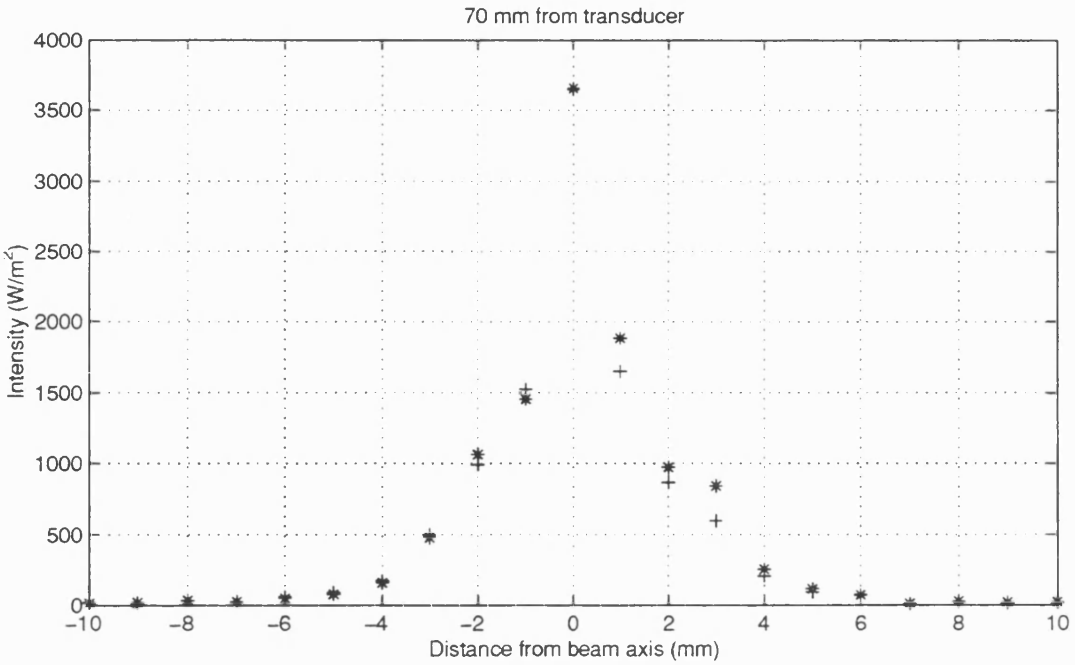

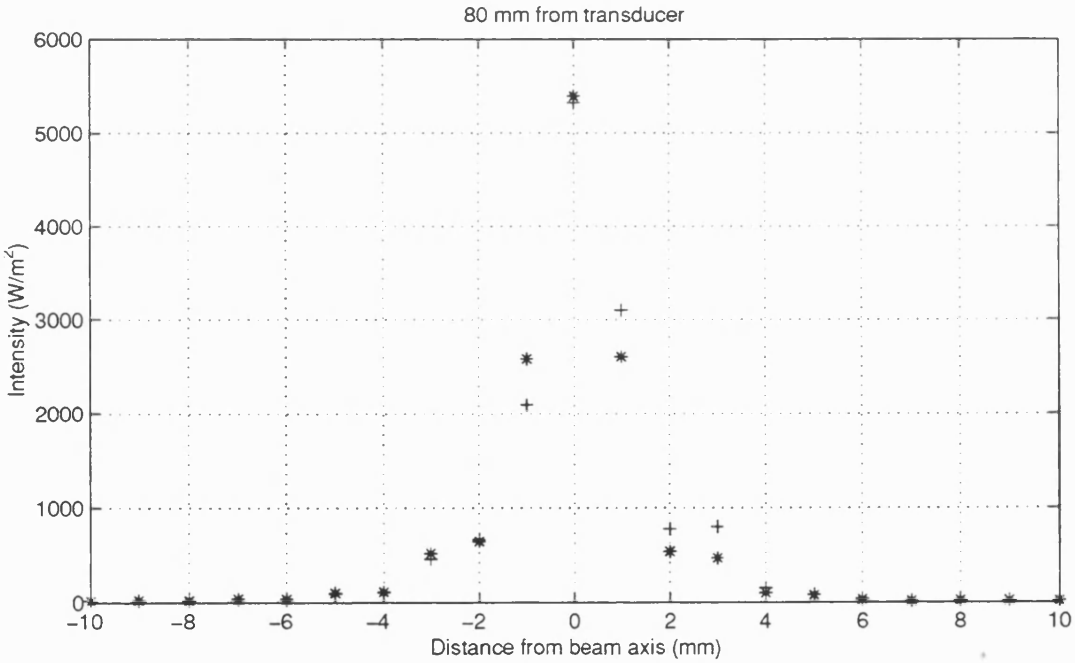

Relative orientation of hydrophone:

\+ 0° * 90°

Figure 5.4: Augmented intensity distribution.

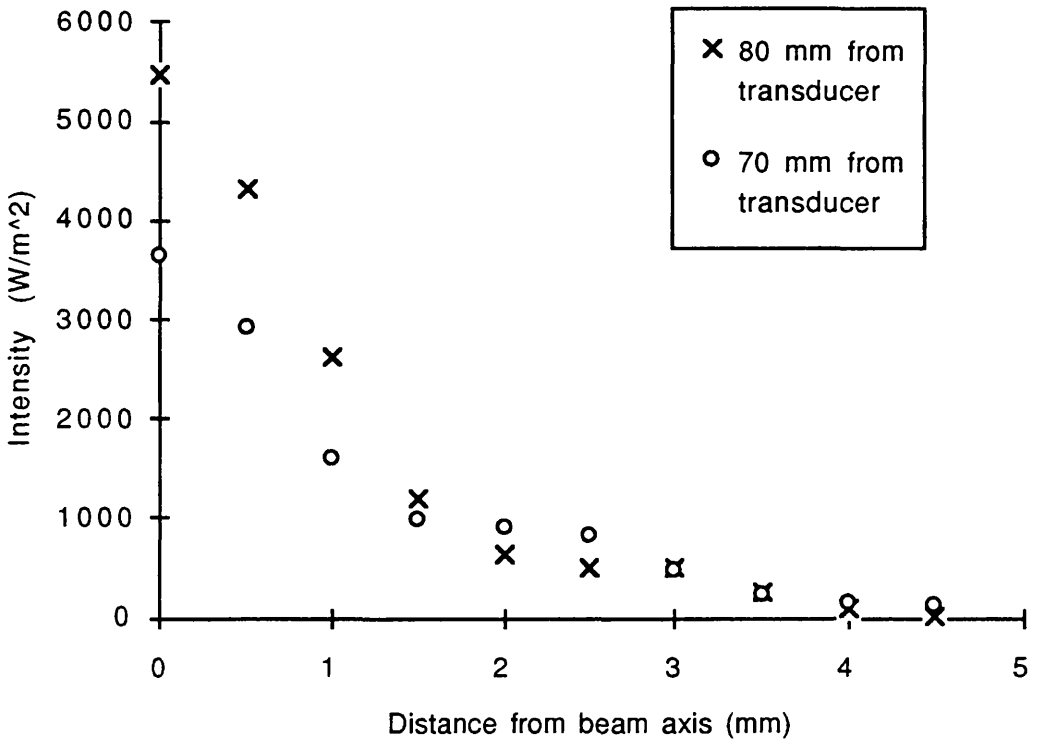

Table 5.3: Beam Characteristics

	Diagnostic equipment in pulsed Doppler mode		Single element probe. Distance from Probe (mm)	
	Range	Typical	70	80
Peak positive pressure (MPa)	0.2-6.4	3.0	0.72	0.95
Peak negative pressure (MPa)	0.1-3.8	1.5	0.58	0.64
-6 dB beam width (mm)	1-5	3	4.5	2.9
I_{spta} (W cm^{-2})	0.11-5.4	1	0.37	0.53
Acoustic power (mW)	9-330	50	50	50
Pulse duration (μs)	0.35-90	0.5	4.4	4.4
Pulse repetition frequency (kHz)	1.5-50	Not given	6.7	6.7

The output power of the transducer was measured using a power balance (Perkins, 1989). This device had been calibrated by NPL at 2.25 MHz and 5 MHz and the indicated power was found to be within 2% of the value determined for the test transducers using the NPL Primary Standard Force Balance. The power balance was used to determine the power, rather than BECA, as it measures power directly rather than measuring the intensity along a line and assuming cylindrical symmetry. It also allowed much quicker determination of output power, allowing this to be regularly monitored. The power output was measured on 10 occasions over a period of 9 months and the power was found to be 50 ± 2 mW (mean ± 1 standard deviation).

A frequency spectrum of the pressure pulse is shown in Figure 5.5. It can be seen that the amplitude of the second harmonic is 20% of the fundamental. This is due to non-linear propagation of the ultrasound as this second peak is only just visible (below the 5% level) when measurements are taken at 25 mm from the transducer face.

5.3. Temperature Sensors

When choosing a temperature sensor it is important that it perturbs the heating pattern as little as possible. Ideally it should be so small that it does not affect the ultrasound beam and it should neither generate heat nor conduct heat away from the region of interest. It was decided that thin wire thermocouples came closest to meeting these requirements. The wire can be readily obtained in small sizes, in this case 50 μm diameter, which means that there should not be a significant distortion of the beam due to scattering and reflection (Hynynen & Edwards, 1989). The small diameter also means that any heat conduction is minimal. K type thermocouples were made from commercially available insulated thermocouple wire (Goodfellow Metals Ltd) with the junctions being twisted and then welded. K type extension cables where used to link these to a thermocouple measurement board (OMD-5508TC, Omega Ltd) that was installed in a personal computer. In order to minimise noise the precautions suggested by Benedict (1984) for avoiding extraneous electrical effects were adopted; these included shielding the extension wires, grounding the shield and using twisted wire pairs in the extension cable.

Figure 5.5: Frequency spectrum of ultrasound pulse at 80 mm from transducer.

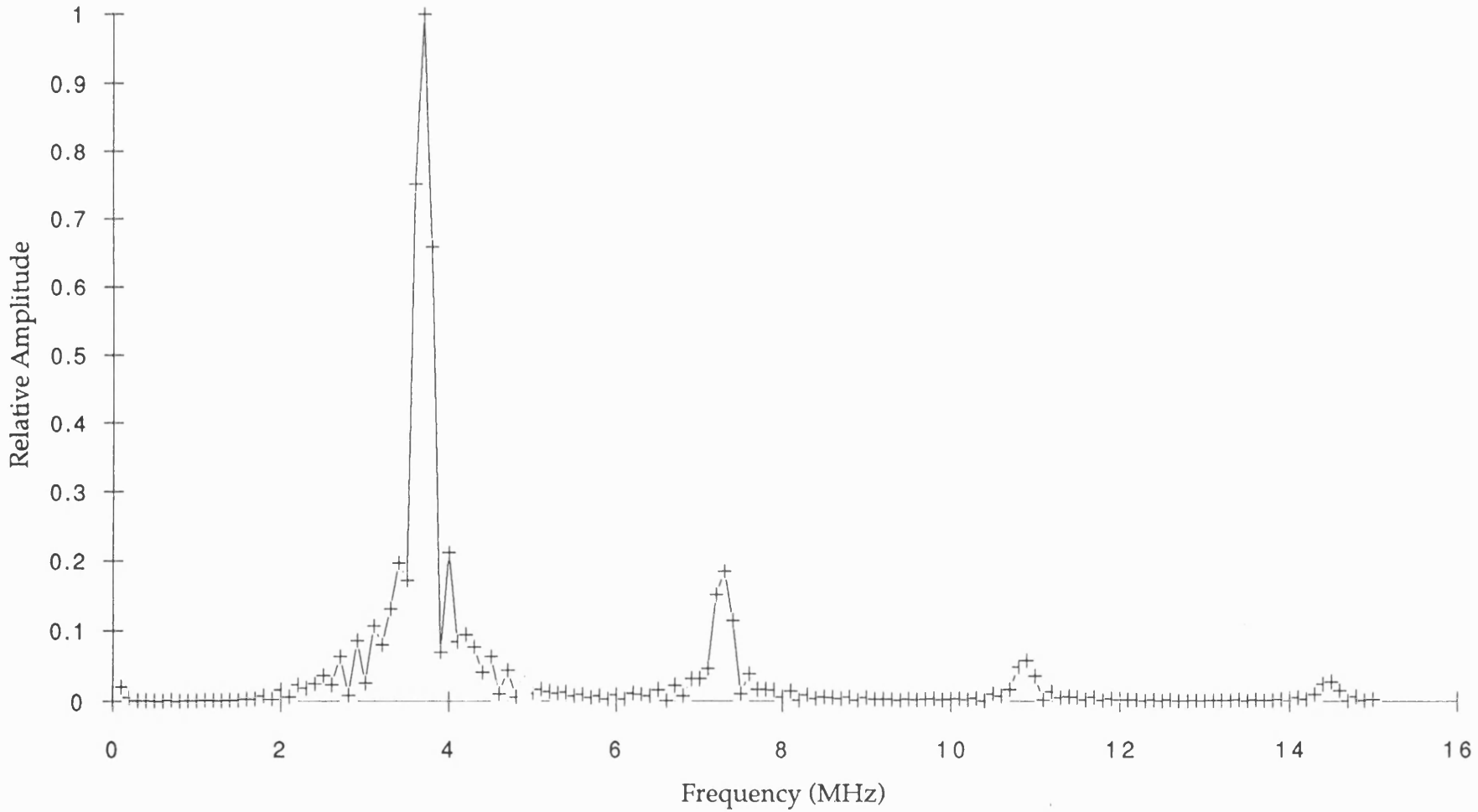

5.4. Calibration

The i/o board to which the thermocouples were connected is capable of cold junction compensation and the software contains calibration data for the type of thermocouple used. The system was tested to ensure that the thermocouples conformed to the calibration data in the software and also to check the stability of the system. This was done by immersing two of the thermocouples in a water bath and comparing the measurements obtained with those from a commercial thermocouple system (Digitron T208). The error quoted for the commercial system was 0.1% of the reading + 0.2°C + 1 digit (0.1°C). This made it necessary to carry out the calibration over a wide temperature range so that the error in the commercial system could be considered insignificant. Readings were taken over the temperature range 18 - 63°C. The sampling frequency was set at 100 Hz and, for the each temperature, three sets of 100 measurements were collected for each of the test thermocouples. The mean of each set of readings was calculated and the mean of these three results was used in the analysis. The commercial system displayed the temperature to one decimal place and it was ensured that this did not alter by more than 0.1°C while the test readings were taken. The results are shown in Figure 5.6. A least squares regression analysis of the results from the test thermocouple against those of the commercial system was carried out. For both test thermocouples the gradient of the resulting graph was 0.98, with the standard error of the gradients being 0.6%. The system appeared, therefore, to be giving a good indication of the temperature.

The precision of the readings was also tested. Sampling at 100 Hz, sets of 100 readings were taken and the standard deviation of each set calculated. The maximum standard deviation of any set was found to be 0.11°C, which was recorded when the mean temperature was 19.2°C. As occasionally there were individual readings that were more than 0.3°C from the mean it was decided that it would be best to use the mean of a series of readings for each data point. It was thought adequate to know the temperature rise in the samples at one second intervals and so, if the temperature was sampled at 100 Hz, the mean value of each 100 readings could be used and, assuming the data has a normal distribution, the standard error due to noise should be 0.01°C. In practice it was found that,

Figure 5.6: Results of thermocouple calibration

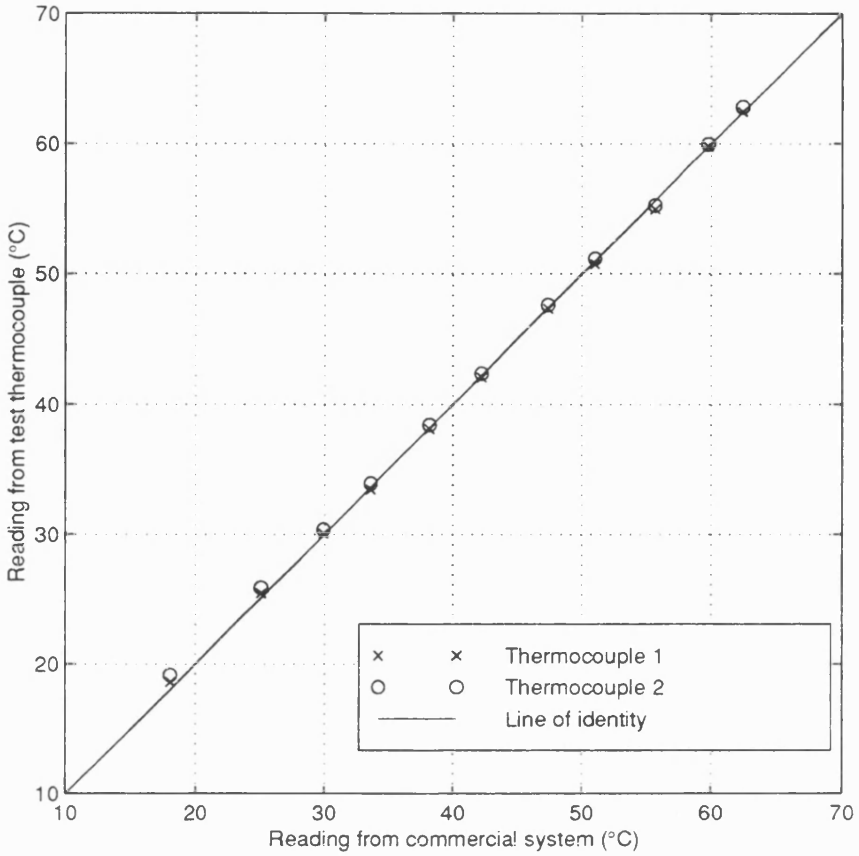

due to the high level of electronic noise within the hospital environment, the noise level was occasionally higher than this but it was still within acceptable limits.

5.4.1. Heating artefacts

The presence of the thermocouple in the ultrasound field can lead to measurement artefacts and so it was important to ensure that these did not lead to unacceptable errors in the results. Three types of error were considered: the effect of the finite heat capacity of the wires, heat conduction by the wires and viscous heating.

The effect of the heat capacity of and the heat conduction by the thermocouple wires was estimated by Fry and Fry (1954). They considered the situation, illustrated in Figure 5.7, in which a thermocouple wire of radius r_0 is embedded in an absorbing medium. A cylinder, of radius r_1, around the wire is considered in the analysis. r_1 is chosen so that the heat

Figure 5.7: System considered when estimating error in thermocouple readings.

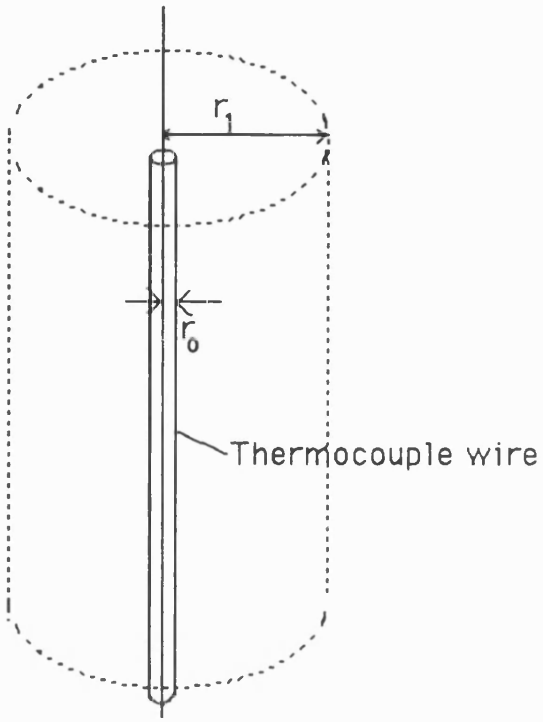

capacity per unit length of the medium within the cylinder is much greater than the heat capacity per unit length of the wire and the ultrasonic intensity is constant to a distance of greater than r_1 from the axis of the wire The error in the temperature reading caused by the heat capacity of the thermocouple wire was estimated to be:

$$\delta T_e = \frac{2\alpha I}{2K} r_o^2 \left(\frac{\rho_w C_w}{\rho C} \right) \ln \left(\frac{r_1}{r_o} \right) \qquad \text{(Equation 5.1)}$$

where the symbols are as defined in the Table of Symbols and subscript w denotes that the properties are those of the wire rather than the medium.

For thermocouples at the surface of bone the situation is more complex, as the wires have different thermal properties on either side and the intensity of the beam decays as it travels through the bone. However Equation 5.1 can be used to obtain an estimate of the magnitude of the error and hence to see whether this effect needs to be studied more closely. To do this the thermal properties of bone were used, as ρC for these was lower than for agar and so gave a higher error. The properties of the thermocouple wire used are shown in table 5.4.

Table 5.4: Properties of Thermocouple Wire.

	Thermal conductivity ($W\ m^{-1}\ K^{-1}$)	Specific Heat ($J\ kg^{-1}\ K^{-1}$)	Density ($kg\ m^{-3}$)
Alumel	19	481	8.5×10^3
Chromel	30 - 32	387	$(8.5 - 8.7) \times 10^3$

The thermal conductivity and density values are those quoted by the manufacturer for 'room temperature' and the specific heat values are those given by Kaye and Laby (1986) at 273 K (the figures at 373K differed by less than 5%). These figures were used, together with the thermal properties of cancellous bone (NCRP, 1992) and an absorption coefficient of 3 Np cm^{-1}. r_1 was taken as 0.25 mm as this radius meant that the heat capacity of the cylinder was more than 100 times that of the wire but the drop of intensity over this distance was only 14%. This gave an error in the temperature rise of less than 0.01K which suggested that this effect was unlikely to be significant.

The effect of the thermal conductivity depends upon the intensity distribution and the difference made by the thermocouple, as a fraction of the total temperature rise is given by:

$$\frac{\delta T}{\Delta T} = -\frac{K_w r_o^2}{2K} \ln\left(\frac{r_1}{r_0}\right) \frac{f''(x)}{f(x)}.$$

where f(x) is a function describing the intensity distribution. In order to estimate this a second order polynomial was fitted to the intensity data measured at 80 mm from the transducer giving the following equation:

$$I = 4 \times 10^8 x^2 - 3 \times 10^6 x + 5416$$

where I is the intensity ($W\ m^{-2}$) and x is the radial distance from the axis (m). This line was seen to have a steeper gradient close to the axis than the real data and so should overestimate the error. The thermal conductivity value used for the wire (K_w) was that of chromel as this was the higher of the two values and r_1 was again taken to be 0.25 mm. Using these values the percentage error in the temperature due to conduction in the wires was found to be less than 1% which was considered to be acceptable.

Viscous heating results from the relative movement of the thermocouple with respect to the surrounding medium, which causes shear forces and local energy absorption at the thermocouple surface (Hynynen & Edwards, 1989). This heating is localised to the boundary between the thermocouple and the medium in which it is embedded and so the temperature rise has a short time constant of the order of 0.1 s (Hynynen, Martin, Watmough, & Mallard, 1983; Carnochan, Dickinson, & Joiner, 1986). A significant amount of viscous heating should, therefore, lead to a fast rise in the measured temperature when the power is turned on and a similar sharp fall in temperature once the power is turned off.

In order to determine the contribution from viscous heating the temperature rise occurring when insonating the 39 week sample was studied. If there is a significant amount of viscous heating present the gradient of the curve should be enhanced during the first few hundred milliseconds and if the temperature data from after this time is extrapolated back to the point at which the exposure started, the intercept will not equal the initial temperature. The difference between this intercept value and the initial temperature rise gives an indication of the amount of viscous heating. This is illustrated in Figure 5.8.

Figure 5.8: Effect of viscous heating on early part of heating curve.

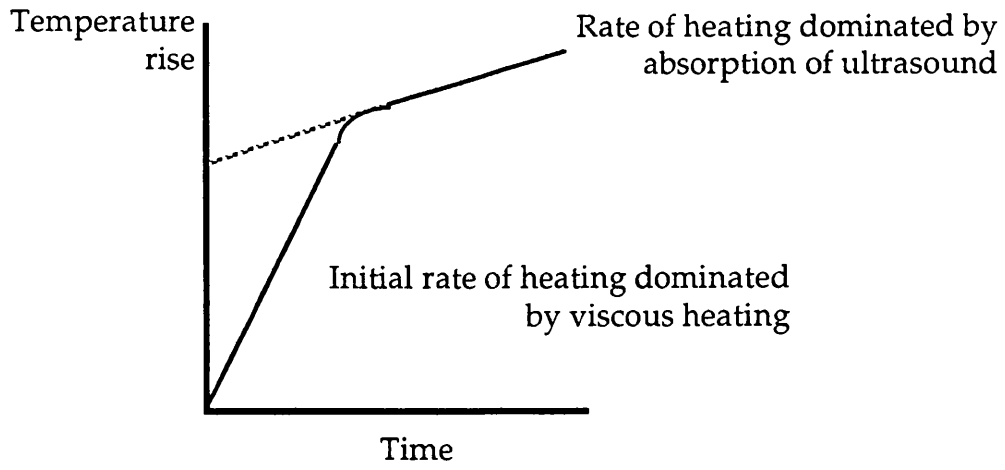

A series of 0.5 s long data segments (i.e. 50 data points) was analysed to see whether this effect could be observed. A linear regression was carried out on each segment and the line through the data was extrapolated back to the time at which the insonation began. Using a 0.5 s data segment meant that there were enough points in the regression analysis to minimise the error in the gradient while ensuring the part of the curve due to tissue heating, which appeared to have a time constant of more than 10s, was

approximately linear over the time considered. The first segment started at the beginning of insonation and the last went from 1.5 to 2 s after insonation commenced. The intercept was within 0.1°C of the temperature value 0.5 s before the power was turned on in all but one case and in this case it was actually lower than the initial value. This indicated that the viscous heating was contributing 0.1°C or less to the temperature rise and, given that the standard deviation in the data sets was typically 0.1°C it may well be much less than this. These results are in keeping with those of Drewniak and Dunn (1996) who observed little viscous heating artefact when heating measurements were carried out on fetal femur. One reason that this artefact was not observed, when it has been noted by other observers, is that the high absorption coefficient of bone means that less power is needed to induce a significant temperature rise in this than in soft tissue. The displacement amplitude of the molecules when heating bone is therefore less than that needed to produce the same temperature rise in soft tissue and this reduces the magnitude of any viscous heating. The high acoustic impedance of the bone also reduces the risk of viscous heating. If this is calculated using the data for infant skull from Fry and Barger (1978), the value obtained is in the range 3.6 - 3.9 x 10^6 Rayl, over twice that of soft tissue. The acoustic impedance is the ratio of the pressure amplitude to the displacement amplitude meaning that, for an identical pressure field, the displacement amplitude in bone, and hence the potential for viscous heating, will be lower. The amount viscous heating in a fluid is dependant on the frequency of the ultrasound (Fry & Fry, 1954) and it would seem likely that, as the frequency affects the movement of the thermocouple, this would also be true for the above measurements. However, as the main results, reported in Section 5.7, were carried out with the probe being driven in the same way, as defined by Table 5.1, as when the above results were obtained, the amount of viscous heating should be the same in both cases.

5.5. Preparation of the Bone Samples.

When planning the measurement procedure for the bone samples a variety of factors needed to be considered. The samples needed either to be used soon after they were obtained or they had to be preserved; they had to be mounted in such a way that they were easy to handle and, for ease of modelling, they had to be embedded in a solid material so that they did not lose heat by convection. They way in which these factors were dealt with is considered next.

5.5.1. The tissue samples

The samples used in the measurements were sections of the thoracic spine from fetuses of gestational age ranging from 14 to 39 weeks (dating from the last menstrual period). These were obtained with the help of the Fetal Medicine Research Unit at the University of Bristol. The spine was used on the advice of the pathologist, as this could be obtained from fetuses undergoing post-mortem examination. The fact that the spine surrounds the spinal cord made it a good choice as one area of concern is heating of the central nervous system caused by nearby bone acting as a heat source. Each sample contained between 3 and 8 vertebral bodies. Photographs and ultrasound images of some of the samples are shown in Figure 5.9. The cross-section of the samples was approximately elliptical although the posterior surface was generally flatter than the anterior. In most cases each vertebra in the sample was approximately the same size but in a few instances there was a noticeable change along the length of the sample. The size of the samples in shown in Table 5.5. It was known that some of the fetuses had suffered from inter-uterine growth retardation (IUGR) and this information is also recorded.

5.5.2. Preservation

For practical reasons it was not possible to carry out all the measurements soon after the sample had been removed from the body and so they needed to be preserved. Two techniques were used: freezing and preservation in formalin. Fixing the samples with formalin was the easier technique, as once this had been carried out they could then be used at room temperature. However, the process of fixation has been found to increase the attenuation coefficient (Fry & Barger, 1978) to a degree that depends upon the frequency of the ultrasound (Bamber, 1986). Bosward et al (1993), however, had found that the peak temperature rise in fresh and formalin-fixed fetal guinea-pig brains, close to bone, was not significantly different. It was decided, therefore, to study samples that had been frozen as well as the formalin fixed ones. The frozen samples were brought to room temperature before measurements were taken and after a set of readings had been obtained they were formalin fixed and heating measurements were repeated in order to assess the effects of fixation. In one case it was possible to carry out measurements on a 'fresh' sample that had been stored in saline since the post-mortem. Measurements were taken and the sample was then fixed in formalin and repeat measurements carried out.

Figure 5.9a: Photograph of 14, 23 and 39 week samples

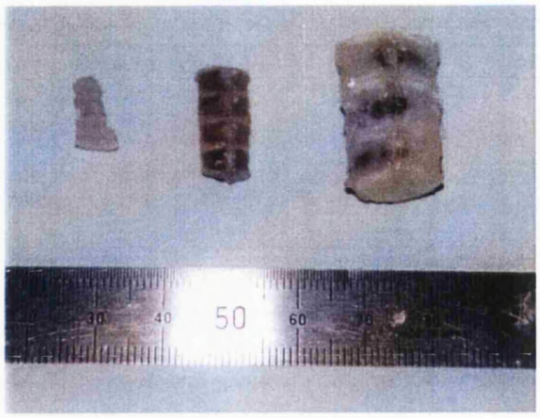

Figure 5.9b: Photograph of 39 week sample

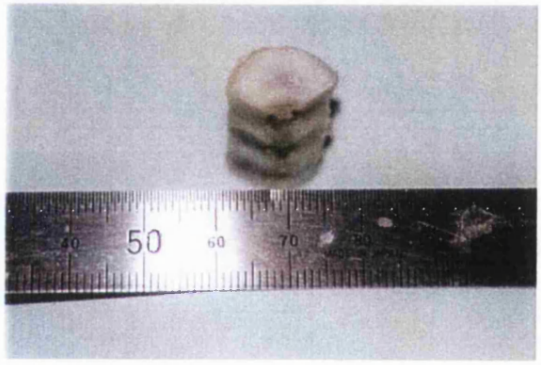

Figure 5.9c: Ultrasound image of 14 week sample

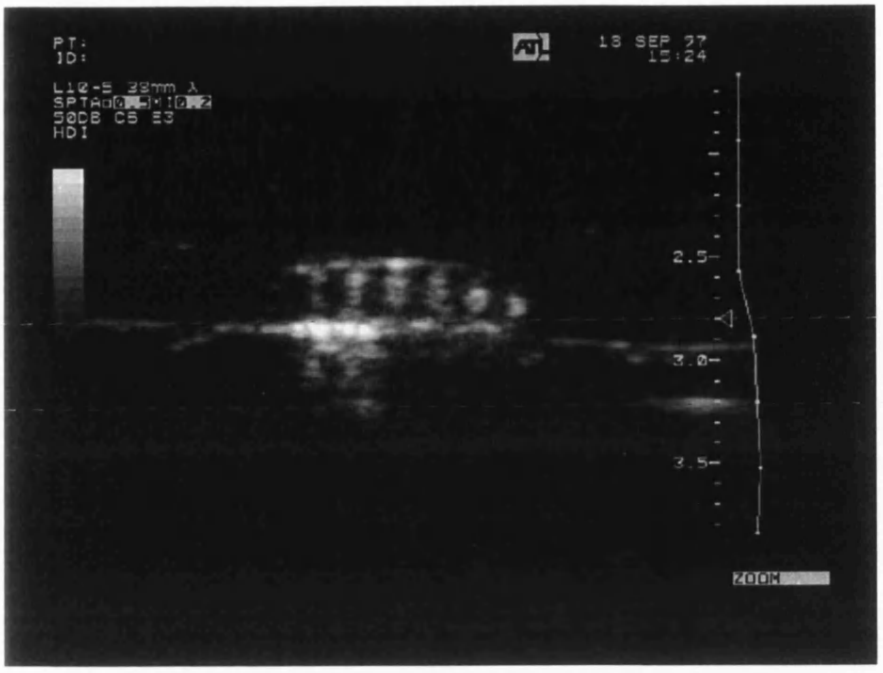

Figure 5.9d: Ultrasound image of 39 week sample

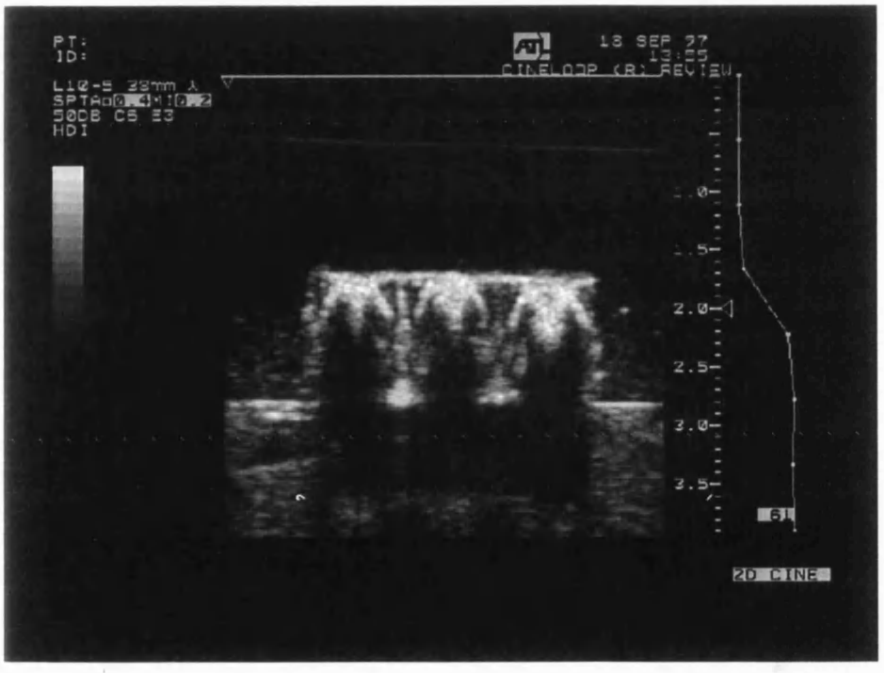

Table 5.5: Details of Bone Samples

Sample age (weeks)	Length of major axis ± 1(unless shown otherwise) (mm)	Length of minor axis ± 1 (mm)	IUGR
14	4	2	
19	7 ± 2	5	
20	10 ± 3	5	
21.5	9	5	
23	9	5	
26	9	5	Y
29	9	5	Y
31	10	7	
34	14 ± 2	9	
36	15	9	
36.5	15	10	Y
39	16 ± 3	10	

5.5.3. Thermocouple attachment and mounting of the samples.

The thermocouples were attached to each sample using a small amount of glue (Loctite Superattak Gel) which was then made to cure within a few seconds using an activator (BSL activator 7455). It was decided not to glue the bead of the thermocouple, as the attenuation of the glue could affect the results but to attach the wire at either side of the bone. This is illustrated in Figure 5.10.

All samples were embedded in 1.5% agar gel before measurements were taken. It was ensured that at least 10 mm of agar was above and below the bone. A small amount of sodium azide (0.02%) was added to the agar to inhibit fungal and bacterial growth. There were two benefits in having the layer of agar: the first was that they could then be mounted in a standard sample holder facilitating ease of measurement; the second was that this meant that any solid liquid interface was at least 10 mm from the bone

Figure 5.10: Attachment of the thermocouples.

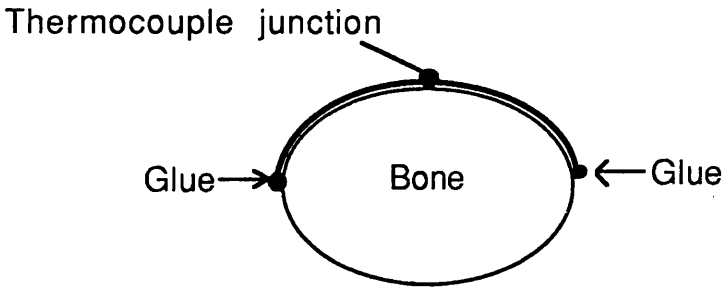

surface and so the effect of convection was minimised. This was desirable as tests had shown that the convection coefficient was not known accurately enough for it to be adequately modelled.

The attenuation due to the agar was measured by immersing the power balance in water and carrying out measurements with and without a layer of agar between the transducer and the power balance target. The agar was found to make very little difference to the readings, at most 2 mW when the total measured power was 45 mW; this was comparable to the reading error of the power balance. Theoretical calculations of the intensity loss due to agar support the theory that the loss is minimal. The attenuation coefficient of 3 - 4% agar gel at 20°C is 2.5×10^{-3} Np m^{-1} MHz^{-2} and the acoustic impedance 1.497×10^6 Rayl (Bouakkaz, Cachard & Gimenez, 1994). The intensity reflection coefficient at an interface is given by:

$$\frac{\text{Reflected intensity}}{\text{Incident intensity}} = \frac{(Z_1 - Z_2)^2}{(Z_1 + Z_2)^2} \qquad \text{(Equation 5.2)}$$

where Z_1 and Z_2 are the acoustic impedance of the two materials on either side of the interface (Miller, 1986). If this is evaluated for the water-agar interface, using the impedance value for water quoted by Bouakkaz et al. (1.483×10^6 Rayl), then it can be shown that less than 0.01% of the power is reflected at the surface of the agar. The fact that the acoustic impedance of agar and water are within 1%, also means that the reflection at the agar-bone interface will be very similar to that which would occur at a water-bone interface. Evaluation of Equation 5.2 with impedance values for bone ranging from 1.5×10^6 - 5×10^6 Rayl, a range that will be shown in

Section 12.3.2 to emcompass the likely value for fetal bone, shows that reflection coefficient is changed by less than 0.005 if the acoustic impedance of agar is substituted for that of water. The attenuation in 23 mm of agar, the maximum amount in front of the bone, is less than 0.2% and so neither the heat generated in the agar or the loss of intensity due its attenuation are likely to significantly affect the results. It is to be expected that 3% agar is less like water than 1.5% gel and so these calculations are likely to overestimate the effect of the agar. If these figures are compared with the uncertainty in the power measurement (4%) and those in the temperature measurements, which will be shown in Section 5.7.4 to be greater than 5%, it appears reasonable to neglect the reflection and absorption losses due to the agar.

5.5.4. Experimental Set-up

The formalin-fixed samples were embedded in a layer of agar, the total thickness of which was in the range 43 - 50 mm. To do this a batch of agar that had previously been prepared was heated to above its melting point and then allowed to cool to below 50°C. The sodium azide was then added and a layer of agar approximately 20 mm thick was poured into the sample holder. Once this base layer had set the sample was placed upon it and more agar added. The agar was left overnight to solidify and the distance from the top of the agar to the bone was then measured using a diagnostic scanner. The mean thickness of the agar layer was 16 mm (± 4 mm S.D).

In order to carry out the heating measurements the sample was placed in a water tank so that the bone was at the required distance from the transducer surface. The water in the tank was at room temperature: 21 ± 3 °C. Figure 5.11 shows the experimental set-up used.

Figure 5.11: Experimental Set-up.

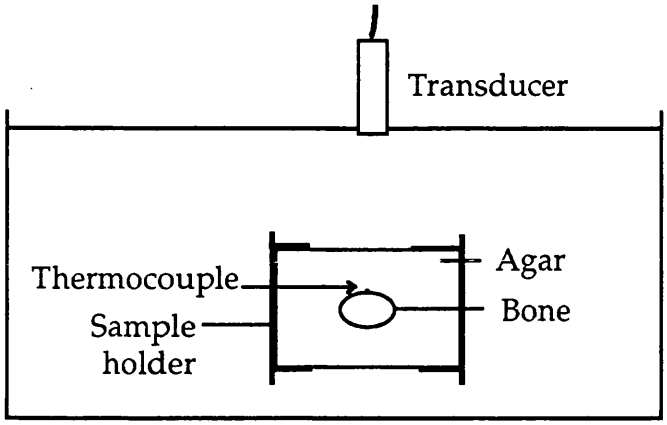

5.6. Positioning the Sample

The ultrasound beam used in the heating measurements had a diameter of a few millimetres at the measurement positions and so it was felt necessary to control the movement of the sample relative to the ultrasound beam in steps of less than 1 mm. As moving the thermocouple in the tissue would be very difficult it was decided to fix the position of this relative to the sample and move the transducer with the aid of a computer controlled translation stage (Unislide, Time and Precision Ltd). This was used to control the movement of the transducer perpendicular to the beam axis. The resolution of the stage was nominally 2.5 μm but tests showed that there was hysterisis of 0.1 mm when changing the direction of travel and so it was decided to position to the nearest 0.2 mm. Along the beam axis a manual translation stage was used and so the precision was ± 2mm. In this direction the critical dimension was the distance of the thermocouple from the bone surface, rather than from the transducer and this depended upon how the thermocouple was attached.

For all the temperature measurements the first step was to align the thermocouple with the centre of the ultrasound beam. This was done by maximising the temperature rise over a short period, typically 10 s, that was long enough to get a reasonable temperature rise while still ensuring that the measurement depended upon the local intensity.

5.6.1. Data acquisition

The aim of this study was to determine the temperature rise that may be caused by diagnostic scanning and so the acquisition needed to have good enough resolution to determine the rate of heating while being long enough to give an indication of 'worse case' results. As has already been discussed, it was necessary to over-sample and then average results in order to reduce noise and this, combined with the memory limitations of the computer, limited the maximum time for which data could be acquired. These factors lead to the decision to sample at 100 Hz for 300 seconds and then to average each hundred points so that, effectively, one data point was acquired per second. The time limit was close to the upper limit imposed by the computer memory but was felt to be adequate as this would be considered a long time dwell time for diagnostic scanning; Duggan and McCowan (1993) had measured the mean exposure time during a pulsed Doppler examination of the carotid artery to be 31 s, range 4 - 80 s. The insonation was not started until 5 seconds after the data acquisition began, allowing a base line temperature to be established.

5.7. Results

5.7.1. Variation of temperature rise with region of insonation

Measurements were carried out with the ultrasound beam incident on what in-vivo would be the anterior and the posterior surfaces of two of the samples (23 weeks and 39 weeks) to determine whether the orientation of the sample, with respect to the beam, influenced the temperature rise. In each case the thermocouple was attached to the uppermost surface of the sample where the beam entered the bone. The temperature plots obtained when the sample-transducer separation was 80 mm are shown in Figure 5.12. It can be seen that in both cases the temperature rise at the posterior was greater than that at the anterior surface. When the sample was closer to the transducer and hence the beam diameter was larger the posterior surface still gave the largest temperature rise but the difference was less: 13% as opposed to over 30%. It was thought that the difference in the temperature rise between the anterior and posterior surfaces could be due to the structure of the bone and so information was obtained on the histology of the samples. Figure 5.13 shows a slice of the 23 week sample stained with haematoxylin and eosin.

Figure 5.12: Temperature rise at surface of vertebra

a) 39 week sample

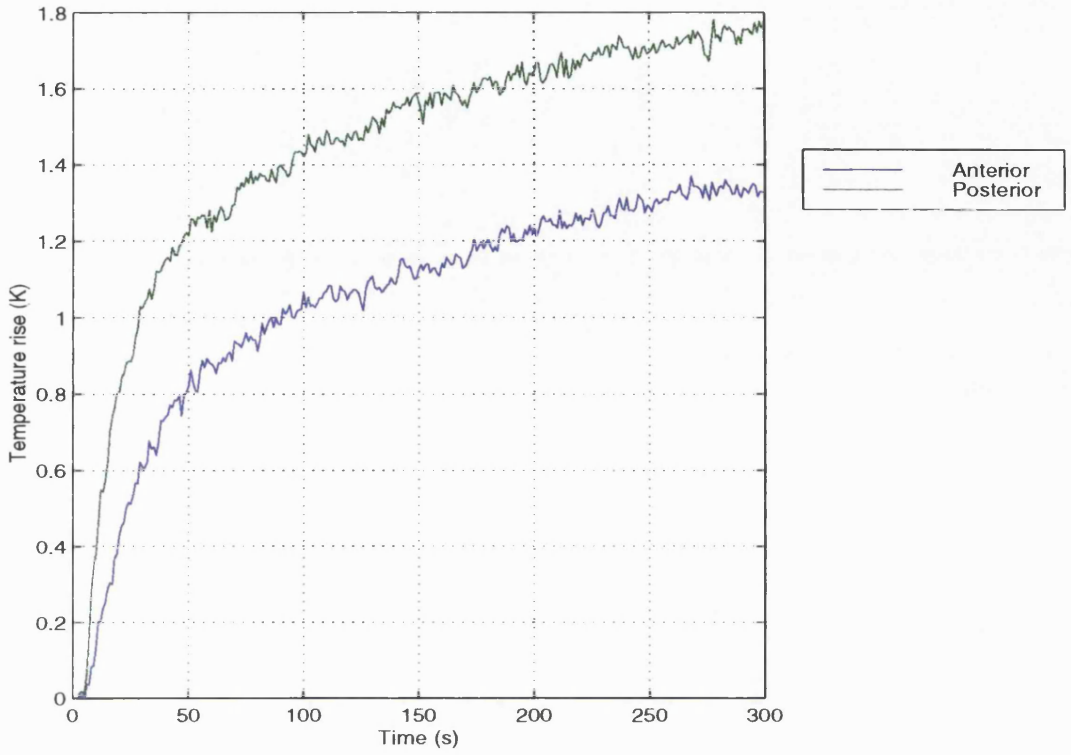

b) 23 week sample

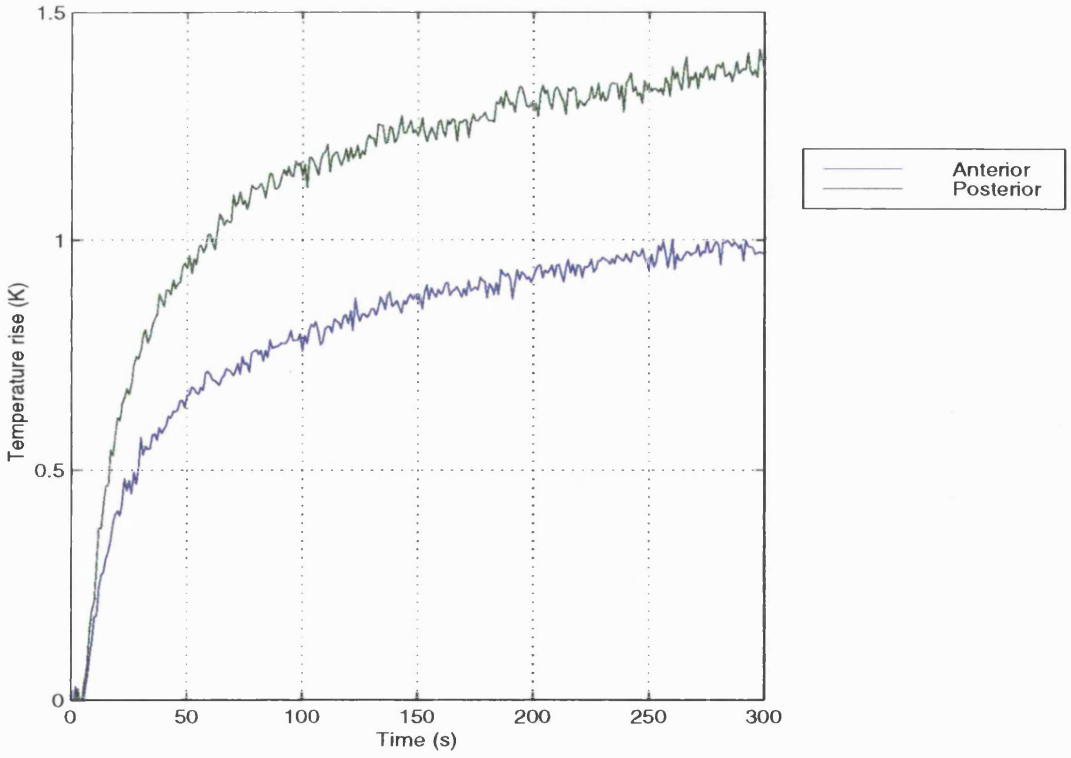

Figure 5.13: Image showing histology of 23 week sample.

Anterior

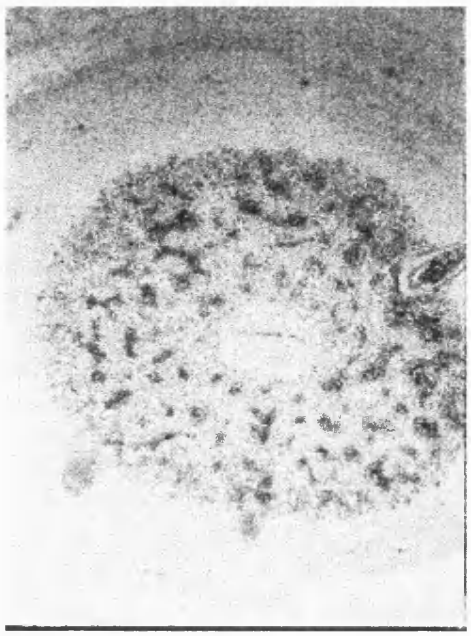

Posterior

Figure 5.14: Structure of the bone samples.

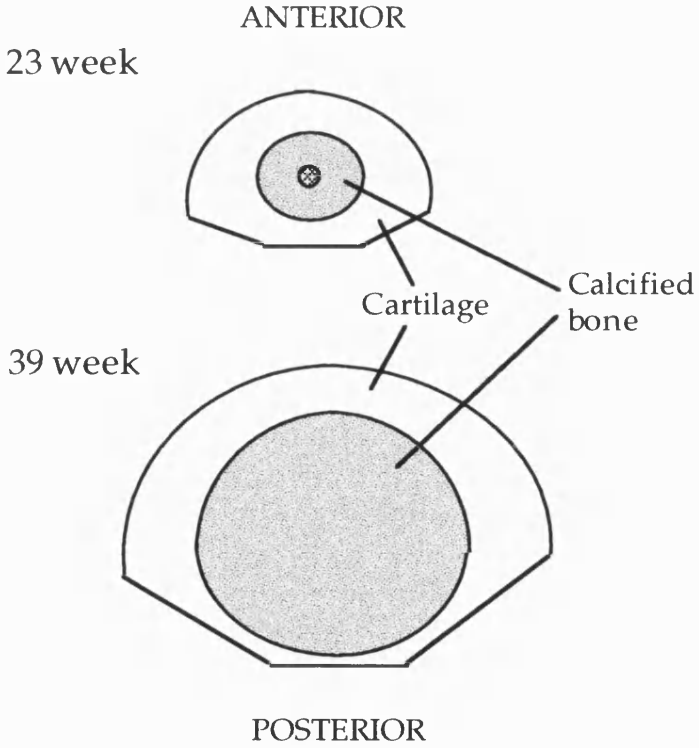

The plain area is cartilage and the mottled area is developing bone tissue. (A slice of the 39 week sample was also stained but its image can not be reproduced here due to the limitations of the equipment used.) It can be seen that there is a layer of cartilage around the developing bone. Figure 5.14 illustrates the distribution of cartilage in the two samples. In both cases the layer of cartilage at the anterior surface was thicker than that at the posterior and, in the 39 week sample, there was very little cartilage at the posterior surface. If, as might be expected, the bone is the more absorbent of the two tissue types, more heat will be generated in this than in the cartilage. When the thermocouple is attached to the posterior surface of the vertebra, and therefore closer to the developing bone, it will, therefore, be expected to record a greater temperature increase. It should be noted, however, that the process of separating the vertebral bodies from the spine involves cutting them away from the vertebral arch and the way this is carried out could affect the amount of cartilage towards the posterior surface of the samples.

5.7.2. Variation of Temperature Rise with Gestational Age

Figure 5.15 shows how the temperature rise at the posterior surface of the sample varied with the gestational age: Figure 5.15a shows the temperature rise recorded after 60 s insonation while Figure 5.15b gives the maximum temperature rise recorded during the five minute acquisition (insonation time 295 s). The posterior surface of the sample was chosen in order to maximise the temperature rise. In both cases there is a factor of three difference between the temperature rise of the youngest sample, which is approximately at the end of the first trimester and oldest sample which was close to term. It can also be seen that between 65 - 75% of the temperature rise occurs during the first minute of insonation. In order to test whether the temperature rise with gestational age was statistically significant a linear regression was carried out and the gradient was tested to see whether it was significantly different from zero. There is no theoretical model to suggest the shape of the curve but from inspection of the graphs it appears that this approximation is reasonable. The variation of the temperature rise with age both at 60 s and at 295 s was shown to vary significantly with gestational age ($p < 0.001$). This was true both when all the results obtained were plotted separately and when the mean temperature rise for each sample was used. This latter group was tested because using all the results meant that some bone samples had

Figure 5.15: Temperature rise vs. gestational age.

a) Temperature rise at 60 s

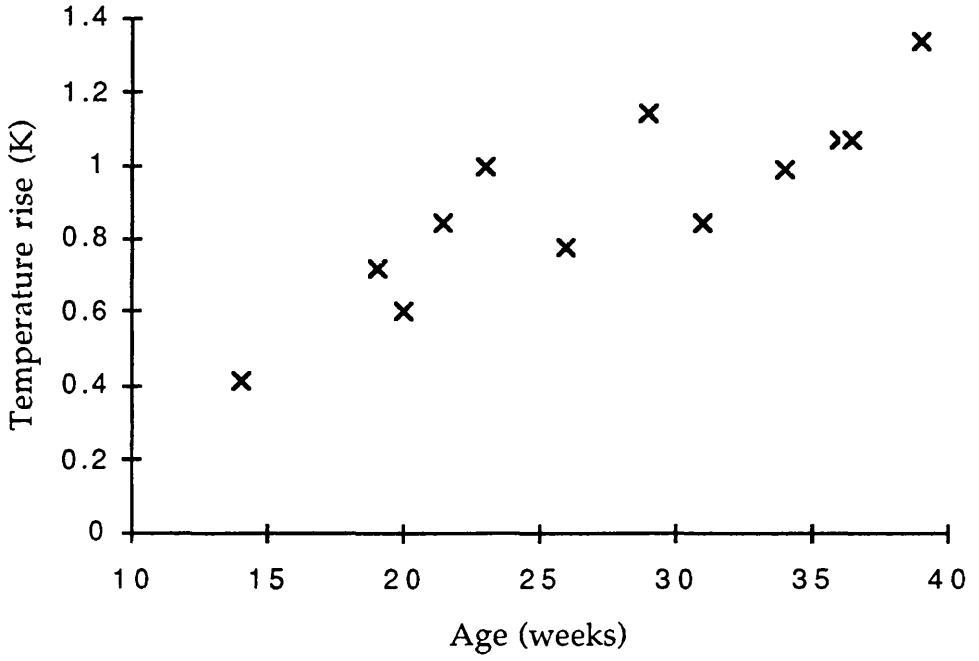

b) Temperature rise at 295 s

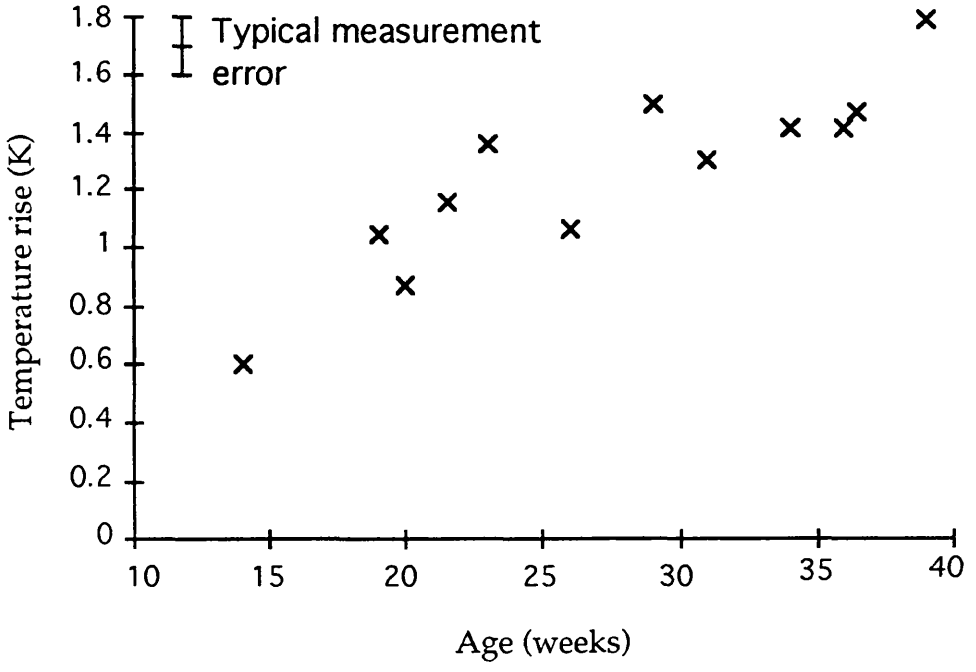

more influence on the regression than others and, while the repeated measurements meant that the standard error of the result for that sample was lower, it could still be that the sample did not give a good indication of the mean result from a population of samples of the same age.

5.7.3. Variation with beam diameter

Measurements were taken at two distances from the transducer in order to observe how the difference in beam diameter changed the maximum temperature rise. The difference in path length of 10 mm should make a difference of less than 1% to the power, assuming an attenuation coefficient for water of 0.0025 Np m^{-1} MHz^{-2} (Preston, 1991). The temperature plots for the 39 week sample placed at 70 and 80 mm from the transducer face are shown in Figure 5.16. The intensity distribution at these distances is shown in Figure 5.3 and the corresponding -6 dB beam diameters are 4.5 and 2.9 mm.

The variation of temperature rise with beam diameter is one of the factors included in the Thermal Index, which is discussed in Chapter 8, and the formula used when bone is at the beam focus assumes that the temperature rise is inversely proportional to the beam diameter. It can be seen that while the temperature rise shown in Figure 5.16 is greater when the beam diameter is smaller, the ratio of the temperature rises at 300 s, 1:1.31, is less than the ratio of the beam diameters, 1:1.55. The difference between the two graphs is, however, increasing with time at 300s and so the steady-state difference will be greater.

5.7.4. Errors and uncertainties

Repeatability measurements were carried out to allow estimates of the errors associated with the measurements to be made. These fell into four categories, those arising when:

- the sample was not moved between measurements;
- the sample was repositioned, as might occur if measurements were taken on successive days;
- measurements made with a new thermocouple attached to the vertebra and hence there was a new layer of agar;
- measurements made on the same sample but a different vertebral body.

Figure 5.16: Variation of temperature rise with beam diameter

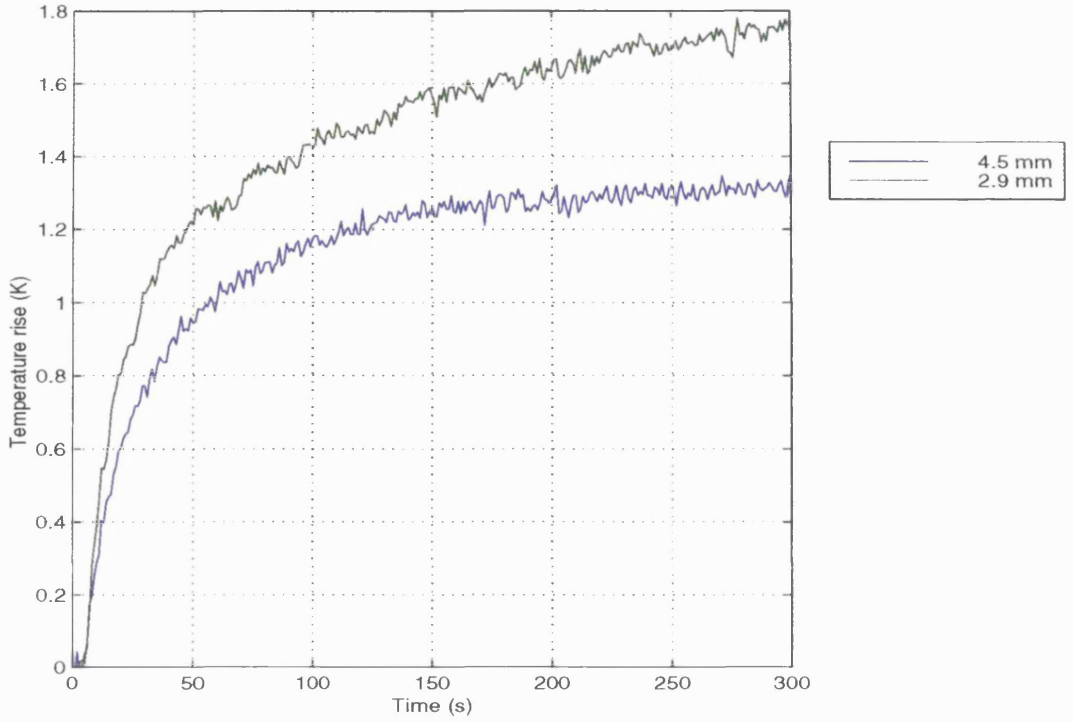

In the first category measurements were made on two samples of significantly different size and age: the 39 week sample which had a cross-section 16 x 10 mm and the 23 week sample which was 9 x 5 mm. Initial sets of three measurements were taken and the standard deviation was found to be 0.07 K for the 39 week sample and 0.02 K for the 23 week sample. Measurements of the error that occurred when the sample was repositioned were also made; this time the youngest and smallest sample (4 x 2 mm) was measured, as it would seem likely that this would be hardest to position repeatably, as well as the oldest. The standard deviation of these was found to be less than the 0.07 K found in the previous set of readings, suggesting that repositioning the sample did not increase the uncertainty in the results.

In order to assess the variation in results when different thermocouples were attached, either to the same vertebrae or to different ones, two of the longer samples were chosen. This allowed measurements to be obtained from three vertebrae without having to use the ones at either end of the sample that may have been affected when the samples were removed from the body. The 20 and 34 week samples were used as each of these had seven vertebral bodies To obtain each reading the temperature rise at 300 s was determined twice, without moving the sample, and the mean of

these values was used (in order to give a standard error of less than 0.05 K). The centre vertebra of each sample was studied on three occasions, with a new thermocouple and layer of agar each time. One set of data was also collected from two other vertebra. The results are tabulated in table 5.6.

Table 5.6: Temperature rise in repeated temperature measurements.

	Thermocouples attached to same vertebra	**Thermocouples attached to different vertebrae**
20 week sample	1.06, 0.84, 0.78 K	0.81, 0.88 K
34 week sample	1.40, 1.49, 1.35 K	1.31, 1.50 K

It can be seen that for the 20 week sample the minimum and maximum results were obtained from the same vertebra suggesting that the difference between different vertebra was less significant than the effect of repositioning the thermocouple. If all the results from the 20 week sample are considered the mean result is 0.87 ± 0.11 K standard deviation. For the 34 week sample the mean of all the results is 1.41 K; the standard deviation of the three results from the same vertebra is 0.07 and this is only increased to 0.08 when all the results are pooled.

It appears that much of the error occurs from replacing the thermocouple. The way that the thermocouples are made, by twisting wires together and then spot welding them, meant that the size of the bead was variable and the size of the thermocouples makes them difficult to handle. Both these factors combine to make it difficult to ensure that the thermocouple bead is in direct contact with the bone surface and, as Wu and Du (1990b) showed, the temperature gradient is very steep at this point. This may lead to an errors in the temperature measurement. This problem will be considered again when the computer models are discussed.

5.7.5. Effect of formalin fixation.

In order to get an indication of the effect of formalin fixation on the results, three of the samples were measured prior to being fixed with formalin. Two of these, the 23 and 39 week samples, were frozen prior to measurements being taken, for logistical reasons, but one was encased in agar on the day of the post-mortem examination, having been stored in

Table 5.7: Effect of formalin fixation on temperature rise.

Sample age (weeks)	Fresh (a)	Sample previously frozen (b)	Sample previously fresh/frozen then formalin fixed (c)	Sample formalin fixed	Percentage change (c - a,b)/(a,b)
23		1.08 K	1.41 K	1.34 K	+30%
31	1.15 K		1.27 K		+11%
39		1.61 K	1.52 K	1.78 K	-6%

saline during the intervening hours. Measurements were taken on the fresh, or defrosted samples, and they were then removed from the agar with the thermocouple still attached and soaked in formalin for at least three days. After this time they were potted in agar and measurements were carried out the next day. Table 5.7 shows the differences in the maximum observed temperature rise that occurred before and after the samples were formalin fixed and also the values obtained from samples that were placed in formalin immediately after they were removed at autopsy. Again the quoted result are the mean of two measurements taken without moving the sample.

It can be seen that the maximum difference occurs with the youngest sample. If the standard deviation of the readings is taken as 0.1K, as suggested by the measurements tabulated in Table 5.6, then the difference between the results obtained from this sample before and after formalin fixation is more than two standard deviations. The likelihood of this happening due purely to chance, with the formalin fixation making no difference, is about 5%. This suggests that the formalin fixation increases the measured temperature rise for this sample. For the other two samples it is not possible to separate the effect of the formalin fixation from the measurement error.

The youngest sample might be expected to exhibit more of a change in temperature rise on fixation for two reasons: this sample will be less ossified than the others and so the process of fixation, which makes soft tissues more rigid, is likely to have most effect; also a set increase in

absorption coefficient will have a more significant effect on a sample which has a lower absorption coefficient to begin with. The decrease in absorption when the 39 week sample was fixed is probably due to the uncertainties in the values obtained, especially as the part of the 39 week sample that had not been previously frozen had a higher value.

5.8. Temperature Rise Generated by a Diagnostic Scanner

While the ultrasound beam used for most of the experiments aimed to be 'Doppler like' there were ways in which it was unlike the real thing. For example, it was generated by a single element transducer rather than the array probe typical of diagnostic scanners. It was decided, therefore, to investigate the temperature rise that could be generated by a diagnostic scanner operating under conditions close to the maximum values allowed by the U.S. Food and Drug Administration (FDA). This sets a maximum derated intensity value of 720 mW cm^{-2}. Derating the intensity means that the intensity values measured in water are scaled down to allow for the attenuation that would occur if the ultrasound beam was travelling through tissue. It is this scaled down intensity value, rather than the measurement value, that must not exceed 720 mW cm^{-2} as this reflects the intensity that will be incident on the target tissue during clinical scanning. As the measurements reported here were carried out with the beam travelling through water and so there was no attenuation in soft tissue, the actual intensity level was set as close as possible to 720 mW cm^{-2}. An ATL Ultramark 9 scanner was used, operating in pulsed Doppler mode. Two probes were used, one of frequency 2.5 MHz and the other of frequency 6 MHz. The equipment settings necessary to obtain an I_{spta} close to 720 mW cm^{-2} from these probes had been determined previously by K. Dixon using BECA and so these settings were used. The output parameters from the probes, measured by K Dixon, are shown in table 5.8. It can be seem that the beam width of the 2.5 MHz probe was very similar to that of the single element probe used.

Measurements were carried out on the 14 week and the 39 week samples. Figure 5.17 shows the rate of heating for the two samples when insonated with the 2.5 MHz probe. In both cases the 50% increase in power output from this probe, compared with the single element probe used for most of the experiments, led to a 50% increase in the temperature rise (to within 0.1K). This is despite the fact that the frequency was lower than that of the

single element transducer. Although it is important not to read too much into one measurement, this does suggest that the temperature rise may not be strongly dependent on frequency. The 39 week sample was also insonated with the 6 MHz probe and figure 5.18 shows the rate of heating of this sample when insonated by the two clinical probes and the single transducer used for most of the measurements.

Table 5.8: Characteristics of ATL probes

	ATL Probe C340R	**ATL 6 MHz Probe**
Frequency (MHz)	2.5	6
Pulsed Repetition Frequency (kHz)	3.7	2.5
Beam width in direction of electronic focusing (mm) [Slice width (mm)]	2.95	1.33 [3.3]
Distance to point of measurement (mm)	65	42.5
I_{spta} (mW $cm^{-2)}$	765	744
Power (mW)	74	55

Figure 5.17: Temperature rise generated using 2.5 MHz probe (C340R).

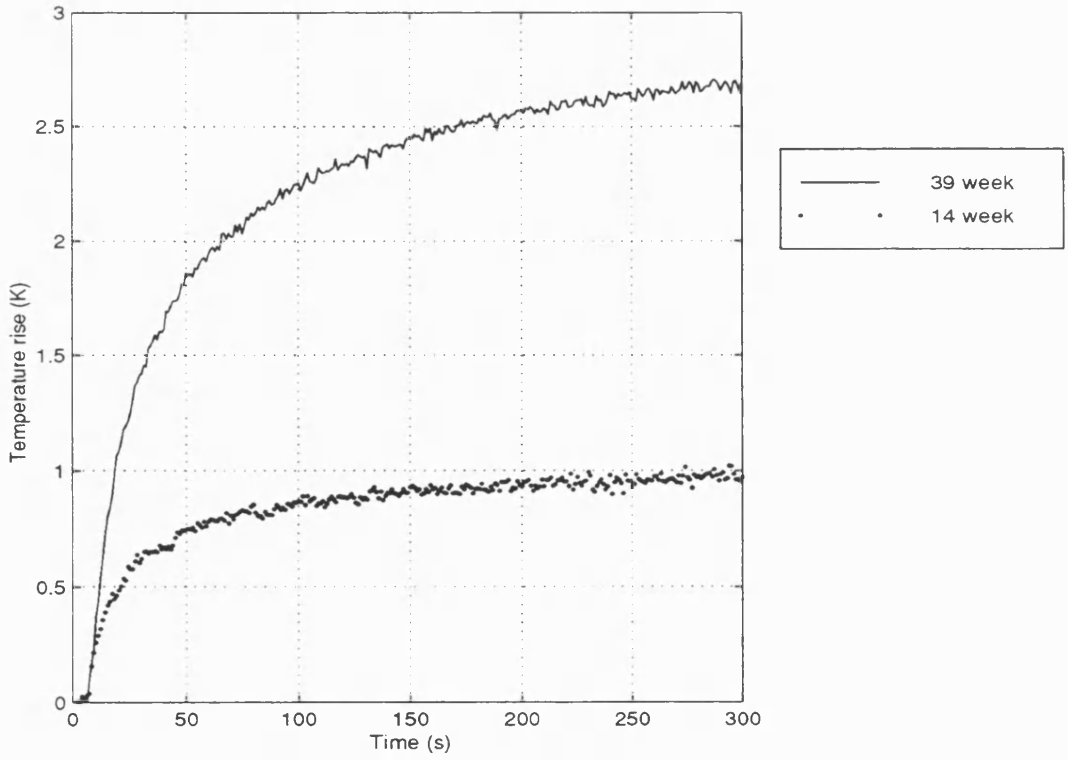

Figure 5.18: Temperature rise generated in 39 week sample

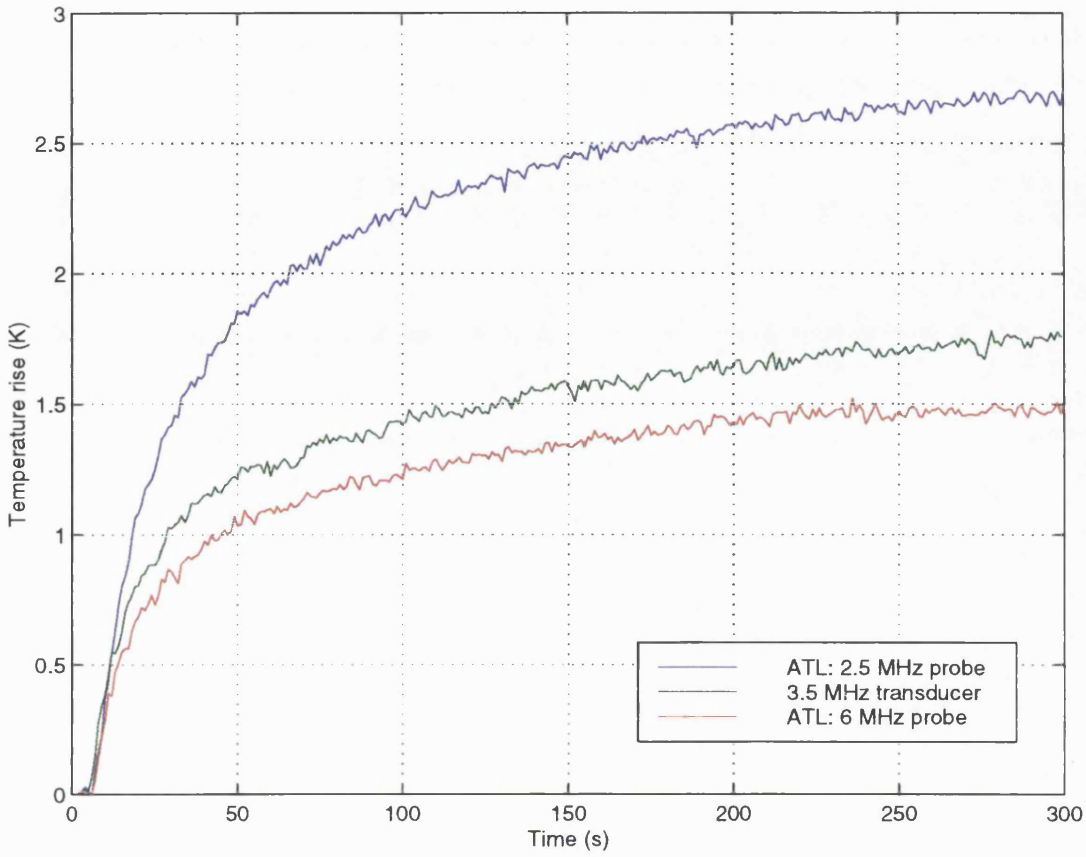

5.9. Discussion

It has been shown that a measurable temperature rise can be generated in fetal bone of 14 weeks gestational age when insonated with an ultrasound beam with power and diameter in the range expected from a diagnostic scanner operating in pulsed Doppler mode. This temperature rise increased as the bone developed and for the oldest sample it was 1.8 K, 45% of the level WFUMB suggest could cause damage if sustained for 5 minutes (WFUMB, 1997). When insonated with a diagnostic scanner, which emitted a power 1.5 times the value used for the original experiments, the temperature rise increased by this same factor, producing a temperature rise of 2.7 K, despite a decrease in the frequency from 3.5 to 2.5 MHz. These results show that the temperature rise that can be generated in fetal bone in vitro, under 'typical' exposure conditions, is not far below that which could be hazardous. It is important therefore to consider how the results from these experiments relate to the temperature rise that might be caused in vivo. This will be discussed in the next chapter.

5.10 Chapter Summary

This chapter has reported on heating measurements made on human fetal thoracic vertebrae ranging in gestational age from 14 to 39 weeks. All the samples were insonated with a 3.5 MHz ultrasound beam with characteristics within the range typical of beams used in pulsed Doppler examinations. The observed temperature rises after one minute ranged from 0.4 to 1.3 K and after 295s these had increased to between 0.6 and 1.8 K. The variation of the temperature rise at both 60 s and 295 s was shown to vary significantly with gestational age. When the position of the sample, and hence the beam diameter, was changed, the fractional change in temperature was less than the corresponding change in beam diameter. Formalin fixation was found to increase the temperature rise by up to 30% although the effect on the older samples was less significant. When insonated with a clinical scanner emitting a beam with of frequency 2.5 MHz and I_{spta} 765 mW cm^{-2} a temperature rise at 295 s of 2.7 K was measured. The temperature rise did not appear to be strongly dependent on frequency.

Chapter 6

Application of the Experimental Results

6.1. Introduction

In order to use the experimental results to predict the likely temperature rise in-vivo a variety of factors need to be considered. These include the typical power output from diagnostic scanners, the attenuation that occurs in tissue and the cooling caused by perfusion. It is only by combining data from a variety of studies, each looking at a different aspect of the problem, that sufficient information can be obtained to produce reasonable predictions.

6.2. Acoustic Power Levels at the Fetus.

The acoustic power output from the single-element transducer used in the measurements was 50 mW, a value given as typical for pulsed Doppler equipment by Duck and Martin in 1991. A more recent survey (Henderson et al., 1995; Henderson et al., 1997) carried out between 1991 and 1997 measured the maximum output values from a range of scanner-probe combinations on over 50 different types of scanner. This found the mean value of these maximum outputs from scanners operating in pulsed Doppler mode to be 124 mW and the maximum output found was 440 mW. The mean value of the I_{spta}, again in pulsed Doppler mode, was 1700 mW cm^{-2} and the maximum 9000 mW cm^{-2}. The authors point out that it is not clear whether there has been a genuine increase in power between the time when their measurements and those of Duck and Martin were performed or purely increased knowledge about which control settings produce the highest power levels. Clearly these values are significantly higher than those used in section 5.7: the mean power being more than twice as large and the mean I_{spta} being three times the value used. It should be remembered, however, that the output survey determined worst case free-field conditions, i.e. the maximum values that could be obtained when carrying out measurements in water and the authors state that, particularly for I_{spta}, these may be much greater than those that the scanner will produce in everyday use. A survey by Patton, Harris & Philips (1994) of output levels reported to the United States Food and Drug Administration (FDA) gave the range of power output levels for general pulsed Doppler equipment as 0.27 - 410 mW with a mean

value of 35 mW. The I_{spta} values ranged from 11 - 1800 mW cm^{-2} and the mean value of these was 449 mW cm^{-2}. These values, however, were obtained using the operating conditions that maximised the 'derated' intensities, i.e. the value after allowing for attenuation in tissue and so may not represent the maximum output values. This may explain the difference between these figures and those of Henderson et al..

6.3. Attenuation in Overlying Tissues.

Another factor that should be taken into account when using the experimental results to predict heating of the fetus is attenuation of the beam in the maternal tissue. The beam used in this study did not undergo the absorption from overlying tissues that would occur when a fetus is scanned and so it is necessary to take this into account. Two basic approaches have been used to model attenuation: homogeneous and fixed path models.

The homogeneous models assume, as the name implies, that the attenuation coefficient does not vary along the beam path and so a constant derating factor per unit length is applied. The FDA (1985) recommends the use of such a model and it has been incorporated into the 'Output Display Standard' (AIUM/NEMA, 1992) which defines the Thermal Index (TI); a parameter which is discussed in Chapter 8. The TI assumes that the value of attenuation depends on the path length and frequency and uses a derating factor of 0.3 dB cm^{-1} MHz^{-1}.

Fixed path models assume that, at any stage of pregnancy, the attenuation depends only on the frequency of the transducer and is not a function of the distance between the transducer and the fetus. This might be visualised by considering a path that consists of a layer of maternal tissue of fixed thickness followed by a minimally attenuating fluid path which can vary in length. NCRP report 113 'Exposure criteria for medical diagnostic ultrasound: 1. Criteria based on thermal mechanisms' (NCRP, 1992) proposes the use of fixed path models for predicting the attenuation in fetal scanning. This is based on the assumption that the minimum path length of attenuating tissues does not change greatly during pregnancy. The values quoted are as follows:

1st trimester:	1 dB MHz^{-1}
2nd trimester:	0.75 dB MHz^{-1}
3rd trimester:	0.5 dB MHz^{-1}.

These are worst case values based on measurements of the minimum thickness of skin, fat and muscle in pregnant women and they do not include attenuation in the placenta which is often not in the path of the beam.

Carson, Rubin and Chiang (1989) measured the thickness of the various tissue layers overlying the fetus in women undergoing amniocentesis. The total attenuation was then calculated using previously published values for the attenuation due to each type of tissue. For 22 second trimester pregnancies the minimum attenuation was found to be 0.8 dB MHz^{-1}, with the mean value being 1.5 dB MHz^{-1}. When the measurements were compared with the FDA derating factor (0.3 dB cm^{-1} MHz^{-1}) it was found that in some cases the derating factor overestimated the amount of attenuation that occurred. In a typical case at 3.5 MHz, the FDA model indicates an attenuation of 7.4 dB compared with the minimum measured value of 2.8 dB. Similar conclusions were reached by Ramnarine, Nassiri, Pearce, Joseph, Patel and Varma (1993) who found the attenuation given by the FDA model to be more than the value obtained by analysing image data in a significant number of first trimester scans, especially those in which the beam passed through the bladder, and in a small proportion of second and third trimester Doppler examinations. The authors of this study suggest that a fixed attenuation value of 0.8 dB MHz^{-1} is representative of worst-case exposure conditions and that a value of 1.0 dB MHz^{-1} be used for common Doppler examinations. The attenuation during third trimester scanning was studied by Kamel (1994) who calculated the attenuation both for the tissues actually seen in the path of the beam, i.e. including placenta if present, and the value only for tissues constantly lying in the tissue path, i.e. excluding placenta. The average value of attenuation due to tissue constantly in the beam path was found to be 1.16 dB MHz^{-1} which, assuming a homogeneous model, gave an average attenuation coefficient of 0.54 dB cm^{-1} MHz^{-1}. The minimum value for attenuation from tissues constantly overlying the fetus was 0.3 dB MHz^{-1} corresponding to an intensity reduction of 1.05 dB (21.5%) at 3.5 MHz. Actual measurements of insertion loss were carried out by Siddiqi, O'Brien, Meyer, Sullivan and Miodovnik (1995) who used a specialised exposimetry system to measure this in first and second trimester pregnancies with a diagnosis of missed abortion. No statistical difference was found between the attenuation in

first and second trimester and a mean value of 3.6 dB MHz^{-1} was obtained. The minimum value measured was 1.1 dB MHz^{-1}.

These studies suggest that the NCRP figures are reasonable estimates of the minimum attenuation likely to occur in maternal tissue. The homogenous model, however, appears to overestimate the attenuation in some cases and this could lead to an underestimate of the acoustic power at the fetus. If the NCRP third trimester values of attenuation are combined with the output values given by Henderson et al (1997) then the power incident on a fetus from a scanner with their mean, worst case output, assuming a 3.5 MHz transducer, is 83 mW. If the maximum output figure is used then the value at the fetus is 293 mW. Both these values are higher than the power used in the heating experiments reported in the previous chapter.

6.4. Perfusion

Perfusion of tissue in-vivo should act to limit the temperature rise but it is 'highly variable and its relevance is difficult to estimate' (Barnett, et al., 1997). A number of authors have measured bone heating in live animals and then repeated the measurements after the animals have been slaughtered. Their findings are summarised in Table 6.1. It can be seen from these figures that it is not easy to give a definitive figure for the reduction in temperature rise due to perfusion. This is perhaps not surprising as it will clearly be influenced by the amount of perfusion in both the bone and the surrounding tissues. This explains the observation of Lehmann that the temperature rise in a well perfused area, such as the bone marrow, is affected by perfusion more than the temperature rise at the surface of the bone. Horder's work on guinea pigs suggests that gestational age must also be taken into account.

While various models for cooling due to perfusion have been proposed, and are discussed in the chapter 7, these rely on knowledge of the amount of blood flow. This information does not appear to be available for fetal spine and so the likely degree of cooling is unclear. It should be noted, however, that the NCRP report 113 (1992) quotes a perfusion rate for bone marrow that is less than an eightieth that of liver and so it may well be in some of the above examples that it is the perfusion in the surrounding soft tissue that is making the difference.

Table 6.1: Measured Perfusion Values.

Author	Year	Tissue heated	Reduction in temperature rise due to perfusion .
Lehmann	1967	Pig thigh - bone surface and spongy bone	23 - 24%
		Pig thigh - bone marrow	46%
Carstensen	1990	Mice skull	12 ± 4%
Duggan	1995	Fetal sheep skull	30 - 43%
Horder	1997	Fetal guinea pig 57 - 61 days gestation	1%
		Fetal guinea pig 62 - 66 days gestation	13%

6.5. Discussion

It can be seen from the above that using the results of in vitro measurements to predict heating in vivo requires consideration of a variety of factors. It appears that the NCRP fixed path values, discussed in Section 6.3, give a reasonable estimate of the minimum attenuation and certainly seem more appropriate to obstetric imaging than homogeneous models. These suggest that during 3rd trimester the power in a 3.5 MHz beam would be reduced by 1.75 dB (3.5 MHz x 0.5 dB MHz^{-1}), i.e. to 67% of its original value. The influence of perfusion is highly variable and under worst case conditions, i.e. those leading to the maximum temperature rise, this appears to have almost no effect on the temperature rise. The effect of formalin fixation was discussed in Chapter 5 and, in order to use the results from fixed samples this too must be allowed for. Fixation was shown to increase the temperature rise by between 0 and 30% and so, if worst cases are being considered, no allowance should be made for this. If all these factors are combined, taking in each case the value that would lead to most heating, the worst case temperature rise in vivo would be 67% of that measured in vitro. The 50 mW beam used in the main set of measurements would,

therefore, be expected to produce, under conditions leading to maximum heating, a temperature rise of 1.2 K. If it is assumed that there in a linear relationship between power and temperature rise, the maximum power output of 440 mW measured by Henderson et al. could produce a temperature rise of 10.6 K after 300 s insonation. It is important, however, to remember that many assumptions underlie this figure, not least that the 440 mW power value relates to a beam which has characteristics, such as frequency and diameter, that are comparable to those of the 50 mW beam. This may not be the case and so, while this figure shows the importance of considering the risk of excessive heating, it should not be given the same weight as a measured value.

6.6. Chapter Summary

It can be seen that the output from transducers operating in pulsed Doppler mode varies greatly and that the distribution of values found depends upon the definition of 'worst-case' conditions. It is clear, however, that it is possible to obtain values of power and intensity that are much larger than those used in the measurements described in Chapter 5. When considering heating in-vivo these values will, however, be reduced due to the attenuation that occurs in the maternal tissue overlying the fetus. It appears that this is adequately modelled using the fixed path approach suggested by the NCRP giving, for a third trimester fetus, a reduction in the intensity of 1.75 dB at 3.5 MHz, as discussed in Section 6.5. Perfusion may act to limit the temperature rise in living tissue but the effect varies greatly and may be as little as 1%. These results suggest that at the maximum power levels measured by Henderson, the in vivo temperature rise could be over 10°C. This figure should be regarded with caution, however, as a full description of the beam that produced the maximum power output is not available and factors such as the beam diameter and frequency would affect the predicted temperature rise.

Chapter 7
Modelling Heating

7.1 Introduction

The fact that the output from diagnostic ultrasound scanners varies, both in terms of the absolute power level and the intensity distribution, means that it is not possible to measure one such scanner and then generalise about tissue heating. Neither is there a readily available test object which can be used to measure the temperature rise that might occur in the fetus. While groups, such as NPL, have developed thermal test objects the relationship between the results from these and heating in fetal tissue is not clear. It is desirable, therefore, to develop mathematical models which, given the appropriate input data in terms of parameters describing the ultrasound beam and tissue, could predict the temperature rise.

The second half of this thesis will, therefore, concentrate on modelling heating. In this chapter the literature on this subject will be reviewed, while in the next the indices of tissue heating given in the 'Output Display Standard' (AIUM/NEMA 1992) will be discussed. The review will concentrate mainly on analytical methods used to predict heating in diagnostic ultrasound but where useful information is available from other sources this will be included. Numerical methods for predicting heating will be discussed in chapter 10.

7.2 Heat Transfer Equations

The basic equations governing the temperature rise in an object can be obtained by considering Fourier's law of heat conduction and the principle of conservation of energy. If heat loss is by conduction only, then the rate of change of temperature, T, with time, t, for a body in which heat is generated at a rate q per unit volume is given by:

$$\frac{\partial T}{\partial t} = k\nabla^2 T + \frac{q}{c_v} \qquad \text{(Equation 7.1)}$$

where k is the thermal diffusivity of the body and c_v is the heat capacity per unit volume. When modelling the temperature rise due to ultrasound the heating term is taken to be the energy lost from the beam through

absorption. For a plane wave travelling in a fluid the heat generation is given by

$$q = 2\alpha_a I \qquad \text{(Equation 7.2)}$$

where I is the intensity of the ultrasound and α_a is the amplitude absorption coefficient. This is true regardless of the absorption mechanism and is approximately correct in the focal region of a focused source (Nyborg, 1986) (the example shown in the paper gave a maximum error of the order of 3%). Commonly the absorption coefficient is assumed to equal the attenuation coefficient and so $q = 2\alpha I$. To fully model heat loss in solids it is necessary to consider shear waves, as these will propagate at a different velocity and with a different absorption coefficient than the longitudinal wave. This has been done using data for adult bone (Chan, Sigelmann & Guy, 1974; Haken, Frizzell & Carstensen, 1992) but the calculations involved in this process are complex and there is limited data available on the values of the parameters involved. More often bone heating is modelled as, effectively, a highly absorbing fluid using Equation 7.2 (ter Haar, 1979; Wu and Du, 1990b; Shaw, 94) Little is known regarding conversion of ultrasonic energy to heat in fetal bone and determining the elastic constants necessary to model conversion of longitudinal waves to shear waves is all but impossible for this type of bone (Drewniak and Dunn, 1996). These authors, therefore, proposed a heat source term for fetal bone that is based on its initial rate of heating.

For in vivo modelling perfusion should be included and Pennes' (1948) bio-heat transfer equation (BHTE) is frequently used:

$$\frac{\partial T}{\partial t} = k\nabla^2 T + \frac{q}{c_v} - \frac{\Delta T}{\tau} \qquad \text{(Equation 7.3)}$$

where ΔT is the temperature rise and τ is the perfusion time constant, which depends upon the rate of blood flow to the tissue and the heat capacity of the blood. The physical interpretation of this model is that blood enters the heated volume and is warmed until it reaches thermal equilibrium with the region, it then leaves the volume taking the 'extra heat' with it. The perfusion is considered to be isotropic. The underlying assumptions are that (Hand, 1997):

- the blood enters the local tissue volume at arterial temperature and leaves at local tissue temperature;
- heat transport related to mass transport of blood is neglected (i.e. there is no change in the volume of blood in the region);
- individual cooling or heating of blood by large vessels is neglected;
- the effects of the venous network is neglected.

The validity of these assumptions has been questioned by authors and other models of perfusion have been proposed. Wulff (1980) pointed out that this did not allow for either the vector nature of blood flow or differences in blood temperature at different points. Chen and Holmes (1980) divided blood vessels into two categories which need to be treated separately: larger vessels that need to be treated individually and small vessels that can be treated as part of the tissue continuum. Weinbaum (1985) suggested that the primary mechanism for blood-tissue energy exchange is incomplete countercurrent heat exchange that occurs between artery-vein pairs rather than the heat exchange at microvascular level assumed by Pennes. In this process the transfer of heat between the vessels going out of the region and those coming in reduces the distance from the heat source at which the blood reaches thermal equilibrium with the tissue. In a review of perfusion modelling Arkin (1994) concluded that the appropriate model depends upon the size of the blood vessels in the heated region and on whether the vessels are paired. Details of vessel size in the heated region is often not available however and so Arkin suggests that due to its simplicity the best practical approach may still be to use the Pennes model.

7.3 Solutions for Soft Tissue Heating

Irrespective of the perfusion model chosen, the solution of these equations is often highly complicated and depends very much on the boundary conditions (Nyborg & Steele, 1983). Simplifying assumptions are generally used, therefore, in order to make the calculations more manageable. The most common of these involve either assuming that the tissue path is homogeneous or defining strict conditions of symmetry on the beam.

Various approaches have been used to solve the basic heat transfer equation (Equation 7.1). Robinson and Lele (1972) obtained solutions for the region near the beam focus by assuming circular symmetry. The temperature

profiles they obtained were then compared with the shape of lesions formed in cats brain and plastic. There was relatively good agreement with the brain lesions although the results were not as good for plastic, probably because they had not allowed for a change in attenuation coefficient with temperature. Conditions of cylindrical symmetry were applied by Filiczynski (1976; 1977) in order to model focused fields such as those used in imaging and Doppler measurements and the results obtained were said to be in approximate agreement with the experimental measurements in muscle tissue by Fry and Fry (1953). Nyborg and Steele (1983) modelled the temperature elevation along the axis of an unfocused beam of ultrasound by considering the region occupied by the beam as being divided into a large number of very thin discs. Each disc acted as a heat source producing a temperature field in the surrounding medium and, by adding the fields produced by all the discs, the total temperature elevation could be calculated. This model did not allow for perfusion.

Nyborg (1988) went on to obtain a solution to the BHTE (Eq. 7.3) and the basis of this technique has since been adopted by many authors. This gives a value for the temperature elevation, ΔT, at a distance, r, from a small source of volume dv which has been generating heat at a rate $q_v dv$ for a time t.

$$\Delta T = (C/r)\{E[2-\mathrm{erfc}(t^*- R)] + E^{-1}\mathrm{erfc}(t^*+ R)\} \qquad \text{(Equation. 7.4)}$$

where erfc is the complimentary error function and the other parameters are defined as follows:

$$C = \frac{q_v dv}{8\pi K},$$

$$E = \exp(-r/L),$$

$$L = \sqrt{k\tau},$$

$$t^* = \sqrt{\frac{t}{\tau}},$$

$$R = \frac{r}{\sqrt{4kt}}.$$

L is known as the perfusion length and is a measure of the distance over which the influence of a heat source is felt in a steady-state temperature field. τ is the perfusion time constant and is indicative, for a fairly uniform

temperature field, of the time required for the temperature to fall after the heat sources are turned off (NCRP, 1992).

The temperature rise due to heating of an extended area can be calculated by integrating the above equation over the volume of the beam. This assumes, however, that the heated region is homogenous and its boundaries are at infinity. As with the solutions for Equation 7.1, use is often made of symmetry in order to reduce the complexity of the problem. The combination of this solution with the technique of considering the field as comprising a series of very thin discs, as described earlier, is often referred to as the heated disc method. This approach has been used by various authors (Dore, 1990; Thomenius, 1990; Wu & Du, 1990a) to study the influence of a range of beam and tissue parameters and it has been shown that beam frequency and focusing play an important role in determining the maximum temperature rise, as do the absorption coefficient and perfusion of the tissue. Wu and Du (1990a) used a range of heat source functions in the region occupied by the transducer to model different boundary conditions and so confirmed Nyborg and Steele's (1983) work which showed that these conditions have a large effect on the temperature rise. If, for example, the thermal conductivity of the transducer is very low the temperature rise at surface is up to twice that obtained if the transducer is assumed to have the same thermal conductivity as the rest of the model.

Wu, Chase, Zhu and Holzapfel (1992b) used a solution to the BHTE developed by Carslaw and Jaeger (1959) for a homogeneous, infinite and nonperfused medium. This gives an analytical solution to the transient temperature rise on axis produced by a beam with cylindrical symmetry. Three intensity distributions were considered: the Nyborg and Steele model, the NCRP model for focused beams and a Gaussian model. The first two each use a 'top hat' distribution in which the intensity at a distance z from the transducer is constant over an area defined by the beam diameter and zero outside; the only difference between these two models being the way that the beam diameter changes with distance from the transducer. In the Gaussian model the intensity is a function of the radial distance from the beam axis as well as the distance from the transducer. When the computed results from the models were compared with experimental measurements in tissue mimicking material there was found to be reasonable agreement although the boundary effects were seen to play an important role. Surface heating of the transducer was found to be an important source of tissue

heating and the fact that the models did not include this led them to underestimate the temperature rise in some situations.

Ellis and O'Brien (1996) developed a general method of predicting heating that does not restrict itself to a specific beam geometry. This considered the source to be made up of a series of acoustic monopoles and summed the contribution from each to calculate the spatial distribution of the acoustic pressure. The pressure field generated by any shape of transducer can therefore be calculated by summing the appropriate terms. The temperature rise at any point was calculated by using the point-source solution to the bioheat transfer equation and adding together the contributions from all the points in the field. The results generated by this technique depend upon the spacing of the monopoles and the points in the acoustic field. The authors deemed that the results were adequate when the monopole source spacing was $\lambda/4$ and the field spacing was 0.01 cm. When results for a circular aperture were compared with those from a heated disc model the magnitude and position of the maximum temperature rise agreed to within 3%. There was a difference of the order of 10% in the predicted heating near the focal zone, however, which was said to be due to the way that the heated disc approach models the beam in this area. This assumes that all the power of the beam is contained within an area defined by the -6 dB diameter and so overestimates the temperature rise.

7.4 Layered Models

As well as being used to model homogeneous tissue, the heated disc approach has been used to try and predict the temperature rise in layered materials. This is done by allowing discs to have different absorption coefficients. The nature of this type of model, however, means that only one set of thermal properties can be used for the whole region. Thomenius (1990) considered a fixed path model, in which there was a layer corresponding to the maternal abdominal wall followed by a non-absorbing layer of amniotic fluid and then the absorbing target tissue. The position of the target relative to the focal point of the ultrasound field was shown to play an important role in determining the temperature increase. The model also predicted that the rise time for the temperature increase in a good absorber, such as bone, would be short: seconds rather than minutes. Wu and Nyborg (1992) modelled the temperature rise generated by a Gaussian beam in a two-layer medium. This is relevant to fetal examinations via the abdominal wall where the beam passes through

weakly attenuating fluids (urine and amniotic fluid) before reaching the fetus. Gaussian intensity distributions were used to approximate the field in the focal region of non-gaussian transducers as they produce a simple expression for the intensity distribution, reducing the complexity of the integration and hence the computer time. It was found that the maximum temperature rise occurred close to the interface even when the beam focus is located in the interior of the second (absorbing) layer.

Carnes, Drewniak and Dunn (1991) used an alternative approach to solving the BHTE which, by modelling the heated volumes as nested parallelepipeds and assuming a Gaussian beam profile, gave an analytical solution. This was used to predict the temperature rise in a mouse fetus inside its dam (mother). The properties of the outer parallelepiped, representing the dam, remained the same in all the models while the size and absorption coefficient of the inner parallelepiped changed to represent fetuses of different ages. Measurements of temperature rise in the fetus were carried out at three gestational ages and the results were compared with the model. In order to obtain agreement between the measured and computed temperature increases, the perfusion constant was chosen to be different at different exposure times. The differences between the computed and measured results were up to 50% of the measured values and it was suggested that a more realistic model would include better determination and modelling of the beam and better approximations of the absorption coefficients and perfusion rates.

The variation in the predicted temperature rise that can occur from using different intensity distributions was demonstrated by Jago, Whittingham and Henderson (1995; Whittingham, Henderson and Jago, 1995). These papers reported calculations of the temperature rise in soft tissue, water/bone and soft tissue/ bone models and it was shown that modelling the intensity distribution using a Gaussian distribution, as opposed to the actual, measured, distribution can give large errors. There were also problems when the heated disc model was used for beams without circular symmetry

7.5 Modelling the Temperature Rise in Bone

Chan, Sigelmann, Guy and Lehmann (1973) obtained a solution for a layered model that included bone using the finite difference technique, a numerical method of solving differential equations. The model was one-

dimensional and was composed of three layers, fat, muscle and bone, with each layer having a different heat source and cooling function. The incident wave was assumed to be normal to the surface and the heat source term in each layer had the form of an exponential, decaying with distance travelled inside the tissue. The cooling term, which modelled perfusion, was a function of the temperature rise and the values of the coefficients were determined by comparing the results with the measurements in pig thigh made by Lehmann and Johnson (1958). It was found that in order to get a good agreement between the calculated values and Lehmann's measurements the value for the power dissipation in the muscle had to be reduced from the one calculated using the absorption coefficient. Once this had been done the theoretical and experimental results in all three layers agreed to within the experimental error for measurements on both live (i.e. perfused) and dead (unperfused) pigs. This group went on to consider how the heat generated in a layered model depends upon the angle of incidence of the wave (Chan, Sigelmann, & Guy, 1974). Fat and muscle were assumed to behave as viscous liquids while bone was modelled as a viscoelastic solid. This meant that bone was considered capable of supporting both longitudinal and shear waves and so the heating from both sources had to be considered. The attenuation coefficient of the shear wave in bone was given as 2.6 Np cm^{-1} compared to 1.52 Np cm^{-1} for the longitudinal wave (a ratio of 1.5 for shear to longitudinal wave attenuation has since been measured by Wu and Cumberley (1997)). The power deposited in the bone is assumed to originate from the frictional loss of the acoustic wave and depends upon the velocity vector and the stress tensor. The amount of heating in each layer was shown to depend to a significant degree upon the angle of incidence of the wave as this affected the transmission coefficients at the boundaries. The maximum power loss per unit volume in the bone was obtained when the angle of incidence was in the range 45 - 60°. When the incident angle was greater than 22° the shear wave was responsible for most of the heating. This paper considers only the heating caused by each type of wave, i.e. the power lost from the beam, and not the temperature rise but clearly if most of the energy deposited in the tissue comes from the shear wave this will play a major factor in determining the local temperature rise.

The steady-state temperature elevation generated by an ultrasound beam striking a tissue-bone interface was studied by Wu and Du (1990a). This model considered a focused Gaussian beam and included the reflection of

the beam at the bone surface. It was assumed that the thermal conductivity in both tissues was the same. The effects of reflection, focusing and perfusion were investigated. It was shown that the maximum temperature rise along the beam axis occurs inside the bone close to the interface, no matter what the focal length of the transducer. The gradient of the temperature rise versus position graph is steepest near the interface and a change in position of 1 mm can reduce the temperature rise from its maximum value to 50% of maximum. This paper also demonstrates the need to consider the absorption of the reflected beam when calculating the temperature rise in the soft tissue.

Carstensen, Child, Norton and Nyborg (1990) attempted to model the temperature rise that they measured in mouse and rat skull. To do this they assumed that all the energy that enters the bone is absorbed in a thin planar sheet at the bone surface. If the heat source term in the point source solution to the BHTE is assumed to be a function of the intensity of the beam at any point and the result is integrated over the area of the sheet then the temperature rise can be calculated. The steady-state temperature rise for three intensity distributions was calculated. These were the distribution proposed by O'Neil for the farfield of a piston source (O'Neil, 1949), the Gaussian distribution and a disc (top hat) distribution. The distribution given by O'Neil is based on a first order Bessel function J_1 and the radial intensity distribution I(r) is given by

$$I(r) = I_0[2J_1(x)/x]^2$$

where I_0 is the axial intensity, r the radial distance from axis and $x = 4.43r/d_6$ where d_6 = -6 dB beam diameter.
The Gaussian distribution is given by

$$I(r) = I_0\exp(-y^2)$$

where $y = 2.35r/d_6$ and in the disc distribution the intensity is constant over the -6 dB diameter. It was shown that, in the absence of perfusion, for the same axial intensity and beam diameter the steady-state temperature rises were in the ratio 1: 0.98: 1.3 (Bessel: Gaussian: Disc) and for the same total acoustic power and beam diameter they are 1: 1.10: 1.06. The rate of heating was then compared with the experimental results. The O'Neilian distribution was used and it was assumed that 60% of the energy incident on the bone was converted to heat. For measurements on rat skull there was

reasonable agreement between the observed and predicted values, although the fact that the first measurement was at 30s meant that most of the temperature rise had occurred by this time. For mice skulls the model overestimated the temperature rise by approximately 20% compared to the measurements on old mice and approximately 75% compared to the measurements on young mice. Factors that would affect the results, but had not been included in the model were given as:

- movement of the mice increasing the effective radius of the beam;
- the thermocouple not being in intimate contact with the bone or exactly on axis;
- the fact that the heat is actually produced over a finite volume and not in a sheet;
- the difference in thermal conductivity and diffusivity of bone compared to water (water values were used throughout).

Shaw (1994) used the measured spatial intensity distributions from three transducers to calculate the temperature increase in layered media by integrating the point source solution to the BHTE. Models with both fluid paths and bone were considered although, again, the thermal properties were constant throughout the region of interest. The predictions from these models were compared with simple estimators of heating produced by the NCRP and AIUM/NEMA and will be discussed in chapter 8.

7.6 Discussion

It can be seen that, while models have been developed that can give reasonable estimates of the temperature rise in homogeneous materials, there is still much work to be done before it is possible obtain an accurate predictions of in-vivo heating. The reasons for this include the following:

- the complexity of the mathematics - analytical solutions have only been found for simplified cases;
- the uncertainty about values for quantities such as the absorption in fetal tissue;
- the difficulty of modelling perfusion.

These difficulties have been addressed in different ways. Standards bodies, who are concerned with safety issues have developed simple equations to act as predictors of worst-case heating and these will be discussed in the next chapter; while some authors, such as Ziskin (1993) have suggested that "at this point in the analysis of thermal bioeffects in diagnostic ultrasound it appears to be highly desirable to bring in the use of numerical methods". These methods can produce solutions to situations for which it is not possible to obtain analytical solution and so could allow modelling of more complex beam and tissue geometries. One such technique, finite element modelling will be discussed later in this thesis.

7.7 Chapter Summary

Techniques based on the point source solution of the BHTE have allowed the influence that a range of factors, such as the frequency and focal length of the transducer, have on temperature rise to be determined and have produced results that are in reasonable agreement with experimental values obtained for soft tissue heating. This approach has also been used to study heating in bone but there is little experimental validation of the results and when this was tried by Carstensen et al. the agreement was only good for one of the three sets of exposure conditions investigated, although there were a range of factors that could have been responsible for this. One limitation of this approach is that it assumes that the thermal properties are constant throughout the model. The finite difference method has also been used to solve the equations governing heating and, by choosing appropriate values for the tissue properties, it was possible to obtain heating predictions for bone that were in good agreement with experimental results. Accurate predictions of heating in bone have not, however, been produced without using the measurements of the temperature rise to refine the input parameters to the model.

Chapter 8

The Thermal Index.

8.1. Introduction

During the past few years there has been a move towards displaying exposure information in terms of biophysical safety indices, as opposed to in more traditional units, such as intensity (Duck, 1997). These indices aim to assist the operator in making risk/benefit decisions about the use of ultrasound. The two indices that can be found on many modern scanners are the Thermal Index (TI) and the Mechanical Index (MI). These are described in the 'Output Display Standard' (AIUM/NEMA, 1992) and their display is a requirement of the US Food and Drug Administration (FDA, 1993). The mechanical index is concerned with damage to tissue from mechanisms such as cavitation, while the thermal index aims to give an indication of the 'reasonable worst case' heating.

8.2. Thermal Index Formulae

TI is the ratio of the acoustic power exposing the tissue to the acoustic power required to raise tissue temperature by 1°C under defined conditions. There are three thermal indices: the soft tissue thermal index (TIS); the bone at focus thermal index (TIB) and the cranial thermal index (TIC). A series of formulae are given for calculating these, each one based on different assumptions about the beam path. These were summarised by Duck (1997) and are shown in table 8.1.

8.3. Assumptions Underlying the Thermal Index Formulae for Bone.

The TIB (scanned model) is based on the assumption that for scanned transducers the greatest temperature rise will occur in the soft tissue next to the transducer. This model, therefore, takes no account of the presence of bone and is based on work carried out by Curley (1993) who calculated the soft tissue temperature rise from 1400 scanned diagnostic transducers. Curley calculated the steady-state heating along the central plane of the acoustic field by integration of all the line sources of heat.

Table 8.1: Summary of the TI Formulae

TI	Target tissue	Position	Transducer type	Formula
TIB, TIS	Soft tissue and bone	At the surface	Scanned	$\frac{W_1 f}{210}$
TIS	Soft tissue	At depth	Not scanned, A>1 cm^{2*}	$\max\left[\min \frac{W_{.3} f}{210}, \frac{I_{.3} f}{210}\right]^{\dagger}$
TIB	Bone	At depth	Not scanned	$\min\left[\frac{\sqrt{W_{.3} I_{.3}}}{50}, \frac{W_{.3}}{4.4}\right]$
TIC	Bone	At the surface	All	$0.025 W \sqrt{\frac{\pi}{4A}}$

Notes:

W and $W_{.3}$ are the total and 'derated' powers in mW;

W_1 is the power through a 1 cm wide segment of the scan;

$I_{.3}$ is the peak 'derated' temporal average intensity;

f is the frequency in MHz;

A is the source area in cm^2;

*For small unscanned transducers, A < 1 cm^2, the formula for scanned transducers is used, substituting W for W_1.

†Measured at a distance from transducer greater than

$$1.5 \times \sqrt{\frac{4 \times \text{Aperture area}}{\pi}}$$

In all cases the tissue path is modelled as a homogeneous structure which attenuates tissue at a rate of 0.3 dB cm^{-1} MHz^{-1}.

The acoustic output per unit scan length (i.e. along the length of the transducer) sufficient to cause at 1°C temperature rise at the surface was given by:

$$\frac{W_{deg}}{X} = \frac{210 \text{ mW MHz cm}^{-2}}{f}$$

where W_{deg} is the power required to generate a 1°C temperature rise and X is the length of the transducer face over which it is emitting power. There was no noticeable dependence of surface temperature on

transducer width. If the power for the central centimetre of the aperture is used this then gives the quoted formula.

The TIB for unscanned modes and the TIC are based on the heated disc model that has already been discussed. For the TIB the following assumptions are made:

- the combined effects of reflection, transmission and perfusion reduce the effective energy absorbed by the bone to 50% of the incident value;
- the absorption coefficient of bone is such that the energy is absorbed very close to the surface;
- tissue overlying the bone attenuates at a rate of 0.3 dB $cm^{-1}MHz^{-1}$;
- the perfusion rate is low, with a perfusion length (L) of 1 cm;

The figure of 50% is based on the experimental and theoretical data on the temperature rise in mouse skulls obtained by Carstensen et al. (1990) in which it was assumed that 60% of the incident energy was absorbed in the bone. If these assumptions are put into the heated disc model and the number 'rounded off' then the power (in mW) needed raise the temperature by one degree is given by the formula:

$$W_{deg} = 40d \text{ mW} \qquad \text{(Equation 8.1)}$$

where d is the beam diameter given in centimetres.
This equation, combined with the definition of the thermal index, gives the TIC.

For the TIB the derivation is taken further by relating the power and peak intensity to the beam diameter. For a 'top hat' distribution the following relationship is used:

$$W = \frac{\pi d^2}{4} I_{ta}$$

where I_{ta} is the temporal average intensity but the relationship is different for other distributions, such as a Gaussian beam. For simplicity the 'top hat' formula is assumed and an equivalent diameter of 1.1d is used in the calculations. If these assumptions are combined with the one stating that the temperature rise will be greatest at the point at which the derated intensity is greatest and numbers are 'rounded off' the first term

in the TIB equation is obtained. The second term comes from the assumption that the minimum effective beam width is 1 mm.

It should be noted that there is another, slightly different, definition of the thermal index laid out in NCRP report 113 (1992). This version of the TI is defined in terms of whether or not a fetus is being insonated, and if it is, in which trimester is the pregnancy. For second and third trimester examinations the thermal index is basically the same as the AIUM TIB (unscanned). The most significant difference between the two versions is the assumptions made about the attenuation of the beam in maternal tissue. The NCRP TI agrees with the AIUM version as far as the point which states that W_{deg} = 40d but then it uses a fixed path attenuation model to account for losses in maternal tissue. This assumes an attenuation factor (A) of 0.75 dB MHz^{-1} in second trimester and 0.5 dB MHz^{-1} in third trimester. The NCRP version of the TI formula is therefore:

$$TI = \frac{W_0}{4d.10^{Af/10}}$$

8.4. Comparison of Thermal Index with Observed Heating.

A series of phantoms have been developed at the University of Vermont that allow the thermal index to be compared to experimental measurements of heating. O'Neill at al (1994) used phantoms which consisted of compact bone, either human or cow, embedded in tissue mimicking material (TMM). The TMM was made so that it had an attenuation coefficient of 0.3 dB $cm^{-1}MHz^{-1}$ in keeping with the assumptions behind the AIUM definition of the TI and the bone was placed 2.22 cm from the transducer, a distance approximately equal to the radius of curvature of the transducers used. The bone samples varied in size but were between 1.4 - 1.6 cm thick. Heating measurements were carried out and the values obtained were compared to predictions from a slightly modified version of the thermal index. This used the TIC formula but derated the power in the beam by 0.3 dB $cm^{-1}MHz^{-1}$ to predict the upper limit to the temperature rise, ΔT_{lim}. At 3.5 MHz ΔT_{lim} was 9.6°C and the observed heating 6.9°C while at 5 MHz ΔT_{lim} was 13°C and a temperature rise of 9.9°C was observed. As the thermal index is meant to

give a worse case estimate of heating the predicted values were seen as reasonable.

Wu et al. (1994) developed a transcranial phantom along similar lines but with the bone 0.5 cm below the surface of the phantom. When heating measurements were carried with only a thin layer of water between the transducer and the phantom and the result compared with those from the TIC formula the measured temperature rises were much higher than the predictions. The observed temperature rises fell, however, when a thicker (> 1cm) layer of water separated the transducer from the phantom. This difference was ascribed to the transducer heating up and, when this was allowed for in the model, there was closer agreement between the TI and the observed heating, although the TI still underestimated the observed temperature rise by amounts ranging from 7 - 51%.

Although these papers give some indication about how the TI values compare with those that occur in practice they do have limitations. Neither phantom can reproduce perfusion and this has been shown to influence heating. Also, although the cranial phantom is using an appropriate piece of bone, human temporal bone, the phantoms used to study the TIB formula contained compact bone. This may not be appropriate for looking at bone heating in a fetus as, as has already been discussed, it may have properties very different to those of fetal bone. O'Neill reports that measurements were carried out on cancellous bone but the results were not as consistent as for the compact bone. It is suggested that, according to preliminary tests, the temperature rise could be higher for cancellous bone than for compact bone.

The TIB for the beam from the single element transducer used in the bone heating measurements described in Chapter 5 was 0.5°C. The definition of the TIB, however, includes the derating factor which is to account for attenuation of the beam as is passes through soft tissue; this was not applicable to the experimental set-up used. When this factor was removed a value of 3.1°C was obtained, compared to a maximum measured temperature rise of 1.8°C.

In order to determine how the TIB compares with other observations of bone heating calculations were carried out using the data given in the literature. This included work on animal fetal bone (Bosward et al., 1993; Duggan et al., 1995) and mice skull (Carstensen et al., 1990). It is not

possible to apply the formula directly, however, as in these measurements the ultrasound was incident directly on the bone and so was not attenuated by overlying tissue, as is assumed in the TIB. Another complication is that the papers quote the beam parameters at the bone surface and these do not necessarily correspond to the focus of the beam. In order to carry out a comparison it was necessary, therefore, to define a simplified version of the TI that did not contain a derating factor and used the data that are available in all the papers. $TI_{adapted}$ is given by:

$$TI_{adapted} = W/44d,$$

where:

W = power incident on transducer surface;

d = -6 dB beam diameter (cm) .

This relies on Equation 8.1; the formula giving W_{deg}, the power needed to generate one degree temperature rise, but includes the factor of 1.1 used in the AIUM/NEMA TIB to allow for different intensity distributions. The $TI_{adapted}$ is the ratio of the actual power to this 'one degree' power. The assumption behind this index, that the power needed to raise the temperature by one degree equals 44d, is also at the heart of the TIB and so if there is a significant mismatch between these values and the experimental ones it is unlikely that the TIB will be a good predictor of heating. The ratio of measured maximum temperature rise to $TI_{adapted}$ is shown in figure 8.1. It should be noted that the measured values are not necessarily at steady state, although by inspection of the graphs, they do not appear to be far from the steady-state values.

The markers on the right-hand side the graph are for studies using either fetal bone or substitutes for it while those on the left represent mature bone. In studies which investigated the variation of heating with gestational age the results from the oldest specimens have been used. It can be seen that for fetal bone the TI tends to overestimate the temperature rise by a larger degree than is the case for mature bone and that, in all but one case, the predicted temperature rise is less than that observed. The exception to this seems to be the Carstensen data for 'old' mice which was used in the derivation of the TI. While these mice had thin skull bones, approximately 0.5 mm, they are probably composed of mature bone and so, as the authors of the paper state, 'should be a conservative model of the fetal skull'.

Figure 8.1: Ratio of Observed Heating to Thermal Index (adapted).

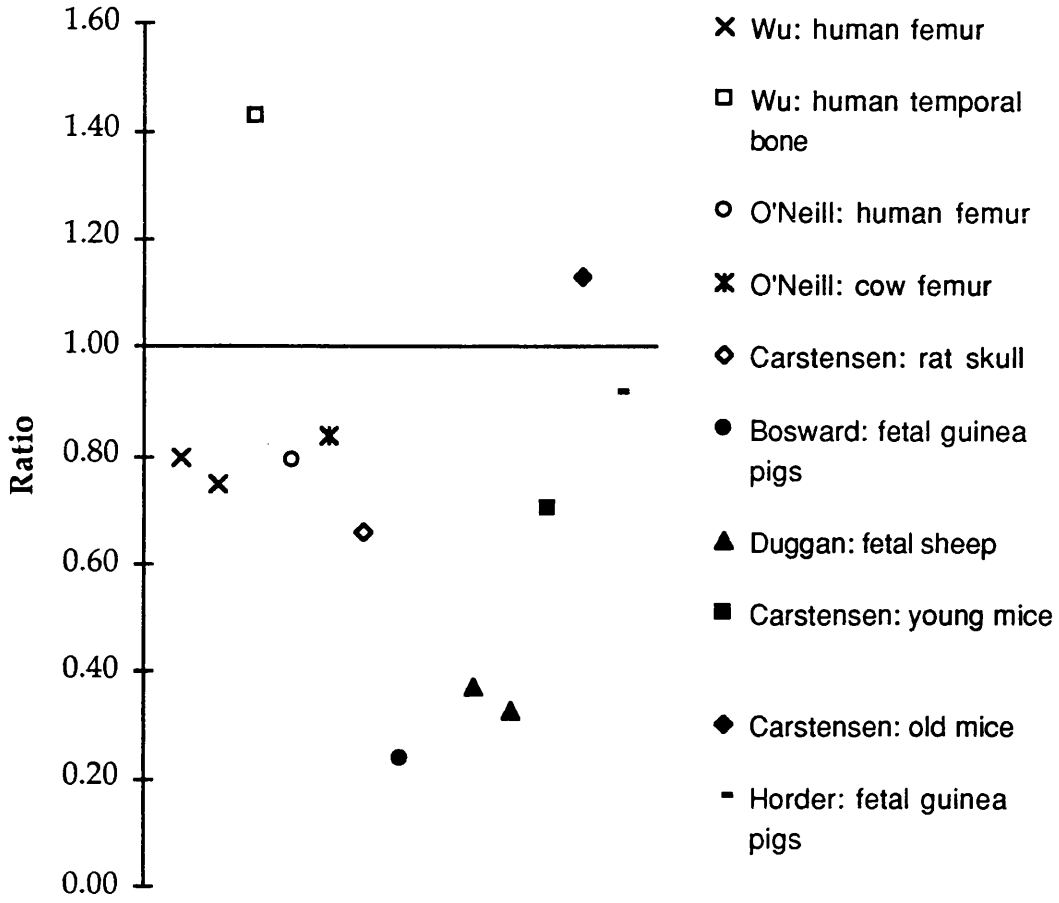

8.5. Use of the Thermal Index to Predict Heating.

Since the publication of the NCRP and AIUM reports various authors have used the thermal index, combined with output data from diagnostic scanners, to estimate the maximum likely temperature rise. Bly, Vlahovich, Mabee and Hussey (1992) used the data on ultrasound field parameters obtained from manufacturers to estimate heating of fetal tissue during pulsed doppler examinations. The NCRP definition of the TI was used. For second and third trimesters, where bone is the target tissue, the majority of systems had TI values of less than 4 although the maximum values found were 7.1 using the second trimester formula and 8.7 using the third. These maximum values came from systems which the manufacturers submissions claimed were intended for peripheral vascular or cardiac use. Patton et al. (1994) compared a 'worst-case' model for fetal exposure with the AIUM TIB. This 'worst-case' model, giving

Table 8.2: Thermal index and 'worst-case' heating values.

	ΔT_{lim} range (K)	TIB range	ΔT_{lim} mean (K)	TIB mean
General imaging	0.0 - 1.6	0.0 - 1.4	0.29	0.21
Pulsed Doppler	0.04 - 5.9	0.03 - 2.8	1.3	0.87

ΔT_{lim}, was effectively the NCRP TI with a fixed path attenuation of 1 dB/MHz. The results are summarised in table 8.2. It can be seen that the maximum value for ΔT_{lim} in pulsed Doppler mode exceeds the 4 K value which the WFUMB state should be considered potentially hazardous if sustained for 5 minutes. The maximum TIB does not predict this level of temperature rise, however. In approximately 75% of cases the TIB was within a factor or two of the corresponding worst-case value (i.e. worst-case < 2TIB). When ΔT_{lim}/TIB exceeded two, it was due mainly to the fact that the transducers had long focal lengths and so the AIUM derating factor was large.

Shaw (1994) used the same adaptation of the NCRP thermal index in his paper on the prediction of temperature rise in layered media. The measured spatial intensity data from three unscanned transducers was used as input to an integral solution of the BHTE. Calculations were performed for a series of layered models in which the acoustic properties of each layer reflected the assumptions behind the various models, for example the AIUM model consisted of a homogeneous material with attenuation coefficient 0.3 dB MHz^{-1} cm^{-1}. The results from the models were then compared with the NCRP and AIUM thermal indices. Cases were found in which the indices over and underestimated the results from the more complex models depending upon the degree of transducer focusing. There was found to be quite good agreement between the simple predictions and the results for the more weakly focused transducer at the distance implied by the simple algorithm, i.e. the position at which the TIB expression is a maximum, but this was not necessarily the position of the maximum temperature rise. The agreement was less good for the strongly focused transducer and the non-cylindrically symmetric transducer. The ratio of the NCRP to the AIUM TIB predictions varied from 0.95 to 2.2.

8.5. Discussion

The Output Display Standard, and with it the display when appropriate of the TI, has now been implemented by most, if not all, manufacturers of ultrasound scanners (Duck, 1997). While this gives the user access to safety information of which they may previously have been unaware, it is important that the limitations of this information are known.

This chapter has looked, in most detail, at the TIB applicable to stationary beams and the results presented in Figure 8.1 suggest that the relationship between beam diameter, acoustic power incident on the bone and temperature that is at the heart of this index gives a reasonable worst-case estimate of the temperature rise in mature bone. For fetal bone the TI can, in some instances, overestimate the temperature rise by a factor of two or more but the fact that the temperature rise in fetal bone increases with gestational age, means that unless the TI were made much more complex it may be difficult to avoid this. There is relatively little experimental work validating the TI as a whole, i.e. including the derating factor and it appears that in some cases this factor can be a source of error. The estimates of attenuation in maternal tissue, discussed in chapter 6, showed that the derating factor in the TIB may not always give a conservative estimate of exposure and the calculations of Patton et al. shown in Table 8.2 suggest that this may lead to the temperature rise predicted by the TIB being, in some cases, more than a factor of two less than that obtained using a fixed-path model for attenuation.

The way in which the intensity measurements, upon which the calculation of TI is based, are performed could also lead to errors. These measurements are carried out in water and it is known that non-linear propagation of ultrasound can occur at diagnostic intensities (Baker, 1991). This effect could lead to excess attenuation in the water bath measurements and so cause the temperature rise in tissue to be underestimated. Christopher and Carstensen (1996) found that ignoring non-linear propagation led to underestimates of the tissue temperature rise that were typically less than 40%.

Another factor that also needs to be addressed is the basic premise upon which the TIB for scanned transducers is based. This is that the maximum temperature rise occurs at the surface and is due to soft tissue

heating. This has not been proven and there is need for work to be carried out to investigate whether this is, in fact, always the case.

Clearly, while the TI gives an indication as to whether caution needs to be exercised when using a particular set of operating conditions, it does not tell the full story of bone heating and there is much work still to be done.

8.6. Chapter Summary

The Thermal Index, as defined in the 'Output Display Standard' is now commonly displayed on ultrasound scanners. The formula used to calculate the TI depends upon the structure being insonated and upon whether the ultrasound beam in scanned or stationary. The TIB (unscanned) is the formula appropriate to the situation where bone is in the focal region of the ultrasound beam as may occur, for example, during pulsed Doppler examination of a third trimester fetus. It appears that the part of this formula that relates the temperature rise to the beam diameter and power incident on the bone gives a reasonable worst-case estimate for mature bone and generally overestimates the temperature rise for fetal bone. The part of the formula that models attenuation of the beam can, however, lead to an underestimate of the power reaching the fetus. It is also possible that non-linear propagation may lead to excessive absorption of the beam when measurements are made in water and this, too, could lead to the power at the fetus being underestimated. The TIB corresponding to the scanned case is in need of experimental verification.

Chapter 9

Application of the Heated Disc Model to Bone Heating

9.1. Introduction

It has been shown that there is considerable uncertainty about the thermal and acoustic properties of bone. This affects our ability to obtain accurate predictions of temperature rise and so, in order to study the degree to which the uncertainty in the properties affects the calculations, a simple heated disc program was implemented. This considered a homogeneous region of tissue, with boundaries at infinity, and calculated the temperature increase on-axis caused by an ultrasound beam of constant diameter undergoing exponential decay due to absorption. This is illustrated in Figure 9.1a. The temperature rise at a point due to the contributions from all points in the beam path was calculated by integrating the point source solution to the BHTE (Eq. 7.4). The procedure for doing this was as follows:

- for one plane integrate over all points that are a distance r from the beam axis, to obtain the temperature rise due to a ring;
- integrate the solution from all rings between r = 0 and r = beam radius, to obtain solution for a disc;
- integrate the solution from all discs in the volume of interest.

It was assumed that all the energy lost from the beam is converted into heat, giving $q = 2\alpha I$. A top hat intensity distribution was assumed, i.e. the intensity was constant within a circular area defined by the -6 dB beam diameter and zero outside. This is simple to implement and was shown by Carstensen et al. (1990) to produce results that are comparable with more realistic intensity distributions. The diameter of the beam was assumed to be constant. A series of programs were written to perform these calculations using the commercial software package called Matlab; examples of these programs are shown in appendix A. The integrals were carried out numerically with the tolerance set at 0.1%.

Figure 9.1a: Heated disc model.

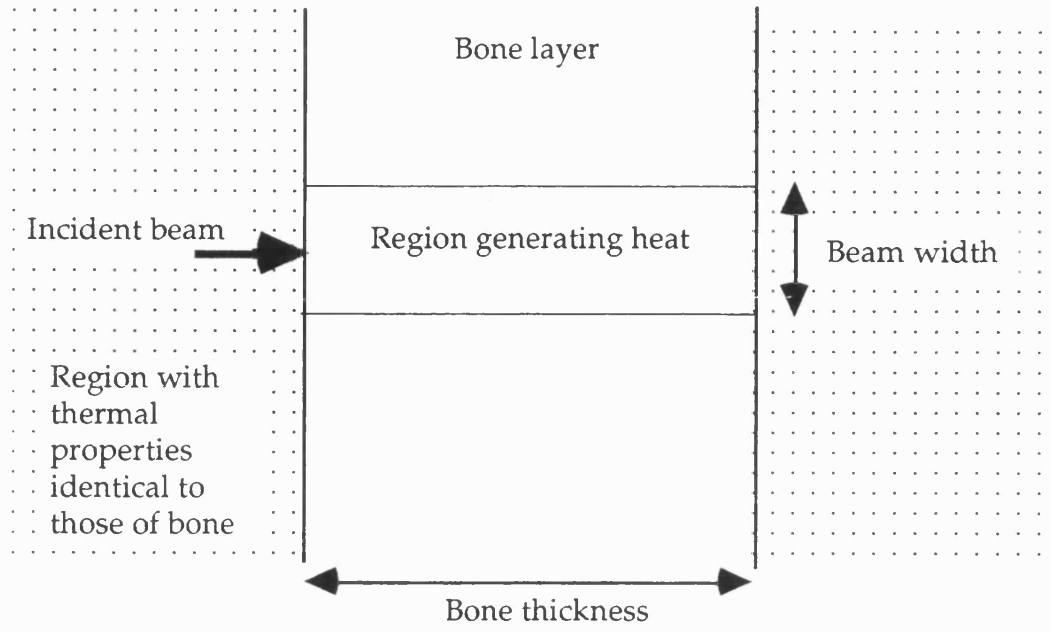

Figure 9.1b: Model used in NCRP report.

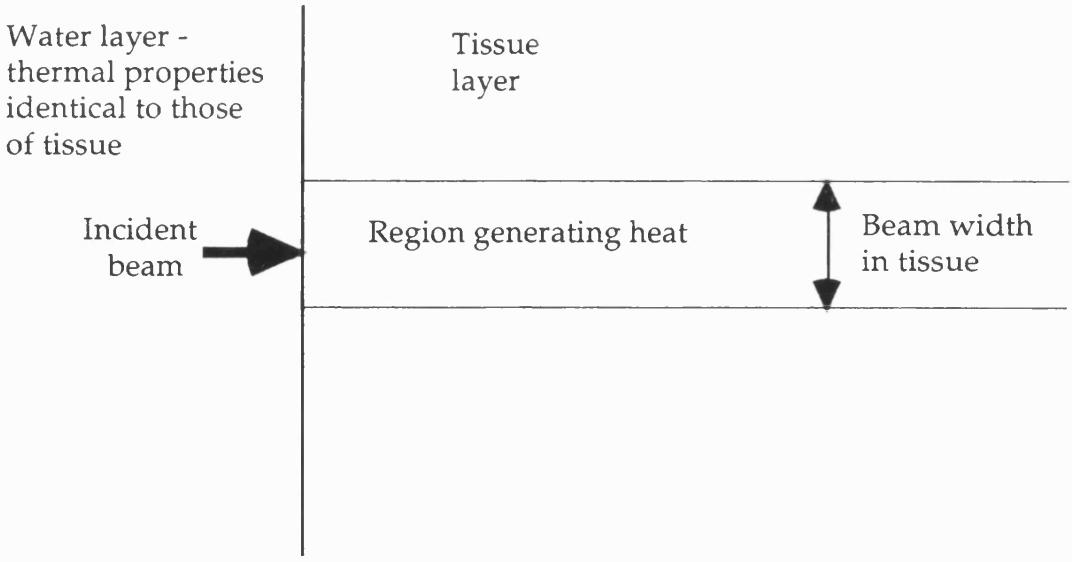

9.2 Validating the Model

The programs were validated by comparing the results with a two-layer model discussed in NCRP Report No. 113 (1992). This model (W2 in table 5.4 of the report) considers an ultrasound beam which passes first through a homogenous, water-like, non-absorbing medium and then into tissue. This is illustrated in Figure 9.1b. The width of the beam within the tissue, which is given, is constant and the model assumes a top hat intensity

distribution. The attenuation coefficient of the tissue is given as 0.05 Np cm^{-1} MHz^{-1}, a value appropriate to soft tissue, and the other acoustic and thermal properties of the material are stated. The tissue parameters are constant throughout the model and if the same values are used in this and the Matlab program both models should be equivalent. The NCRP model was used in the report to estimate the minimum power required to generate a steady-state temperature rise of 1 K. This made the assumption that the maximum temperature rise was twice that at the boundary and so, if the power level stated in the table generated a maximum temperature rise of 1 K, it heated the boundary by 0.5 K. In order to compare the results from this and the Matlab program the temperature rise generated at the tissue boundary by a 100 mW beam was calculated. If W_{deg} is the power in mW which the NCRP report states will cause a temperature rise of 1 K, the temperature rise at the boundary for a 100 mW beam should be $(100/W_{deg}) \times 0.5$ The thickness of the tissue layer in the Matlab program was set to 100 cm. The value used in the NCRP model is not stated; it was only said to be much larger than the perfusion length, L, which is 1.2 cm. The results obtained when the comparison was performed for a range of values of beam width and frequency are shown in Table 9.1.

Table 9.1: Comparison of Heated Disc model with NCRP model.

Frequency (MHz)	Beam width (mm)	Temperature Rise (K)	
		NCRP model	Matlab program
3	3.5	0.89	0.91
5	2.1	1.7	1.7
7.5	1.4	2.9	2.8
10	1.05	3.9	4.0

It can be seen that in all cases the results agreed to within 4%. This was thought to be acceptable as this error was comparable to that in the power values in the NCRP report, due to the fact that only two significant figures were quoted.

9.2. Beam Parameters used to Model Bone

In was decided to use as input data for the model the beam parameters that had been used for most of the heating measurements described in Chapter 5. These are shown in Table 9.2.

Table 9.2: Default Values used in Modelling

Acoustic Power	50 mW
Beam diameter	3 mm
Frequency	3.5 MHz

While, at one level, the choice was unimportant as the aim was to see the degree to which the input values affected the results, using these values ensured that the output values were of the right order of magnitude. Unless stated otherwise, it was assumed that the layer of bone was 1 cm thick, as this was in the middle of the range of thicknesses of the bone samples studied in Chapter 5. The perfusion constant was set to 10^6 in order to describe a situation in which there was, effectively, no perfusion.

9.3. Influence of Thermal Parameters

As has already been discussed the thermal properties of bone are poorly defined and so it was decided to study the difference in result obtained when using a set of values from each end of the central range, i.e. what remains when the outliers are excluded. The values used were those quoted for human cancellous bone by Biyikli (1986) and by Sekins and Emery (1983); this latter set being the values given in the NCRP report 113 (1992). These are shown in Table 9.3, together with the values quoted by the NCRP for liver which are often used as 'typical' soft tissue values. These data are for adult bone as data for fetal bone are not available. For both sets of thermal data the value of the absorption coefficient was taken as 1.5 Np cm^{-1}. This is at the bottom end of the range of values quoted in Table 3.5 and so seemed an appropriate estimate for fetal bone. The predicted temperature rise against time at the front of a 10 mm thick layer of bone are shown in Figure 9.2.

Table 9.3: Bone Tissue Parameters

	NCRP	Biyikli	NCRP liver
Thermal Conductivity (W m^{-1} K^{-1})	0.58	0.3	0.57
Specific Heat (J kg^{-1} K^{-1})	1600	2200	3600
Thermal Diffusivity (mm^2s^{-1})	0.28	0.11	0.15
Density (kg m^{-3})	1300	1100	1050

Figure 9.2: Rate of Heating for Biyikli and NCRP Values.

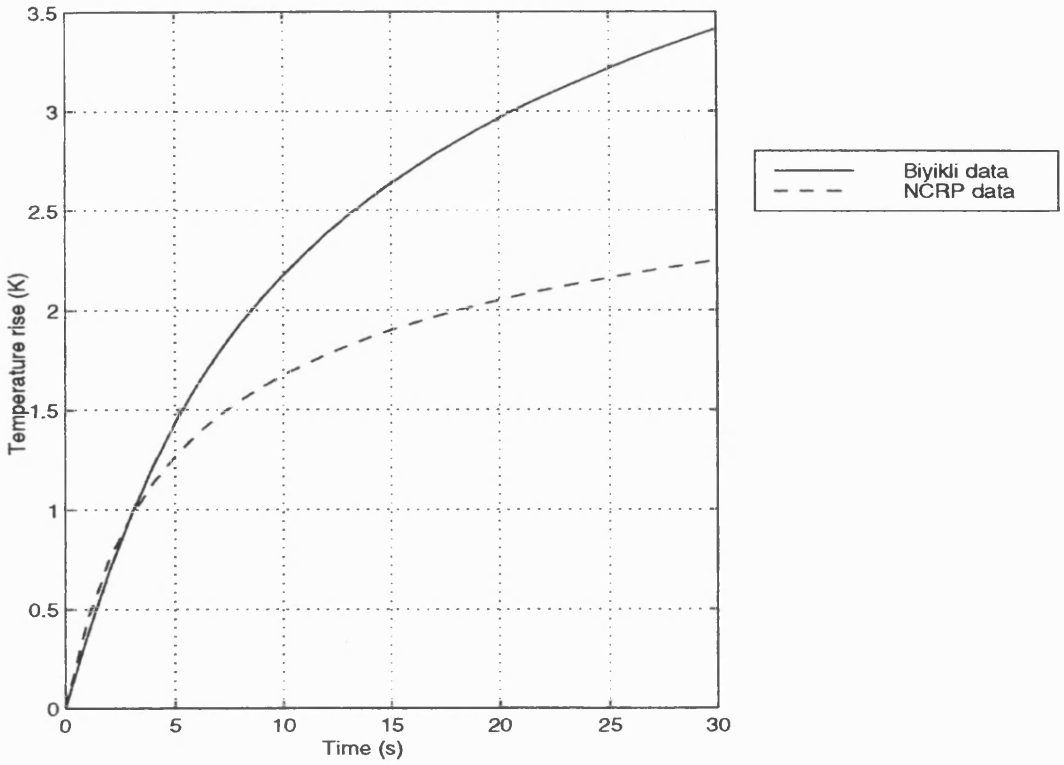

It can be seen from this that the temperature rise at 30 s using the Biyikli data is 50% greater than that predicted using the NCRP data. This model, however, is based on an infinite region in which the thermal properties are constant. In practice the bone is likely to be surrounded by soft tissue and so the temperature rise will depend not only on the thermal properties of the bone but also on the properties of the soft tissue.

9.4. Influence of Absorption Coefficient

Another important factor which does not have a well defined value is the absorption coefficient. For adult bone a range of values have been obtained from measurements made at, or close to, 3.5 MHz. A lower limit for the absorption at this frequency would appear to be around 1.5 Np cm^{-1} while the value suggested in the NCRP report of 1.5 Np cm^{-1} MHz^{-1} gives a values at 3.5 MHz of 5.25 Np cm^{-1}, which seems to be higher than any of the values measured directly. The variation in temperature at the front of the absorber after 300 s insonation was determined over this range using both the NCRP and Biyikli thermal values. The results are shown in Figure 9.3.

Figure 9.3: Effect of Absorption Coefficient on Temperature Rise at 300 s.

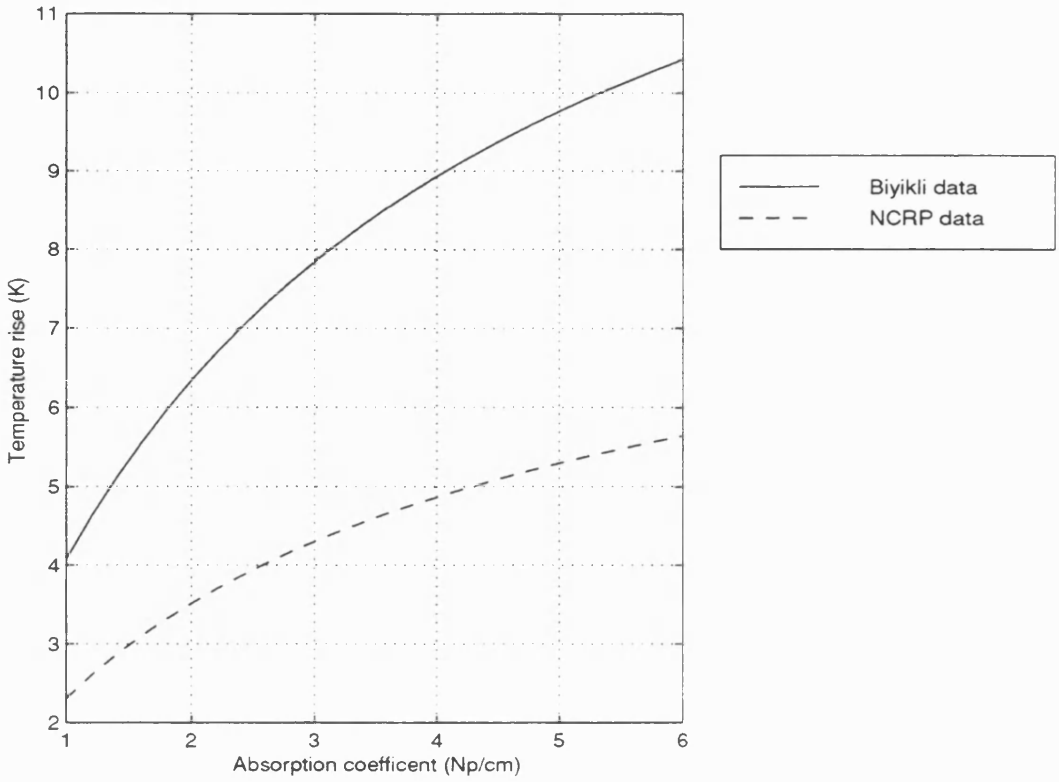

Not surprisingly the absorption coefficient plays an important part in determining the temperature rise. For both sets of thermal values changing the coefficient over the described range changes the temperature rise by a factor of over two. It is not clear, however, how to relate these results to fetal bone which may be closer to cancellous bone than to the compact form. Most of the data available are for adult compact bone and it has been suggested that cancellous bone may experience a larger temperature rise (O'Neill, et al., 1994). Fry and Barger (1978), however, found that infant skull had a smaller absorption coefficient than adult compact bone and so would be expected to heat less.

The influence of absorption coefficient on a thin absorber (1 mm thick) was also studied and it was found that whereas for the 1 cm thick absorber the range of absorption values changed the predicted temperature rise by a factor of approximately 2.5, for the thinner absorber the factor was nearly 4.

Figure 9.4: Effect of Absorption Coefficient on Temperature rise at 300 s in 1 mm thick absorber.

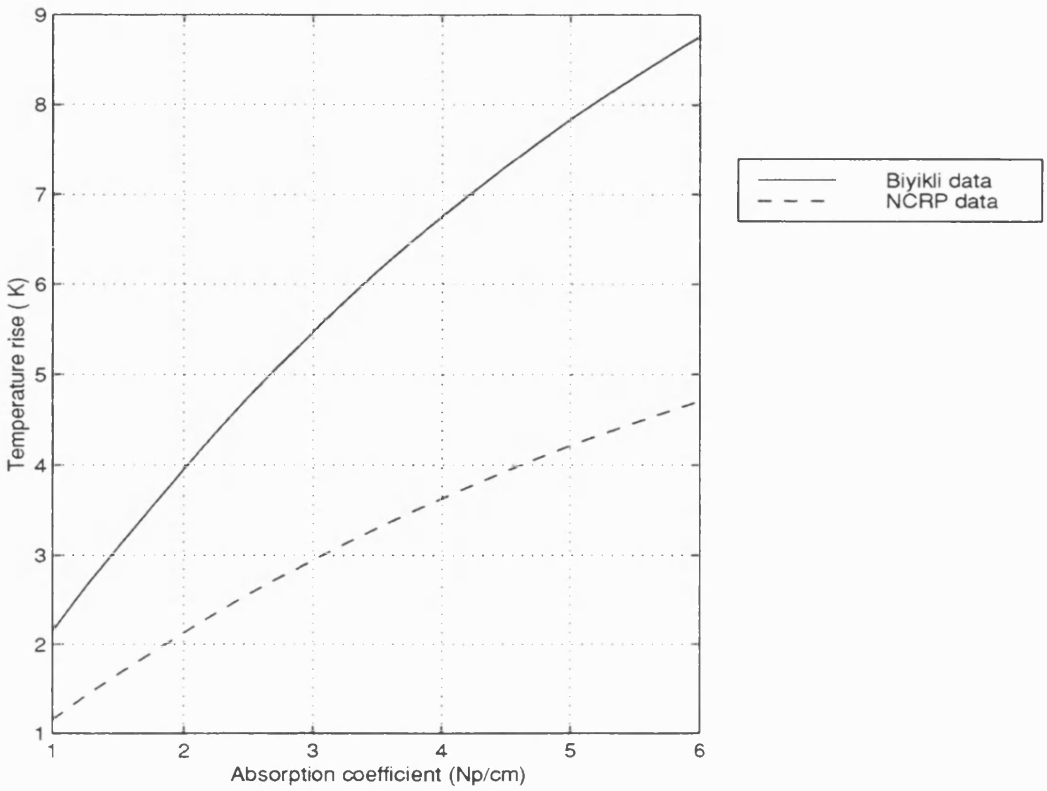

9.5. Influence of Bone Thickness.

It can be seen, from the above, that the bone thickness influences the temperature rise and so this was investigated further. The temperature rise for a range of thicknesses was calculated for both sets of parameters. An absorption coefficient of 1.5 Np cm^{-1} was used. The results are shown in Figure 9.5.

The importance of this graph becomes clear when it is recalled that the thickness of the occipital bone, the thickest skull bone, is only 0.3 mm at 4 - 5 months gestation (Ohtsuki, 1977) and grows to approximately 1.6 mm towards term. This increase in thickness leads to a doubling of the predicted temperature rise.

Figure 9.5: Variation of Temperature Rise with Bone Thickness.

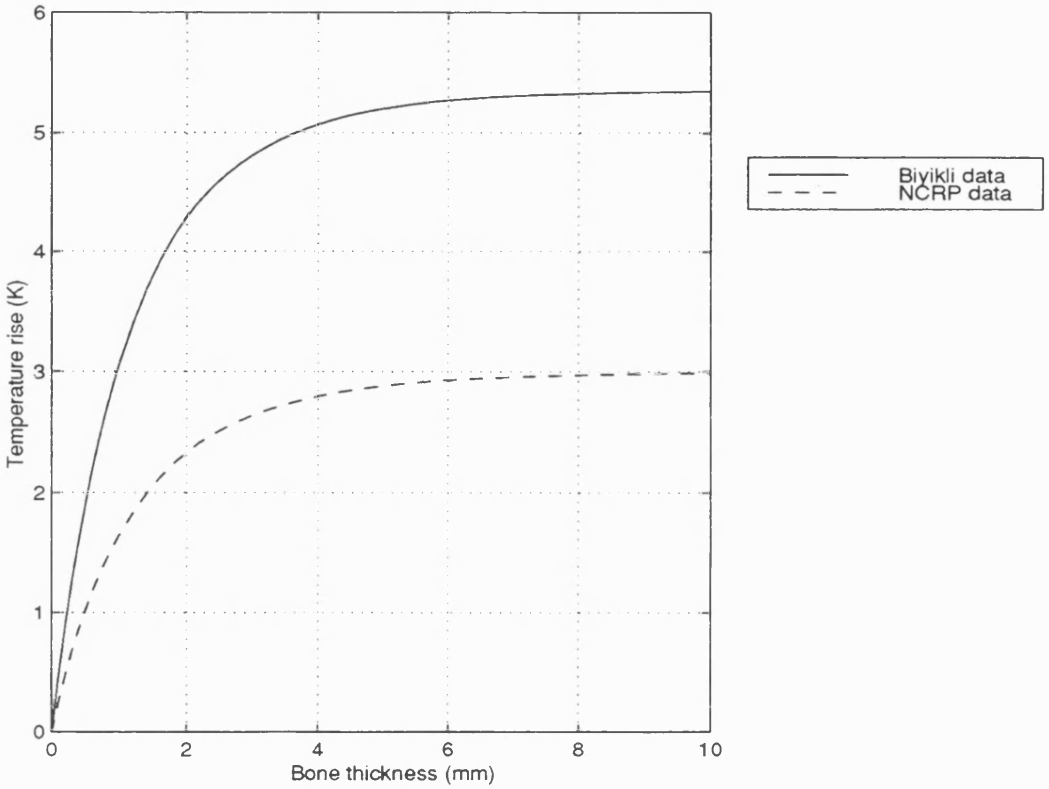

9.6. Temperature Rise Inside Bone

Although the measurements carried out in this study were all at the bone surface the heated disc model can predict the temperature rise inside a layer of bone. This was done using both sets of thermal parameters and for two values of the absorption coefficient: 1.5 Np cm^{-1} and 5.25 Np cm^{-1}. Figure 9.6 shows the temperature rise at 300 s in the front 5 mm of a 10 mm thick absorber. In all cases the maximum temperature rise was inside the bone between 0.5 and 1.5 mm from the surface. The difference between the maximum temperature rise and that at the surface was greatest for the lower value of absorption coefficient using the Biyikli thermal data; under these conditions the surface temperature rise was 75% of the maximum value.

Figure 9.6: Temperature rise inside absorber at 300 s.

a) Absorption coefficient: 1.5 Np cm^{-1}

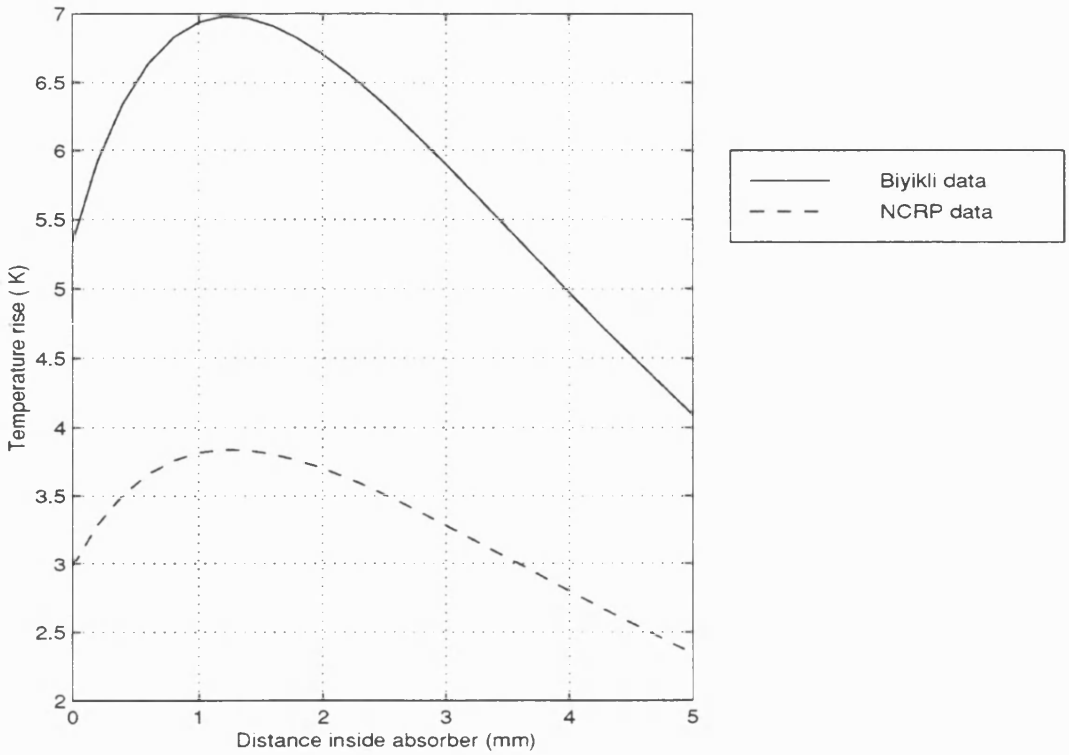

b) Absorption coefficient: 5.25 Np cm^{-1}

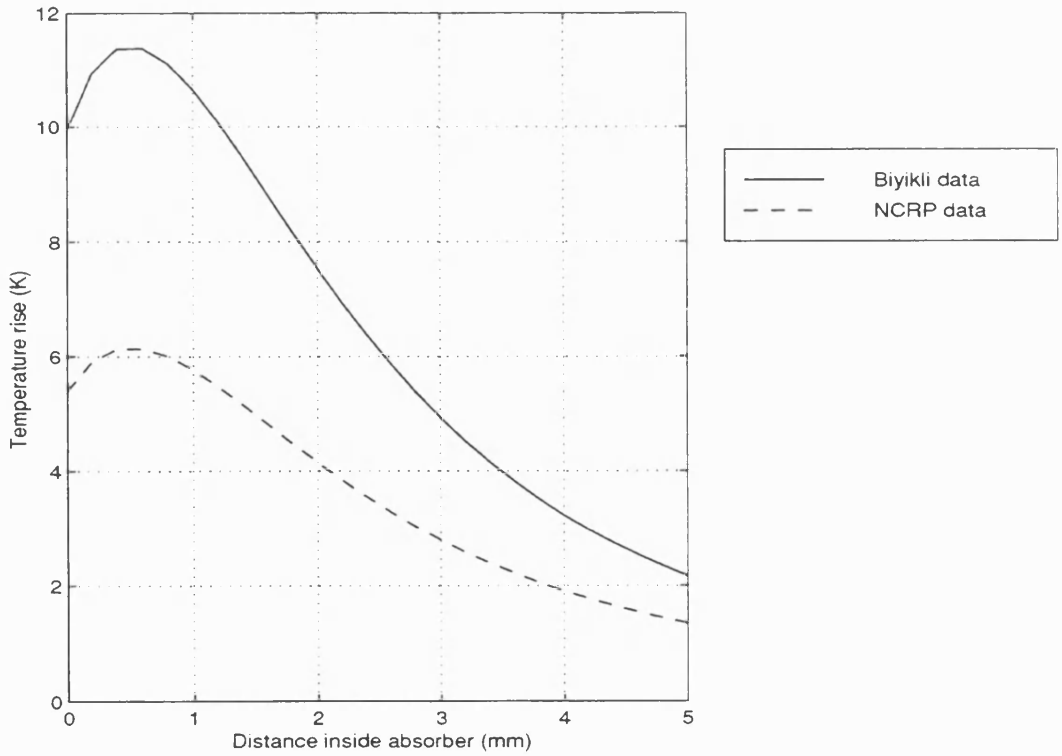

9.7. Discussion

It can be seen that a variation in the input parameters to the model leads to a large variation in the predicted temperature rise. The uncertainty about the correct choice of input values for the following parameters can lead to an uncertainty of at least 50% in the temperature rise:

- thermal properties of bone;
- bone thickness;
- absorption coefficient.

While the heated disc method may make these more significant than they would be in a layered model, where the properties of other layers might mitigate the effect, the size of the uncertainties suggests that they are unlikely to be reduced to an insignificant level. The situation is further complicated by the fact that the effect of changing one parameter by a known amount depends upon the value of the others. So, for example, changing the absorption coefficient from 1.5 to 5.25 Np cm^{-1} changes the result by a factor of 2.5 in a 1 cm layer of bone but by nearly 4 in a 1mm layer. From the point source solution to the BHTE it is clear that uncertainties in parameters such as the thermal conductivity are going to be highly significant, as this value multiplies the rest of the solution. Analytical solutions are not available however for the error due to the absorption coefficient and this will depend upon the limits of integration. This means that the most straightforward way of estimating the errors is to create models with input values over the range of interest. This will have to considered when layered models are produced.

While the heated disc model has proven useful in examining how our uncertainty of the properties of bone affects predictions of heating it does have limitations. These include that fact that any model can only use one set of thermal parameters. This will lead to errors when modelling layers of tissue in which the thermal properties differ. The heated disc approach also makes the assumption that heat loss is due only to conduction and so it is not possible to impose, for example, convective boundary conditions. The affect of these limitations will clearly depend

upon the degree to which the situation being modelled needs to be simplified. It may be that, if the values given by Biyikli for bone are correct and bone has a thermal conductivity that is approximately half that of soft tissue, they cause significant errors when the heated disc model is used for bone surrounded by soft tissue. This will be examined in Chapter 11 when heated disc and finite element models of the same structure are compared.

9.8 Chapter Summary

A heated disc model has been implemented in order that the influence of a range of parameters on the temperature rise in bone might be determined. This has shown that our current uncertainty about the thermal properties and the absorption coefficient of fetal bone lead to uncertainties of at least 50% in the predicted temperature rise. It has also been shown that the maximum temperature occurs inside the bone and the temperature rise at the surface may only be 75% of the maximum value. For bone layers less than 4 mm thick the temperature rise varies significantly with bone thickness and this should be taken into account when modelling fetal skull.

Chapter 10

The Finite Element Technique

10.1. Numerical Modelling Techniques

The previous chapters have discussed a variety of techniques used to estimate the temperature rise in an ultrasound beam. Many of these use the point source solution of the BHTE and so have only been able to use one set of thermal parameters. The solutions have also made use of symmetry to reduce the complexity of the problem and so have analysed relatively simple geometries, e.g. those with cylindrical symmetry. One way of overcoming these limitations is to adopt numerical modelling techniques, as 'these will permit a more precise determination of surface and focal heating effects and will allow a more general evaluation of fixed path models especially for the fetal bone case.' (Ziskin & Lewin, 1993). Two numerical approaches commonly used to model heat transfer are the finite difference method and the finite element method, both of which produce approximate solutions to differential equations. In the finite difference method the continuous domain is replaced by a mesh of discrete points and the temperature rise is calculated at these points. The partial derivatives in the differential equation are approximated using terms in a Taylor's series expansion and so the problem is reduced to solving a set of linear equations. In finite element modelling (FEM) the region of interest is divided into a series of elements, each of which has a function relating the temperature at any point within it to that at certain points called nodes. Within an element the variation in temperature may, for example, be linear while over the whole of the region the distribution may be far more complex. The functions used to predict the temperature at points between the nodes are generally polynomials and these form part of the formulation of the problem. The solution technique finds the temperature at the nodes and then the polynomials can be used to obtain the value at any other point. The theory behind the finite element technique is described in appendix B.

The finite difference technique has been used successfully to model ultrasound heating in layered tissues (Chan et al., 1973). However, if a range of geometries is being considered finite element techniques are more suitable (Lapidus & Pinder, 1982; Thomas, 1992). The disadvantage

of the finite difference technique is that in order to model tissue inhomogenities or complex contours very small grid sizes have to be used, whereas the use of, for example, triangular elements in FEM allows these models to represent the complex contours of the body more easily (Chatterjee & Adams, 1994). FEM also has the advantage that as soon as the results at the nodes are obtained the solution is available at all points in the model whereas the finite difference model is strictly discrete, giving only the solution at the nodes, and additional calculations are needed to obtain the solutions at points between the nodes. The price paid for this advantage is that the relatively large amount of algebra associated with the discretization process in FEM (Shih & Chen, 1983; Paulsen, Jia & Sullivan, 1993).

It was decided to investigate the finite element technique as it was hoped to model both bone mimicking material and fetal vertebrae and the ability of FEM to easily adapt to structures of different shapes would seem to make it well suited to this.

10.2. Use of the Finite Element Technique to Model Tissue Heating.

FEM has been used to model the temperature rise produced in tissue by a range of heat sources. Kagawa, Takeuchi and Yamabuchi (1986) produced a 2-D model of a simplified cross-section of the human body undergoing ultrasound hyperthermia. Both the acoustic wave field and the temperature distribution were obtained using finite element techniques. This study modelled ultrasound of frequency 100 kHz, lower than that usually used in hyperthermia, as this gave a longer wavelength and hence allowed for a coarser mesh and reduced computational time. This model was used to study the effect of perfusion and of phase differences between the three transducers used. The results were said to 'look promising'. No comparison was made with experimental results however. It should be noted that this paper is over 10 years old and so the limitations on mesh size imposed by the 'prohibitive computation time' may not apply now.

FEM has also been used to help determine the accuracy of simpler techniques used in microwave hyperthermia. Wong, Mechling, Jones and Strohbehn (1988) developed FE models which included various patterns of tumour perfusion and then investigated how the values of

specific absorption rate and blood flow predicted by the established methods compared with the 'true' values from the FE model. Clegg, Samulski, Murphy, Rosner and Dewhirst (1994) used FEM to produce known temperature distributions and then studied the sensitivity of the SPE algorithm, which is used in hyperthermia to reconstruct the temperature distribution, to errors in its input data, specifically the perfusion function. Both these papers used a two dimensional finite element model. Paulsen, Jia and Sullivan (1993) demonstrated that a three dimensional anatomically conforming model for hyperthermia treatment analysis could be implemented on a workstation and suggested this technique as a practical alternative to finite difference time domain computations. Chatterjee and Adams (1994) used a commercially available finite element package, ANSYS, to model microwave hyperthermia treatment. They produced a 2-D model of the prostate region based on data from a CT scan. The main disadvantage, noted by the authors, was the absence of a term to include perfusion. This was overcome however by using the heat convection term. More recently Shaw, Preston & Bacon (1996) have proposed a method of calculating the perfused temperature at any time given the unperfused temperature history and the perfusion time constant, τ. This could also be used to include perfusion in models such as this.

FEM has also been used in other areas where it is important to know about the temperature rise in tissue. Diller and Hayes (1983) studied burn injury resulting from the application of a hot cylinder to the skin surface. One advantage of FEM for this situation was that a range of element sizes could be used, making it possible to have a high concentration of elements at the skin surface where the thermal gradient was highest. Glenn, Rastegar and Jacques (1996) studied coagulation in laser irradiated tissue and used FEM to determine how the uncertainty in optical properties and surface convection affected the temperature profiles in the tissue.

It appears that FEM not only allows the temperature rise at any point in a model to be predicted; it also allows the influence of the various input parameters to be studied. This would be useful as the thermal parameters of bone as so poorly defined. The ability to handle large thermal gradients, noted by Diller and Hayes, is also important as these may well be a result of the high absorption coefficient of bone.

10.3. Construction and Use of a Finite Element Model.

ANSYS, the package used successfully by Chatterjee and Adams (1994) was readily available and so this was used to model the temperature rise in the bone samples and to see how the uncertainty in the input values affects the results. The steps involved in setting up the model where as follows:

- construction of the model;
- imposition of loads and boundary conditions on the model;
- solution and analysis of results.

10.3.1. Construction of the Model

The construction of the model involves the following steps:

- defining the structure to be modelled;
- dividing the structure into areas representing different tissue types;
- defining the physical parameters for each layer;
- dividing each area into a number of elements (meshing).

Defining the structure and setting the parameters for each layer.

While, as has already been stated, it is possible to model any geometry using FEM, implementing a fully 3-D model requires significant computer time and memory. The ultrasound beam used in the experiments possessed axial symmetry and this fact was used to limit the complexity of the model and so reduce usage of computer resources. (This would not necessarily be appropriate, however, for a beam emitted from a modern scanner where the probe may have rectangular elements and so would not produce an axially symmetric beam.) The symmetry allowed a three dimensional cylinder to be represented by a two dimensional axisymmetric system, as illustrated in Figure 10.1, greatly reducing the size of the computer model. Different parts of the model were defined as particular materials, such as bone or agar gel, and properties assigned accordingly. For a thermal model it is necessary to define the specific heat, thermal conductivity and density of each material.

Meshing.

Meshing, the process of subdividing each area into elements, has important implications for the accuracy of the model. The decisions associated with this step involve defining the type of element used and

Figure 10.1: Application of axial symmetry.

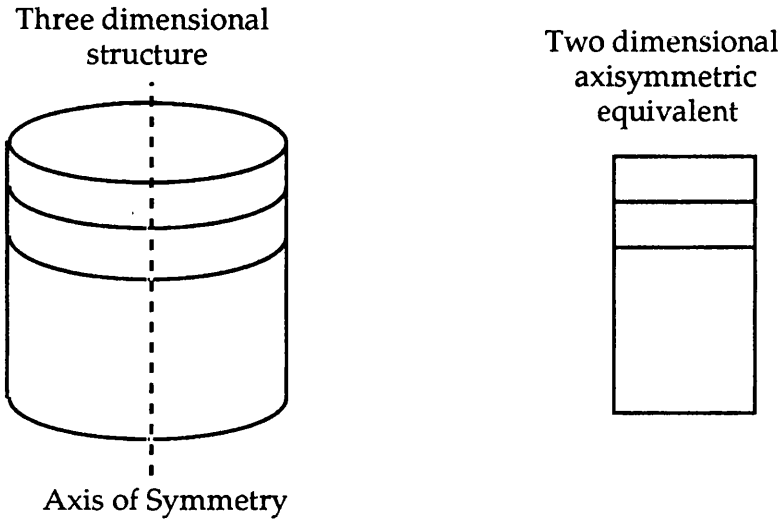

the size of the elements. Within ANSYS a range of element types are available. The simplest four-sided element has a node at each corner and the temperature within the element is a linear interpolation of the temperature at the nodes. Higher order elements are available, which have more nodes and use higher order terms of the polynomial in the interpolation. These increase the complexity of the calculations but allow more complex temperature distributions to be modelled within each element and so may allow larger, and thus fewer, elements to be used. The relationship between the nodal temperatures and the temperature rise at any other point for elements with 4 and 8 nodes is shown in figure 10.2. As the power dissipation in the model was exponential and the gradients at the bone surface were likely to be high, it was decided to use an 8 node element. This resulted in a second order polynomial being used for the shape function.

In this study, another factor important in the choice element size was the power dissipated by the ultrasound beam. This was calculated at each node and so, in order that it be modelled with reasonable accuracy, it was

Figure 10.2: Element shape functions

2-D and Axisymmetric 4 Node Quadrilateral Solid

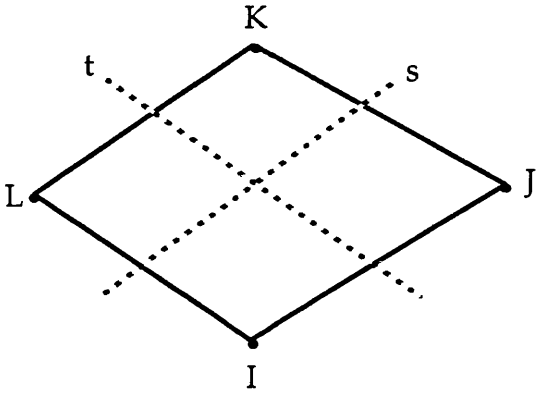

Co – ordinates of nodes (s,t):

I = (-1,-1) J = (1,-1) K = (1,1) L = (-1,1)

Temperature at any point:

$$T = \frac{1}{4}\left(T_I(1-s)(1-t)+T_J(1+s)(1-t)+T_K(1+s)(1+t)+T_L(1-s)(1+t)\right)$$

2-D and Axisymmetric 8 Node Quadrilateral Solid

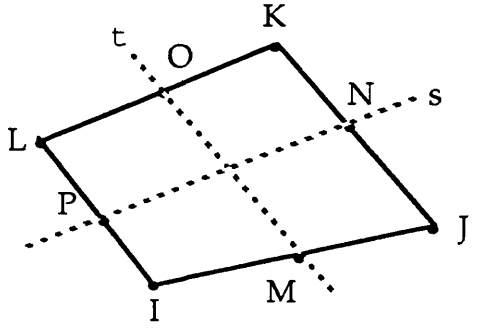

$$T = \frac{1}{4}\begin{pmatrix} T_I(1-s)(1-t)(-s-t-1)+T_J(1+s)(1-t)(s-t-1) \\ +T_K(1+s)(1+t)(s+t-1)+T_L(1-s)(1+t)(-s+t-1) \end{pmatrix}$$

$$+\frac{1}{2}\left(T_M(1-s^2)(1-t)+T_N(1+s)(1-t^2)+T_o(1-s^2)(1+t)+T_P(1-s)(1-t^2)\right)$$

important that the node spacing and hence the element size was not too large. Using ANSYS it is possible to specify the element size in critical areas, give an upper limit for the rest of the model and instruct the software to mesh the model with suitable elements. This facility was used with typical element lengths in the bone tissue being 0.2 mm andthe maximum element length in the model being 5 mm. The meshing process then ensured that there were not excessive jumps in size between adjacent elements. The effect of element size on the results is considered in section 11.4.1.

10.3.2. Imposition of loads and boundary conditions

Once the model had been constructed loads needed to be applied. Two types of loads were used; the heat source functions arising from the absorption of the ultrasound beam and surface loads used to model the convection or conduction at solid-liquid interfaces. As explained earlier, the rate of heat production per unit volume in a plane wave can be approximated to $q = 2\alpha I$. Although this is a simplification, it was decided to use this formula to calculate the heat source functions as it is simple and has been used by the NCRP and AIUM when formulating their models (AIUM, 1992; NCRP, 1992). It was assumed that the intensity of the beam at the surface of the bone was known and that it undergoes exponential decay with the attenuation coefficient being the same as the absorption coefficient. Heating due to absorption in the agar was neglected because, as was discussed in section 5.5.3, the total power loss due to the agar, i.e. from reflection and absorption, had been shown to be comparable to the reading of error of the power balance. This produced a maximum uncertainty of 5% in the power value.

Loads were applied to the surface of the model to include heat loss due to convection. It has been shown that a fluid interface can make a significant difference to the temperature rise in bone (Wu, Winkler, & O'Neill, 1994) and so it was necessary to include this. The value to be used for the convection coefficient is not clear however. Thomas quotes a range of 200 - 600 $W\,m^{-2}{}^{\circ}C^{-1}$ for free convection in water (Thomas, 1992) and so values within this range were tried. The model did not include perfusion.

10.4. Solution and Analysis of the Results.

Once the model had been set up and the loads imposed the next step was to obtain the solution. The software does this by using matrix techniques to solve a set of simultaneous equations. The derivation of these matrices is described in appendix B.

It was possible to obtain either the steady-state solution or, if a transient analysis was carried out, the rate of heating. In a transient solution it is necessary to define the minimum and maximum values of the time step. An equation for the minimum time step is given in the ANSYS documentation as:

$$\text{initial time step} = \delta^2/4k$$

where δ = minimum conducting length, effectively the shortest element dimension;

k = thermal diffusivity.

The maximum time step was set to 10 s as this gave adequate resolution in the latter part of the curve while ensuring that the results file did not become too large. The software automatically increased the time between solution steps as the thermal gradients decreased.

10.4.1. Error estimates.

It must be remembered that FEM is an approximate technique and so it was important to determine the accuracy of the results. ANSYS estimates the error in the results due to the size of the elements. First the heat flow for each element is calculated by averaging the nodal values for that element. For each node within the element the difference between this value and the average value from all the elements to which it is attached can then be used to estimate the thermal energy error. Unfortunately, this process can be inaccurate when the model contains a mix of materials where the difference in heat flow in the elements to which a node is attached may be due to the different thermal properties. This leads the error estimator to overestimate the degree of error but does imply that this figure should give an upper limit to the error due to mesh size. The software will also display the regions of the model in which the errors occur and so, as long as the errors on the boundaries of the layers are ignored, this can be used to help refine the mesh.

10.5. Discussion

After the initial familiarisation period it was found that ANSYS could be used to produce layered models with reasonable ease. One attractive feature of this software is that it can be run in either interactive or batch mode and the log file automatically generated during interactive use can be converted into a command file for batch mode operation. The commands that were found, interactively, to create acceptable models could therefore be used repeatably without the risk of mistyping a value and, unknowingly, changing the model. This facility also meant that slight variations to a model could be easily implemented. The use of macro files, effectively subroutines to which variables could be passed, meant that the process of loading each node with its heat generation rate could also be automated.

Unlike the heated disc model it was not possible to find out quickly how altering one parameter over a range of values changed the predicted temperature rise, as a full solution had to be obtained for each value of the parameter. The software was run on a multi-user UNIX server and so the time taken to run each analysis varied, depending upon the number of users on the machine. The CPU time was of the order of 1000 s but the actual run-time was typically in the range 0.5 - 2 hours. The solution time for the heated disc model also varied, depending on how quickly the numerical integration converged, but obtaining the result for a range of input values rarely took more than 1 hour.

It was important to check that the models produced were giving reasonable results and to see how they could be optimised. This will be considered in Chapter 11.

10.6. Chapter Summary

Finite element modelling has been used by many authors to model the temperature distribution in parts of the human body caused by a range of factors. It can represent the contours of organs more easily than the other technique commonly used for numerical modelling of heating, finite difference modelling, and once the model has been solved the temperature at all points in the model is available. The steps involved are: construction of the model; imposition of loads and boundary conditions and solution and analysis of the results. FEM, however, is an approximate technique and it is important to validate the results.

Chapter 11

Validation of the Finite Element Model

11.1. Introduction

It has already been pointed out that finite element modelling is a technique which produces approximate solutions to differential equations and so the results from any model have an uncertainty associated with them. The degree of uncertainty depends upon a variety of factors including the size of the elements, the type of shape functions used and the way that loads, such as heat generation, are modelled. To help assess the way that these factors might affect any bone model, and to determine how the uncertainty could be minimised, a well defined experiment was modelled and the predicted and measured temperature rises were compared. The uncertainty about the thermal properties of bone made this an unsuitable material for these measurements and so a phantom was produced which contained a bone mimic with well defined properties.

11.2. The Phantom

The phantom consisted of two layers, 15 mm of 1.5% agar gel and 5 mm of glass filled PTFE, with a K type thermocouple sandwiched between them. This is shown in figure 11.1.

Figure 11.1: Diagram of the phantom.

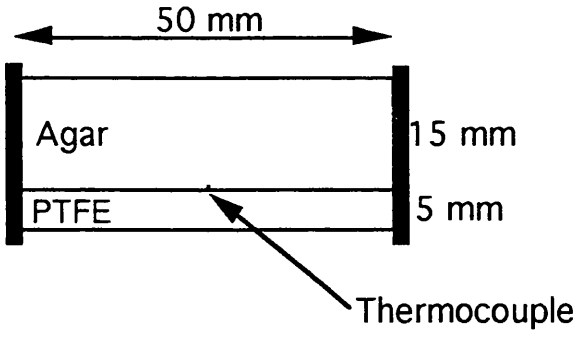

The bone mimic was suggested by the National Physical Laboratory (NPL) and its thermal and acoustic properties had been characterised by them. It consisted of PTFE filled with 60 μm diameter glass fibres to a concentration of 25%. The properties of this material are shown in table

11.1. The agar gel had thermal properties very close to those of water but its presence meant that the thermocouple was not in direct contact with liquid and so made the boundaries conditions less important.

Table 11.1: Properties of Glass-filled PTFE.

Ultrasound Propagation Speed	1400 ± 20	$m\ s^{-1}$
Attenuation coefficient at 3.5 MHz	3.9 ± 0.5	$Np\ cm^{-1}$
Density	2200	$kg\ m^{-3}$
Thermal conductivity at 20°C	0.33 ± 0.02	$W\ m^{-1}\ K^{-1}$
Specific heat at 21 ± 2.5°C	1600 ± 500	$J\ kg^{-1}\ K^{-1}$
Thermal diffusivity at 20°C	$(0.9 \pm 0.3) \times 10^{-7}$	$m^2\ s^{-1}$

The uncertainties quoted are the limits of the 95% confidence interval except for the specific heat and thermal diffusivity values. The specific heat varies considerably over the temperature range of interest and the uncertainty figure quoted is a measure of this variability, rather than the measurement uncertainty. The value is quoted at 21 ± 2.5°C as this range includes all the temperatures at which the measurements were carried out (including the temperature of the PTFE when heated). The thermal diffusivity is calculated using the value of specific heat and so shares its large uncertainty.

The agar gel was made by mixing agar with distilled water to a concentration of 1.5% (weight/volume). Duck (1990) gives the thermal conductivity of gel of this concentration as 0.609 $W\ m^{-1}\ K^{-1}$ and the specific heat as 4289 $J\ kg^{-1}\ K^{-1}$. The density was assumed to be 1000 $kg\ m^{-1}$. The fact that the acoustic impedance of both the agar gel and the PTFE were known meant that the reflection coefficient at the surface of the PTFE could be calculated. The intensity reflection coefficient at the agar-PTFE boundary was calculated to be 12%.

11.3. Measurements

A series of heating measurements were carried out in order to test the modelling under a range of conditions. The beam parameters, the separation of the thermocouple from the transducer and the data

acquisition were the same as those used in the bone heating measurements. Measurements were taken with the beam passing through the agar and into the PTFE and also with the phantom turned over so that the beam passed through the PTFE before reaching the thermocouple. These two configurations are shown in figure 11.2. In both cases the thermocouple was positioned at the interface between the PTFE and agar. An acoustic absorber, a layer of carpet, was placed beneath the phantom to minimise reflections from the bottom of the tank.

Figure 11.2: Experimental set-up

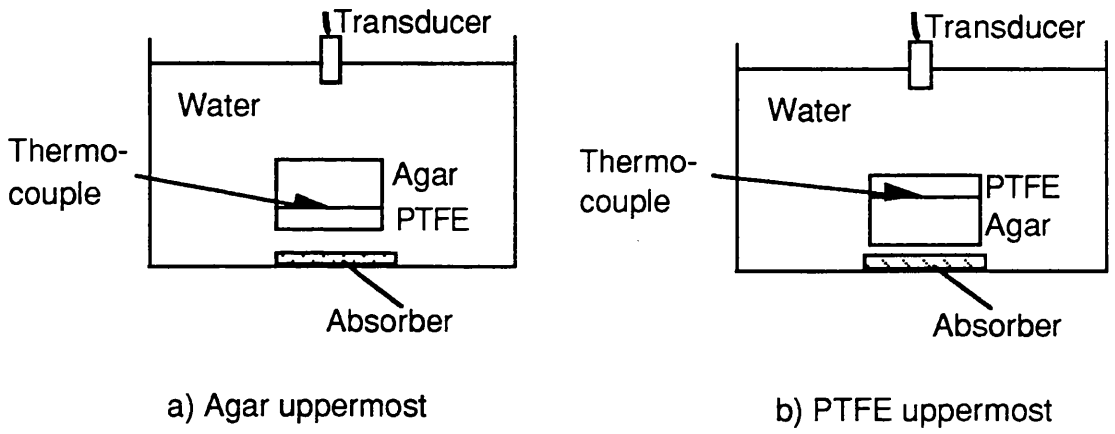

11.4. Modelling

11.4.1. Choice of element size

Finite element models were set up to predict the temperature rise for each of the experimental arrangements. The structure of the model and a typical arrangement of elements is shown in figure 11.3. The model has the beam entering from the bottom as this meant that it was travelling in the direction of increasing x, as defined by ANSYS. The elements were smallest in and around the part of the PTFE which absorbed the ultrasound beam. A range of values was used to model the beam width but in order to avoid having to change the model each time an area of radius 7.5 mm, corresponding to the largest beam radius considered, was defined in which the element size was keep small. This is in keeping with the requirement of FEM. that elements should be smallest where the largest temperature gradients are expected.

Figure 11.3: Finite element model of bone mimic.

a) Structure and boundary conditions.

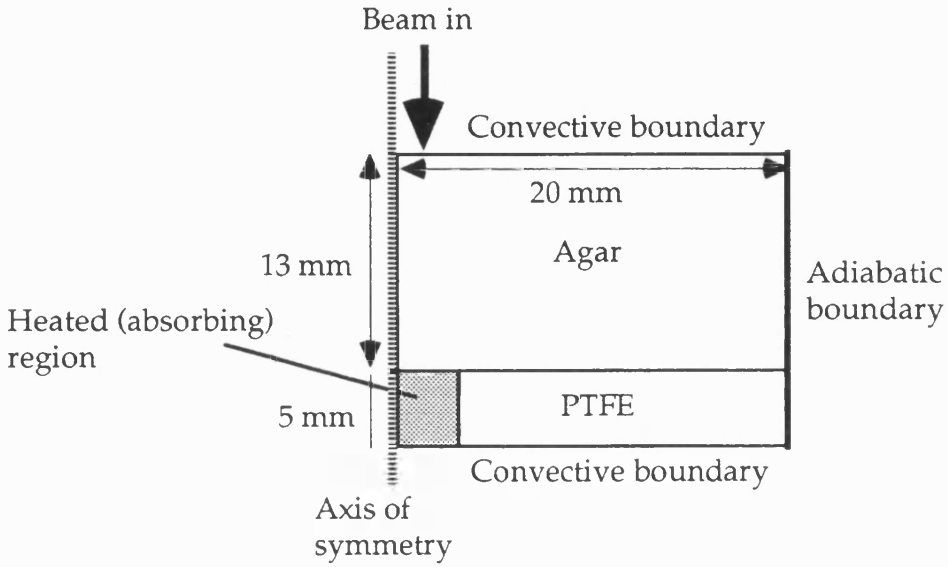

b) Typical arrangement of elements.

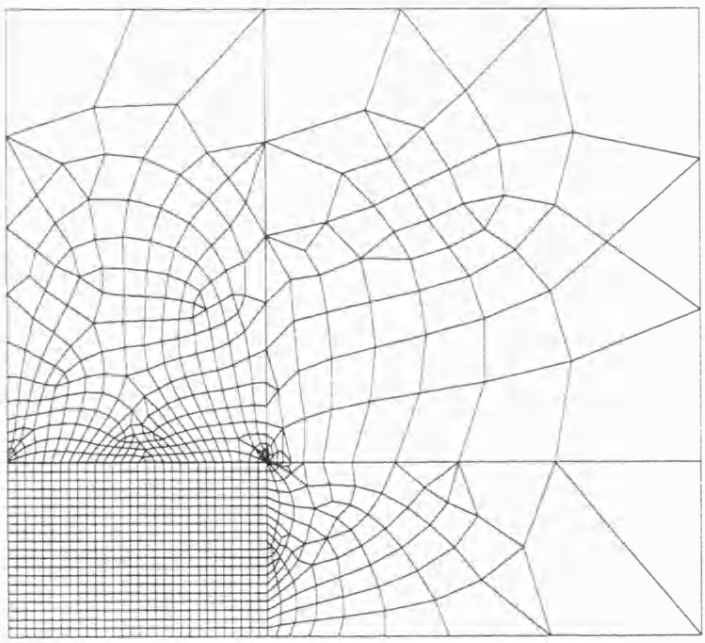

The heat generation loads were applied at the nodes and so, having small elements where the beam passed through the PTFE but larger elements elsewhere, allowed the exponential decay of the beam to be modelled with acceptable accuracy while still keeping the number of elements to a minimum. This limited the computer resources needed to handle the model.

The error that was incurred by calculating the heat generation at the nodal points, rather than using the correct integral solution, depended upon the size of the elements. The difference between the integral solution and that obtained using the mean nodal value can be determined by considering a linear element of cross-sectional area A going from y = 0 to Y = L.

Assuming that the intensity at any point is given by $I = I_0 \exp(-2\alpha y)$
and that the heat generation per unit volume is $2\alpha I$.
If q is the heat generated within the element:

$$q = 2A\alpha I_0 \int_{y=0}^{y=L} \exp(-2\alpha y)dy$$

$$= AI_0[1-\exp(-2\alpha L)].$$

If, however, the mean value of the heat generation rate at the nodes is used, for an element with a node at either end, the mean nodal rate is

$\alpha I_0[1+\exp(-2\alpha L)]$.

Multiplying by the volume of the element to obtain the total heat generation within the element gives:

$q = AL\alpha I_0[1+\exp(-2\alpha L)]$.

For an element with unit cross-sectional area and which an absorption coefficient, α, of 3.9 Np cm^{-1} the values obtained for the heat generation per unit intensity using these two techniques are shown in Table 11.2.

Table 11.2: Integral and mean nodal solution for heat generation.

L (mm)	Integral solution	Mean nodal solution
0.1	0.0750	0.0751
1	0.542	0.569

It can be seen that using an element size of 1 mm leads to a difference of 5% in the heat generation. However, if the element size is reduced, such that L = 0.1 mm the difference of less than 0.2%.

The FEM calculation of heat generation depends upon the shape function as well as the nodal heat generation rates, as can be seen from the definition of the load vector (see Appendix B). An element with 2 nodes on each side would use a linear shape function and so the heat generation within the element would be related in a linear fashion to the loads applied at the nodes. This is equivalent to using the average value to calculate the heat generation within the element, as was done above. Higher order elements, which have more nodes, would use higher order polynomials. This makes the relationship more complex and so it is not possible to make a general statement about the error. The information gained from the linear case can, however, be used to give an indication of the appropriate element size and would suggest that elements sizes less than 1 mm should be tried.

An 8 node quadrilateral element was used in the models. This has three nodes on each side and hence a quadratic shape function. This allowed for more complex temperature distributions than would be possible using the same number of elements and linear shape functions. This element type can also become a triangle, rather than a quadrilateral, if this is necessary to model the shape of the object.

Another factor that needed to be considered was the heat generation at the front of the PTFE. The way the model was defined means that there is a node at the boundary between the PTFE and the agar and any load applied to this would influence all of the elements which share this node: some in the agar and some in the PTFE. Applying a heat generation load to this node, therefore, is equivalent to having some heat generation in the agar, while if no load were placed upon it the heating at the front of the PTFE is under-represented. This could make a significant difference to the result as the thermocouple is situated at such a node. To minimise this problem it was decided to have a layer of very thin elements, 1×10^{-5} m thick, directly in front of the PTFE, so that, although these would be generating heat, the volume affected would be so small that it should not add a significant amount to the total heat generation in the region. When the results obtained with this thin layer of elements were compared with those without, for a model in which the minimum

element size, apart from this layer, was 0.25 mm, the predicted temperature rise fell by 10%. This was because in the model with the thin layer of elements, the agar element attached to the node at the boundary, was ony 4% of the width of the equivalent element in the model without this layer and so significantly less heat generated was within it.

The one unknown in the system was the convection coefficient at the solid-fluid interfaces. It was decided to choose a value for this that was within the expected range and then to see how changing this value altered the result.

11.4.2. Modelling the Intensity Distribution

It was necessary to convert the measured intensity distribution within the beam into heat generation rates for the elements. This involved making decisions about the resolution with which the beam profile should be entered and the radius out to which the beam should be modelled. The hydrophone elements of BECA are 0.5 mm in diameter and they are spaced at 1 mm intervals. This governed the resolution with which the intensity values could be modelled. The radial intensity distribution was modelled as a step function and the heat generation applied to a node depended upon its distance from the axis. A single set of intensity values acquired by BECA could give a step size of 1 mm, due to the element spacing, whereas when two sets of readings were taken, with the hydrophone moved by 0.5 mm in-between, placing the hydrophone elements in the gaps in the previous set of readings, a step size of 0.5 mm could be used. The two intensity functions at 80 mm from the transducer are shown in figure 11.4. To ensure that the intensity values were in line with the total power measurement obtained from the power balance, the values were integrated out to a distance of 7.5 mm. This gave a power value of 46 mW compared to 50 mW from the power balance. Given the errors associated with intensity measurements from BECA this was considered acceptable.

The radial distance of each node from the beam axis was used to determine the intensity of the beam at the PTFE surface and then an exponential decay factor was applied to this to give the local intensity, accounting for attenuation. This result was then multiplied by 2α to give the heat generation at the position of the node.

Figure 11.4: Intensity distributions used in the model.

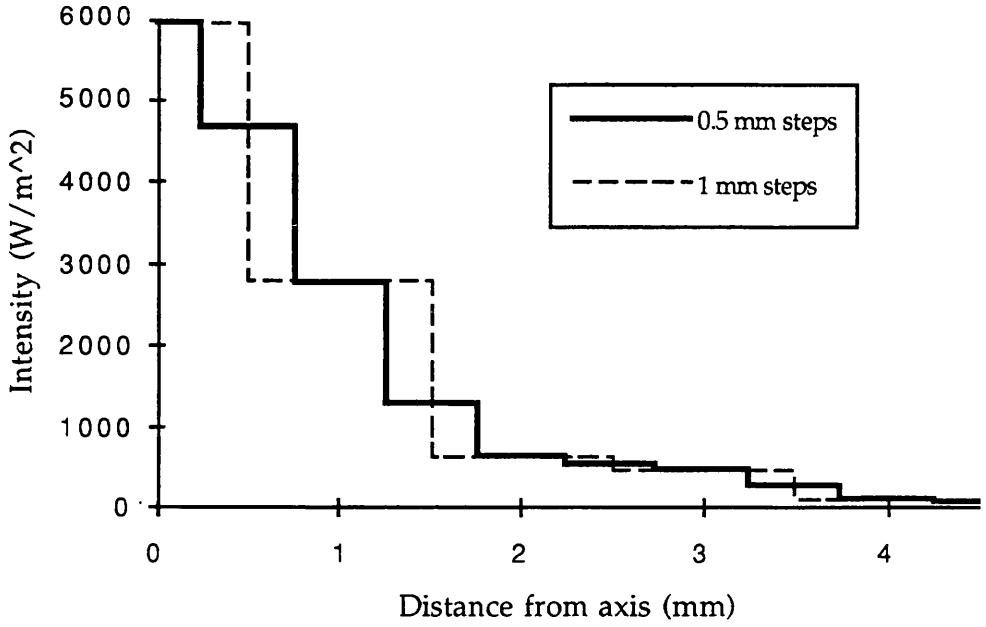

It was also necessary to consider the effective radius of the beam that should be used in the model. The beam did not have a clean cut-off point at which the intensity fell to zero but it was necessary to impose one on the model in order to avoid either having to use an excessive number of very small elements in the model or having to change the element size across the heated area. A range of values were tried and the results compared.

11.5. Results

11.5.1. Element and step size

The first parameter to be studied was the element size in the PTFE. The calculations shown above had suggested that the element size should be less than 1 mm and so three sizes were tried 0.1, 0.25 and 0.5 mm. Early attempts at modelling had indicated that there was some interaction between the effect of element size and the resolution to which the beam profile was modelled and so models were generated with a step size in the intensity distribution of 0.5 and 1 mm. Table 11.3 shows the temperature rise at the front of the PTFE at 300 s for each combination of element and step size. This is for the orientation in which the agar is

uppermost and so the beam passes through the agar before reaching the PTFE.

Table 11.3: Temperature rise at front of PTFE at 300 s

Intensity step size (mm)	Element size (mm) 0.1	0.25	0.5
0.5 mm	3.15	3.13	2.75
1 mm	3.28	3.20	3.07

It can be seem that for both steps sizes the difference between an element size of 0.1 and 0.25 mm causes a change in the maximum temperature of less than 3% while changing the element size to 0.5 mm causes a change in the maximum temperature of over 12% for the 0.5 mm step and over 6% for the 1 mm step. An element size of 0.25 mm would therefore seem to be an appropriate choice. Figure 11.5 shows the rate of heating at the front of the PTFE for elements of size 0.25 mm using step sizes of 0.5 and 1 mm.

Figure 11.5 - Heating at front of PTFE

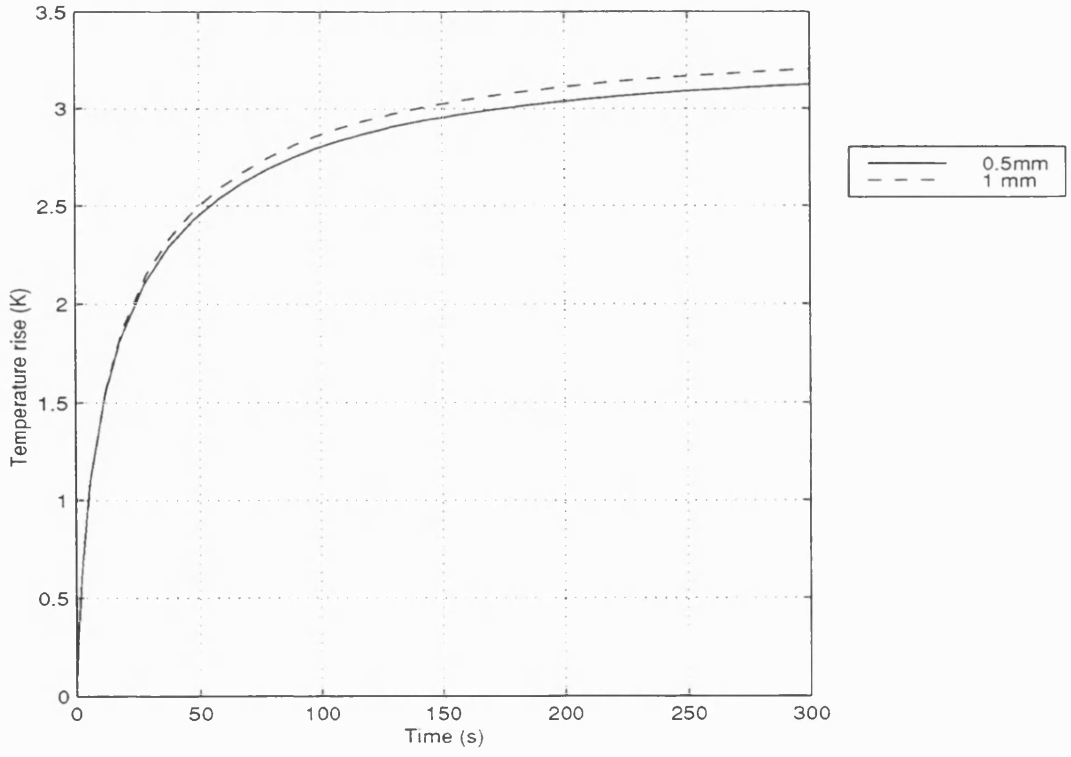

The increase in step size, from 0.5 to 1 mm, increases the maximum temperature rise by 5%. Part of the reason for this can be seen by considering the degree to which the power generated close to the axis determines the temperature rise. This can be estimated by using the heated disc model to predict the temperature rise from a disc of radius 0.5 mm over which the intensity is 547 mW cm^{-2} (the intensity value in the first step). This predicts a temperature rise of 1.4K purely from this small area, demonstrating the importance of the intensity in this region. The central hydrophone element spanned the axis of the ultrasound beam, and hence the axis of symmetry in the model. This meant that, as far as the model was concerned, the first step was half the size of the others, ending at 0.25 for the smaller step size and 0.5 mm for the larger. This meant that for the smaller step size two intensity values were used for the distance 0 - 0.5 mm. When the intensity values out to 0.5 mm were integrated, to give the power for both cases, the result was 19% lower for the smaller step size. This leads to the lower predicted temperature rise on axis observed in figure 11.3. While the smaller step size led to a lower intensity value between 0.25 - 0.5 mm, the intensity was greater between 0.5 - 0.75 mm and if the integration is carried out to distance of 4.5 mm the power is only 3% less for the smaller steps. The fact that intensity was 'moved away' from the axis reduces the on-axis temperature rise however.

The temperature rise along the axis was also investigated to see whether the maximum temperature rise was affected by the element size. The maximum was found to occur inside the PTFE, as had been suggested by the heated disc model and the ratio of the maximum temperature rise to that at the surface was 1.36 ± 0.01 for all three choices of element size. Figure 11.6 shows the axial temperature rise from 2mm in front of the PTFE to 2 mm inside [element size 0.25 mm, step size 0.5 mm]. It was decided to use an element size of 0.25 mm and a step size of 0.5 mm as standard, as this gave a model of manageable size while not introducing excessive errors due to the coarseness of the model.

11.5.2. Effective beam radius.

The heat generation in an element makes less of a contribution to the axial temperature rise as the distance of the element from the axis increases. This is due not only to the distance from the axis but also to the fact that the intensity decreases with distance from the axis. Three cut-off values were tested, therefore, to see to what distance from the axis

Figure 11.6: Temperature rise along the axis.

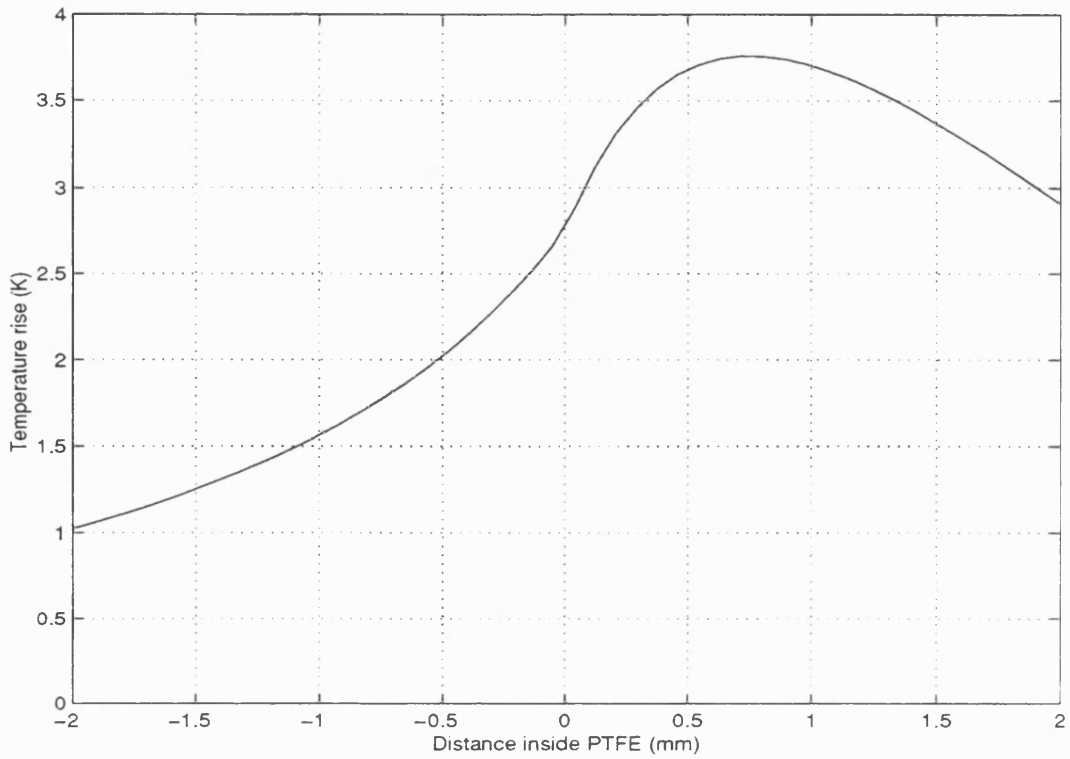

it was necessary to 'load' the elements with heat generation rates. The cut-off distances used were 3.5, 4.5 and 7.5 mm corresponding to beam diameters of 7, 9 and 15 mm and the step size was 1 mm. The corresponding power levels were 38 mW, 41 mW and 46 mW. The structure of the finite element model was the same, in all cases, with only the number of elements with a heat generation load being changed. For a transducer-PTFE separation of 80 mm, giving a measured -6 dB beam diameter of 2.9 mm, the difference in the predicted axial temperature rise at 300s for cut-off radii of 3.5 and 7.5 mm was less than 4%, with the 4.5 mm value falling almost exactly at the mid-point between these values.

The results for a transducer-PTFE separation of 70 mm, giving a -6 dB diameter of 4.5 m are shown in Table 11.4. Here the power in the three distributions was 37, 42 and 48 mW. It can be seen that the 4.5 mm cut-off gave a predicted temperature rise within 0.1 K, and 3%, of the maximum value obtained. This was considered acceptable given the large uncertainty in the actual intensity values.

Table 11.4: : Effect of cut-off radius on predicted temperature rise.

	Cut-off radius (mm)		
	3.5	4.5	7.5
Temperature rise (K)	2.56	2.67	2.75

11.5.3. Convection.

Another parameter whose value needed to be determined was the convection coefficient. Thomas (1992) quotes a range for natural convection in water of 200 - 600 W m^{-2} K^{-1}. The exact value depends upon a wide range of factors including the orientation and shape of the surface and whether the flow is laminar or turbulent (Zemansky & Dittman, 1981). The initial models used the values in the middle of the range quoted, i.e. 400 W m^{-2} K^{-1}, but it was thought important to determine the effect that changing this value had on the result. Table 11.5 shows the temperature rise at the surface of the PTFE and the maximum temperature rise for three values of convection coefficient.

Table 11.5: Effect of convection coefficient when agar uppermost.

	Convection Coefficient (W m^{-2} K^{-1})		
	200	400	600
Temperature rise at surface (K)	3.17	3.13	3.11
Maximum temperature rise (K)	4.33	4.27	4.24

It can be seem that the uncertainty in the convection coefficient did not lead to a significant uncertainty in these modelling results. The effect of changing the thickness of the agar layer was also studied as this effected the distance between the PTFE and the convective surface. While this had been constant for the PTFE it had differed between bone samples. When the thickness was increased from 13 mm to 20 mm (mean value plus one standard deviation for the bone samples) the temperature rise changed by less than 0.1K

The convection coefficient was found to be more significant when considering the situation when the phantom was turned over so that the beam entered the PTFE directly from the water. This resulted in a greater temperature rise at the PTFE-water interface and so a correspondingly greater heat loss. Table 11.6 shows how the predicted temperature rise at the PTFE-water interface and at thermocouple site varied with convection coefficient. Here the range of values quoted for the convection coefficient caused the predicted temperature rise at the site of the thermocouple to vary by approximately 20% as opposed to 2% when the agar was in front of the PTFE.

Table 11.6: Temperature rise when beam incident on water/PTFE interface.

	Convection Coefficient (W m^{-2} K^{-1})				
	200	**300**	**400**	**500**	**600**
Temperature rise at interface (K)	4.16	3.38	2.86	2.49	2.20
Temperature rise at thermocouple (K)	0.88	0.81	0.76	0.73	0.71

Another factor that needed to be considered was the boundary condition at the outer edge of the phantom. The PTFE and agar were enclosed in a PVC tube of diameter 50 mm in order to give the phantom some strength and it was assumed that this surface was far enough away from the beam not to make a significant difference to the result. In the models discussed above this surface was defined as adiabatic, i.e. it was assumed that there was no heat flow across this boundary, but it was thought necessary to test this assumption. A model was therefore generated in which convective boundary conditions were applied to this surface. The convection coefficient on all the surfaces was set to 400 W m^{-2} K^{-1}. When this model was solved the predicted axial temperature rise was found to be within 0.01K of the result as obtained for adiabatic boundary conditions.

11.6. Comparison of Finite Element and Heated Disc Models.

11.6.1. Models with identical thermal properties.

One way of checking the validity of the results from the finite element model was to compare a FE model with a heated disc one of the same structure. To do this a FE model of the bone mimic was constructed in which all the layers in the model had the thermal properties of PTFE. This is shown in Figure 11.7.

Figure 11.7: FE model used for comparison with heated disc models.

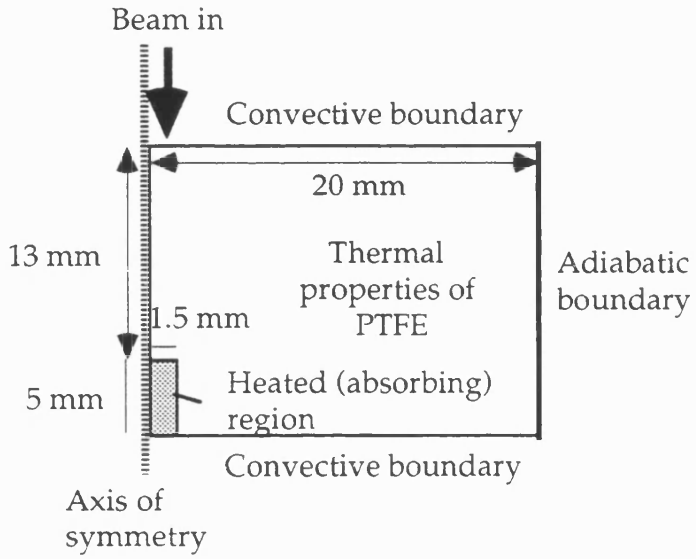

Although the regions occupied, in reality, by the PTFE and agar were both assigned the thermal properties of PTFE, the only area where heat was generated was the part of the model that corresponded to the PTFE layer. The corresponding heated disc model consisted of a disc of thickness 5 mm and width 1.5 mm in which heat was generated, but inherent in the nature of this type of model is the assumption that the heated region is surrounded by an infinite area with the same thermal properties. A 'top hat' intensity distribution was used in both models. For a transducer-PTFE separation of 80 mm the intensity value within 1.5 mm of the axis was 7074 W m^{-2}, 30% greater than the maximum value used in the stepped intensity distributions. The results obtained from the two models are shown in figure 11.8.

Figure 11.8: Finite element and heated disc results for the same structure.

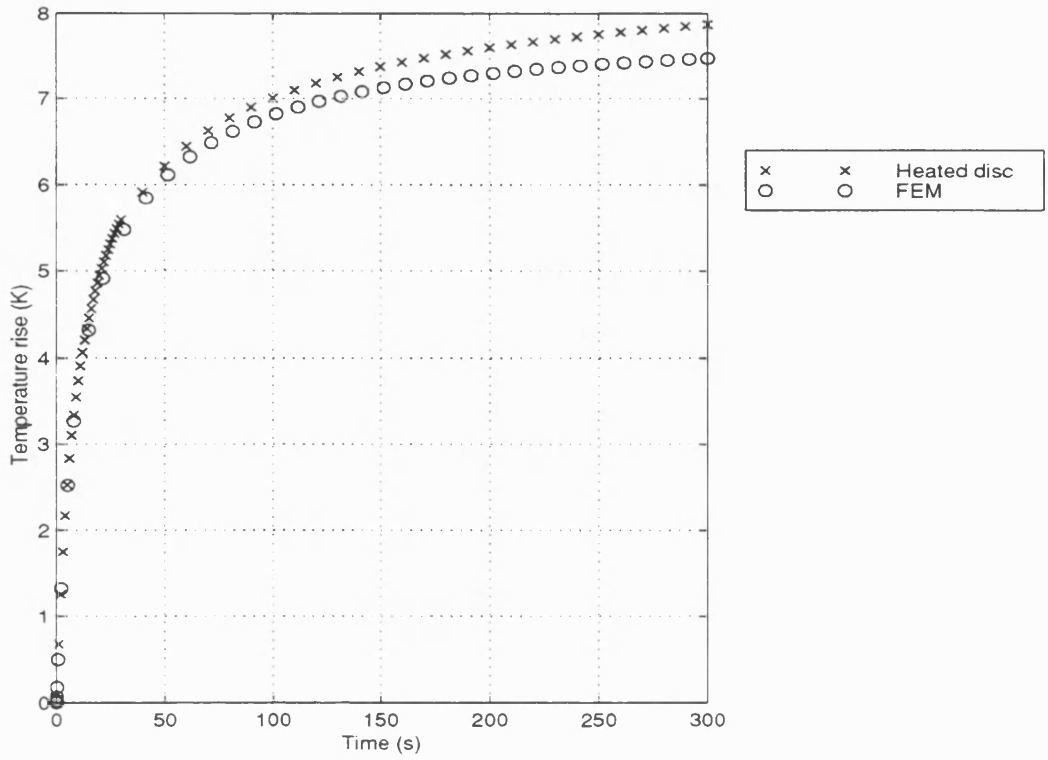

It can be seen that the early part of both curves is very similar but that they start to diverge after 30 s. and at 300 s there is a 6% difference in the temperature rise. This is due to difference in the boundary conditions between the two models. The convective boundary conditions at the back of the PTFE removed more heat than the conduction that is inherent in the heated disc model and so the finite element model experienced a slightly lower temperature rise. As this difference was due to the fact that the finite element model could represent the situation more accurately, it was not thought to be a problem.

11.6.2. Comparison of heated disc and finite element layered model

The added complexity of FEM is only worthwhile if the results obtained using this technique are more accurate than those from the heated disc model. The next finite element model, therefore, contained distinct PTFE and agar layers in which the thermal properties are correct, a feature that cannot be included in the heated disc model. This is shown in figure 11.9.

Figure 11.9: FE layered model used for comparison with heated disc models.

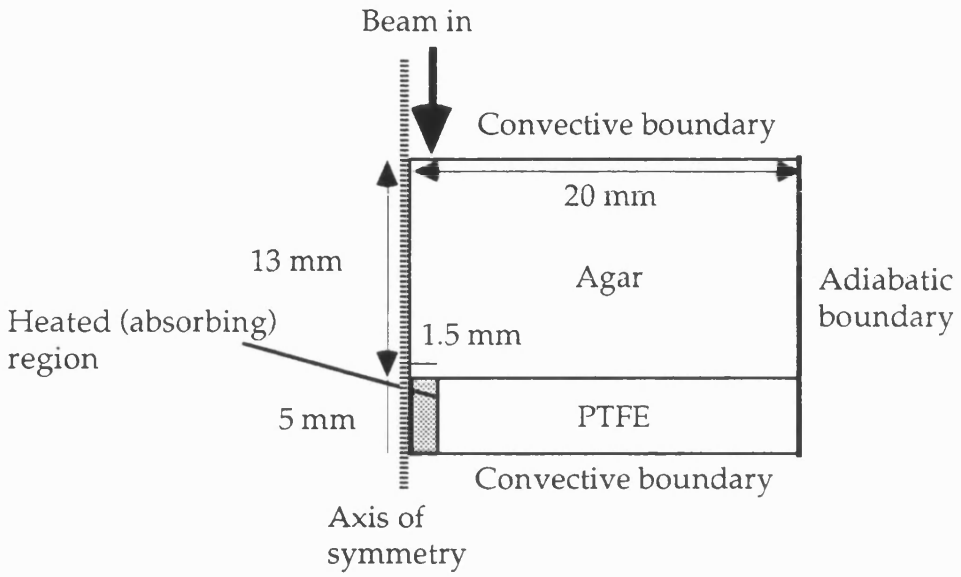

The results from this were then compared with two heated disc models; one using PTFE properties throughout (as above) and the other agar properties. The same 'top hat' intensity distribution was used in all the models. The results are shown in Figure 11.10. It can be seen that there is a difference of over 3 K between the two sets of results obtained using the heated disc technique and that the results from the FE model are closer to those obtained when the thermal properties of agar were used. This demonstrates the difficulty in using the heated disc technique in layered materials where the thermal properties of adjacent layers are significantly different. If this approach is adopted and the thermal data for PTFE used in the model, the predicted temperature rise at 300 s is nearly 50% higher than that obtained using the FE model in which each layer has the correct thermal properties.

The model discussed so far used a 'top hat' intensity distribution in order to carry out the comparisons with the heated disc model. It has already been shown that the way that the intensity distribution is modelled plays an important role in determining the results. This is demonstrated further if the results from the stepped intensity distribution (0.5 mm step

Figure 11.10: Results from FE layered model and heated disc models.

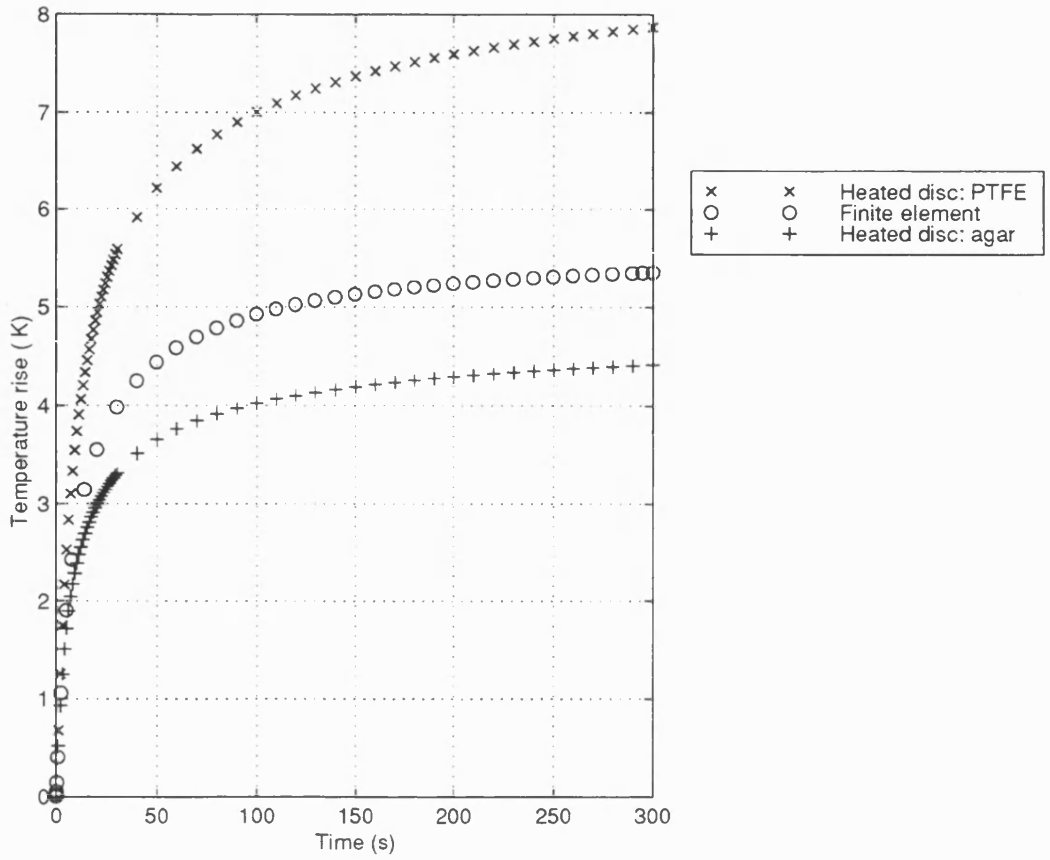

size) and the 'top hat' distribution are compared. This is shown in Figure 11.11. It can be seen that there is a difference in over 2 K in the temperature rise at 300 s. This is much greater than the 6% difference in temperature rise calculated for different intensity distributions in NCRP report 113 (1992). In this the steady state temperature rise was calculated for a point at the front of a highly absorbing sheet which was surrounded by material which had the same thermal properties. Three intensity distribution were compared: a top hat, a Gaussian and an O'Neillian distribution which is based on a first order Bessel function; in each case the total power and the diameter of the beam were the same. These, and the stepped distribution used in the FE model are shown in Figure 11.12. In each case the total power is 40 mW, as the step distribution did not give the total power in the beam, and the - 6dB diameter was 3 mm.

Figure 11.11: Comparison of results from stepped and 'top hat' intensity distribution.

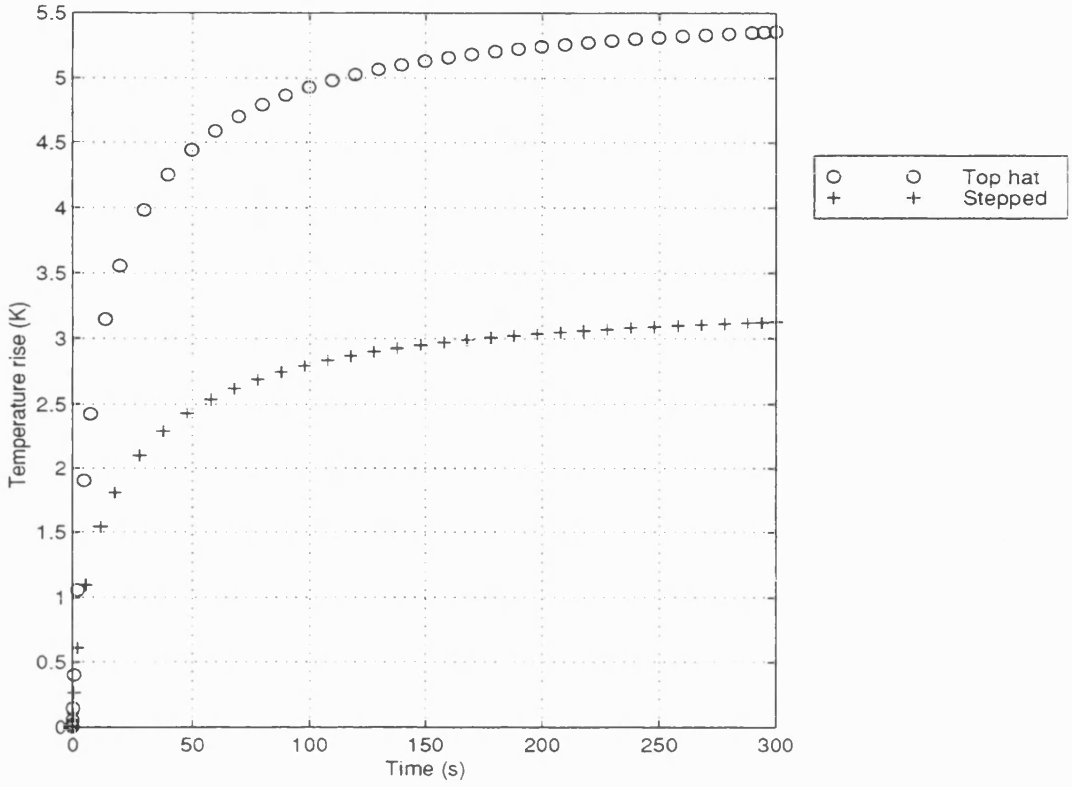

It can be seen that for the three intensity distributions considered by the NCRP, the peak intensity is higher than the value in the stepped distribution. Also more of the power comes from the portion of the beam that is close the axis; in particular, all of the power in the top hat distribution is in an area within 1.5 mm of the axis, while for the stepped distribution less than half the power (47%) in concentrated in this area. If the radius of the top hat distribution is increased to 3 mm, so that it encompasses an area which contains three-quarters of the temperature rise in the stepped distribution, the predicted temperature rise at 300 s falls to 1.3 K. This demonstrates the importance of not just the total power but also the intensity distribution. This is in agreement with the work of Jago et al. (1995) who found large differences in the predicted temperature rise in soft tissue and bone models, when they compared a Gaussian intensity distribution with measured intensity distributions.

Figure 11.12: Intensity distributions.

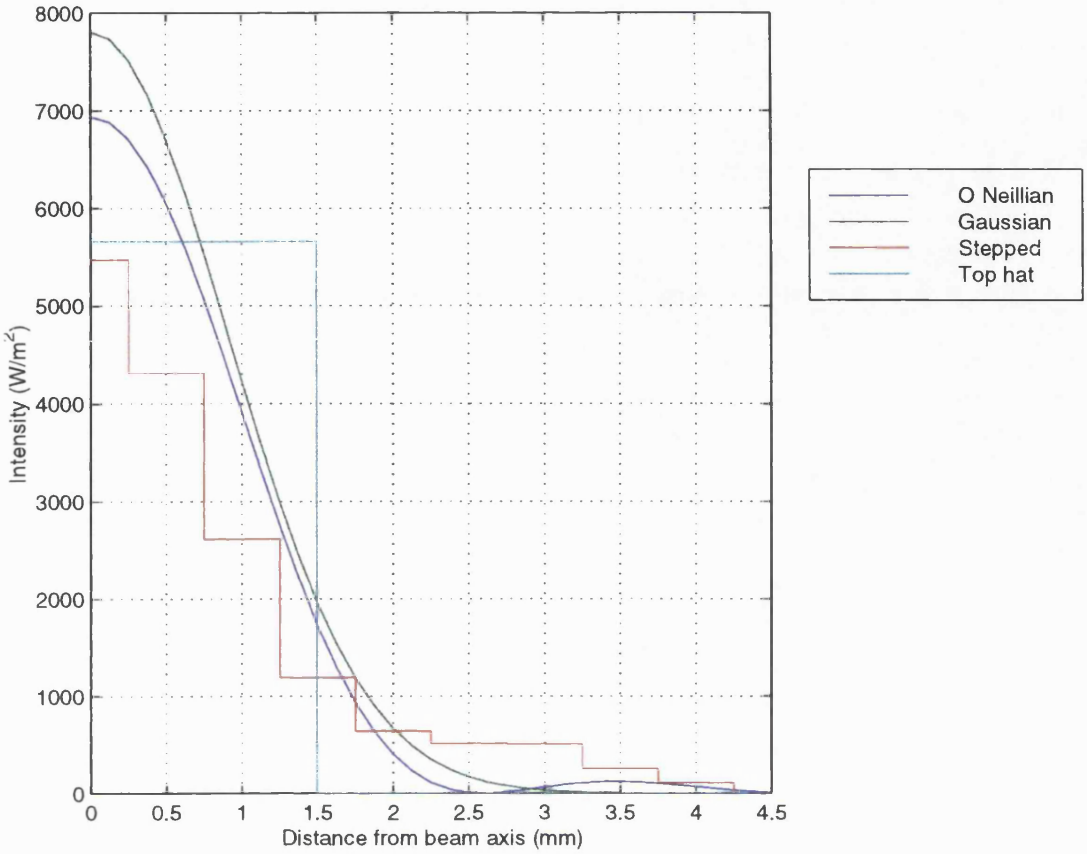

The other main difference between the model considered by the NCRP and the FE model was the fact that the former considered a region in which the thermal properties were constant; a thermal conductivity value of 0.58 W m^{-1} K^{-1} being used throughout. This value was 1.75 times the value of thermal conductivity used for the PTFE and it was thought that this might reduce the significance of the intensity distribution. A FE model was constructed, therefore, in which the thermal conductivity of the PTFE layer was set at 0.6 W m^{-1} K^{-1}. This led to a reduction in the temperature rise at 300 s of 20% for both distributions and changed the ratio of values obtained from the two distributions by less than 1%.

11.7. Comparison of Model and Experiment Results.

In order to compare the results from the model with the experimental measurements allowance had to be made for the reflection that occurred at the surface of the PTFE. As this lead to a reduction in intensity of 12%

and as the temperature rise is proportional to the intensity, this was achieved by reducing the output from the model by 12%.

Figure 11.13 shows the measured and modelled temperature rise at the front surface of the PTFE for the case where the beam passed through the agar before entering the PTFE. The transducer - PTFE separation was 80 mm and a value of 400 W m^{-2} K^{-1} was used for the convection coefficient.

Figure 11.13: Measured and modelled temperature rise of front of PTFE.

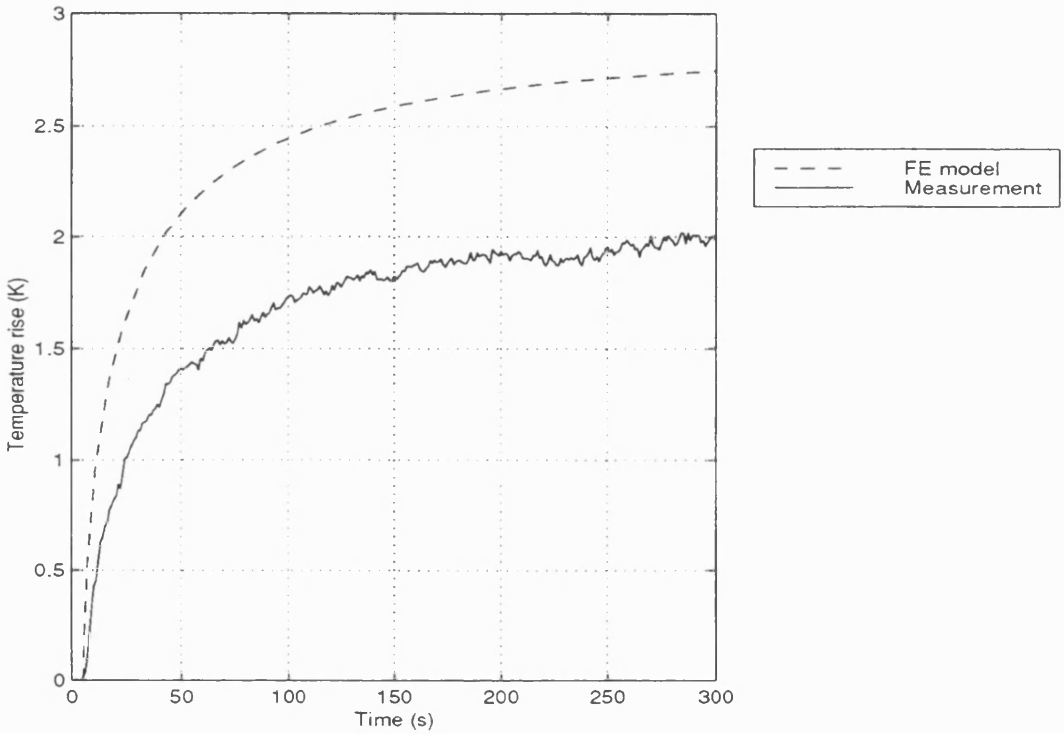

It can be seen that the predicted temperature rise exceeds the measured value by 38%. A number of factors could contribute to this error including the position of the thermocouple and the uncertainty in the properties of the PTFE and the intensity values.

The steep temperature gradient at the front of the PTFE means that a relatively small displacement from the surface leads to large changes in the measured temperature. It has already been observed in the bone heating measurements that the positioning of the thermocouple can introduce errors and the nature of the PTFE, a large flat surface, made it more difficult to attach the thermocouples to this material than to bone. The modelled axial temperature distribution close to the surface of the

PTFE was shown in Figure 11.6 and it can be seen that relatively small displacements of the transducer can cause significant changes in the measured temperature. In this case moving 0.5 mm from the front of the samples reduces the temperature rise to the measured value. If this factor is the cause of some, or all, of the error it should be observed in all the measurements taken with this phantom as the thermocouple was in the same position throughout. Figure 11.14 shows the rate of temperature rise at the PTFE surface and 0.5 mm from the surface, inside the agar layer for three sets of measurement conditions. The first case is the one just considered, the second is similar except that the transducer-PTFE separation is 70 mm and in the third the phantom is turned over so that the thermocouple is now at the back of the PTFE. It can be seen that the temperature rise at 0.5 mm from the PTFE surface appears to give a better prediction of the measured temperature rise than the heating at the surface. While these results suggest a possible caused for the discrepancy between the predicted and measured values it is important to investigate other possible causes.

The large uncertainty in the specific heat of the PTFE, and hence the thermal diffusivity, was mentioned earlier in this chapter and so the model was rerun using a value for the specific heat that was at the top end of the range of measured values, 2200 J kg^{-1} K^{-1}. Figure 11.15 shows the rate of heating produced by this model compared to the original. It can be seen that altering the specific heat value changes the initial part of the curve but that this difference decreases with time, making a difference of only 1% at 300 s.

The effect of increasing the thermal conductivity was also studied. This was found to make more of a difference as the exposure time increased but a 10% difference in the thermal conductivity reduced the predicted temperature rise at 300s by less than 3%.

Another property of the PTFE which could alter the result is the absorption coefficient. There are two ways in which this could cause errors: the first is if the value used is inaccurate and the second is if the assumption that the absorption coefficient equals the attenuation coefficient is incorrect. The uncertainty in the attenuation coefficient measurement is known and the two extreme values, 3.4 and 4.4 Np cm^{-1} were entered into the model to determine the effect of this uncertainty on

Figure 11.14: Predicted temperature rise at surface and 0.5 mm in front of PTFE.

a)Transducer-PTFE separation 80 mm.

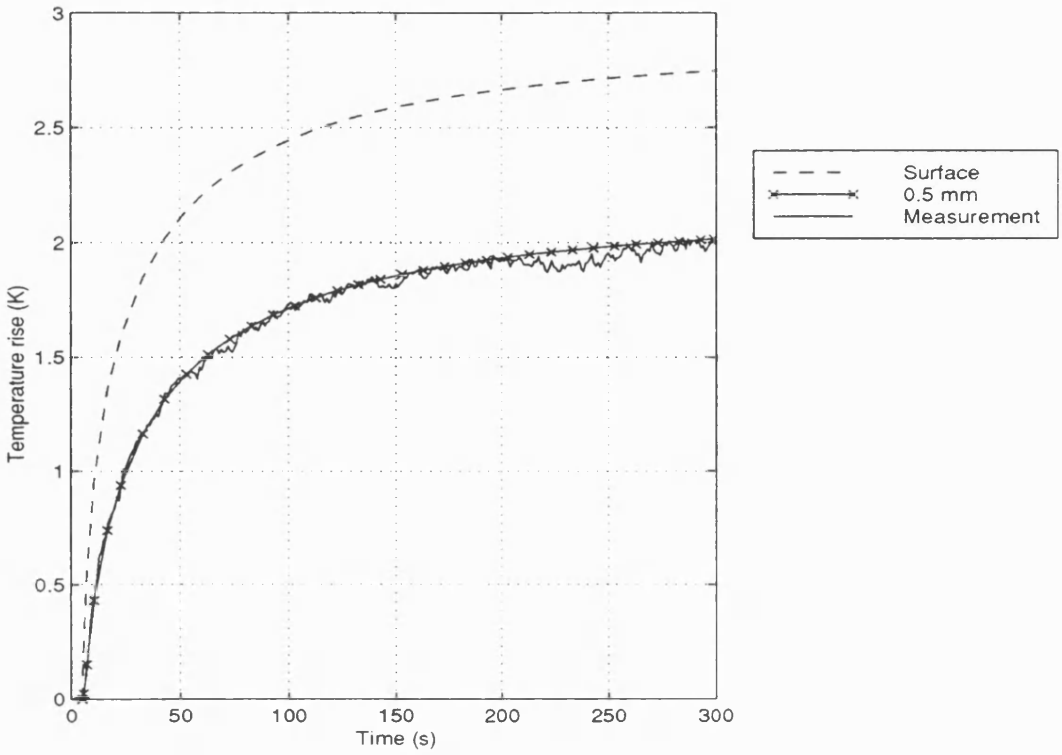

b) Transducer-PTFE separation 70 mm.

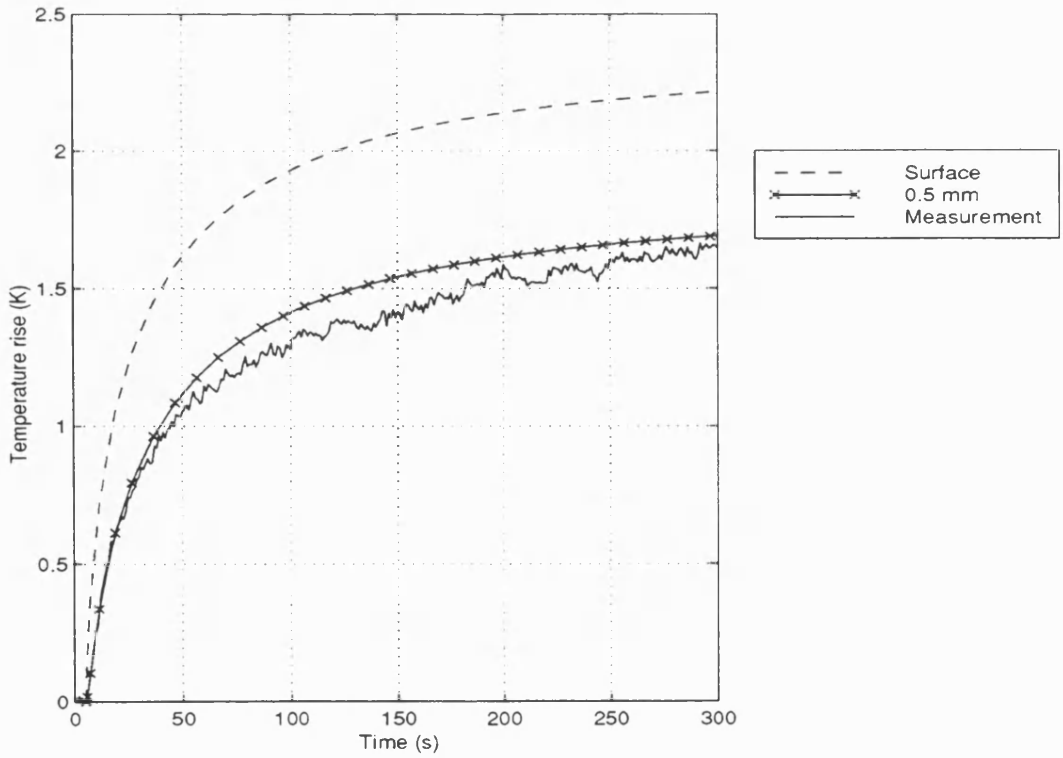

c) Heating at back of sample.

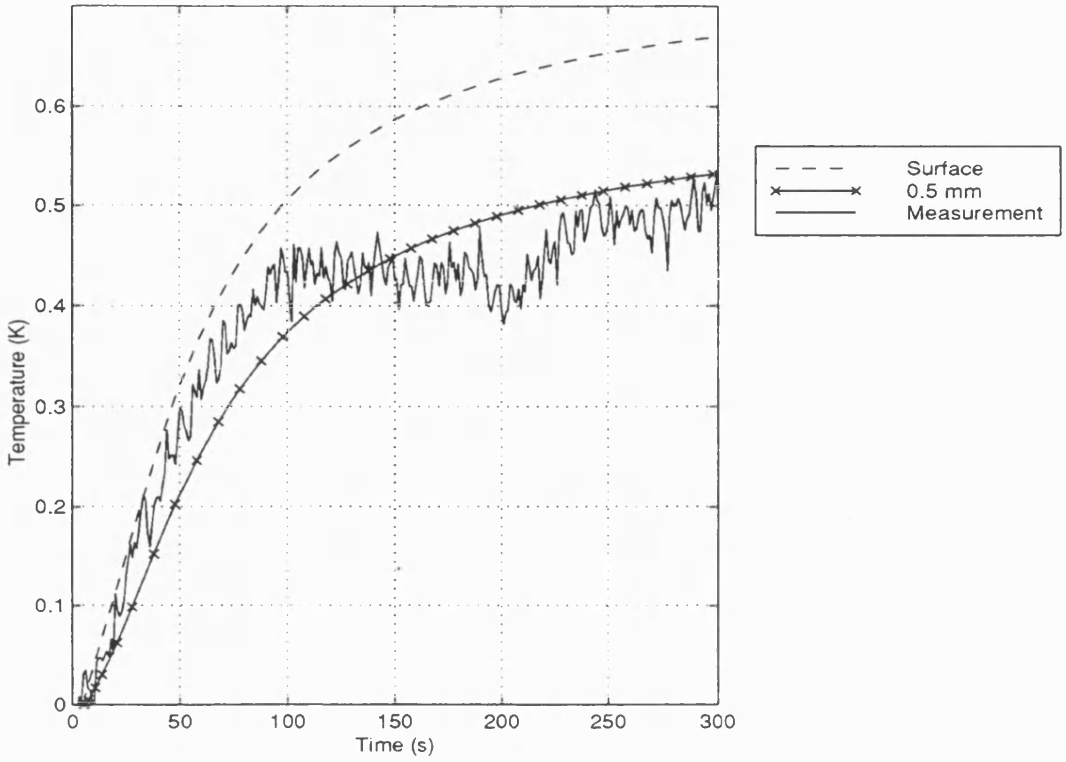

Figure 11.15: Influence of the specific heat on the predicted temperature rise.

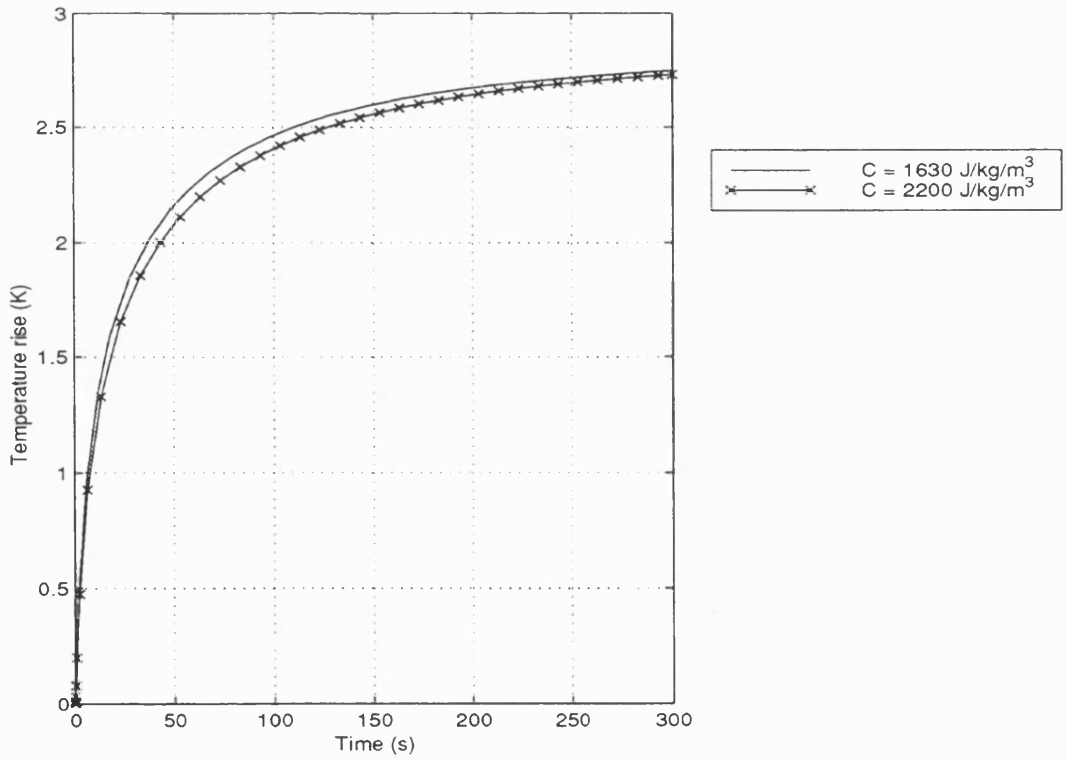

the predicted temperature rise. Using these values caused the predicted temperature rise at the measurement position to decrease by 6% and increase by 5%. The effect of a scatter component in the attenuation coefficient is more difficult to quantify. The level of the attenuation coefficient is such that the intensity is reduced to half its initial value in a distance of 0.9 mm and so, unless the attenuation is strongly dominated by scattering, any part of the beam that is scattered would be expected to be absorbed relatively close to the original scattering position. It has been shown however, in the discussion on the effect of the intensity distribution, that a relatively small change in the intensity distribution can affect that measured temperature rise.

Another factor which could lead to too high a temperature rise being predicted is an over-estimate in the intensity values. A 30% uncertainty is associated with the I_{spta} measurement from BECA and as nearly all of this is systematic error it can not be reduced significantly by taking more readings. A variety of factors contribute to this error, including the calibration of the elements and the gain of the system. Different sources of error will affect the intensity distribution in different ways: errors in calibration of the hydrophone elements could change the shape of the intensity distribution while errors in the gain of the system would act equally on all the hydrophone elements. Any error in the gain should, therefore, increase all the predicted temperature by a constant factor. Figure 11.16 shows the normalised plots of the predicted and measured temperature rise. It can be seen that the shape of the two curves is different and so this alone cannot account for the error.

The way that inaccuracies in the calibration of the individual elements would affect the predictions would depend upon the way these changed the shape of the intensity distribution. If the elements close to the beam axis were overestimating the intensity by 30%, due to inaccuracies in the gain and calibration, this could lead to a significant error in the predicted temperature rise.

Table 11.7 summarises the possible causes of error that could lead to a disagreement between the measurements and the predictions from the models. It shows how each source of error would affect the ratio of the modelled to measured results both for the initial rate of heating and for the maximum temperature rise.

Figure 11.16: Normalised predicted and modelled temperature rise.

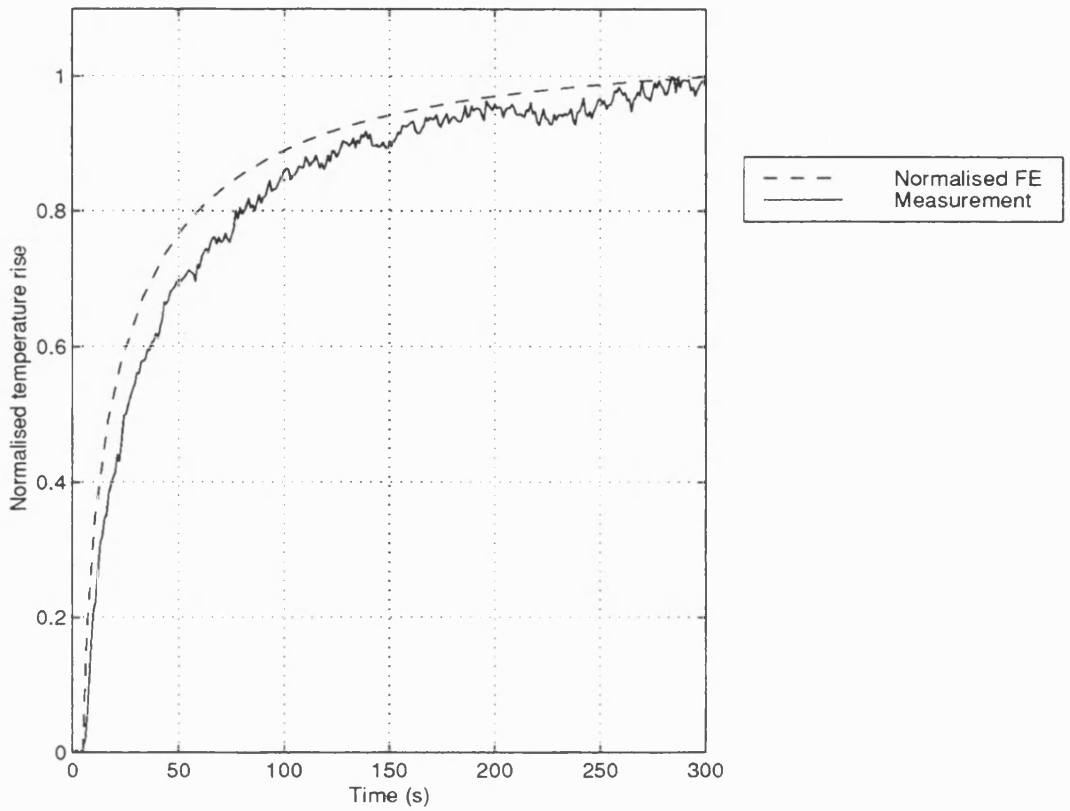

The highlighted figures indicate which of these two ratios is most affected (when both are affected equally neither figure is highlighted). The observed results were that both the initial rate of heating and the maximum temperature rise in the model were greater than the measured values but that the ratio of the modelled to measured results was greatest when the rate of heating was considered. The measured temperature rise at 10 s, for example, was 54% of the modelled value while at 300 s it was 73%. This pattern could be caused by an overestimate in the attenuation coefficient of the PTFE or a significant proportion of the attenuation being due to scatter; a large amount of absorption in the agar or a displacement of the thermocouple away from the surface of the PTFE. The fact that the attenuation coefficient was measured by NPL, the national standards laboratory, would make it unlikely that an overestimate in this is the cause of the error. Neither would attenuation

Table 11.7: Effect of errors on the initial rate of heating and the maximum temperature rise.

	Modelled/measured heating	
Error	**Initial rate of heating**	**Maximum temperature**
Underestimate thermal conductivity in PTFE	Little effect	**>1**
Underestimate specific heat of PTFE	**>1**	Little effect
Overestimate attenuation	**>1**	>1
Significant scattering	**>1**	> 1
Uniformly overestimate intensity	> 1	> 1
Off-axis intensity ignored	Little effect	<1
Significant absorption in agar	**>1**	>1
Thermocouple not at interface	**>1**	>1

in the agar seem a likely cause, as the measurements carried out on this showed that this reduced the power reaching the PTFE by less than 5%, much less than is necessary to explain the observations. The effect of a scattering component in the attenuation is difficult to quantify without knowing the scattering coefficient but the fact that the glass fibres were much smaller than the wavelength of the ultrasound (diameter of fibres 15% of the wavelength) would suggest that scattering is unlikely to make such a large difference in the results. This would seem to indicate that displacement of the thermocouple is the most likely cause and the fact that the agreement between the measurements and the predicted temperature rise at 0.5 mm from the surface is good for three different sets of exposure criteria gives credence to this.

11.8. Discussion

It can be seen that there are difficulties associated with modelling even relatively well defined situations. The factors that generate the most significant errors in the model include:

- the size of the finite elements;
- uncertainties in the intensity values;
- the resolution to which the intensity in modelled.

These factors interact in such a way that, for example, the effect of changing the size of the finite elements depends upon the intensity step size.

The situation gets more complicated still when the predictions are compared with measured values. Here the most significant cause of error is associated with not knowing the exact position of the thermocouple.

The large temperature gradient at the front of the PTFE means that a displacement of 0.5 mm can lead to an error of over 30% in the recorded temperature. The way the thermocouples are made, by twisting 50 μm wire together and then welding, mean that the size of the bulb is likely to be at least 200 μm and that it does not lie in line with the rest of the wire. It is also difficult to attach the bulb to the surface of the PTFE. It was thought that any material used to stick the bulb to the surface could effect the result, either by increasing the absorption or changing the thermal conductivity and so the thermocouple was attached by taping the wire to the PTFE at 1 cm from the bulb. This did mean, however, that thermal contact between the thermocouple and the PTFE could not be ensured. The sensitivity of the measured temperature rise to the position of the thermocouple demonstrates the difficulty in taking measurements in vivo. It may be that some of the animal studies in which thermocouples have been placed close to the bone have underestimated the temperature rise at the bone surface.

11.9 Chapter Summary

A finite element model of a layer of bone mimic encased in agar has been constructed and the sensitivity of the results to a range of input factors has been determined. It was been shown that models in which only one set of thermal properties are used, as is necessarily the case when using

techniques based on the point source solution to the BHTE, can produce significant errors when there is a large difference in the thermal properties of the different layers. The way that the intensity distribution is modelled was shown to affect the predicted temperature rise to a greater extent than has been suggested by other authors. This appears to be because significantly more of the energy in the beam was outside the -6 dB diameter than is the case in the intensity distributions commonly considered. When the results from the model were compared with the experimental measurements they were found to overestimate the temperature rise by 38%. This is thought to be due to the thermocouple not being directly in contact with the surface of the bone mimic. If it is assumed that the thermocouple is 0.5 mm in front of the bone mimic, good agreement is obtained between the predicted and measured temperature rise for a variety of exposure conditions.

Chapter 12

Finite Element Model of Vertebrae Heating

12.1. Introduction

Producing a model of the vertebrae was a more complex procedure than developing the model of the bone mimic. One reason for this was the shape of the samples. It can be seen from Figure 5.9 that these did not possess the axial symmetry used when modelling the bone mimic. To overcome this, while still keeping the model to a size that could be handled using available computing resources, simplifications were made and then the effect of these was tested.

The models allowed the uncertainty caused by the lack of information about the thermal and physical properties of the bone to be examined and comparison of the results with the experimental measurements allowed an estimate of the attenuation coefficient to be obtained. Comparing models in which the shape of the bone sample was modelled in different ways also gave information about the degree to which the complexity of the model structure affects the results.

12.2. The Finite Element Model.

Although ANSYS, the finite element package used, has the capability to perform three-dimensional modelling, doing so increases the number of nodes, and consequently the processing time. The 'computational cost', an indicator of processing time, was calculated by Ottosen and Peterson (1992) for a simple heat flow calculation in one, two and three dimensions. For models with 5, 5 x 5 and 5 x 5 x 5 nodes respectively the ratio of computational costs was 1:61:6400. For this reason it was decided not to attempt a three-dimensional model but to use a two dimensional axisymmetric approximation. The model used is illustrated in Figure 12.1.

Although the use of axial symmetry was not completely appropriate for the vertebrae it gave a good representation of the ultrasound beam. The likely effect of this simplification will be considered later in this chapter.

Figure 12.1: Model of vertebra embedded in agar.

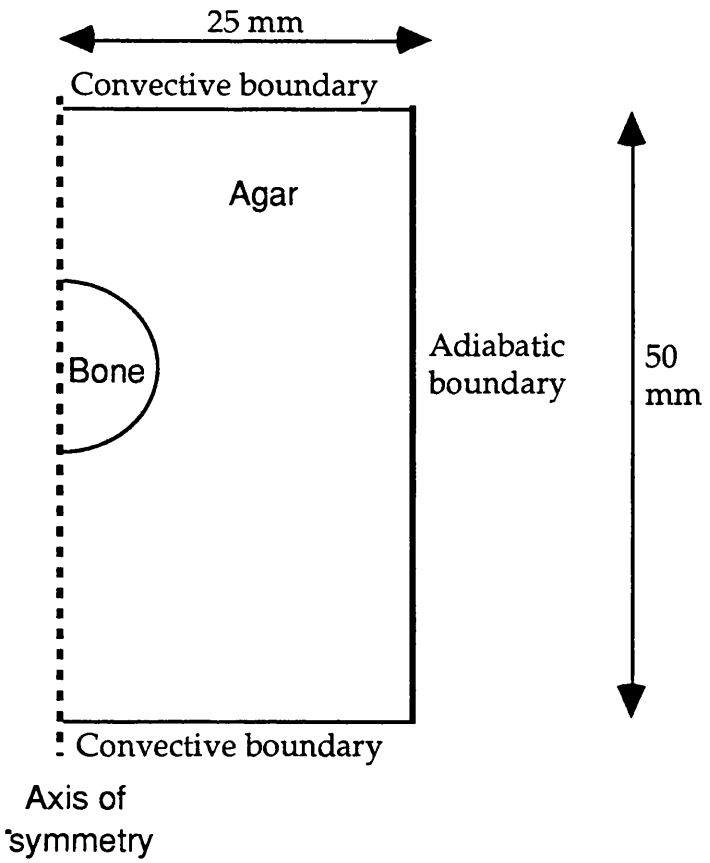

The maximum element length was 0.25 mm within the bone and 5 mm in the agar and care was taken to ensure that there was not a sudden change in size between adjacent elements. Around the bone was a layer of very thin elements, 0.01 mm wide. This served the same purpose as the thin layer of elements in front of the bone mimic; it ensured that the heating load on the nodes at the agar-bone interface only affected a small volume of agar and hence did not lead to a significant overestimate in the heat generation (see Section 11.4.1). The configuration of elements used in the 39 week model is shown in Figure 12.2.

The two sets of thermal parameters used in chapter 9 were also applied to this model; for convenience these and the properties of the agar are restated in table 12.1.

Once the model had been constructed it was necessary to apply the heating loads. The intensity at any point within the bone now depended on both the distance off axis and the distance from the front of the curved bone-agar interface. The way the loads were calculated is illustrated in figure 12.3.

Figure 12.2: Arrangement of elements in the model of the 39 week sample.

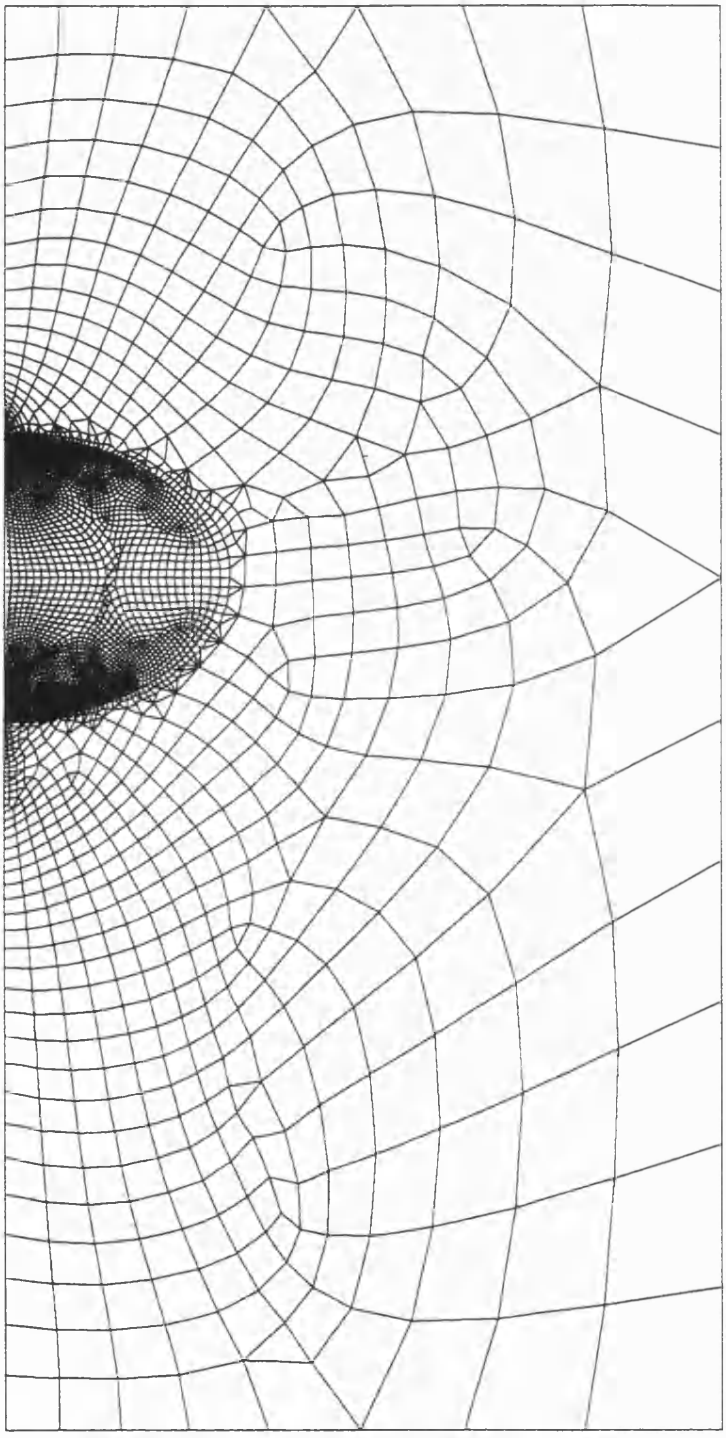

Table 12.1: Thermal properties of bone and agar

	Bone NCRP	Bone Biyikli	Agar
Density kg m^{-3}	1300	1100	1000
Thermal conductivity $Wm^{-1}K^{-1}$	0.58	0.30	0.609
Specific heat $J\,kg^{-1}K^{-1}$	1600	2200	4289
Thermal diffusivity mm^2s^{-1}	0.28	0.11	0.14

Figure 12.3: Geometry used in calculating path length through bone.

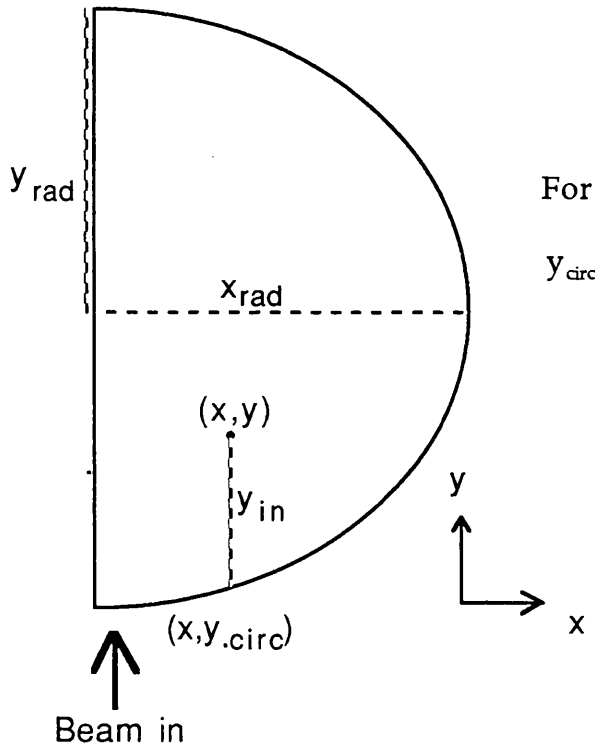

For an ellipse centred on $0,y_o$

$$y_{circ} = y_o - \sqrt{y_{rad}^2 - \frac{x_{rad}^2}{y_{rad}^2}x^2}.$$

Once y_{circ}, the co-ordinate of the ellipse directly in front of the bone, is known the path length through the bone, y_{in}, can be calculated. The intensity at the bone surface is then derated using a factor of $\exp(-2\alpha y_{in})$ in order to give the intensity at the point of interest. Refraction and mode conversion to shear waves at the bone surface were neglected as it was thought that the properties of the bone were not well enough defined to

model these adequately; this decision is discussed in Section 12.6. The effect of reflection at the bone surface was incorporated at a later stage (see section 12.3.2). The intensity distribution at the front of the bone was modelled using the step function, with step size 0.5 mm, that was used when modelling the bone mimic. The cut-off point for the beam was taken as 4.5 mm.

The total thickness of the agar layer was taken as 50 mm, of which 15 mm was in front of the bone and the distance from the model axis to the outer edge of the agar was 25 mm. Convective boundary conditions with h = 400 W $K^{-1}m^{-2}$ were applied to the upper and lower surface of the agar, while the outer edge, which was surrounded by the PVC tubing, was modelled as having no heat flow across it. The modelling of the bone mimic had shown that these conditions did not introduce significant errors.

A transient analysis was carried out which produced solutions at a series of time steps between 0 and 300 s. The initial time step was set at 0.04 s and the maximum step was 10 s. The ANSYS automatic time stepping routine, described in appendix B was used to determine the time increments.

12.3. Modelling the 39 Week Sample.

The first model produced was of the 39 week sample; as this is the most mature of all the samples its properties should be most like the values quoted for adult bone. The bone was considered to be homogeneous because, although this was known to be a simplification, the physical properties of the layers within the bone were not known accurately enough to justify a more complex model. The ellipse used to define the bone volume had axes ($2x_{rad}$ and $2y_{rad}$ in Figure 12.3) of length 15 and 10 mm. The appropriate value to use for the attenuation coefficient was unclear, as has already been discussed, and so the first set of models used a range of values and compared the predictions with the experimental measurements.

12.3.1. The effect of the attenuation coefficient on the temperature rise.

The uncertainty in the value of the attenuation coefficient of bone was discussed in section 3.4 and it was shown that for a frequency of 3 MHz values in the range 1.5 - 4 Np cm^{-1} had been measured; while NCRP

report 113 (1992) quotes a value of 1.5 Np $cm^{-1}MHz^{-1}$ which for the frequency used (3.5 MHz) gives 5.25 Np cm^{-1}. Three values of attenuation coefficient spanning this range were therefore input into the model: 1.5, 3.5 and 5.25 Np cm^{-1}. As there is also uncertainty about the thermal properties of the bone, models were produced with the two sets of thermal data used previously. Table 12.2 shows the predicted temperature rise on axis after 300 s at the surface of the bone and the maximum temperature rise in the bone at this time. It can be seen that there is a factor of over two difference between the lowest and highest value for the maximum temperature rise. If the difference due purely to the range of values of the attenuation coefficient is considered, i.e. data using each set of thermal parameters is considered separately, the largest effect is seen at the surface of the bone, where the predicted temperature rise using an attenuation coefficient of 5.25 Np cm^{-1} is a factor of 1.8 ± 0.1 greater than that obtained using a value of 1.5 Np cm^{-1}.

Table 12.2: Surface and maximum temperature rise (in K) at 300 s .

Absorption coefficient (Np cm^{-1})	NCRP data		Biyikli data	
	Surface	Max.	Surface	Max.
1.5	1.7	2.2	2.0	3.5
3.5	2.6	3.1	3.1	4.6
5.25	3.0	3.5	3.7	5.1

These results also show the difference between the surface and the maximum temperature rise and it can be seen that for the Biyikli data this can be over 50%. This is important as most experimental studies measure the temperature rise at the bone surface and, while this will indicate the temperature rise experienced by the soft tissue around the bone, it may be much less than the maximum temperature rise inside the bone.

12.3.2. Comparison of predicted and observed temperature rise.

In order to compare the predicted results with the experimental measurements it was necessary to allow for reflection of the beam at the bone surface. To obtain an estimate of the transmission coefficient two sources of data were considered: Fry and Barger's (1978) measurements of the velocity and density of infant skull and the data used by Carstensen et al. (1990) when they attempted to model the temperature rise in mouse

skull. Fry and Barger give the density of the infant skull as 1740 kg m^{-3} and the velocity as either 2060 or 2260 m s^{-1} depending upon the measurement technique. This would suggest an intensity transmission coefficient in the range 79 - 83%. Carstenson et al., while obtaining a measurement of 9% as the lower limit of the reflection coefficient used a transmission coefficient of 75% in their calculations. In the light of these results the transmission coefficient was assumed to be 80%. No attempt was made to account for the fact that the bone surface was at an angle to the beam, as it was felt that the simplification in the geometry of the model and the uncertainty about parameters such as the speed of sound made this level of complexity inappropriate. The possible effect of this will be considered later in this chapter. Figure 12.4 compares the predicted and measured values for the 39 week model. It can be seen that the highest value of absorption coefficient significantly overestimates the temperature rise and that, for both sets of thermal data, the measurements fall somewhere between the predictions obtained using values of 1.5 and 3.5 Np cm^{-1} for the attenuation coefficient.

The measurements on the bone mimic, however, had suggested that the measured temperature rise could underestimate the true value due to distance of the thermocouple from the surface. The difference in the predicted temperature rise at the bone surface and 0.5 mm in front of this was therefore calculated in order to estimate the error in the measured temperature. It was found that, for all the combinations of attenuation coefficient and thermal properties, the predicted temperature rise 0.5 mm from the surface of the bone was between 0.72 and 0.76 times that at the surface. If this factor is applied to the measured values it would suggest that the temperature rise at the bone surface might actually be as high as 2.5 K. This is likely to be an upper limit of the temperature rise as the shape of the bone samples meant that it was easier to attach the thermocouples to these than to the bone mimic and so the thermocouple may well have been closer to the bone surface than it was to the bone mimic. The temperature rise along the beam axis close to the surface of the bone is shown in Figure 12.5. These graphs also show how the attenuation coefficient affects the temperature distribution. The higher values of attenuation coefficient give a greater temperature rise at the front of the sample but this falls off more quickly as less of the power in the beam penetrates the sample.

Figure 12.4: Comparison of predictions with experimental measurements.

a) NCRP data

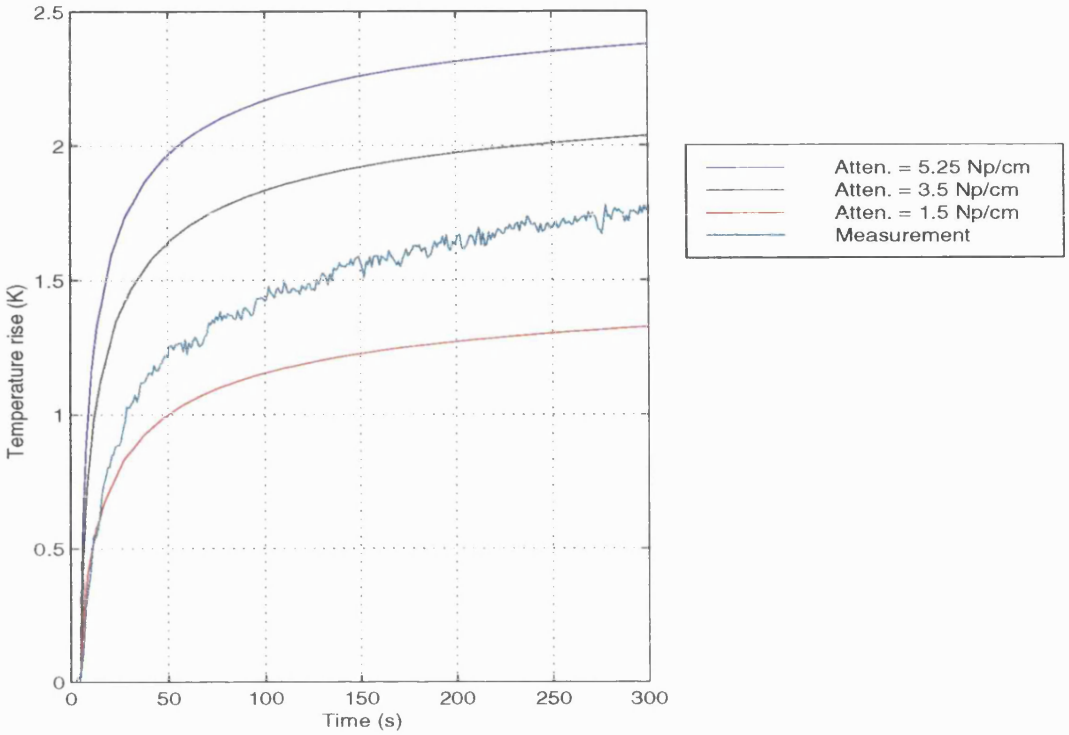

b) Biyikli data

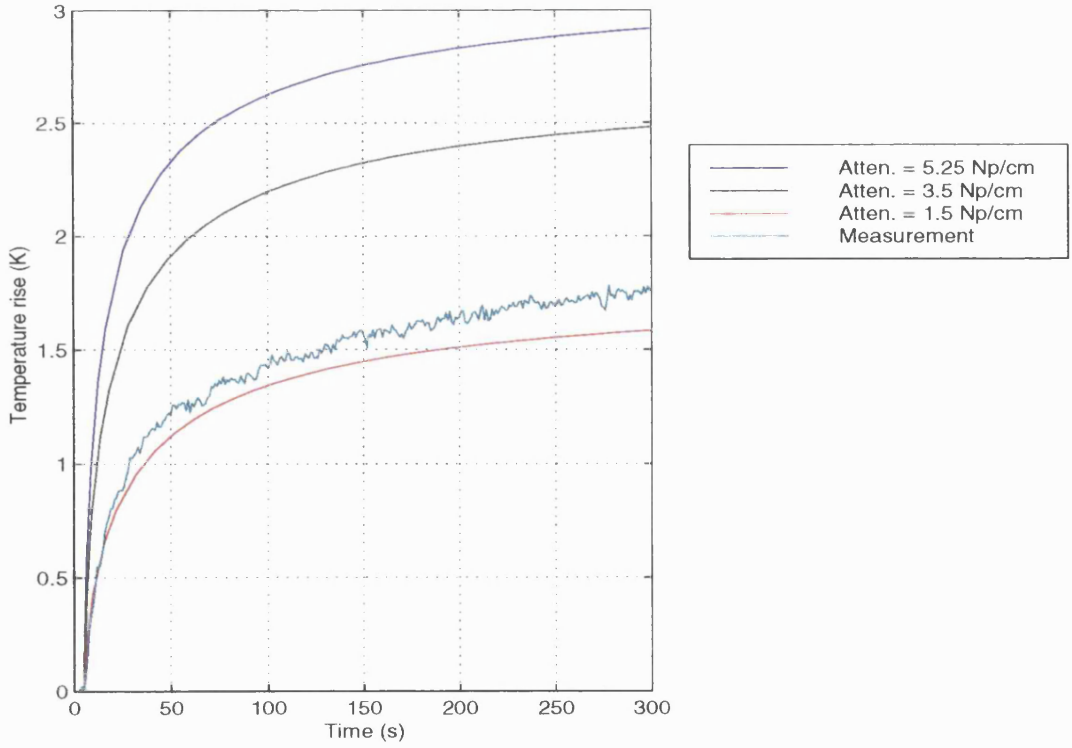

Figure 12.5: Axial temperature rise.

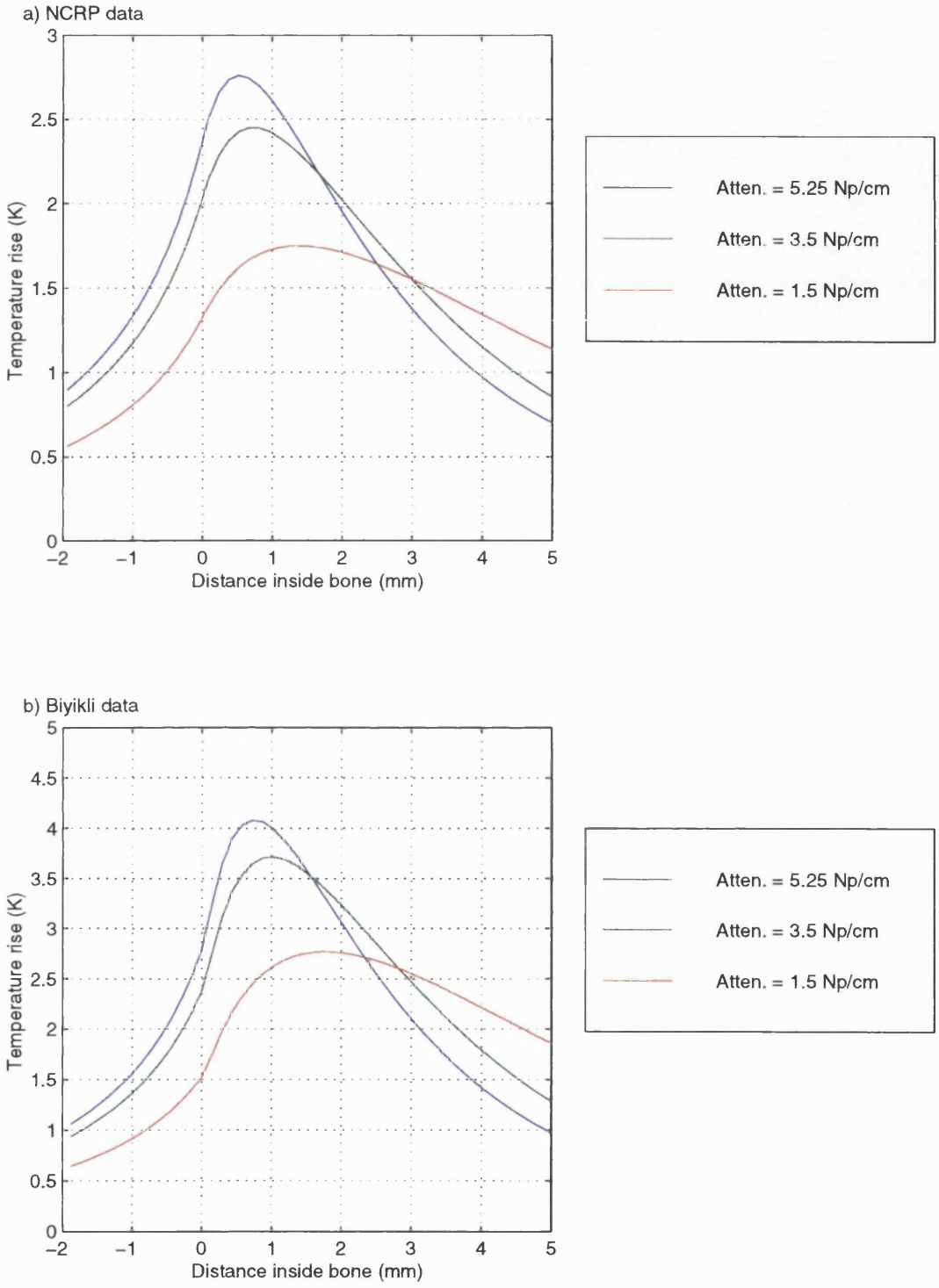

12.4. Modelling the 23 Week Sample.

The measurements on the bone samples had shown that the measured temperature rise increased with the age of the bone sample. Two possible reasons for this are the smaller size of the younger samples and the fact that the composition was changing with age; for example the older samples might be expected to have more calcified tissue and less cartilage. A model of one of the younger samples could give information about how reducing the size of the bone affected the predicted temperature rise and demonstrate the degree to which this, rather than the difference in composition, lead to the lower temperature rise. The 23 week sample was chosen as major axis of this was of length 9 mm which corresponded to the width of the ultrasound beam used in the model. Figure 12.6 shows the predicted and measured temperature rise; the NCRP thermal data was used and a reflection coefficient of 20% was assumed, as was done previously.

Figure 12.6 Predicted and measured temperature rise for 23 week sample (NCRP data).

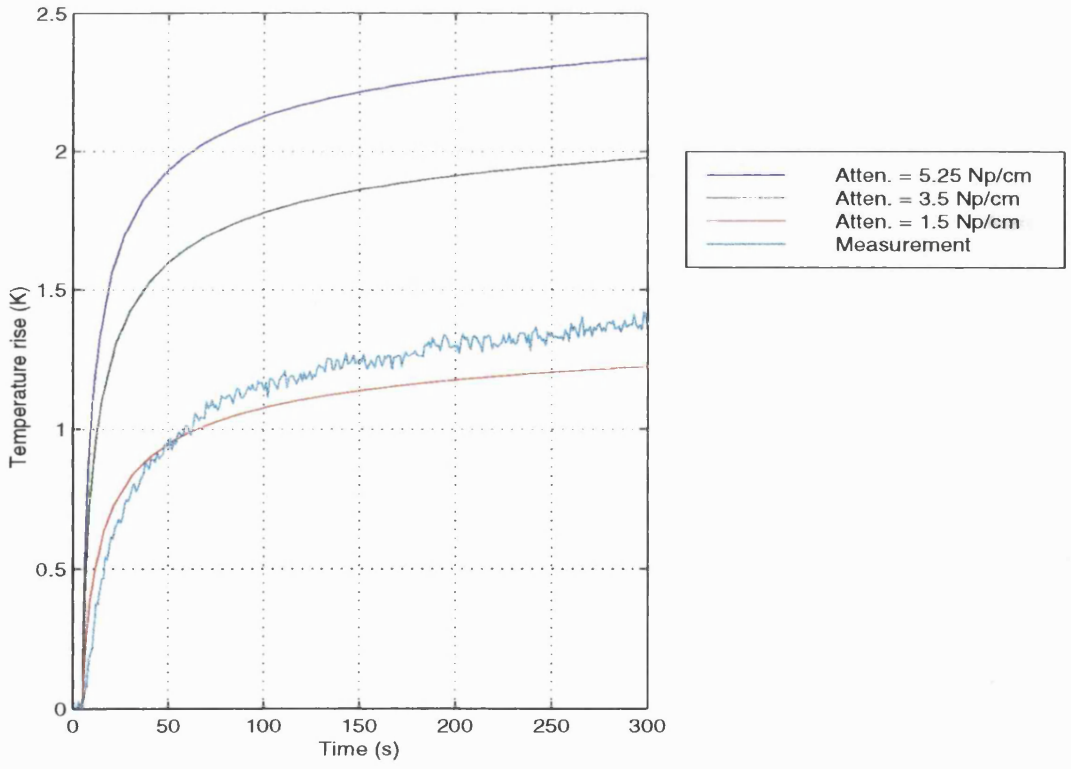

It can be seen that the measured temperature rise is much closer to that obtained using an attenuation coefficient of 1.5 Np cm^{-1} than was the case

for the 39 week sample. When the Biyikli data was used in the model the predicted temperature rise obtained using this value for the attenuation coefficient was above the measured temperature rise, as can be seen in Figure 12.7. This apparent reduction in the attenuation coefficient, relative to the 39 week sample, reflects the difference in the composition of the two samples that was illustrated in Figure 5.13. The 23 week sample is less calcified and so it might be expected to have a lower attenuation coefficient. Figures 12.6 - 12.7 are consistent with the value of attenuation coefficient of 1.44 ± 0.23 Np cm^{-1} reported by Dussik, Fritch, Kyriazidou, Sear (1958) for cartilage at 3 MHz.

Figure 12.7: Predicted and measured temperature rise for 23 week sample (Biyikli data).

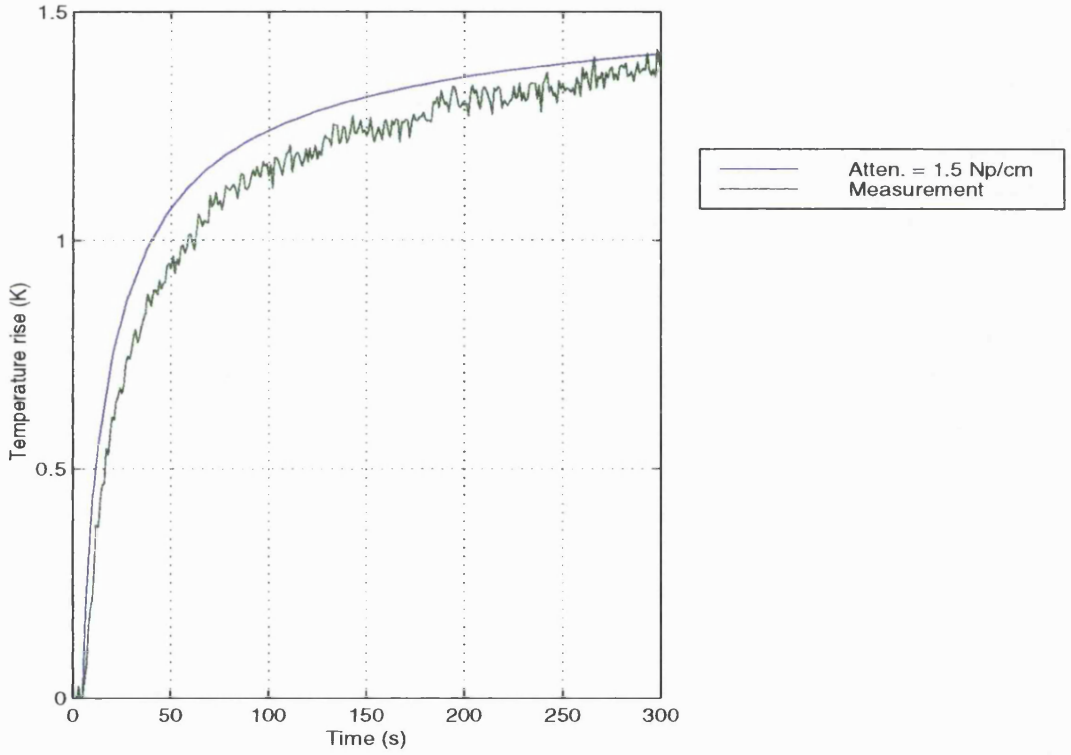

Initially, however, the bone appears to heat up more slowly than is suggested by the model although with increasing time the measured values approach, and for the NCRP data overtake, the predicted values. One reason for this may be that the thermocouple is not in contact with the surface of the bone but it may also be to do with the structure of the bone. It was shown in Figures 5.13 that in the 23 week sample there was a layer of cartilage covering the posterior surface of the bone, while there was very little cartilage at this position in the 39 week sample. This layer

could lead to an initial rate of heating that reflected the attenuation coefficient of the cartilage followed by a later contribution from the bone as the heat diffused across to the measurement position. As the attenuation coefficient of cartilage is lower than that of bone, this could lead to a curve of the shape seen in Figures 12.6 - 12.7. The uncertainty about the thermal properties of the bone and the exact measurement position, however, means that while this is a possible explanation for the shape of the heating curve, no definite conclusions can be drawn.

12.5 Comparison with the Heated Disc Model

The FEM results obtained for the 39 week sample were compared with the predictions from a heated disc model similar to those discussed in Chapter 9. The heated disc model considered a plane layer of bone that was 10 mm thick surrounded, as must always be the case when using the heated disc approach, by a region with identical thermal properties and a top hat intensity distribution was used. Both techniques assumed a reflection coefficient of 20%. The finite element model was found to predict a lower temperature rise than the heated disc model. Figure 12.8 shows the finite element and heated disc results obtained using a value of 1.5 Np cm^{-1} for the absorption coefficient.

There are two reasons why the finite element model predicted a lower temperature rise: the fact that the intensity distribution is entered more accurately in the finite element model and the fact that this model can include the properties of the agar gel as well as those of the bone. The effect of the intensity distribution was considered in the previous chapter and shown to have a considerable effect on the predicted temperature rise. A small part of the observed difference could be due to the fact that the cut-off radius imposed on the beam in the finite element model meant that the total power in this model was only 41 mW, compared to 50 mW in the heated disc model. It was shown in Chapter 11, however, that increasing the cut-off radius to 7.5 mm so that the power in the beam was 46 mW only increased the predicted temperature rise by 2%. It appears, therefore, that it is the intensity distribution rather than the difference in power that is causing the difference. To determine the effect of this the model was re-run using the 'top hat' distribution. The results obtained are shown in Figure 12.9. It can be seen that when the NCRP data are used, giving the agar and bone layers similar values of thermal conductivity, there is little difference between the results generated by the

Figure 12.8: Comparison of results from finite element and heated disc models.

a) NCRP data

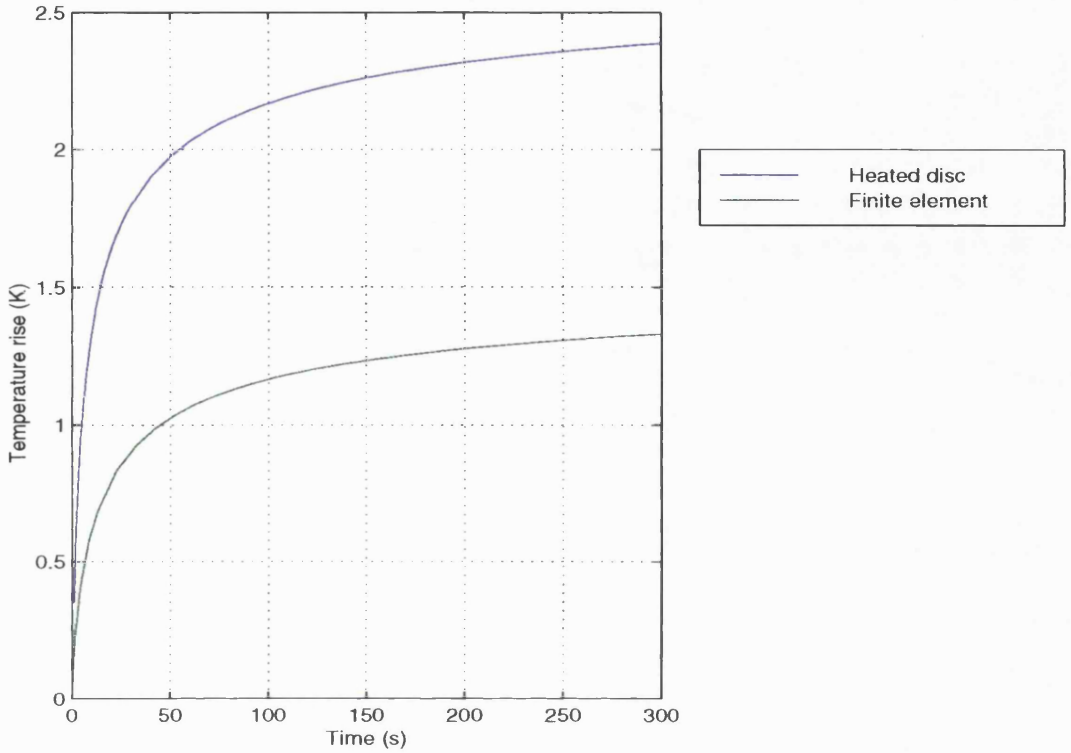

b) Biyikli data

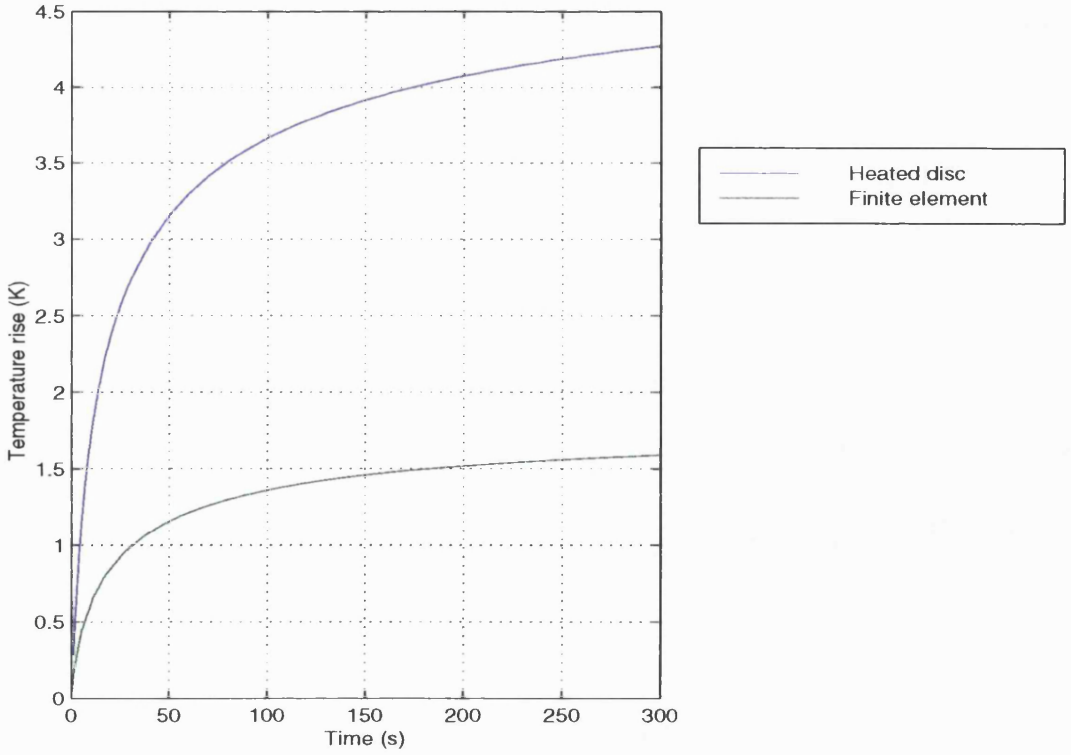

Figure 12.9: Comparison of results from finite element and heated disc models when using top hat intensity distribution.

a) NCRP data

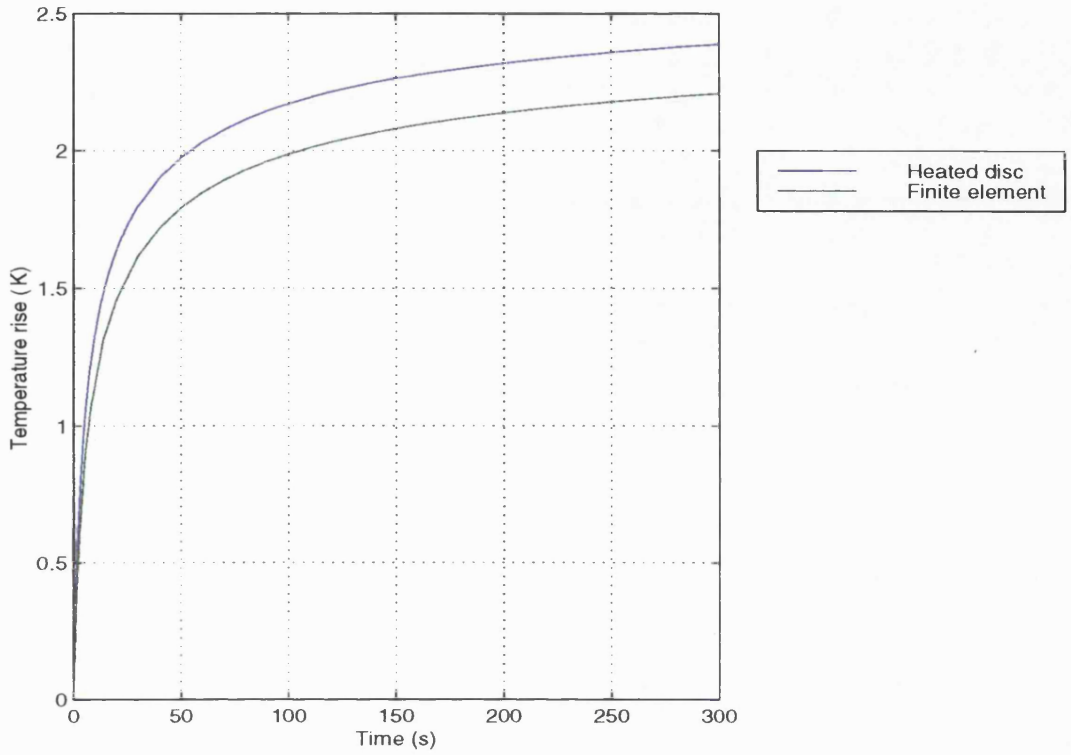

b) Biyikli data

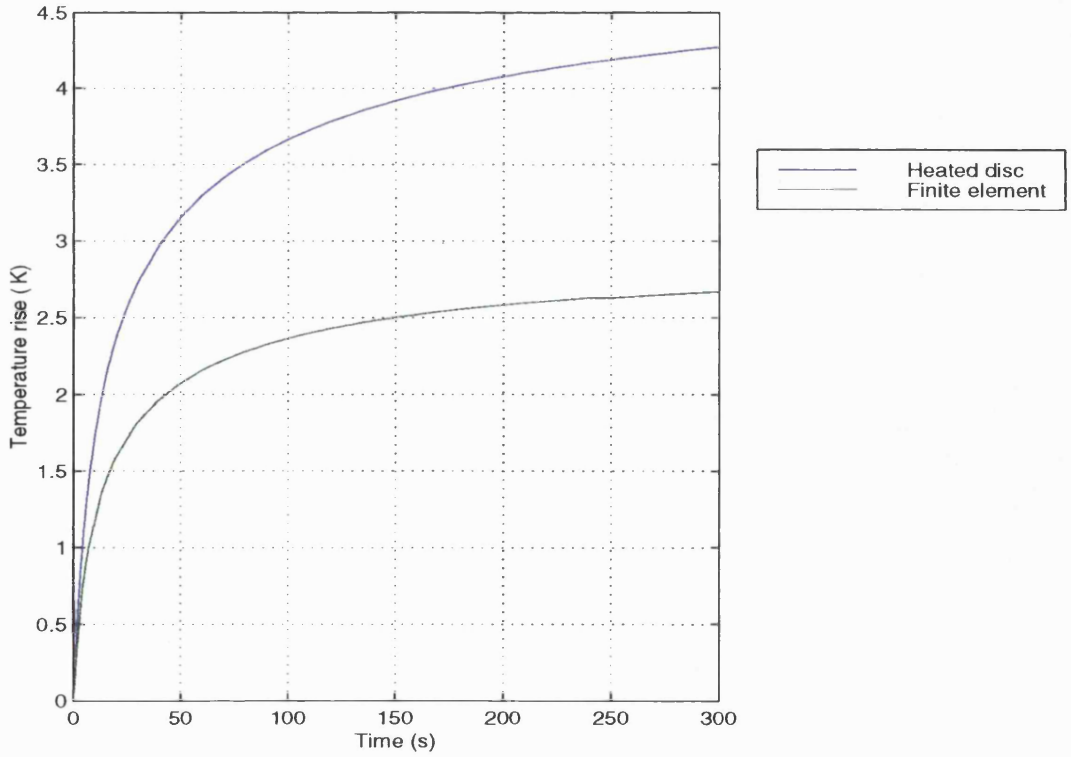

two techniques. However, when the Biyikli data are used and the thermal conductivity of the bone is approximately half that of the agar, the fact that the heated disc model cannot allow for this leads it to overestimate the temperature rise by over 50%.

As might be expected, the results from the finite element model are affected less by the properties of bone than are the heated disc results. The difference in the predicted temperature rise at the bone surface is reduced to a factor of 1.2 compared to 1.8. This is because the temperature rise at this point is now affected by the properties of the agar as well as those of the bone. The maximum temperature rise predicted with the Biyikli data is still 50% greater than that observed with the NCRP figures however.

12.6. The Effect of Simplifications in the Model

Restrictions on computer resources and uncertainties about the detailed structure of the bone made it necessary to include various simplifications in the model. The effect of these simplifications will now be discussed.

12.6.1. The effect of the simplified geometry.

The imposition of axial symmetry led to the shape of the bone being modelled as an ellipsoid despite the fact that they were really cylinders with an elliptical cross-section. This imposition underestimated the amount of bone. The effect of this could be estimated by comparing the model used so far with one in which the plane of the model is along the bone. This leads to the bone being represented as a rectangle and when axial symmetry is adopted modelled as a disc. This is illustrated in Figure 12.10. This approach overestimates the amount of bone, as opposed to the model used so far which underestimates it and so the true representation would fall somewhere between these two extremes. It will produce a model similar to that used for the agar-PTFE phantom except that there will be a layer of agar behind the bone. The configuration of the elements in this model is shown in Figure 12.11. This is for the 39 week sample and so the thickness of the bone layer was 10 mm, the value previously used for the minor axis of the ellipse. Figure 12.12 compares the rate of heating obtained from this model with the results from the ellipsoidal model when an attenuation coefficient of 3.5 Np cm^{-1} was used. It can be seen that the temperature rise at 300 s is almost independent of the model chosen (less than 0.1 K) but that the rate of heating is different. This is due to the fact that the biggest difference between the thermal properties

Figure 12.10: Geometry of bone models.

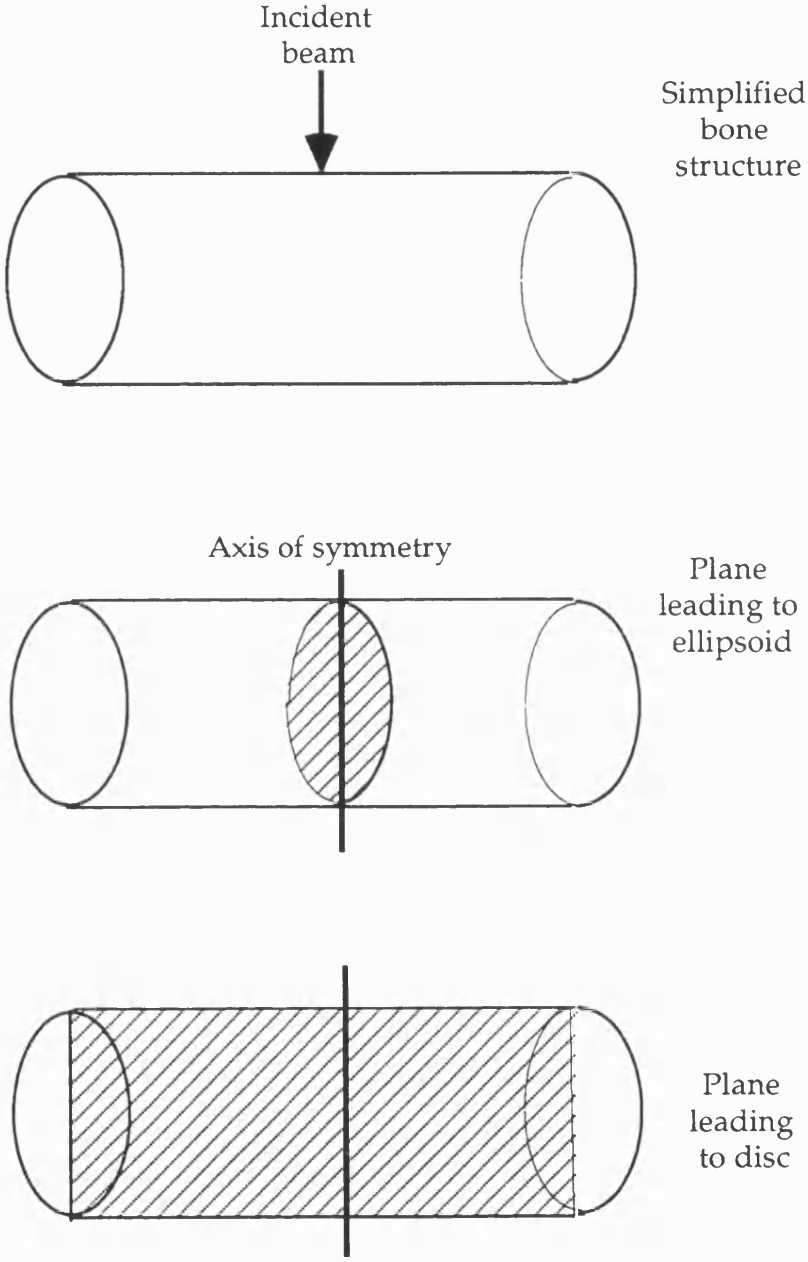

Figure 12.11: Configuration of elements when plane of model rotated.

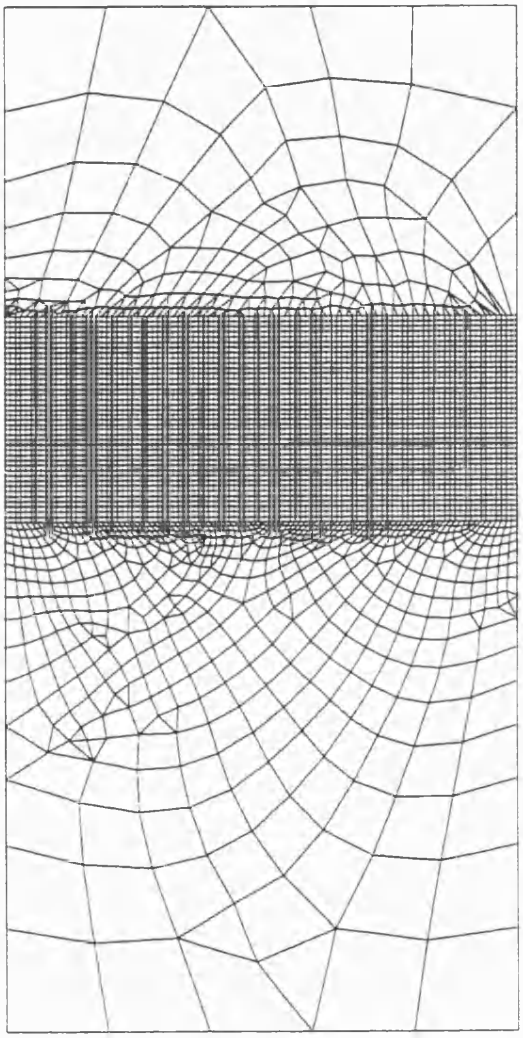

Figure 12.12: Effect of changing the plane of the model.

a) NCRP data

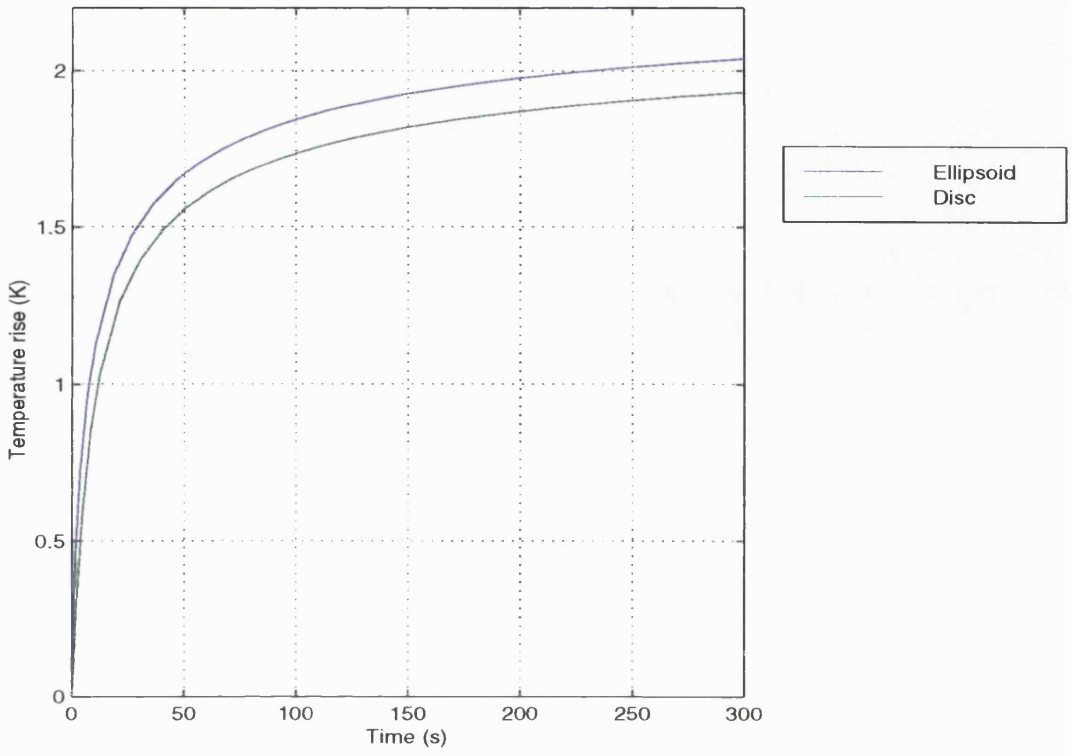

b) Biyikli data

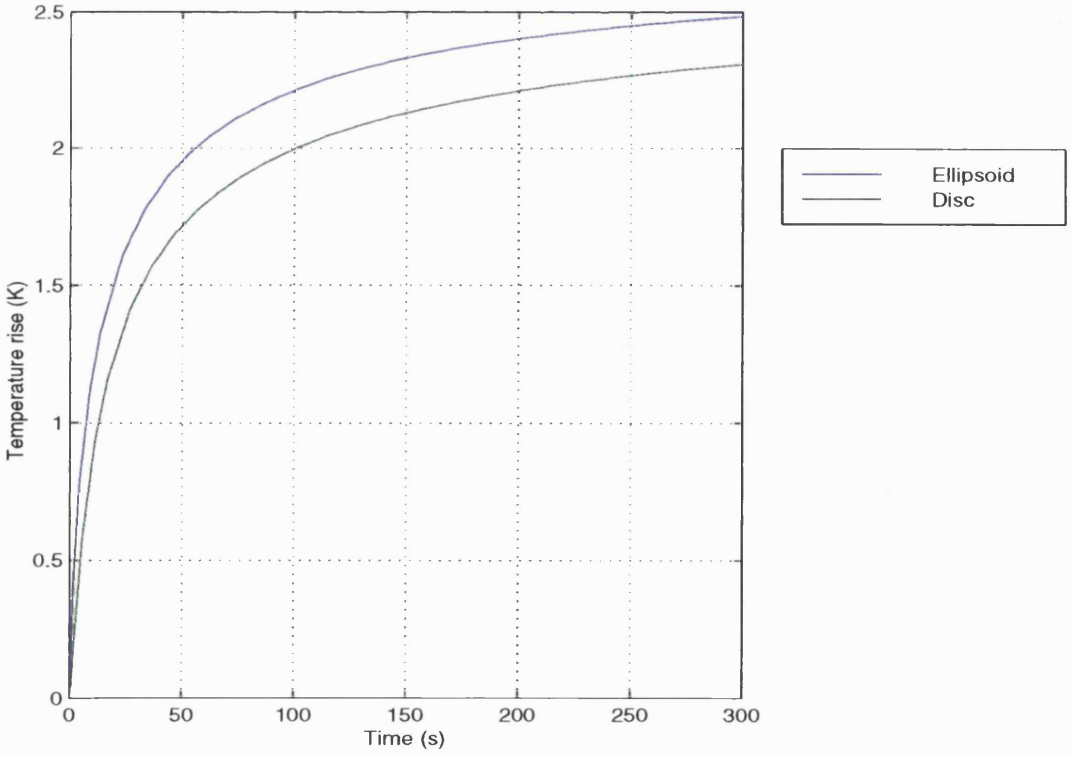

of bone and agar gel is in the specific heat which is 1900 ± 300 J kg^{-1} K^{-1} for bone and 4289 J kg^{-1} K^{-1} for agar gel. This means that in the ellipsoidal model, in which there is more agar, the temperature rise occurs more slowly. The specific heat plays no part in the steady state temperature however. While there is also a difference in the thermal conductivity between the two materials this appears to make little difference to the final results. This may be because the difference in structure is outside the beam area.

12.6.2. The agar-bone interface

One important feature of the agar-bone interface, which is different to that of the bone mimic is that it is curved. This affects the transmission of the ultrasound into the bone in two ways: the change in transmission coefficient with angle of incidence and the effect of refraction.

The transmission coefficient depends upon the angle of incidence of the ultrasound beam and so, as the curved surface means that the angle of incidence increases with distance from the centre of the bone sample, it was necessary to determine the effect of this. If mode conversion into shear waves is neglected then the fraction of the incident power transmitted into the bone is given by:

$$T = \frac{4Z_1Z_2\cos\theta_i\cos\theta_r}{(Z_1\cos\theta_r + Z_2\cos\theta_i)^2}. \qquad \text{(Equation 12.1)}$$

where θ_i is the angle of incidence and θ_r is the angle of refraction (Miller, 1986). In order to calculate this it is necessary to consider how the angle of the surface of the bone changes with position. This can be achieved by expressing the loci of the ellipse in its parametric form, $x = a\cos\phi$, $y = b\cos\phi$, where a and b are the length of the axes (x_{rad} and y_{rad} in Figure 12.2) and the choice of ϕ defines the point on the surface of the ellipse. If this is done the gradient of the normal to the ellipse, m, is given by $m = (a/b)\tan\phi$ and so the angle between the vertical and the normal, θ_i, is given by $\tan^{-1}(1/m)$. This is illustrated in Figure 12.13.

Figure 12.13: The normal of the ellipse

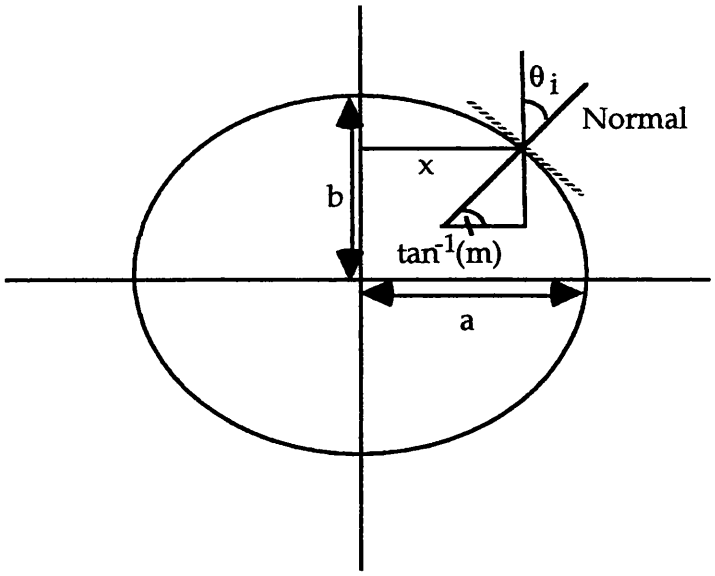

The relationship between the angle of incidence and the angle of refraction can then be calculated using Snell's law:

$$\frac{c_a}{c_b} = \frac{\sin\theta_i}{\sin\theta_r}$$

where c_a and c_b are the speed of sound in the agar and bone respectively. These were taken as 1480 ms^{-1} for agar and 2200 ms^{-1} for bone, this value being in the range quoted by Fry and Barger (1978) for infant skull. It is assumed that the beam is a plane wave which is travelling vertically, as in the region where the measurements were taken the diameter of the beam changes by less than 3% in the 5 mm on either side of the measurement position. Table 12.3 shows the values of θ_i for a range of positions across the bone and the corresponding values of θ_t and the transmission coefficient T_{coeff}. Distances up to 3.5 mm from the beam axis were considered as it had been shown for the bone mimic that over 95% of the temperature rise is due to heating of this area. It can be seen that for the larger ellipse, which has dimensions corresponding to those of the 39 week sample, there is very little change in transmission coefficient over this range and even for the smaller ellipse, corresponding to the 23 week sample, it is only when the distance from the beam axis exceeds 3 mm that the transmission coefficient is reduced by more than 10% of its value on-axis. These results are, however, very dependent on the velocity of the wave in bone and using a larger value, closer to those

Table 12.3: Angle of incidence and refraction of beam and corresponding transmission coefficient.

	x (mm)	θ_i (degrees)	θ_t (degrees)	T_{coeff}
x_{rad} = 7.5 mm, y_{rad} = 5mm				
	1	5	7	0.80
	2	11	15	0.80
	3	16	24	0.79
	3.5	20	29	0.78
x_{rad} = 4.5 mm, y_{rad} = 2mm				
	1	7	10	0.80
	2	15	23	0.79
	3	26	40	0.75
	3.5	35	55	0.67

normally quoted for adult bone, would increase the change in transmission coefficient with angle.

The degree of refraction of the beam can also be seen from these results. Again it is at the edge of the smaller sample that this effect is most pronounced, with the angle between the beam and the normal to the ellipse increasing by 20°. The effect of this will depend, among other things, upon the attenuation of the bone as this will determine how far the beam penetrates into the bone but the relatively small change in angle close to the axis, for example 8° at 2 mm from the axis which corresponds to an increase in beam width of 0.14 mm per 1 mm depth, suggests that this is unlikely to contribute significantly to the overall uncertainty in the model.

12.6.3. Shear waves

Another simplification in the model is the fact that shear wave generation in the bone has not been considered. Bamber (1997) pointed out that equation 12.1 does not adequately describe the situation at interfaces involving solids, where mode conversion between longitudinal and shear waves may take place. Modelling mode conversion requires a degree of complexity which is beyond the scope of this model. Some insight can be gained by considering the figures quoted

by other authors for generation and attenuation of shear waves. The attenuation coefficient of shear waves in compact bone has been shown to be 1.5 times that of longitudinal waves in the range 4 - 10 MHz (Wu & Cubberly, 1997). This is similar to the ratio used by Chan et al. (1974) when they calculated the heat generated by ultrasound in fat-muscle-bone layers and in this case it was found that at angles of incidence greater than 22° the shear wave is responsible for most of the tissue heating. While care must be taken not to rely too much on these figures, as the properties of fetal tissue may be different to the compact bone considered, they would seem to suggest that heating from shear waves is unlikely to be the dominant heat source close to the measurement site. More generally, where the beam may strike the bone at any angle, it appears that the introduction of shear waves introduces an error comparable to those already present due to uncertainty about the thermal and physical properties of the bone.

12.7. Discussion

It has been shown that it is possible to used a two-dimensional axisymmetric model to produce predictions of the temperature rise in and around fetal bone and that, after the early stages of heating, the simplification due to the geometry of the model does not significantly affect the results. The results from this model agree with the experimental measurements to within the limits of uncertainty but these are large due to limitations in our present knowledge of the properties of fetal bone. The model of the younger sample suggests that the change in these properties with gestational age may need to be considered in order to obtain accurate predictions of bone heating.

The uncertainty in the attenuation coefficient can lead to a difference in the predicted temperature rise at the bone surface that is close to a factor of two, which is significant as the higher results are less than 0.5 K below the level which WFUMB (1997) state could be hazardous under certain conditions. Comparison of the modelled and measured results would suggest that the value of attenuation coefficient given in NCRP report 113 (1992) of 1.5 Np cm^{-1} MHz^{-1} overestimates the attenuation in fetal bone at 3.5 MHz, although the uncertainty in the position of the thermocouple, means that more work needs to be carried out before this can be proved to be the case.

The range of possible values for the thermal properties of the bone also leads to uncertainty in the results. The significance of these is reduced compared to the predictions from the heated disc model, and for the surface temperature rise the difference is now only of the order of 20%, but differences of the order of 50% are still observed between the maximum predicted temperature rise.

The similarity between the predicted temperature rise at 300s obtained when the plane of the model cut through the bone in two orthogonal directions shows that the shape of the bone layer is less important than its thermal and acoustic properties. The way that the intensity distribution is modelled can have a significant effect on the result however. The implications of these results and suggestions for work that needs to be carried out will be discussed in the next chapter.

12.8. Chapter Summary

Two-dimensional finite element models of fetal bone in agar have been produced and used to obtain predictions of the temperature rise in the bone. The simplification needed to allow a two-dimensional model to be used did not appear to cause a significant error in the temperature rise. The results obtained suggest that the attenuation coefficient for the most mature bone sample, which was of 39 weeks gestational age, is less than the 1.5 Np cm^{-1} MHz^{-1} quoted for adult bone in NCRP report 113. It also appears that the lower temperature rise observed in the younger samples may be due to changes in the structure rather than the size of the vertebrae. The finite element model was shown to predict temperature rises that were, in some instances, less than half those predicted using a heated disc model. Both the way in which the intensity distribution was modelled and the ability of the finite element model to use the correct thermal properties in each layer contributed to this.

Chapter 13
Discussion

This thesis has considered the degree to which diagnostic ultrasound can heat fetal bone. This is important because excessive heating has been shown to cause a variety of unwanted effects ranging from reversible changes in the electrical signals generated by the spinal cord (Yamane et al, 1992) to developmental abnormalities such as neural tube defects and even prenatal death (WFUMB, 1992). It was decided to study bone because its high absorption coefficient means that it will heat up more than soft tissue. To date the only reported data on heating of human fetal bone is a study of fetal femurs which only considers samples up to 108 days gestational age. Concern over the damage that could be caused by heating has lead the WFUMB to produce a list of recommendations based on thermal effects (WFUMB, 1997) and these include the statement that "A diagnostic exposure that elevates embryonic and fetal in situ temperature above 41°C (4°C above normal temperature) for five minutes or more should be considered potentially hazardous." This can be used as a benchmark against which to compare measured temperature rises.

The measurements carried out demonstrated that the temperature rise that occurred when fetal thoracic vertebrae were exposed to a diagnostic-like beam varied with gestational age; an observation previously made for younger fetal bone samples by Drewniak et al (1989). The observed temperature rise after 295 s exposure to a beam of power 50 mW ranged from 0.6°C for a sample of gestational age 14 weeks to 1.8°C for a 39 week sample. These were generated using a transducer which had a power output that was 40% of the mean value found in a recent survey of maximum outputs from clinical scanners operating in pulsed Doppler mode (Henderson et al, 1997). In order to apply these results to in-vivo heating of the fetus it is necessary to make assumptions about the effect that formalin fixation has on the samples, the degree to which the power in the beam is attenuated by maternal tissue and the effect of perfusion. If this is done, using in each case the values likely to lead to the maximum temperature rise, i.e. assuming that perfusion and formalin fixation have

no effect and that attenuation in maternal tissue reduces the intensity by 33%, the temperature rise that would be generated in-vivo is 1.2°C.

It is not a straightforward task to relate this result to the temperature rise that might occur during a typical pulsed Doppler examination of a fetus. Both Henderson et al. and Patton et al. (1994) found the maximum output from transducers operating in this mode to be over 400 mW but the range of values they recorded was very wide and the mean output value reported in the two studies is significantly different: Henderson et al. 124 mW, Patton et al. 35 mW. This difference is likely to be due to the fact that the results reported by Patton correspond to operating conditions that maximised the 'derated' intensities and so may not represent the maximum values. Neither group, however, report typical output levels and for this it is necessary to go back to the study published by Duck and Martin in 1991 from which the value of 50 mW used in the measurements was obtained. There is evidence, however, of an upward trend in output levels (Henderson et al., 1995) and so typical values may have increased since this value was obtained. From a safety point of view, however, it is the maximum value of the power output that must be safe, not just the typical value. If the measurements in this thesis are scaled up, so that the output corresponds to the maximum free field value of 440 mW recorded by Henderson et al., a temperature rise of over 10 K is obtained. It should be noted, however, that the extent to which the beams measured by Henderson et al. and Patton et al. are like the one used in the measurements reported here is unclear and if the frequency and diameter are significantly different it may generate a temperature rise that is far smaller than this. The figure of 10 K also corresponds to the temperature rise at 295 s, a longer exposure time than the range of 4 - 80 s that Duggan and McCowan (1993) recorded for pulsed Doppler examinations of the fetal carotid artery. Short exposure times may act to limit the temperature rise although this was found to reach approximately 75% of its maximum values within the first minute. It should also be noted that a large number of assumptions have been made about factors such as perfusion and formalin fixation, in order to obtain this value and, as the values leading to the greatest temperature rise were chosen each time, it is likely to be an overestimate. The fact that the value obtained is much higher than the 4 K level, however, demonstrates the need for more work in this field.

If the bone thermal index (TIB) is calculated for the output conditions used in the measurements a value of 0.5 is obtained. The formula for TIB, however, assumes that there is soft tissue between the transducer and the bone and includes a factor (0.3 dB cm^{-1} MHz^{-1}) to account for attenuation in this tissue. In the experiments presented in this thesis, however, the beam path was composed of water and agar, both of which are only weakly attenuating (total attenuation < 0.5 dB), and so this factor is not appropriate; if it is removed and it is assumed that no attenuation occurs in the beam path, the 'TIB' = 3.1. This is more than 1 K higher than the maximum temperature rise measured (1.8 K) and suggests that the formula used to predict the temperature rise when a beam of known power is incident on bone is, if anything, an overestimate for fetal bone. This overestimate was also found when results from other studies of fetal bone were analysed. It has been shown by other authors, however, that the derating factor of 0.3 dB $MHz^{-1}cm^{-1}$ used in the TIB formula to account for attenuation in overlying tissue may lead to an overestimate of the attenuation that occurs in fetal scanning (Carson et al., 1989; Ramnarine et al., 1993) In cases were the focal length of the transducer is large it has been shown to overestimate the attenuation by more than a factor of two (Patton and Harris 1994). This could lead to the power level at the fetus being underestimated and may mean that the TIB would not always overestimate the temperature rise in fetal bone. The question of whether the assumptions in the TIB are appropriate to fetal scanning is further complicated by the fact that the measurement procedure used to characterise the output from a transducer involves pressure measurements in water. Finite amplitude effects can lead to increased attenuation in water and it has been shown that this can cause the heating to be underestimated by 40% (Christopher and Carstensen, 1996). It appears, therefore, that while the basic formula relating absorbed power to temperature rise is reasonable, the way in which the TIB determines the power incident on bone is more problematic. The degree of uncertainty in the predictions is significant because the measurements have shown that potentially hazardous temperature rises can be induced with currently available equipment and the difference between a temperature rise which the WFUMB state can be used without reservation on thermal grounds (1.5°C) and one which, under certain conditions, should be considered potentially hazardous (4°C) is less than a factor of three.

The development of computer models allows the way in which the properties of bone affect the predicted temperature rise to be examined more closely. While the heated disc model can give an indication of which parameters have most effect on the rate of heating, this approach was seen to predict temperature rises that were much higher than those obtained using the finite element model. This is due, in part, to the fact that the heated disc approach can only include one set of thermal data and the specific heat and thermal conductivity of agar are higher than bone; using the thermal properties of bone throughout the model therefore underestimates the flow of heat out of the bone. Even in the finite element model, where different thermal properties were assigned to the bone and agar, uncertainty about the acoustic and thermal properties of fetal bone adversely influence our ability to produce accurate estimates of temperature rise. The uncertainty in two parameters, the attenuation coefficient and the thermal conductivity of the bone can cause a difference in the predicted temperature rise that is close to a factor of two. These models can still produce useful information however. Plots of the temperature rise along the beam axis showed that the temperature rise at the surface of the bone may be less than two-thirds of the maximum temperature rise. The temperature at the surface of the bone may be the critical value, as this indicates the temperature rise in the tissue around the bone and tissue from the central nervous system is seen as one of the areas most susceptible to damage. The maximum temperature rise should not be ignored, however, as Eriksson and Albrektsson (1983) showed bone could be changed by heat and so it is important to realise that the temperature recorded at the surface may not be the maximum. The steep temperature gradient at the front of the bone means that a displacement of the thermocouple by 0.5 mm could lead to an underestimate in the recorded temperature of approaching 30%. This needs to be considered when measurements carried out on animal fetuses are studied, as often in these the exact distance of the thermocouple from the bone is unknown. Although the models consisted of bone and agar the findings are also applicable to models containing bone and soft tissue as the thermal conductivity and specific heat of liver are within 10% of those of agar.

One noticeable feature of the modelling was the fact that the shape of the bone layer was relatively unimportant, so that changing from an ellipsoid to a disc made a difference of less than 10% in the maximum predicted

temperature rise at the surface. Larger differences in the temperature rise were observed, however, when the intensity distribution in the model was changed. Models of the bone mimic had shown that the 'top hat' distribution, in which the intensity is considered constant over a diameter defined by the -6 dB diameter of the beam and zero outside, gave a temperature rise 70% higher than the value obtained using a more accurate intensity distribution. This is much larger than the differences obtained from using different intensity distributions (Gaussian, Bessel and disc) reported in NCRP 113 (1992) which were less than 10%. This appears to be mainly due to the fact that the beam profile used in the models had a significant proportion of the power (> 50%) outside the area defined by the -6dB beam diameter. This profile corresponds to that of the beam used in the measurements and how the intensity profile of this compares to typical diagnostic beams is not known. If many diagnostic beams are like this, then the perception that the exact intensity distribution is relatively unimportant may be incorrect. In models of the bone mimic and those which used the Biyikli thermal data for bone, the relatively low thermal conductivity of the bone (mimic) added to the importance of the intensity distribution. The fact that the temperature rise at 300 s is modelled, rather than the steady state rise, may also contribute to this although an inspection of the curves does not appear to indicate that this would greatly affect the result.

The uncertainty in the properties of bone produced a large uncertainty in the predicted temperature rise. This made it difficult to determine the degree to which the simplifications in the model, such as assuming the bone to be homogenous and neglecting shear waves, were valid. Haken et al. (1992) studied mode conversion and showed that the power deposited in 1 cm on either side of a bone-muscle boundary did not depend greatly on the angle of incidence but as has just been discussed the pattern of heat generation appears to be important and if this changed it will affect the temperature rise.

12.1 Further Work

It is clear that if accurate predictions of the in-vivo temperature rise in fetal bone are to be made more information is needed. The present uncertainty about both the absorption coefficient and the thermal conductivity of bone means that predictions can differ by more than a factor of two, depending on the choice of input data used in the model.

The range of values quoted for the thermal conductivity of adult human bone suggests that getting a definitive figure even for mature bone is difficult. Two factors that contribute to this are the inherent difficulty in carrying out the measurements on small samples of poor conductors and the natural variability in bone. Both these factors are likely to be worse in fetal bone and so it may be that even with further work there is a limit to the precision with which this value can be determined. Fetal bone changes as it develops and so it is necessary to determine the age of fetal bone that should be studied before measurements can be carried out. If it was decided, for example, that the temperature rise at the end of the first trimester is more critical than the one closer to full term, even though the latter is higher, it would be better to determine that properties of the bone at this stage in development.

Once the properties of fetal bone are known more accurately it may then be appropriate to refine the model. Three major simplifications in the model are its geometry, the fact that the bone is considered to be homogenous and the omission of shear waves. The fact that the result did not change greatly when the bone was modelled as a disc, rather than an ellipsoid, suggests that the assumption of axial symmetry is reasonable and so this is likely to be a minor effect but not enough data is available to be certain of the effect of the other assumptions. The histology data on the 23 week sample has shown that there are distinct layers within the bone but their relative properties are not known and the limited data available of mode conversion considers tissue which may have properties quite different to those of fetal bone.

The measurements reported in this thesis suggest that the temperature rise generated by a 'typical' pulsed Doppler beam is unlikely to reach the 4 K level that WFUMB state could be hazardous under certain conditions, even if the 'typical' output has doubled since 1991. The definition of typical used here, however, is that of Duck (1991) and relates to an approximate median value of the worst case exposures from a range of probes. Henderson et al. (1997) have reported a wide range of acoustic power values, however, up to nearly nine times the typical value: 440 mW as opposed to 50 mW. A beam with acoustic power of 440 mW and diameter and frequency similar to those used in the measurements reported in Chapter 5 could generate a temperature rise of over 10 K under worst case conditions. In order to determine whether a

temperature rise of this magnitude could occur in vivo it is necessary to know the dimensions and frequency of the beam and these are not included in the paper by Henderson et al. A study which measured not only the maximum acoustic power emitted by a probe but also the characteristics of the beam would allow better estimates of the temperature rise to be obtained.

The fact that most fetuses in the Western world are now exposed to ultrasound and that it appears that the power output from clinical scanners is rising make it necessary regularly to re-evaluate the safety of this technology. In order to do this it is necessary to have evidence on which to base decisions and the degree to which bone is heated by ultrasound is part of this. This thesis has presented the results of experimental measurements on fetal vertebrae and produced a computer model in order to predict heating. While the thermal index gives the user an indication of the temperature rise that may occur it is clear that there is still work to be done before accurate predictions can be made.

References

Adler, L. & Cook, K. (1975). Ultrasonic parameters of freshly frozen dog tibia. *Journal of the Acoustic Society of America,* **58**(5), 1107-1108.

AIUM/NEMA (1992). *Standard for the real-time display of thermal and mechanical acoustic output indices on diagnostic ultrasound equipment* , AIUM, Rockville Maryland, USA

Andrews, H. (1993). Normal first trimester appearance using transvaginal ultrasound. *BMUS Bulletin,* **1**(3), 8-12.

Arkin, H., Xu, L. X. & Holmes, K. R. (1994). Recent developments in modelling heat transfer in blood perfused tissues. *IEEE Trans. Biomed. Eng.,* **41**(2), 97-107.

Baker, A. C. (1991). Prediction of non-linear propagation in water due to diagnostic medical ultrasound equipment. *Physics in Medicine and Biology,* **36**(11), 1457-1464.

Bamber, J. C. (1986). Attenuation and Absorption. In C. R. Hill (Eds.), *Physical Principles of Medical Ultrasonics* , Chichester: Ellis Horwood Limited.

Bamber, J. C. (1997). Acoustical characteristics of biological media. In M. J. Crocker (Eds.), *Encyclopedia of Acoustics,* John Wiley.

Barnett, S. B., Edwards, M. J. & Martin, P. (1991). Pulsed ultrasound induces temperature elevation and nuclear abnormalities in bone marrow cells of guinea-pig femurs. In *6th WFUMB Congress in Ultrasound.*

Barnett, S. B., Haar, G. R. T., Ziskin, M. C., Nyborg, W. L., Maeda, K. & Bang, J. (1994). Current status of research on biophysial effects of ultrasound. *Ultrasound in Medicine and Biology,* **20**(3), 205-218.

Barnett, S. B., Rott, H., Haar, G. R. t., Ziskin, M. C. & Maeda, K. (1997). The sensitivity of biological tissue to ultrasound. *Ultrasound in Medicine and Biology,* **23**(6), 805-812.

Bender, L. F., Herrick, J. F. & Krusen, F. H. (1953). Temperatures produced in bone by various methods used in ultrasonic therapy. *Archives of Physical Medicine and Rehabilitation,* **34**, 424-433.

Bender, L. B., Janes, J. M. & Herrick, J. F. (1954). Histologic studies following exposure of bone to ultrasound. *Archives of Physical Medicine and Rehabilitation,* **35**, 555-559.

Benedict, R. P. (1984). *Fundamentals of Temperature, Pressue and Flow Measurements.* (3rd ed.). Wiley.

Bhatia, A. (1967). *Ultrasonic Absorption*. Oxford: Clarendon Press.

Biyikli, S., Modest, M. F. & Tarr, R. (1986). Measurements of thermal properties for human femora. *Journal of Biomedical Materials Research*, **20**, 1335-1345.

Bly, S. H. P., Vlahovich, S., Mabee, P. R. & Hussey, R. G. (1992). Computed estimates of the maximum temperature elevations in fetal tissues during transabdominal pulsed doppler examinations. *Ultrasound in Medicine and Biology*, **18**(4), 389-397.

Bosward, K. L., Barnett, S. B., Wood, A. K. W., Edwards, A. J. & Kossoff, G. (1993). Heating of guinea-pig fetal brain during exposure to pulsed ultrasound. *Ultrasound in Medicine and Biology*, **19**(5), 415-424.

Bouakkaz, A., Cachard, C. & Gimenez, G. (1994) Evaluation de l'agar, matériau solide présentant des charactéristiques acoustiques équivalentes à celles de l'eau. *Journal de Physique IV, C5*, **4**, 1221-1224

Bowman, H. F. (1981). Heat transfer and thermal dosimetry. *Journal of Microwave Power*, **16**, 121-133.

Brown, N. T., Galloway, W. D. & Henton, W. W. (1981). Reflex development following in utero exposure to ultrasound. In *Meeting of AIUM*, San Francisco.

Campbell, J., Elford, R. & Brant, R. (1993). Case-control study of prenatal ultrasonography exposure in children with delayed speech. *Can. Med. Assoc. J*, **149**, 1435-1440.

Carnes, K., Drewniak, J. & Dunn, F. (1991). In utero measurement of ultrasonically induced fetal mouse temperature increases. *Ultrasound in Medicine and Biology*, **17**(4), 373-382.

Carnochan, P., Dickinson, R. J. & Joiner, M. C. (1986). The practical use of thermocouples for temperature measurement in clinical hyperthermia. *Int. J. Hyperthermia*, **2**(1), 1-19.

Carslaw, H. & Jaeger, J. (1959). *Conduction of heat in solids*. (2 ed.). Oxford Press.

Carson, P. L., Rubin, J. M. & Chiang, E. H. (1989). Fetal depth and underlying path lengths through overlying tissues. *Ultrasound in Medicine and Biology*, **15**(7), 629-639.

Carstensen, E. L., Child, S. Z., Norton, S. & Nyborg, W. (1990). Ultrasonic heating of the skull. *Journal of the Acoustic Society of America*, **87**(3), 1310-1317.

Chan, A. K., Sigelmann, R. A. & Guy, A. W. (1974). Calculations of therapeutic heat generated by ultrasound in fat-muscle-bone layers. *IEEE Trans. Biomed. Eng.*, **BME-21**, 280-284.

Chan, A. K., Sigelmann, R. A., Guy, A. W. & Lehmann, J. F. (1973). Calculations by the method of finite differences of the temperature distribution in layered tissues. *IEEE Trans. Biomed. Eng.*, **BME-20**, 86-90.

Chatterjee, I. & Adams, R. E. (1994). Finite element thermal modelling of the human body under hyperthermia conditions. *Int. J. of Computer Applications in Technology*, **17**(3-6), 151-159.

Chen & Holmes (1980). Microvascular contributions in tissue heat transfer. *Annals of New York Academy of Science.*, **335**, 137-150.

Christopher, T. & Carstensen, E. L. (1996). Finite amplitude distortion and its relationship to linear derating formulae for diagnostic ultrasound systems. *Ultrasound in Medicine and Biology*, **22**(8), 1103-1116.

Clegg, S. T., Samulski, T. V., Murphy, K. A., Rosner, G. L. & Dewhirst, M. W. (1994). Inverse techniques in hyperthermia: A Sensitivity Study. *IEEE Trans. Biomed. Eng,*. **41**(4), 373-380.

Craigmyle, M. (1986). *A Colour Atlas of Histology* (2nd ed.). London: Wolfe Medical Publications Ltd.

Curley, M. (1993). Soft tissue temperature rise caused by scanned diagnostic ultrasound. *IEEE Trans. on Ultrasonics, Ferroelectrics and Frequency Control*, **40**(1), 59-66.

David, H., Weaver, J. B. & Pearson, J. F. (1965). Doppler ultrasound and foetal activity. *British Medical Journal*, **2**, 62-64.

DeForest, R. E., Herrick, J. F., Janes, J. M. & Krusen, F. K. (1953). Effects of ultrasound on growing bone. *Archives of Physical Medicine and Rehabilitation*, **34**, 21-31.

Dekhtyar, Y., Gamza, A., Tatarinov, A. & Jansons, H. (1995). Electron and mechanical properties of bone during heating, evaluated by exoelectron emission and ultrasound. *Biomaterials*, **16**(11), 861-863.

Diller, K. R. & Hayes, L. J. (1983). A finite element model of burn injury in blood-perfused skin. *Trans. ASME J. Biomechanical Engineering*, **105**, 300-307.

Dillon, E. H., Case, C. Q., Ramos, I. M., Holland, C. K. & Taylor, K. J. W. (1993). Endovaginal pulsed and color doppler in first-trimester pregnancy. *Ultrasound in Medicine and Biology*, **19**(7), 517-525.

Dore, G. R. (1990). *Evaluation of a model for the prediction of temperature rise in tissue due to the absorption of ultrasound.* No. RSA (EXT) 13). National Physical Laboratory, Teddington, England

Drewniak, J. L., Carnes, K. I. & Dunn, F. (1989). In vivo ultrasonic heating of fetal bone. *Journal of the Acoustic Society of America,* **86**(4), 1254-1258.

Drewniak, J. L. & Dunn, F. (1996). An experimentally obtainable heat source due to absorption of ultrasound in biological media. *Journal of the Acoustic Society of America,* **100**(2), 1250-1253.

Duck, F. (1990). *Physical Properties of Tissue.* London: Academic Press.

Duck, F. A. (1991). Exposure measurement of diagnostic equipment. In M. F. Docker & F. A. Duck (Eds.), *The Safe Use of Diagnostic Ultrasound* London: British Institute of Radiology.

Duck, F. A. & Martin K. (1993) Trends in diagnostic ultrasound exposure. *Physics in Medicine and Biology,* **38**, 1423-1432

Duck, F. A. (1997). The meaning of thermal index and mechanical index values. *BMUS Bulletin,* **5**(4).

Duck, F. A. (1998) Personal communication.

Duck, F. A. & Henderson, J. (1998). Acoustic output of modern ultrasound equipment: is it increasing? In S. B. Barnett & G. Kossoff (Eds.), *Safety of Diagnostic Ultrasound* Carnforth, Lancs: Parthenon Publishing.

Duggan, P. (1993) *Pulsed Ultrasound and the Fetal Sheep Brain.* Doctor of Medicine, University of Auckland.

Duggan, P. M. & McCowan, L. (1993). Reference ranges and ultrasonic exposure conditions for pulsed doppler sonographic studies of the internal carotid artert. *J. Ultrasound Med.,* **12**, 719-722.

Duggan, P. M., Liggins, G. C. & Barnett, S. B. (1995). Ultrasonic heating of the brain of the sheep in utero. *Ultrasound in Medicine and Biology,* **21**(4), 553-560.

Dussik, K. T., Fritch D. J., Kyriazidou, M., & Sear, R. S. (1958). Measurement of articular tissue with ultrasound. *American Journal of Physical Medicine.* **37**, 160-165.

Edmonds, P. (1982). The molecular basis of ultrasonic absorption by proteins. *Bioelectromagnetics.,* **3**, 157-165.

EFSUMB (1996). New clinical safety statement for diagnostic ultrasound. *EFSUMB Newsletter,* **10**(2), 9.

Ellis, D. S. & O'Brien Jnr, W. D. (1996). The monopole-source solution for estimating tissue temperature increases for focused ultrasound fields. *IEEE Trans. on Ultrasonics, Ferroelectrics and Frequency Control*, **43**(1), 88-97.

England, M. A. (1990). *A Colour Atlas of Life Before Birth.* Aylesbury, England: Wolfe Medical Publications.

Eriksson, A. & Albrektsson, T. (1983). Temperature threshold levels for heat-induced bone tissue injury: a vital-microscopic study in the rabbit. *The Journal of Prosthetic Dentistry*, **50**(1), 101-107.

Evans, J. A. (1986). Wave propagation in tissues. In J. A. Evans (Eds.), *Physics in Medical Ultrasound* London: Institute of Physical Sciences in Medicine.

Filipczynski, L. (1976). Thermal effects in soft tissues developed under the influence of focussed fields of short duration. *Archives of Acoustics*, **1**, 309-322.

Filipczynski, L. (1977). Thermal effects in soft tissues developed under the action of ultrasonic fields of long duration. *Archives of Acoustics*, **2**, 297-303.

Fitzgerald, H. J. T. (1978). *Human Embryology: a Regional Approach.* Harper Row.

Food and Drug Administation (1985). *Document 510 (k) Guide for measuring and reporting acoustic output of diagnostic ultrasound medical devices*, US Department of Health and Human Sciences, Rockville, MD

Food and Drug Administation (1993). *Revised 510(k) Diagnostic Ultrasound Guidance for 1993* , US Department of Health and Human Sciences, Rockville, MD

Fry, F. J. & Barger, J. E. (1978). Acoustical properties of the human skull. *Journal of the Acoustic Society of America*, **63**(5), 1576-1590.

Fry, W. J. & Fry, R. B. (1953). Temperature changes produced in tissue during ultrasonic radiation. *Journal of the Acoustic Society of America*, **25**, 6-11.

Fry, W. J. & Fry, R. B. (1954). Determination of Absolute Sound Levels and acoustic Absorption Coefficients by Thermocouple Probes - Theory. *Journal of the Acoustic Society of America*, **26**(3), 294-310.

Glenn, T. N., Rastegar, S. & Jacques, S. L. (1996). Finite Element Analysis of Temperature Controlled Coagulation in Laser Irradiated Tissue. *IEEE Trans. Biomed. Eng.*, **43**(1), 79-87.

Goldberg, B. (1997). Presidential Message. *WFUMB News*, **4**(2), 1.

Hand, J. (1997). Ultrasound Hyperthermia. In *3rd Mayneard Philips Summer School* .

Hedrick, W. R. & Hykes, D. L. (1991). Biologic Effects of Ultrasound. *Journal of Diagnostic Medical Sonography*, **7**, 264-275.

Henderson, J., Whittingham, T. & Dunn, T. (1997). A Review of the acoustic Output of Modern Diagnostic Ultrasound Equipment. *BMUS Bulletin*, **5**(4), 10-14.

Henderson, J., Willson, K., Jago, J. R. & Whittingham, T. A. (1995). A survey of the acoustic outputs of diagnostic ultrasound equipment in current clinical use. *Ultrasound in Medicine and Biology*, **21**(5), 699-705.

Herrick, J. F. (1953). Temperature produced in tissues by ultrasound. Experimental study using various techniques. *Journal of the Acoustic Society of America*, **25**, 12-16.

Heuter, T. F. (1952). Ultrasonic absorption measurements in human skull bone and their dependance upon frequency. In F. Dunn (Eds.), *Ultrasonic Biophysics*

Holmes, A. & Challis, R. (1996). Acoustic absorption due to proton transfer in solutions of proteins, peptides and amino acids at neutral pH. *Journal of the Acoustic Society of America*, **100**(3), 1865-1877.

Horder, M. M., Barnett, S. B., Edwards, M. J. & Kossoff, G. (1997). In Utero Measurement of Ultrasound-induced heating in guinea-pig fetal brain. In *AIUM Annual Convention*, San Diego.

Hynynen, K. & Edwards, D. K. (1989). Temperature measurements during ultrasound hyperthermia. *Med. Phys.*, **16**(4), 618-626.

Hynynen, K., Martin, C. J., Watmough, D. J. & Mallard, J. R. (1983). Errors in temperature measurement by thermocouple probes during ultrasound induced hyperthermia. *British Journal of Radiology*, **56**, 969-970.

Kagawa, Y., Takeuchi, K. & Yamabuchi, T. (1986). A simulation of ultrasonic hyperthermia using a finite element model. *IEEE Trans. Ultrasonics, Ferroelectrics and Frequency Control*, **33**(6), 765-777.

Kamel, I. R. (1994). An evaluation of overlying tissues to determine fetal exposure to ultrasound during the third trimester. *Ultrasound in Medicine and Biology*, **20**(1), 41-51.

Kaye, S. W. & Laby, T. H. (1986). *Tables of Physical and Chemical Constants* (15 ed.). Longman Scientific and Technical.

Kieler, H., Axelsson, O., Haglund, B., Nilsson, S. & Salvensen, K. (1998). Routine ultrasound screening in pregnancy and the children's subsequent handedness. *Early Human Development*, **50**, 233-245

Kishimoto, T. (1958). Ultrasonic absorption in bones. *Acustica*, **8**, 179-180.

Kurjak, A., Alfirevic, Z. & Miljan, M. (1988). Conventional and color Doppler in the assessment of fetal and maternal circulation. *Ultrasound in Medicine and Biology*, **14**(5), 337-354.

Kuttruff, H. (1991). *Ultrasonics: Fundamentals and Applications*. London: Elsevier Applied Science.

Lakes, A., Yoon, H. & Katz, J. (1985). Ultrasonic wave propagation and attenuation in wet bone. *J. Biomedical Engineering*, **8**, 143-148.

Lapidus, L. & Pinder, G. F. (1982). *Numerical Solution of Partial Differential Equations in Science and Engineering*. John Wiley and sons.

Lees, S. & Klopholz, D. Z. (1992). Sonic velocity and attenuation in wet compact cow femur for the frequency range 5 to 100 MHz. *Ultrasound in Medicine and Biology*, **18**(3), 303-308.

Lehmann, J. F., Delateur, B. J., Warren, C. G. & Stonebridge, J. B. (1967). Heating produced by ultrasound in bone and soft tissue. *Arch. Phys. Med. Rehab.*, **48**, 397-401.

Lehmann, J. F. & Johnson, E. W. (1958). Some factors influencing the temperature distribution in thighs exposed to ultrasound. *Arch. Phys. Med. Rehabil.*, **39**, 347-356.

Lehmann, J. (1983). *Therapeutic Heat and Cold*. Baltimore: Williams and Wilkins.

Lele, P. P. (1977). Thresholds and mechanisms of ultrasonic damage to 'organized' animal tissues. In D. G. Hazard & M. L. Litz (Ed.), *Symposium on Biological Effects and Characterizations of Ultrasound Sources*, DHEW.

Liebeskind, D., Padawer, J., Wolley, R. & Bases, R. (1982). Diagnostic ultrasound: time-lapse and transmission electron microscopic changes of cells insonated in vitro. *Brit. J. Cancer*, **45**, 176-186.

Liebeskind, D., Padawer, K., Wolley, R. & Bases, R. (1981). Diagnostic ultrasound: Time-lapse and transmission electron microscopic studies of cells insonated in vitro. In *10th L.H. Gray Conference*, . Oxford:

Margulies, N., Abraham, V., Way, J. S. & Ziskin, M. C. (1992). Effect of Ultrasound on Neonatal Rat Brain. *Ultrasound in Medicine and Biology*, **18**(5), 459-464.

Mason, W. P. (1950). *Piezoelectric crystals and their application to ultrasonics.*

McKelvie, M. L. & Palmer, S. B. (1991). The inteaction of ultrasound with cancellous bone. *Physics in Medicine and Biology,* **36**(10), 1331-1340.

Miller, E. B. (1986). Basic acoustic theory. In C. R. Hill (Eds.), *Physical Principles of Medical Ultrasonics.* Chichester: Ellis Horwood Ltd.

Miller, M. & Ziskin, M. (1989). Biological Consequences of Hyperthermia. *Ultrasound in Medicine and Biology,* **15**, 707-722.

Miller, M. W., Miller, D. L. & Brayman, A. A. (1996). A Review of in vitro bioeffects of inertial ultrasonic cavitation from a mechanistic perspective. *UMB,* **22**(9), 1131-1154.

Montenegro, N., Matias, A., Areias, J. C. & Barros, H. (1997). Ductus Venosus revisited: a doppler blood flow evaluation in first trimester pregnancy. *Ultrasound in Medicine and Biology,* **23**(2), 171-176.

Moses, W. M., Witthaus, F. W., Hogan, H. A. & Laster, W. R. (1995). Measurement of the Thermal Conductivity of Cortical Bone by an Inverse Technique. *Experimental Thermal and Fluid Science,* **11**, 34-39.

Murai, N., Hoshi, K. & Nakamura, T. (1975). Effects of diagnostic ultrasound irradiated during the foetal stage on on development of orienting behaviour and reflex ontogeny in rats. *Tohoku J. Exp. Med.,* **116**, 17-24.

NCRP (1992). *Exposure Criterea for Medical Diagnostic Ultrasound: 1. Criterea based on Thermal Mechanisms* No. 113). NCRP.

Newnham, J. P., Evans, S. F., Michael, C. A., Stanley, F. J. & Landau, L. I. (1993). Effects of frequent ultrasound during pregnancy: a randomised controlled trial. *The Lancet,* **342**(October 9), 887-891.

Nicholson, P., Haddaway, M. & Davie, M. (1994). The dependence of ultrasonic properties on orientation in human vertebral bone. *Physics in Medicine and Biology,* **39**(6), 1013-1024.

Nyborg, W. L. (1986). Sonically produced heat in a fluid with bulk viscosity and shear vicoscity. *Journal of the Acoustic Society of America,* **80**(4), 1133-1139.

Nyborg, W. L. (1988). Solutions of the bio-heat transfer equation. *Physics in Medicine and Biology,* **33**(7), 785-792.

Nyborg, W. L. & Steele, R. B. (1983). Temperature elevation in a beam of ultrasound. *Ultrasound in Medicine and Biology,* **9**(6), 611-620.

O'Neil, H. (1949). Theory of focusing radiators. *Journal of the Acoustic Society of America*, **21**, 516-526.

O'Neill, T. P., Winkler, A. J. & Wu, J. (1994). Ultrasound heating in a tissue-bone phantom. *Ultrasound in Medicine and Biology*, **20**(6), 579-588.

Ohtsuki, F. (1977). Development changes of the cranial bone thickness in the human fetal period. *Americal Journal of Physical Anthropology*, **46**, 141-154.

Ottosen, N. & Peterson, H. (1992). *Introduction to the Finite Element Method*. Prentice Hall: Hertfordshire.

Overgaard, J. (1983). Histopathologic effects of hyperthermia. In F. K. Storm (Eds.), *Hyperthermia in Cancer Therapy* Boston: G.K. Hall.

Pansky, B. (1982). *Review of Medical Embryology*. MacMillan.

Patton, C. A., Harris, G. R. & Phillips, R. A. (1994). Output levels and bioeffects indices from diagnostic ultrasound exposure data reported to the FDA. *IEEE Trans. on Ultrasonics, Ferroelectrics and Frequency Control*, **41**(3), 353-359.

Paulsen, K. D., Jia, X. & Sullivan, J. M. (1993). Finite element computations of specific absorption rates in anatomically conforming full-body models of hyperthermia treatment analysis. *IEEE Transactions on Biomedical Engineering.*, **40**(9), 933-945.

Pennes, H. H. (1948). Analysis of tissue and arterial blood temperatures in the resting human forearm. *J. Appl. Physiol.*, **1**, 93-122.

Perkins, M. A. (1989). A versitile force balance for ultrasound Power measurement. *Physics in Medicine and Biology*, **34**(11), 1645-51.

Pilla, A. A., Mont, M. A., Nasser, P. R., Khan, S. A., Figueiredo, M., Kaufman, J. J. & Siffert, R. S. (1990). Non-invasive low-intensity pulsed ultrasound accelerate bone healing in the rabbit. *J. Orthopaedic Research*, **4**(3), 246-253.

Preston, R. C. (1988). The NPL ultrasound beam calibrator. *IEEE Trans. Ultrasonics, Ferroelectrics and Frequency Control*, **35**, 122-139.

Preston, R. C. (1991). *Output Measurements for Medical Ultrasound*. Springer-Verlag.

Ramnarine, K. V., Nassiri, D. K., Pearce, J. M., Joseph, A. E. A., Patel, R. H. & Varma, T. R. (1993). Estimation of in situ ultrasound exposure during obstetric examinations. *Ultrasound in Medicine and Biology*, **19**(4), 319-329.

Reher, P., Elbeshir, E., Harvey, W., Meghji, S. & Harris, M. (1997). The stimulation of bone formation in vitro by therapeutic ultrasound. *Ultrasound in Medicine and Biology*, **23**(8), 1251-1258.

Robinson, T. C. & Lele, P. P. (1972). An analysis of lesion development in the brain and in plastics by high-intensity focused ultrasound at low-megahertz frequencies. *Journal of the Acoustic Society of America*, **51**(4), 1333-1351.

Salvensen, K. (1997). Epidemiology of diagnostic ultrasound exposure during human pregnancy. *BMUS Bulletin*, **5**(4), 32-34.

Salvensen, K., Vatten, L., Bakketeig, L. & Eil-nes, S. (1994). Routine ultrasonography in utero and speech development. *Ultrsasound Obstet Gynaecol.*, **4**, 101-103.

Salvensen, K. A., Vatten, L. J., Eik-Nes, S. H., Hugdahl, K. & Bakketeig, L. S. (1993). Routine ultrasonography in utero and subsequent handedness and neurological development. *British Medical Journal*, **307**(17 July 1993).

Sapereto, S. A. & Dewey, W. C. (1984). Thermal dose determination in cancer therapy. *Int. J. Radiat. Oncol. Biol. Phys.*, **10**, 787-800.

Schwartz, J. (1995). *Skeleton Keys*. New York: Oxford University Press.

Sekins, K. & Emery, A. (1983). Thermal science for physical medicine. In J. Lehmann (Eds.), *Therapeutic Heat and Cold.* (pp. 70-132). Baltimore/London.: Williams and Wilkins.

Shaw, A. (1994). Prediction of temperature rise in layered media from measured ultrasonic intensity data. *Physics in Medicine and Biology*, **39**(8), 1203-1218.

Shaw, A., Preston, R. C., Bacon, D. R. (1996). Perfusion corrections for ultrasonic heating in nonperfused media. *Ultrasound in Medicine and Biology*, **22**(2), 203-206.

Shih, T. M. & Chen, Y. N. (1983). Comparison of finite difference method and finite element method. In T. M. Shih (Ed.), *Numerical Properties and Methodologies in Heat Transfer*: Springer Verlag.

Siddiqi, T. A., Jr, W. D. O., Meyer, R. A., Sullivan, J. M. & Miodovnik, M. (1995). In Situ human obstetrical ultrasound exposimetry: estimates of derating factors for each of three different tissue models. *Ultrasound in Medicine and Biology*, **21**(3), 379-391.

Siddiqi, T. A., Plessinger, M. A., Meyer, R. A. & Woods, J. R. (1990). Bioeffects of diagnostic ultrasound on auditory function in the neonatal lamb. *Ultrasound in Medicine and Biology*, **16**(6), 621-627.

Slutsky, L. (1981). Ultrasonic chemical relaxation spectroscopy. In P. Edmonds (Eds.), *Methods in Experimental Physics. Volume 19* London: Academic Press.

Slutsky, L. (1996). On the possible contribution of chemical relaxation to acoustic absorption in biological systems. *IEEE Trans. on Ultrasonics, Ferroelectrics and Frequency Control*, **UFFC-33**(2), 156-161.

Stark, C. R., Orleans, M., Haverkamp, A. D. & Murphy, J. (1984). Short- and long-term risks after exposure to diagnostic ultrasound in utero. *Obstetrics and Gynaecology*, **63**, 194-200.

Tarantal, A. F., Gargosky, S. E., Ellis, D. S., O'Brien, W. D. & Hendrickx, A. G. (1995). Hematologic and growth-related effects of frequent prenatal exposure in the long-tailed macaque (Macaca Fascicularis). *Ultrasound in Medicine and Biology*, **21**(8), 1073-1081.

ter Haar, G. (1996). Commentary: safety of diagnostic ultrasound. *British Journal of Radiology*, **69**, 1083-1085.

ter Haar, G. R., Duck, F., Starritt, H. & Daniels, S. (1989). Biophysical chaacterization of diagnostic ultrasound equipment - preliminary results. *Physics in Medicine and Biology*, **34**, 1533-1542.

Thomas, L. C. (1992). *Heat Transfer*. New Jersey: Prentice Hall.

Thomenius, K. E. (1990). Thermal dosimetry models for diagnostic ultrasound. *Ultrasonics Symposium*, 1399-1407.

Travakoli, M. B. & Evans, J. A. (1992). The effect of bone structure on ultrasonic attenuation and velocity. *Ultrasonics*, **30**(6), 389-395.

Trotter, M. (1972). Percentage ash weight of fetal skeleton. *Growth*, **36**, 145-153.

Uchiyama, S., Yashiro, K., Takahashi, H. & Homma, T. (1989). An experiemental study of spinal cord evoked potenetials and histologic changes following spinal cord heating. *Spine*, **14**, 1215-1219.

Wang, S., Lewallen, D. G., Bolander, M. E., Chao, E. Y. S., Ilstrup, D. M. & Greenleaf, J. F. (1994). Low intensity ultrasound treatment increases strength in a rat femoral fracture model. *J. Orthopaedic Research*, **12**(1), 40-47.

Weinbaum, S. & Jiji, L. M. (1985). A new simplified bioheat equation for the effect of blood flow on local average tissue temperature. *Journal of Biomechanical Engineering*, **107**, 131-139.

WFUMB (1992). Symposium on safety and standardisation in medical ultrasound. *Ultrasound in Medicine and Biology*, **18**(9), 731-814.

WFUMB (1997). Ultrasound safety statement. *WFUMB News*, **4**(2), 2-4.

Williams, A. R. (1983). *Ultrasound: Biological Effects and Potential Hazards*. Manchester: Academic Press.

Williams, A. R. (1991). A critical evaluation of bioeffects reports and epidemiological surveys. In M. F. Docker & F. A. Duck (Eds.), *The Safe use of Diagnostic Utrasound*. (pp. 30-33). London: British Institute of Radiology.

Wong, T. Z., Mechling, J. A., Jones, E. L. & Strohbehn, J. W. (1988). Transient finite element analysis of thermal methods used to estimate SAR and blood flow in homogeneously perfused tumour models. *Int. J. Hyperthermia*, **4**(6), 571-592.

Wu, J., Chase, J. d., Zhu, Z. & Holzapfel, T. P. (1992). Temperature rise in a tissue-mimicking material genrated by unfocused and focused ultasonic transducers. *Ultrasound in Medicine and Biology*, **18**(5), 495-512.

Wu, J., Cubberley, F., Gormley, G. & Szabo, T. L. (1995). Temperature rise generated by diagnostic ultrasound in a transcranial phantom. *Ultrasound in Medicine and Biology*, **21**(4), 561-568.

Wu, J. & Cubberley, F. (1997). Measurement of velocity and attenuation of shear waves in bovine compact bone using ultrasonic spectroscopy. *Ultrasound in Medicine and Biology*, **23**(1), 129-134.

Wu, J. & Du, G. (1990a). Temperature elevation generated by a focused Gaussian beam of ultrasound. *Ultrasound in Medicine and Biology*, **16**(5), 489-498.

Wu, J. & Du, G. (1990b). Temperature elevation generated by a focused Gaussian ultrasonic beam at a tissue-bone interface. *Journal of the Acoustic Society of America*, **87**(6), 2748-2755.

Wu, J. & W, L. N. (1992). Temperature rise generated by a focussed Gaussian in a two-layer medium. *Ultrasound in Medicine and Biology*, **18**(3), 293-302.

Wu, J., Chase, J. D., Zhu, Z., & Holzapfel, T. P. (1992b). Temperature rise in a tissue-mimicking material generated by unfocused and focused ultasonic transducers. *Ultrasound in Medicine and Biology*, **18**(5), 495-512.

Wu, J., Winkler, A. J. & O'Neill, T. P. (1994). Effect of acoustic streaming on ultrasound heating. *Ultrasound in Medicine and Biology*, **20**(2), 195-201.

Wulff, W. (1980). Discussion Paper: Alternatives to the Bio-Heat Transfer Equation. *Annals New York Academy of Sciences.*, **335**, 151-154.

Yamane, T., Tateishi, A., Cho, S., Manabe, S., Yamanashi, M., Dezawa, A., Yasukouchi, H. & Ishioka, K. (1992). The effects of hyperthermia on the spinal cord. *Spine*, **17**(11), 1386-1391.

Zemansky, M. & Dittman, R. (1981). *Heat and Thermodynamics*. London: McGraw-Hill.

Ziskin, M. C. & Lewin, P. A. (1993). *Ultrasonic Exposimetry*. CRC Press.

Ziskin, M. C. & Petitti, D. B. (1988). Epidemiology of human exposure to ultrasound: a critical review. *Ultrasound in Medicine and Biology*, **14**(2), 91-96.

Appendix A

Examples of Heated Disc Programs

All programs run under Matlab version 4.
Lines starting % are comments

A.1. Program Heattime

```
% heatime.m
% program for calculating heating over an extended area
% includes defaults
% this version allows you to study a range of times

% Define some globals so that the functions can get to them
global absorp L Kcond kdiff time tstar diam zfront I

% Lets clear the screen
clc
clear totheat

% See if the user wants to enter the rest
defl = input('Do you want to use the defaults? ','s');
if strcmp(defl,'y') == 1
        kdiff = 0.28;
        tau = 1000;
        pow = 0.1;
        diam = 0.4;
        thick = 67;
        Kcond = 0.6;
else
kdiff = input('Enter k (mm2/s): ');
Kcond = input('Enter K (W/m/K): ');
tau = input('Enter tau (s): ');
diam = input('Beam diameter (cm): ');
diam = diam/100;
area = (diam/2)^2 * pi;
pwin = input('Do you want to enter the power or the intensity (p/i)? ','s');
if strcmp(pwin,'p') == 1
        pow = input('What is the intial power: (W) ');
        I = pow/area;
else
        I = input('What is the intensity: (W/cm2)');
        I = I * 1E4;
end
thick = input('What is the thickness of the absorber (mm): ');
end

tm1 = input('What is the start time (s): ');
```

```
tm2 = input('What is the total exposure time (s): ');
tms = input('What time interval (s): ');

% Find out the distance from the point of interest to the front of the
absorber
zfront = input('What is the distance to the front of the absorber (cm): ');

%Get everything into SI units
kdiff = 1E-6 * kdiff; %convert to m2/s
zfront = zfront/100;
thick = thick/1000;

% Work out the dependents
L = sqrt(kdiff * tau);

% Ask for the absorption coefficient
% At the moment lets assume absorption equals attenuation
absorp = input('What is the absorption coefficient (Np/cm): ');
absorp = absorp*100;    %work in metres

loop = 1;
for time = tm1:tms:tm2;
        fprintf('time  %d\n',time);
        tstar = sqrt(time/tau);
        % Integrate the disc solutions over the thickness of the absorber
        zback = zfront+thick;
        totheat(loop) = quad8('heatdisc2',zfront,zback)
        loop = loop + 1;
end
ver = 1;
flname = sprintf('res-%s-%g',date,ver);
flnmtot = [flname '.mat'];
while exist(flnmtot) ~= 0,
ver = ver + 1;
flname = sprintf('res-%s-%g',date,ver);
flnmtot = [flname '.mat'];
end
eval(['save ' flname])
fprintf('Saved data to file %s',flnmtot);
```

A.2.. Program Heatabs

```
% heatabs.m
% the main program for calculating heating over an extended area
% calculates heating for a range of absorption coeffs
% includes defaults

% Define some globals so that the functions can get to them
global absorp L Kcond kdiff time tstar diam zfront I
```

```
% Lets clear the screen
clc

% Lets define default values
tau = 1000;
Kcond = 0.6;

% See if the user wants to enter the rest
defl = input('Do you want to use the defaults? ','s');
if strcmp(defl,'y') == 1
        kdiff = 0.28;
        pow = 0.1;
        diam = 0.4;
        time = 1E6;
        thick = 100;
else
kdiff = input('Enter k (mm2/s)');
pow = input('What is the intial power: (W) ');
diam = input('Beam diameter (cm): ');
time = input('What is the duration of exposure (s) ');
% Ask for the thickness of the absorber
thick = input('What is the thickness of the absorber (mm): ');
end

% Find out the distance from the point of interest to the front of the
absorber
zfront = input('What is the distance to the front of the absorber (cm): ');

%Get everything into SI units
kdiff = 1E-6 * kdiff; %convert to m2/s
diam = diam/100;
zfront = zfront/100;

% Work out the dependents
L = sqrt(kdiff * tau);
area = (diam/2)^2 * pi;
I = pow/area;
tstar = sqrt(time/tau);
thick = thick/1000;

% Ask for the absorption coefficient
% At the moment lets assume absorption equals attenuation
a1 = input('What is the minimum absorption coefficient (Np/cm): ');
a2 = input('What is the maximum absorption coefficient (Np/cm): ');
as = input('What step size? ');
%absorp = absorp*100; %work in metres
% Integrate the disc solutions over the thickness of the absorber
zback = zfront+thick;
```

```
loop  = 1;
for abrpcm = a1:as:a2;
        absorp = abrpcm * 100;
%       fprintf('absorp coeff = %2.2f Np/cm\n',abrpcm)
        totheat(loop) = quad8('heatdisc2',zfront,zback);
        loop = loop + 1;
end
ver = 1;
flname = sprintf('res-%s-%g',date,ver);
flnmtot = [flname '.mat']
while exist(flnmtot) ~= 0,
ver = ver + 1;
flname = sprintf('res-%s-%g',date,ver);
flnmtot = [flname '.mat'];
end
eval(['save ' flname])
```

A.3. Subroutines Used in All Programs

A.3.1. Heatdisc

```
function y=heatdisc2(z)
% heatdisc2.m
% This version calculates the heating due to a disc a distance
% z from the point of interest

% Lets this function know about the globals
global absorp L kdiff Kcond time tstar diam zfront I

% z might be negative so make a variable which is positive
zpos = abs(z);

%Maximum distance from ring diam d
rtot = sqrt(z.^2 + (diam/2)^2);

% Work out how far into the absorber you are
zin = z - zfront;

% Calculate the intensity at this point
inten = I*exp(-2*absorp*zin);

% Hence the amount of heat produced
ht = 2*absorp*inten;

for loop = 1:length(z)
        intgl(loop) = quad8('ring_sol2',zpos(loop),rtot(loop));
end
```

```
y = ht/(4*Kcond).*intgl;
```

A.3.2. Ring_sol

```
function y=ring_sol2(x)
% ring_sol2.m
% the solution to the bioheat transfer equation
% for a ring

global absorp L kdiff time tstar

E = exp(-x/L);
term2 = x/sqrt(4*kdiff*time);
nummin = tstar - term2;
numplus = tstar + term2;

ef1 = erfc(nummin);
ef2 = erfc(numplus);

y = E.*(2-ef1)+ef2./E;
```

Appendix B

Finite Element Theory

B.1. Introduction

The finite element method (FEM) is a numerical approach which can be used to obtain approximate solutions to differential equations. The characteristic feature of this technique is that the region of interest is divided into elements and the approximation is carried out over each element. For example, it may be adequate to assume that the solution is linear over each element even if the distribution is far more complex over the whole region. Each element has a series of nodes at which the unknown, which in this study is temperature, is determined and the temperature at intermediate points is interpolated using a series of shape functions which are an integral part of the finite element analysis.

The basic steps in producing a finite element model can be summarised as follows (Ottosen & Peterson, 1992):

1. Establish the strong formulation of the problem;
2. Obtain the weak form of the problem;
3. Make an element-wise approximation over the entire body of the unknown function;
4. Choose the weight function.

These will be illustrated with reference to a one-dimensional heat flow problem.

B.2. The Strong Form

Consider a bar of length L and cross-sectional area A(x) with heat input Q per unit time per unit length.

The steady state equation can be obtained by considering conservation of energy, which gives:

$$\frac{\partial}{\partial x}(Aq) = Q$$

where q is the heat flux and Fourier's law of conduction:

$$q = -k\frac{\partial T}{\partial x}$$

Combining these gives the following differential equation:

$$\frac{\partial}{\partial x}\left(Ak\frac{\partial T}{\partial x}\right) + Q = 0 \qquad \text{for } 0 \le x \le L$$

The boundary conditions will depend upon the exact nature of the problem but for illustrative purposes assume that the heat flux at one end of the bar, x = 0, is known and denoted by h and the temperature at the other end, x = L, is g . The boundary conditions are then:

$q(x = 0) = h$

$T(x = L) = g$

These boundary conditions, together with the differential equation are known as the strong form of the problem.

B.3. The Weak Form.

To establish the weak form of the equation the strong form is multiplied by a function, known as the weighting function, and then integrated. In ANSYS, the finite element package used in this study, the multiplying function is a virtual change in temperature δT, which is a function of x.

This process gives

$$\int_0^L \left[\delta T \frac{\partial}{\partial x}\left(Ak \frac{\partial T}{\partial x} \right) + (\partial T) Q \right] dx = 0$$

Integrating by parts turns the first term into:

$$\left[(\delta T) Ak \frac{\partial T}{\partial x} \right]_0^L - \int_0^L \frac{\partial (\delta T)}{\partial x} Ak \frac{\partial T}{\partial x} dx$$

and so the equation becomes

$$\int_0^L \frac{\partial (\delta T)}{\partial x} Ak \frac{\partial T}{\partial x} dx = \left[(\delta T) Ak \frac{\partial T}{\partial x} \right]_0^L + \int_0^L (\delta T) Q \, dx$$

The boundary conditions can be incorporated into the second term:

$$\left[(\delta T) Ak \frac{\partial T}{\partial x} \right]_0^L = \left((\delta T) Ak \frac{\partial T}{\partial x} \right)_{x=L} - \left((\delta T) Ak \frac{\partial T}{\partial x} \right)_{x=0} = -((\delta T) Aq)_{x=L} + ((\delta T) A)_{x=0} h$$

This process gives what is known as the weak form of the problem:

$$\int_0^L \frac{\partial (\delta T)}{\partial x} Ak \frac{\partial T}{\partial x} dx = -((\delta T) Aq)_{x=L} + ((\delta T) A)_{x=0} h + \int_0^L (\delta T) Q \, dx$$

$T(x = L) = g$

In the weak form the unknown function T is only differentiated once whereas in the strong form the second derivative appears. This means that the weak form has the advantage when it comes to choosing an

approximating function for T as it does not need to be twice differentiable. This means that the weak form can cope with temperature variations that do not vary smoothly and which would give a discontinuity in $\frac{\partial T}{\partial x}$.

B.4. Choice of Approximating Function.

The approximating function is used to calculate the temperature within each element using the temperature at the nodes. When choosing the form of this function the following points need to be considered:

- any choice of approximating function must, if the elements were infinitely small, come infinitely close to the real temperature distribution;
- even though the approximation is carried out on an element-by-element basis, the temperature approximation must be continuous over element boundaries.

It can be shown (Ottosen & Peterson, 1992) that polynomials are a convenient and commonly used choice of function. The simplest form is to use a first order polynomial such as $T = \alpha_1 + \alpha_2 x$, where T is the temperature at point x within the element and α_1 and α_2 coefficients which have values that need to be determined. In matrix form this is represented as:

$T = \overline{N}\alpha$

where

$$\overline{N} = \begin{bmatrix} 1 & x \end{bmatrix} \text{ and } \alpha = \begin{bmatrix} \alpha_1 \\ \\ \alpha_2 \end{bmatrix}$$

In order to find the value of α, which has two unknowns, it is necessary to have two equations and, in finite element terms, this means that each element must have two nodes. As the order of the polynomial used to estimate T is increased, the number of nodes in each element also increases.

If

$$\mathbf{a_e} = \begin{bmatrix} T_i \\ \\ T_j \end{bmatrix}, \; C = \begin{bmatrix} 1 & x_i \\ \\ 1 & x_j \end{bmatrix} \text{ and } \alpha = \begin{bmatrix} \alpha_1 \\ \\ \alpha_2 \end{bmatrix}$$

where T_i is the temperature at x_i, then $\mathbf{a_e} = C\alpha$ and multiplying both sides by C^{-1} gives $\alpha = C^{-1}\mathbf{a_e}$.

The formula giving the approximate temperatures, $T = \bar{N}\alpha$, can also be expressed in terms of the nodal temperatures:

$T = \mathbf{N_e a_e}$

where $\mathbf{N_e} = \bar{N}\mathbf{C}^{-1}$

As the inverse of **C** is given by

$$\mathbf{C}^{-1} = \frac{1}{L}\begin{bmatrix} x_j & -x_i \\ -1 & 1 \end{bmatrix} \text{ where } L = x_j - x_i$$

the elements of $\mathbf{N_e}$ are

$N_e^i = -\frac{1}{L}(x - x_j)$ which is 1 at x_i and 0 at x_j

and

$N_e^j = \frac{1}{L}(x - x_i)$ which is 0 at x_i and 1 at x_j.

These terms are known as the element shape functions and they contain the information about the geometry of the body. One advantage of this formulation is that terms influenced by geometry, the shape functions ($\mathbf{N_e}$) have been separated from those influenced by physics, the nodal temperatures ($\mathbf{a_e}$). This is particularly useful for computer packages as the shape function of each element depends only of the element type and not of the loads applied.

The weak form of the heat flow equation contains the gradient of the temperature T. As $T = \mathbf{N_e a_e}$ and $\mathbf{a_e}$ does not depend on x

$$\frac{\partial T}{\partial x} = \frac{\partial \mathbf{N_e}}{\partial x}\mathbf{a_e}$$

If matrix $\mathbf{B_e}$ is defined as $\frac{\partial \mathbf{N_e}}{\partial x}$

then $\frac{\partial T}{\partial x} = \mathbf{B_e a_e}$

In the above example

$$\mathbf{B_e} = \begin{bmatrix} -\frac{1}{L} & \frac{1}{L} \end{bmatrix}$$

This gives the shape function and its derivative for one element but it is necessary to consider the entire body. Global shape functions are defined in such a way that there is one function per node, rather than one per element.

Consider a system with two elements and three nodes where the temperature at the nodes is given by T_1, T_2, T_3. The temperature at any point is approximated by:

$$T = T_1N_1 + T_2N_2 + T_3N_3$$

where N_1, N_2 N_3 are the global shape functions. These are constructed from the appropriate terms of the element shape functions and take the value 1 at 'their' node and zero at all others. The relationship between element and global shape functions is illustrated in figure B.1.

If the components of the element shape function for element 1 are N_1^i and N_1^j and for element 2 are N_2^i and N_2^j etc. then

$$N_1 = \begin{cases} N_1^i \text{ for x in element 1} \\ 0 \quad \text{otherwise} \end{cases}$$

$$N_2 = \begin{cases} N_1^j \text{ for x in element 1} \\ N_2^i \text{ for x in element 2} \\ 0 \quad \text{otherwise} \end{cases}$$

$$N_3 = \begin{cases} N_2^j \text{ for x in element 2} \\ 0 \quad \text{otherwise} \end{cases}$$

This process can be expanded to a system of many elements with the global shape function for a specific node only ever differing from zero in those elements containing that node. A global shape function matrix **N** can be defined such that its elements are the global shape functions and if matrix **a** contains the temperature at the nodal points then $T = \mathbf{Na}$.

Figure B.1: Relationship between element and global shape functions.

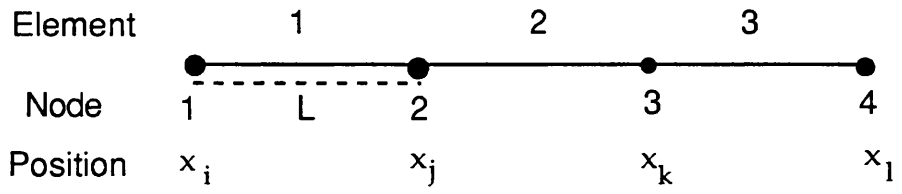

Element shape functions for element 1

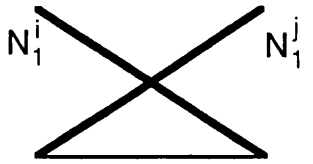

$$N_1^i = -1/L(x - x_j)$$

$$N_1^j = 1/L\,(x - x_i)$$

Global shape function for node 1

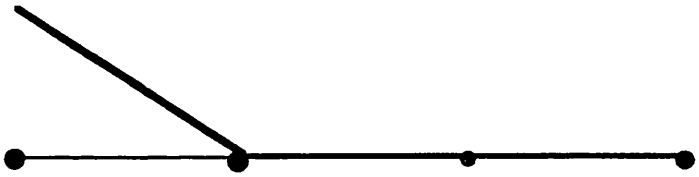

Global shape function for node 2

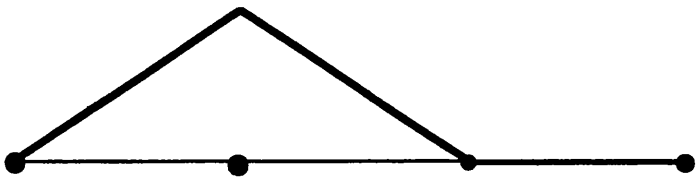

B.5. The Weight Function

In order to get the weak form of the equation, the strong form was multiplied by a virtual change in temperature δT; which is called the weight function. Different methods of finite analysis choose the weight function in different ways but ANSYS uses the Galerkin method. In this

the weight function δT is assumed to vary in the same way as T, the actual temperature distribution, i.e.

$$\delta T = \mathbf{N}\delta\mathbf{a} \text{ and } \frac{\partial(\delta T)}{\partial x} = \mathbf{B}\delta\mathbf{a}$$

When these are substituted into the weak form of the heat flow equation it becomes:

$$\int_0^L \mathbf{B}^T \delta a A k \mathbf{B} a dx = \left[\mathbf{N}^T \delta a A k \mathbf{B} a\right]_0^L + \int_0^L \mathbf{N}^T \delta a Q dx$$

where $\mathbf{B}^T$ is the transpose of **B**.

$\delta\mathbf{a}$ and **a** are dependent only on the values at the nodes and do not vary over the element, they can therefore be taken outside the integrals or cancelled, leaving:

$$\int_0^L \mathbf{B}^T A k \mathbf{B} dx\, \mathbf{a} = \left[\mathbf{N}^T A k \mathbf{B} a\right]_0^L + \int_0^L \mathbf{N}^T Q dx$$

$k\mathbf{B}\mathbf{a} = -\,q$ (since $q = -k\frac{\partial T}{\partial x}$) giving:

$$\int_0^L \mathbf{B}^T A k \mathbf{B} dx\, \mathbf{a} = -\left[\mathbf{N}^T A q\right]_0^L + \int_0^L \mathbf{N}^T Q dx$$

This can be expressed as:

$$K\,\mathbf{a} = f_b + f_l$$

where

$$\mathbf{K} = \int_0^L \mathbf{B}^T A k \mathbf{B} dx$$

$$f_b = -\left[\mathbf{N}^T A q\right]_0^L$$

$$f_l = \int_0^L \mathbf{N}^T Q dx$$

K, the 'Stiffness matrix', is a square matrix of dimension n x n, where n is the number of nodes and it contains the information about physical properties of the body, such as the thermal conductivity. f_b the boundary vector describes the heat flow at the surface and f_l the load vector describes the heating of the bulk of the material, both have dimension n x 1. This equation describes a set of simultaneous equations which can be solved to find **a**, the temperature at the nodes; once this is known the temperature at any arbitrary point can be estimated ising the formula T =

Na. A worked example of a simple heat flow calculation is included in appendix C.

B.6. Convective Boundary Conditions

In order to model an body immersed in fluid it is necessary to include convection. The is done by considering Newton's law of convection which states that the heat flow from the body into the fluid is given by:

$$q = h(T - T_\infty)$$

where

h = convection coefficient;

T = temperature at surface of body;

T_∞ = temperature of the bulk of the fluid.

To see how this fits into the above formulation assume that convection occurs at the end of the bar (x = L) . The boundary vector $\mathbf{f_b}$ is given by:

$$\mathbf{f_b} = -\left[\mathbf{N}^T\mathbf{A}q\right]_0^L = -\left(\mathbf{N}^T\mathbf{A}q\right)_{x=L} + \left(\mathbf{N}^T\mathbf{A}q\right)_{x=0}$$

Using the above

$$(q)_{x=L} = h(T_{x=L} - T_\infty).$$

Since $T_{x=L} = \mathbf{N}_{x=L}\mathbf{a}$

$$(q)_{x=L} = h\mathbf{N}_{x=L}\mathbf{a} - hT_\infty$$

and the boundary vector becomes:

$$\mathbf{f_b} = -h(\mathbf{A}\mathbf{N}^T\mathbf{N})_{x=L}\mathbf{a} + hT_\infty(\mathbf{A}\mathbf{N}^T)_{x=L} + (\mathbf{N}^T\mathbf{A}q)_{x=0}.$$

Convection can therefore be included by modifiying the stiffness matrix and the boundary vector such that:

$$(\mathbf{K} + \mathbf{K_C})\mathbf{a} = hT_\infty(\mathbf{A}\mathbf{N}^T)_{x=L} + (\mathbf{N}^T\mathbf{A}q)_{x=0} + \mathbf{f_l}$$

where

$$\mathbf{K_C} = -h(\mathbf{A}\mathbf{N}^T\mathbf{N})_{x=L}$$

B.7. Transient Analysis

FEM can be used to determine the rate of heating as well as the steady state solution. The matrix formulation of the problem is given by:

$$\mathbf{C}\dot{\mathbf{a}} + \mathbf{K}\mathbf{a} = \mathbf{f}$$

where

$\mathbf{C}$ = specific heat matrix;

$\dot{\mathbf{a}}$ = rate of change of nodal temperatures with time;

$\mathbf{a}$ = nodal temperatures;

$\mathbf{f} = \mathbf{f_b} + \mathbf{f_l}$.

The specific heat matrix is given by:

$$\mathbf{C} = \rho\int \mathrm{CNN}^{\mathrm{T}}\mathrm{d}x$$

where

C = specific heat;

ρ = density.

The relationship between the temperature at time steps n and n + 1, separated by a time interval Δt is estimated using:

$$\mathbf{a}_{n+1} = \mathbf{a}_n + (1-\theta)\Delta t\dot{\mathbf{a}}_n + \theta\Delta t\dot{\mathbf{a}}_{n+1}$$

where θ is the transient integration parameter which defaults to 0.5

As

$$\mathbf{C}_{n+1}\dot{\mathbf{a}}_{n+1} + \mathrm{K}\mathbf{a}_{n+1} = \mathbf{f}$$

substituting for $\dot{\mathbf{a}}_{n+1}$ gives

$$\left(\frac{1}{\theta\Delta t}\mathbf{C}+\mathbf{K}\right)\mathbf{a}_{n+1} = \mathbf{f}+\mathbf{C}\left(\frac{1}{\theta\Delta t}\mathbf{a}_n + \frac{1-\theta}{\theta}\dot{\mathbf{a}}_n\right)$$

This equation represents a set of simultaneous equations and can be solved using the same techniques as used for the static analysis.

It is necessary to know, or assume, the initial values of $\mathbf{a}_n$ and $\dot{\mathbf{a}}_n$. In the program used they were both set to zero.

B.8. Time Step Optimisation

When carrying out a transient analysis it is necessary to determine the frequency of the time steps. To do this various factors are considered; these include the rate of change of temperature between the two previous steps, the thermal conductivity and the specific heat. The first step is to calculate the response eigenvalue which is given by:

$$\lambda_T = \frac{\Delta \mathbf{a}^T \mathbf{K} \Delta \mathbf{a}}{\Delta \mathbf{a}^T \mathbf{C} \Delta \mathbf{a}}$$

where:

$\Delta \mathbf{a}$ = substep solution vector $(\mathbf{a}_n - \mathbf{a}_{n-1})$

$\mathbf{C}$ = specific heat matrix

The oscillation limit is given by $\Delta t_n \lambda$ where λ is the maximum eigenvector. and $\Delta t_n \lambda >> 1$ should be avoided

The above equation for λ_T gives the dominant value rather than the maximum and so in ANSYS the time step restriction is set to:

$\Delta t_n \lambda_T \approx f$ where f defaults to 0.5.

The allowable change in step size is therefore given by:

$$\frac{\Delta t_{n+1}}{\Delta t_n} = \frac{f}{\lambda_T \Delta t_n}$$

Limits are imposed on the step size, both by the user who defines maximum and minimum values and by the ANSYS software which sets the maximum increase or decrease to be a factor of 3.

Appendix C

Example of the Application of the Finite Element Technique

The application of the finite element technique was illustrated by Ottosen and Peterson (1992). Consider a bar going from point a at x = 2 m to point b at x = 8 m with the following properties:
cross-sectional area A = 10 m^2
thermal conductivity k = 5 W $°C^{-1}m^{-1}$
heat supply Q = 100 W s^{-1}

The equation defining the steady state temperature distribution is

$$\frac{\partial}{\partial x}\left(Ak\frac{\partial T}{\partial x}\right)+Q=0 \qquad a \le x \le b$$

The boundary conditions are:
T(x=a) = 0°C,
q(x=b) = 15 W m^{-2}.

The bar is divided into three elements, each with a node at each end giving linear shape functions.

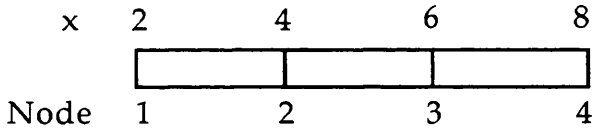

For each element the shape function is given by:

$$N_e = [-\frac{1}{L}(x - x_j) \quad \frac{1}{L}(x - x_i)]$$

For the first element, therefore
N_e = [-0.5(x-4) 0.5(x-2)]
and

$$B_e = \frac{\partial N_e}{\partial x} = [-0.5 \quad 0.5].$$

As explained earlier, it is possible to convert the element formulation into a global one so that the temperature approximation over the region of interest is given by:

$$T = \mathbf{Na}$$

where **N** is the global shape function matrix and **a** contains the temperature at the nodes.

The components of the global shape function, **N**, are

$$N_1 = \begin{cases} -0.5(x-4) & \text{in element 1} \\ 0 & \text{otherwise} \end{cases}$$

$$N_2 = \begin{cases} 0.5(x-2) & \text{in element 1} \\ -0.5(x-6) & \text{in element 2} \\ 0 & \text{otherwise} \end{cases}$$

$$N_3 = \begin{cases} 0.5(x-4) & \text{in element 2} \\ -0.5(x-8) & \text{in element 3} \\ 0 & \text{otherwise} \end{cases}$$

$$N_4 = \begin{cases} 0.5(x-6) & \text{in element 4} \\ 0 & \text{otherwise} \end{cases}$$

The first step in obtaining **a** is to calculate the stiffness matrix, **K**, and for this the components of **B**, are needed, where $\mathbf{B} = \frac{\partial \mathbf{N}}{\partial x}$.

$$B_1 = \begin{cases} -0.5 & \text{in element 1} \\ 0 & \text{otherwise} \end{cases}$$

$$B_2 = \begin{cases} 0.5 & \text{in element 1} \\ -0.5 & \text{in element 2} \\ 0 & \text{otherwise} \end{cases}$$

etc.

The first component of the stiffness matrix is given by

$$K_{11} = \int_L B_1 A k B_1 dx$$

This will only be non - zero in elements containing node 1 and so becomes

$$\int_2^4 B_1 A k B_1 dx = \int_2^4 (-0.5(10)(5)(-0.5)dx = 25$$

The elements on the diagonal, such as K_{22}, are calculated by adding the contribution from two elements:

$$K_{22} = \int_{2}^{L} B_2 A k B_2 dx = \int_{2}^{\text{element 1}} B_2\, AkB_2 dx + \int_{4}^{\text{element 2}} B_2\, AkB_2 dx$$

$$= \int_{2}^{4} (0.5(10)(5)(0.5)dx + \int_{4}^{6} (-0.5(10)(5)(-0.5)dx = 50$$

As K_{ij} will be zero unless nodes i and j occur in the same element many of the components are zero. The whole stiffness matrix can be shown to be

$$K = \begin{bmatrix} 25 & -25 & 0 & 0 \\ -25 & 50 & -25 & 0 \\ 0 & -25 & 50 & -25 \\ 0 & 0 & -25 & 25 \end{bmatrix}.$$

The boundary vector $f_b = -\begin{bmatrix} [N_1 Aq]_a^b \\ [N_2 Aq]_a^b \\ [N_3 Aq]_a^b \\ [N_4 Aq]_a^b \end{bmatrix}$

with $[N_i Aq]_a^b = -(N_i Aq)_{x=b} + (N_i Aq)_{x=a}$

Most of the components of the global shape funtion matrix are zero at x = a and x = b, due to the form of the global shape functions.

$$N_i(x = a) = \begin{cases} N_1(x = a) = -0.5(2-4) = 1 & \text{if } i = 1 \\ 0 & \text{if } i \neq 1 \end{cases}$$

$$N_i(x = b) = \begin{cases} N_4(x = b) = 0.5(8-6) = 1 & \text{if } i = 4 \\ 0 & \text{if } i \neq 4 \end{cases}$$

Therefore

$$f_b = \begin{bmatrix} (Aq)_{x=a} \\ 0 \\ 0 \\ -(Aq)_{x=b} \end{bmatrix} = \begin{bmatrix} (10q)_{x=2} \\ 0 \\ 0 \\ -150 \end{bmatrix}$$

The load vector $f_l = \begin{bmatrix} \int_a^b N_1 Q dx \\ \int_a^b N_2 Q dx \\ \int_a^b N_3 Q dx \\ \int_a^b N_4 Q dx \end{bmatrix} = Q \begin{bmatrix} \int_2^4 N_1 dx \\ \int_2^4 N_2 dx + \int_4^6 N_2 dx \\ \int_4^6 N_3 dx + \int_6^8 N_3 dx \\ \int_6^8 N_4 Q dx \end{bmatrix} = \begin{bmatrix} 100 \\ 200 \\ 200 \\ 100 \end{bmatrix}$

The equation Ka = f therefore equates to

$$\begin{bmatrix} 25 & -25 & 0 & 0 \\ -25 & 50 & -25 & 0 \\ 0 & -25 & 50 & -25 \\ 0 & 0 & -25 & 25 \end{bmatrix} \begin{bmatrix} 0 \\ T_2 \\ T_3 \\ T_4 \end{bmatrix} = \begin{bmatrix} (10q)_{x=2} \\ 0 \\ 0 \\ -150 \end{bmatrix} + \begin{bmatrix} 100 \\ 200 \\ 200 \\ 100 \end{bmatrix}.$$

This can be solved to give

$$\begin{bmatrix} T_2 \\ T_3 \\ T_4 \end{bmatrix} = \begin{bmatrix} 14 \\ 20 \\ 18 \end{bmatrix}$$

As

$-25T_2 = (10q)_{x=2} + 100$

$q_{x=2} = -45\ Jm^{-2}s^{-1}$

As the shape functions and the nodal temperatures are known, the temperature at any point in the bar can be estimated.

Appendix D

Examples of Finite Element Batch Files

All models created using ANSYS 5.1
Lines starting with ! are comments

D.1. File to Create Model of Bone Mimic in Agar

```
/BATCH
/FILNAM,nv24c
/TITLE,Modelling Agar-Bone mimic
/stitle,1,real beam - mean values out to 4.5 mm
/stitle,2,very thin layer in front of bone
/stitle,3,0.5 mm increments, 0.25 mm elements
/UNITS,SI
/PREP7
! material 1 = Agar
mp,dens,1,1000
mp,kxx,1,0.609
! remember C = heat capacity
mp,c,1,4289
! material 2 = ptfe
mp,dens,2,2200
mp,c,2,1630
mp,kxx,2,0.332
et, 1,plane77
keyo, 1, 3, 1
dep0=12.99e-3
dep1=13e-3
dep2=18e-3
wid1=7.5e-3
wid2=20e-3
rectng,0,wid1,0,dep0
rectng,0,wid1,dep0,dep1
rectng,0,wid1,dep1,dep2
rectng,wid1,wid2,0,dep1
rectng,wid1,wid2,dep1,dep2
aglue,all
save
! sort out element size for axial line in front of bone
lesize,4,,,,5
! set default line size
lesize,all,5e-3
! select lines within the heated bit
lsel,s,loc,y,dep1,dep2
lsel,r,loc,x,0,wid1
lsel,a,line,,3
lesize,all,2.5e-4,,,,1
```

```
!invert selection
lsel,inve
lsel,u,line,,4
! Adjust element sizes so that no jump is bigger than 5, maximum
reduction 10
ldva,0,5,10
save
!select ptfe
asel,s,loc,y,dep1,dep2
mat,2
amesh,all
asel,inve
mat,1
amesh,all
allsel,all
save
finish
/solu
asel,s,loc,y,dep1,dep2
asel,r,loc,x,0,wid1
nsla,s,1
! Apply heat generations loads
heatn5,390,dep1
allsel,all
! Apply convection loads
lsel,s,line,,     1
lsel,a,line,,     11
lsel,a,line,,     26
lsel,a,line,,     28
sfl,all,conv,400
! the following select commands were generated by the allsel command
vsel,all
asel,all
lsel,all
ksel,all
esel,all
nsel,all
! Set up to do a transient analysis
timint,on
kbc,1
time,300
autots,on
deltim,0.2e-2,0.2e-2,10
outpr,,none
outres,nsol,1
solve
finish
exit
```

D.1.1 Subroutine for applying heat generation loads to disc

```
! heatn5.mac
! applies heating at nodes but for flat sample
! 'Hard-wired' intensity values
! small step size
atten=arg1
dep1=arg2
*get,ndn,node,,num,min
*get,ndct,node,,count
*do,I,1,ndct
        nd=ndn
        *get,xp,node,nd,loc,x
        *get,yp,node,nd,loc,y
        yin = yp - dep1
        *if,xp,lt,2.5e-4,then
                iref=5472
        *elseif,xp,lt,0.75e-3
                iref=4317
        *elseif,xp,lt,1.25e-3
                iref=2618
        *elseif,xp,lt,1.75e-3
                iref=1193
        *elseif,xp,lt,2.25e-3
                iref=642
        *elseif,xp,lt,2.75e-3
                iref=514
        *elseif,xp,lt,3.25e-3
                iref=507
        *elseif,xp,lt,3.75e-3
                iref=257
        *elseif,xp,lt,4.25e-3
                iref=107
        *elseif,xp,lt,4.5e-3
                iref=27
        *else
                iref=0
        *endif
        iy = iref*exp(-2*yin*atten)
        Pow=2*atten*iy
        bf,nd,hgen,Pow
        *get,ndn,node,nd,nxth
*enddo
```

D.2. File to Create Model of Vertebra in Agar

```
/BATCH
/filenam,ja8
/title 80 mm separation, h = 400
/stitle,1,small heating increments to 4.5 mm
/stitle,2,NCRP values
/stitle,3,mixed elements in bone 0,25,0.5 mm
/stitle,4,rim of small elements around bone
/prep7
! Material 1 = agar
mp,dens,1,1000
mp,kxx,1,0.609
mp,c,1,4289
! Material 2 = Bone
mp,dens,2,1300
mp,kxx,2,0.58
mp,c,2,1600
et,1,plane77
keyopt,1,3,1
! Distance to top of bone
dep1=15e-3
! Total thickness of agar
dep2=50e-3
! Dimensions of ellipse
rady = 5e-3
radx = 7.5e-3
wid1 = 25e-3
K,1,0,dep1
K,2,radx,dep1+rady
K,3,0,dep1+(2*rady)
K,4,0,dep1+rady
K,5,0,dep1-1e-5
K,6,radx+1e-5,dep1+rady
K,7,0,dep1+(2*rady)+1e-5
! Change to cylinrical co-ords
LOCAL,11,1,0,dep1+rady,,,,,0.66
L,1,2
L,2,3
L,5,6
L,6,7
csys,0
A,1,2,4
A,4,2,3
A,5,6,4
A,4,6,7
bopt,yes
aadd,3,4
```

```
rectng,0,wid1,0,dep2
asba,6,5
aadd,1,2
asba,5,8
adel,3
adel,4
adel,5
adel,6
adel,8
ldel,9,10
ldel,14
aglue,all
save
lesize,all,5e-3
csys,11
allsel,all
! Small elements in bone
asel,s,area,,1
lsla,s,0
lesize,all,2.5e-4,,,,1
! Curved lines, do element size in terms of angle
lsel,s,line,,1
lsel,a,line,,3
lesize,all,,3,,,1
asel,s,area,,2
lsla,s,0
lesize,all,5e-4,,,,1
lsel,s,line,,2
lsel,a,line,,4
lssize,all,,3,,,1
asel,a,area,,1
lsla,s,0
! Adjust number of divisions to avoid large jumps
LDVA,0,5,5
! the following select commands were generated by the allsel command
vsel,all
asel,all
lsel,all
ksel,all
esel,all
nsel,all
lsel,s,line,,15,16
lesize,all,2e-3,,,,1
ldva,1,5,5
! the following select commands were generated by the allsel command
vsel,all
asel,all
lsel,all
ksel,all
```

```
esel,all
nsel,all
ldva,1,5,5
save
mat,2
amesh,1,2
mat,1
amesh,7,9
! the following select commands were generated by the allsel command
vsel,all
asel,all
lsel,all
ksel,all
esel,all
nsel,all
save
finish
/solu
! Apply convection loads
sfl,11,conv,400
sfl,13,conv,400
save
csys,0
asel,s,area,,1
asel,a,area,,2
nsla,s,1
! Apply heat generation loads using subroutine
heates,525,dep1,radx,rady
allsel,all
save
! Transient analysis
timint,on
kbc,1
time,150
autots,on
deltim,0.04,0.04,10
outpr,,none
outres,nsol,1
solve
save
finish
/exit
```

D.2.1. Subroutine to apply heat generation loads in ellipse

```
! heates.mac
! loading for ellipse
! Hard wired small steps
atten=arg1
```

```
dep1=arg2
arad=arg3
brad=arg4
*get,ndn,node,,num,min
*get,ndct,node,,count
bsqd = brad*brad
boasqd = bsqd/(arad*arad)
*do,I,1,ndct
        nd=ndn
        *get,xp,node,nd,loc,x
        *get,yp,node,nd,loc,y
        *if,bsqd,lt,(boasqd*xp*xp),then
                *if,xp,lt,(arad+0.1e-3),then
                xp = arad
                *endif
        *endif
        yellip = dep1+brad-sqrt(bsqd-(boasqd*xp*xp))
        yin = yp - yellip
        *if,yin,gt,(2*brad+0.1e-3),then
        *msg,error,xp,yin
        xp = %G,yin = %G
        *cycle
        *endif
        *if,xp,lt,2.5e-4,then
                iref=5472
        *elseif,xp,lt,0.75e-3
                iref=4317
        *elseif,xp,lt,1.25e-3
                iref=2618
        *elseif,xp,lt,1.75e-3
                iref=1193
        *elseif,xp,lt,2.25e-3
                iref=642
        *elseif,xp,lt,2.75e-3
                iref=514
        *elseif,xp,lt,3.25e-3
                iref=507
        *elseif,xp,lt,3.75e-3
                iref=257
        *elseif,xp,lt,4.25e-3
                iref=107
        *elseif,xp,lt,4.5e-3
                iref=27
        *else
                iref=0
        *endif
        iy = iref*exp(-2*yin*atten)
        Pow=2*atten*iy
        bf,nd,hgen,Pow
```

```
        *get,ndn,node,nd,nxth
*enddo
```

Appendix E

Nomenclature

The following is a list of the symbols used in the main body of thesis and their meaning:

c	speed of sound
c_v	heat capacity per unit volume
C	specific heat
d_6	-6 dB beam diameter
I	ultrasonic intensity
I_{sata}	spatial average temporal average intensity
I_{spta}	spatial peak temporal average intensity
J_1	first order Bessel function
k	thermal diffusivity
K	thermal conductivity
L	perfusion length
p_+	peak positive pressure
p_-	peak negative pressure
q	heat flux
t	time
T	temperature
ΔT	temperature rise
W	acoustic power
α	amplitude attenuation coefficient
α_a	amplitude absorption coefficient
λ	wavelength
ρ	density

Appendix F
Glossary

anisotropic: showing difference of property in different directions.

AIUM: American Institute of Ultrasound in Medicine.

BECA: (NPL) beam calibrator.

BHTE: bioheat transfer equation.

cancellous: porous or spongy; applied to the honeycomb type of bone.

caudal: pertaining to the tail.

cavitation: formation and activity of gas or vapour-filled cavities in a medium.

cephalic: pertaining to the head.

collagen: a protein constituent of connective tissue.

cortex: the outer layer of an organ.

cranial: pertaining to the skull.

CT: computed tomography.

derating (derating factor, derated): a factor applied to the acoustic output parameters intended to account for ultrasonic attenuation of tissue between the source and a particular location in the tissue.

diploe: the cancellous tissue between the inner and outer layers of the skull.

dorsal: relating to the back or posterior part of an organ.

EFSUMB: European Federation of Societies for Ultrasound in Medicine and Biology.

embryo: animal in earliest stages of development, for humans this up to two months gestation.

FDA: Food and drug administration, US regulatory body.

FEM: finite element modelling

fetus: developing animal after organs are formed, for humans this is after two months gestation.

fibrosis: fibrous tissue formation

fibroblasts: a connective tissue cell.

NCRP: National council for radiation protection and measurements.

intensity, spatial average temporal average (I_{sata}): the temporal-average intensity over the beam cross-sectional area.

intensity, spatial peak temporal-average (I_{spta}): the value of the of the temporal-average intensity at a point in the acoustic field where the temporal-average intensity is a maximum, or is a local maximum in a specified
region.

intensity, temporal average: the time average of the intensity at a point in space.

in vitro: literally 'in glass', in the test tube, i.e. the opposite of in vivo

in vivo: in the living organism.

IUGR: inter-uterine growth retardation.

medially: towards the midline.

mesenchyme: part of the mesoderm that develops into connective tissue.

mesoderm: the middle layer of the embryo giving rise to muscle, bone and connective tissue.

microcephaly: abnormal smallness of the head.

neonatal: referring to the first month of life.

oedema: accumulation of fluid in tissue spaces.

organogenesis: the development of living organs.

ossification: the laying down of bone mineral.

parietal: two bones forming part of the roof and sides of the skull.

perfusion: blood flow.

periosteum: the fibrous membrane covering the surface of bone.

PVDF: polyvinylidene fluoride.

sphenoid: the central part of the base of the skull.

teratogenic: causing abnormal growth in a fetus.

thermal index (TI): the ratio of the total acoustic power to the acoustic power required to raise the temperature by 1°C under defined assumptions.

TIB: bone at focus thermal index.

TIC: cranial thermal index.

TIS: soft tissue thermal index.

TMM: tissue mimicing material.

trabeculae: structural bands or beams.

trimester: a three month period, often used to refer to a third of a pregnancy.

WFUMB: World federation for ultrasound in medicine and biology.